ILLINOIS POLLUTION CONTROL BOARD

IN THE MATTER OF:	)	
	)	
PROPOSED DETERMINATION OF	)	
NO SIGNIFICANT ECOLOGICAL	)	PCB 78-61
DAMAGE FOR THE QUAD CITIES	)	
GENERATING STATION,	)	
COMMONWEALTH EDISON COMPANY.	)	

N O T I C E

TO: Russell R. Eggert, Esq.
Assistant Attorney General
Environmental Control Divison
188 W. Randolph, Suite 2315
Chicago, Illinois 60601

Alan B. Miller, Esq.
Hearing Officer
Friedman & Koven
208 South LaSalle Street
Chicago, Illinois 60604

PLEASE TAKE NOTICE that on September 29, 1978, we filed the attached Motion For Reconsideration with the Clerk of the Pollution Control Board.

ISHAM, LINCOLN & BEALE

By A. Daniel Feldman
A. Daniel Feldman

Attorney for Commonwealth Edison Company.

ISHAM, LINCOLN & BEALE
One First National Plaza
Suite 4200
Chicago, Illinois 60603
(312) 786-7500

ILLINOIS POLLUTION CONTROL BOARD

IN THE MATTER OF:	)	
	)	
PROPOSED DETERMINATION OF	)	
NO SIGNIFICANT ECOLOGICAL	)	PCB 78-61
DAMAGE FOR THE QUAD CITIES	)	
GENERATING STATION,	)	
COMMONWEALTH EDISON COMPANY.	)	

MOTION FOR RECONSIDERATION

Commonwealth Edison Company, pursuant to Rule 333 of the Procedural Rules of this Board, requests reconsideration of the Board's Interim Order of September 7, 1978 requiring the filing of a supplementary petition. The request is made on the following grounds:

1. The consultants report establishing the theoretical and actual plume dimensions during all seasons at Quad Cities is appended hereto. (Iowa Institute of Hydraulic Research Report No. 204, the University of Iowa, June 1977.)

2. The essential requirements of Rule 602 are, however, already met by the petition. They are not, however, stated in the manner or style to which the Board is accustomed, because the diffuser discharge is of unusual design.

The requirements of Rule 602(c)(2) and (3) contemplate the presentation of the kind of plume diagram

which shows a series of concentric isolines on the surface of a body of water, together with some indication, by a drawing or in a table, of plume depths. Two factors make that kind of theoretical plume study inappropriate for the Quad Cities station.

The first factor results from the fact that the Quad Cities discharge comes from a series of individual discharge ports in two large pipes located along the bottom of the Mississippi River. The pipes discharge at high velocity and the condenser discharge is fully mixed with the Mississippi River before the plume ever reaches the surface of the River. As a result, there is no surface plume. Said another way, the size of the worst case plume, if Rule 602 anticipates a surface plume, is zero. What does appear on the surface of the River is a fully mixed discharge having a water temperature which is something higher than ambient; that "plume", which comprises the river itself, persists for miles down stream since any further temperature reduction comes from surface cooling.

The second factor is that the discharge from each exit port comprises a separate plume, spheriod in shape, until it is fully mixed with the River some numbers of feet downstream of the port. That distance depends upon the volume of water passing over that discharge port. Since the

ports are 20 feet apart, a calculation of the size of each plume depends on the volume of water moving through a segment of the Mississippi River 20 feet wide above that discharge port.

Most theoretical plume studies are mathematically derived, and they assume flow rates for the entire body of water adjacent to the discharge port. Since the plume calculation of the Quad Cities diffuser is particularly sensitive to the flow of the River in segments not normally calculated, because they have dimensions which are difficult to measure in the real world, one obtains more accurate predictions by physically modeling the contours of the river and its total flow rates. Such a physical model was constructed for Quad Cities by the Iowa Institute of Hydraulic Research. The model is equipped with rows of temperature sensors. The data from those sensors yields a series of snapshots of the plume from each individual port at a series of distances downstream from the discharge port. The plume isolines for Quad Cities are, therefore, presented in the record in this record as a series of vertical cross-sections downstream from the diffuser, rather than as a plane view of the surface of the River with isolines drawn on it. They appear as Figures 2 through 4 of Dr. Sayre's testimony. The worst case plume is described in words on page 25 of the

Petition. Average and minimum flows for every month are shown on Table 3 (p. 21) of the Petition. Using them, one can calculate average and worst case plume size for any month.

A diagram of a discharge plume appears as Figure 13 (p. 19) to the Petition. Drawing isolines on an inclined subsurface plane was not, however, the primary method of representation used by the Company's consultants. We trust that the Board will accept the technical judgment of the Iowa Institute of Hydraulic Research that the cross-sections which comprise Figures 2 through 4 of Dr. Sayer's testimony are a more informative presentation of the data. If it were translated to an inclined plane view, the discharge would resemble the teeth of a comb, with each tooth being the discharge from a single exit port, as in Figure 13. The discret nature of the discharges is, of course, the reason for the extremely large zone of passage stated in Dr. Sayer's testimony.

These background facts were made part of record in the original proceeding relating to the Quad Cities Station, entitled, Mississippi River Thermal Standards, PCB R70-16, (1971) and in the Quad Cities Nuclear proceeding under title VI, In re Quad Cities Nuclear Generating Station, PCB 71-20, order expunged May 3, 1972. Those proceedings are not, of

course, a part of the record in this proceeding, and we apologize for not having incorporated enough of the background data to make the present showing fully comprehensible.

Nevertheless, the record does include all of the required data. The data required by Rule 602 appears in Table 1 of Professor Sayre's testimony following page 15 of the transcript. The table shows the river flow required to achieve the range of fully mixed temperatures shown at the top of the exhibit. The frequency with which the plume might be that size or larger is the inverse of the frequencies shown in each column. The range of fully mixed temperatures is from 1 to 5 degrees Farenheit above ambient. The mean temperature increase of Quad Cities at the surface is slightly less than 1.6°F. above ambient, testimony of Dr. William Sayre, in evidence as Ex. 2, p. 1, following TR p. 15.

3. The two-dimensional isolines of the plume are represented in the series of cross-sections contained in Figures 2, 3 and 4 of Dr. Sayre's testimony. The theoretical calculation called for by Rule 602(c)(3) appears in Figure 5, where the theoretical plume is diagrammed against the observed plume. In neither case do these exhibits take into account variations in ambient water or air temperature.

They are omitted because a subsurface plume is unaffected by ambient air temperature, and the ambient water temperature is relevant only in showing that the 5 degree above ambient and monthly maximum temperatures are not exceeded. That showing is made by way of the monthly maximum temperatures at the Quad Cities Station shown in Table 4, on page 23 of the Petition. (One has to read Table 4 against Table 1 of Dr. Sayre's testimony, which shows the predicted percentage of time any combination of plant load and river flow will exceed the standard stated in Rule 203(i)(4).)

4. While the Petition only describes in words the plume size and temperature for the theoretical worst case temperature result, it also includes in graphic form a showing that temperature standards were not violated even under physical conditions worse than those required by the theoretical worst case analysis.*/ Actual river flow conditions in October and November, 1976 were substantially below the once in ten year seven day low flow, and therefore were worse than the worst case posited by the standards. As

---

*/ The theoretical worst case, since the plume size is directly dependent on longitudinal flow rate, assumes the regulatory low flow, viz.; the once in ten year seven day low flow, and the highest ambient temperatures of record. The frequency of occurrence of those two events was calculated in the Mississippi River Thermal Standards proceeding, PCB R-70-16 and is incorporated in the excursion clause of Rule 204 [i.e., 3° less than 1% of the hours.]

Figure 18 on page 31 of the Petition shows, the plant, operating at full capacity on several days during that period, did not exceed the 5 degree above ambient temperature limitation. Evidence that the 65 degree standard for November was not exceeded under those circumstances comes from Table 4 of the Petition, which shows a maximum observed temperature of 55 degrees during the 10 years of record for November at the representative temperature monitoring location. Given a maximum increase above ambient of less than 5°, the 65° limit is not violated.

5. Theoretical and observed plume studies made at Quad Cities by the Iowa Institute of Hydraulic Research under the supervision of Drs. Kennedy and Sayre are memorialized in its report No. 204, which presents the data at much greater length. A copy of that report is appended hereto; it was referred to, but not incorporated into the record in the footnote on page 2 of Dr. Sayre's testimony.

Thus, the Petition and record herein does supply the data required by Rule 602, in somewhat less convenient form that it might have. It shows that the Quad Cities diffuser never violates the State Water Quality Standard, because the plume is always less than 600 ft. in areal plane at all flows equal to or above the once in ten year seven day low flow.

WHEREFORE, the Petitioner respectfully requests that the Order entered on September 7, 1978 be reconsidered, or that the Board regard the Petition as having been supplemented by the appended exhibit, and by this motion, and that the Petition be granted.

ISHAM, LINCOLN & BEALE

By _____
A. Daniel Feldman

Attorney for Commonwealth Edison Company.

ISHAM, LINCOLN & BEALE
One First National Plaza
Suite 4200
Chicago, Illinois 60603
(312) 786-7500

PROTOTYPE AND MODEL STUDIES OF THE DIFFUSER-PIPE SYSTEM FOR DISCHARGING CONDENSER COOLING WATER AT THE QUAD-CITIES NUCLEAR POWER STATION

by

Alfred David Parr and William W. Sayre

Sponsored by
The Commonwealth Edison Company
Chicago, Illinois

IIHR Report No. 204

Iowa Institute of Hydraulic Research
The University of Iowa
Iowa City, Iowa

June 1977

PROTOTYPE AND MODEL STUDIES OF THE DIFFUSER-PIPE SYSTEM FOR DISCHARGING CONDENSER COOLING WATER AT THE QUAD-CITIES NUCLEAR POWER STATION

by

Alfred David Parr and William W. Sayre

Sponsored by
The Commonwealth Edison Company
Chicago, Illinois

IIHR Report No. 204

Iowa Institute of Hydraulic Research
The University of Iowa
Iowa City, Iowa

June 1977

ACKNOWLEDGMENTS

This investigation was sponsored by the Commonwealth Edison Company (CECO) of Chicago, Illinois as part of a long-range study of the thermal and biological regimes of the Mississippi River in the vicinity of the Quad Cities Nuclear Power Station to identify and evaluate effects of the thermal discharge from the station on the local ecology of the river. Key roles in coordinating various parts of the study have been played by John H. Hughes, Director of Water Quality for CECO, and Harry F. Bernhard, staff biologist in the CECO water quality group.

The river surveys were performed by Iowa Institute of Hydraulic Research (IIHR) field crews under the direct supervision of the writers. In addition to the first writer, the principal participants included Alfred Schulze of Princeton, Iowa, who supplied much valuable background knowledge of the river, and J.R. Goss, R.E. Hamer, E.J. Miller, and S.E. Stutzman, all of the IIHR. Supplementary data on station operating conditions and plant intake and discharge temperatures were provided by the Technical Staff of the Quad Cities Station, and the NALCO Environmental Sciences (formerly Industrial Bio-Test Laboratories) Fish Laboratory at the Station. The laboratory model investigation was conducted by the first writer.

John R. Glover (IIHR) was responsible for the development and maintenance of the instrumentation systems used in both the field and laboratory phases of the investigation. Other experimental equipment

was fabricated and maintained under the able supervision of Dale C. Harris (IIHR), who also coordinated the logistics for the field surveys.

TABLE OF CONTENTS

		Page
ACKNOWLEDGMENTS		i
LIST OF TABLES		vii
LIST OF FIGURES		ix
LIST OF NOMENCLATURE		xv
ABSTRACT		xix
CHAPTER		
1	INTRODUCTION	1
	1.1 Waste Heat from Electrical Power Generation	1
	1.2 Quad Cities Nuclear Power Station	4
	1.3 Thermal Standards for Large Rivers in Iowa and Illinois	9
	1.4 Purpose and Scope of Study	10
	1.5 Characteristics of Multiport Diffusers	12
2	PREVIOUS STUDIES OF SUBMERGED JETS	14
	2.1 Single Jets	14
	2.1.1. Momentum Jet	14
	2.1.2. Buoyant Jet	16
	2.1.3. Effect of Crossflow	18
	2.1.4. Free-Surface and Bottom Effects	21
	2.2 Multiport Diffusers	23
	2.2.1. Round Jet Interference	23
	2.2.2. Equivalent Slot Diffuser Concept	25
	2.2.3. Two-Dimensional Channel Model	26
	2.2.4. Three-Dimensional Models	28
3	TWO-DIMENSIONAL CHANNEL MODEL OF THE QUAD CITIES MULTIPORT DIFFUSER	29
	3.1 Objectives of the Study	29
	3.2 Characteristics of the Quad Cities Multiport Diffuser	31

CHAPTER Page

3.3 Modeling Considerations 32

4 EXPERIMENTAL EQUIPMENT AND PROCEDURES 35

4.1 Prototype Studies 35

4.1.1. Temperature and Velocity Measuring Equipment 35
4.1.2. Boat and Positioning Equipment 36
4.1.3. Experimental Procedure 37

4.1.3.1. Single-Port Surveys 37
4.1.3.2. Cross-Sectional Surveys 39

4.2 Model Study 40

4.2.1. Experimental Equipment 40

4.2.1.1. Flume and Hot Water Supply 40
4.2.1.2. Temperature Measuring Equipment 42
4.2.1.3. Velocity Measuring Equipment 46

4.2.2. Experimental Procedure 47

4.2.2.1. Planning of Experiments 47
4.2.2.2. Temperature Measurements 51
4.2.2.3. Velocity Measurements 52

5 PROTOTYPE EXPERIMENTAL RESULTS 55

5.1 Cross-Sectional Surveys 55

5.1.1. Two-Pipe Surveys 55

5.1.1.1. Background Data 56
5.1.1.2. Temperature Data 60
5.1.1.3. Velocity and Heat Flux Data ... 73

5.1.2. One-Pipe Surveys 82

5.1.2.1. Background Data 85
5.1.2.2. Temperature Data 88
5.1.2.3. Velocity and Heat Flux Data ... 92

CHAPTER Page

5.2 Single-Port Prototype Surveys 98

5.2.1. Background Data 98
5.2.2. Temperature Data 101
5.2.3. Velocity Data 105

6 MODEL EXPERIMENTAL RESULTS 106

6.1 Introduction 106
6.2 Comparison of Model and Prototype Results for Single-Port Surveys 108
6.3 Zones-of-Passage for Entire Channel 116
6.4 Jet Characteristics 130

6.4.1. Zone of Flow Establishment 130
6.4.2. Centerline Dilution 133
6.4.3. Maximum Excess Velocity 142
6.4.4. Jet Spreading 147
6.4.5. Jet Trajectories 151

6.5 Individual-Jet, Transition, and Two-Dimensional Regions 158

7 PREDICTING ZONES-OF-PASSAGE 164

7.1 Preliminary Considerations 164
7.2 Expressions for P_A and P_Q 169
7.3 Determination of $P_{A_{max}}$ and $P_{Q_{max}}$ 170

7.3.1. Using Simplifying Assumptions 170
7.3.2. P_A and P_Q as Functions of x/D 171

7.4 Comparisons with Experimental Data 175

8 SUMMARY AND CONCLUSIONS 184

8.1 Cross-Sectional Prototype Surveys 184

8.1.1. Two-Pipe Surveys 184
8.1.2. One-Pipe Surveys 189

8.2 Single-Port Studies 192
8.3 General Laboratory Results 193
8.4 Predicting Zones-of-Passage 194

REFERENCES 196

APPENDICES

		Page
A	REGULATIONS OF THE IOWA WATER QUALITY COMMISSION AND THE ILLINOIS POLLUTION CONTROL BOARD CONCERNING THE DISCHARGE OF WASTE HEAT INTO THE MISSISSIPPI RIVER NEAR CLINTON, IOWA	200
B	EXCESS TEMPERATURE PLOTS FOR CROSS-SECTIONAL SURVEYS	207
C	EXCESS TEMPERATURE AND VELOCITY PLOTS FOR SINGLE-PORT SURVEYS	224

LIST OF TABLES

TABLE		Page
5.1	Background Data for Two-Pipe Cross-Sectional Surveys	57
5.2	Background River Flow and Plant Effluent Data	58
5.3	Performance Characteristics of Diffuser Pipe 500 ft Downstream at Points where Minimum Dilution was Obtained	68
5.4	Heat Recovery Ratios 500 ft Downstream from Diffuser Pipe	81
5.5	Background Data for One-Pipe Cross-Sectional Surveys	86
5.6	Background River Flow and Plant Effluent Data when Operating with Spray Canal and/or One Diffuser Pipe Only	87
5.7	Performance Characteristics of Diffuser Pipe at Points where Minimum Dilution was Obtained when Operating with Spray Canal and/or One Diffuser Pipe Only	93
5.8	Background Data for Single-Port Prototype Studies in 1973 and 1974	99
5.9	Results for Single-Port Prototype Studies	104
6.1	Conditions for Model Runs Simulating Single-Port Surveys	107
6.2	Background Data for Model Experiments	109
6.3	Dimensionless Parameters for Model Runs	111
6.4	Comparison of Model and Prototype Results for Single-Port Surveys	114

TABLE Page

6.5 Rate of Centerline Excess Velocity Reduction for Single-Port Prototype Surveys 147

7.1 Comparison Between Measured and Predicted P_A and P_Q for Single-Port Surveys 182

8.1 Estimated Proportions of Waste Heat and Condenser Cooling Water Discharged Through Diffuser Pipe when Combined System was in Operation 191

LIST OF FIGURES

Figure		Page
1.1	Site of Quad Cities Nuclear Power Station	5
1.2	Quad Cities multiport diffuser pipe	7
2.1	Schematic representation of jet diffusion	15
2.2	Schematic diagram of a round jet in a uniform cross stream	20
2.3	Jet interference for a submerged multiport diffuser	24
2.4	Three-dimensional flow field for a submerged diffuser, two-dimensional behavior in center portion	27
3.1	Round jets in a flowing environment—terms defined	34
4.1	Boat and measuring equipment	38
4.2	Schematic layout of cold and hot water supply systems	41
4.3	Schematic diagram of flume	43
4.4	Discharge ports	44
4.5	Block diagram for dual pressure—transducer velocity measuring system	48
4.6	Calibration curve for dual pressure—transducer velocity measuring system	49
4.7	Temperature measurement grid within a transverse section of the flume	53
5.1	Observed temperatures in °C 200 ft upstream and 500 ft downstream from diffuser pipe on December 3, 1973	61

Figure		Page
5.2	Transverse distribution of depth-averaged temperature 500 ft downstream and ambient temperature 1000 ft upstream from diffuser pipe on November 28, 1972	62
5.3	Transverse distribution of normalized depth-averaged excess temperature 500 ft downstream from diffuser pipe	64
5.4	Observed excess temperatures in °F 500 ft downstream from diffuser pipe on February 20 and July 23, 1973	67
5.5	Observed excess temperatures in °F 500 ft downstream from diffuser pipe	70
5.6	Maximum excess temperature 500 ft downstream from diffuser pipe for full plant load versus river discharge	72
5.7	Normalized transverse distributions of river flows	75
5.8	Average normalized transverse distributions of river discharge 200 ft upstream and 500 ft downstream from diffuser pipe and diffuser pipe normalized discharge distribution at the pipe	77
5.9	Estimated transverse distribution of normalized excess temperature near the diffuser pipe	78
5.10	Transverse distribution of normalized excess heat flux 500 ft downstream from diffuser pipe for Q_R = 30,000 to 40,000 cfs	80
5.11	Schematic diagram of combined spray canal-diffuser pipe cooling system	83
5.12	Transverse distribution of normalized depth-averaged excess temperature 500 ft downstream from diffuser pipe	89
5.13	Normalized transverse distribution of river discharge per unit width 200 ft upstream from the diffuser pipe on April 15 and July 23, 1974	95

Figure		Page
5.14	Normalized transverse distributions of river discharge 200 ft upstream and 500 ft downstream from diffuser pipe	96
5.15	Excess temperature in °F and velocity in ft/sec measured 15 ft downstream from a main channel diffuser pipe port on October 30, 1974	102
6.1	Run numbers for different velocity ratios and relative depths	113
6.2	Normalized mixing zone areas versus distance downstream	118
6.3	5°F isotherms at a section 8.3 jet diameters downstream from a port	121
6.4	Measured transverse and vertical velocity profiles for run 22	122
6.5	Normalized discharge within 5°F isotherms	125
6.6	Minimum zone-of-passage with respect to total river discharge	129
6.7	Normalized excess temperature and velocity profiles just downstream from a port	131
6.8	Centerline excess temperature dilution versus distance downstream	134
6.9	Generalized minimum excess temperature dilutions	138
6.10	Ratios of initial to maximum excess velocity along centerline of jet	143
6.11	Slopes of curves for 3-port series in Fig. 6.10	145
6.12	Estimated standard deviations of vertical and transverse temperature distribution	149
6.13	Estimated transverse and vertical standard deviations of excess velocity distribution	152

Figure		Page
6.14	Jet trajectories	154
6.15	Transverse excess temperature distributions through centerlines of three adjacent jets when interaction begins	161
6.16	Individual jet, transition, and two-dimensional regions for 3-port series	162
7.1	Definition sketch for single-port region	165
7.2	Variation of $\tilde{u}^{\Lambda}_{\Delta T}/U_a$ with x/D for different values of k, according to Eq. (7.7)	168
7.3	Relationships between F and V for $\alpha = 0.7$ and $\alpha = 1$ according to Eq. (7.17), for determining $P_{Q_{max}}$ according to Eq. (7.18)	172
7.4	Predicted A_5/A_j and Q_5/Q_j vs x/D using generalized experimental excess temperature and velocity distributions	174
7.5	Comparison between observed $P_{A_{max}}$ and $P_{Q_{max}}$ and predicted relationships which assume constant $\tilde{u}^{\Lambda}_{\Delta T}/U_a$ and α^2	176
7.6	Comparison between observed $(A_5/A_j)_{max}$ and $(Q_5/Q_j)_{max}$ and predicted relationships for $\Delta T_E/\Delta T_C = 4.6$ based on generalized experimental excess temperature and velocity distributions	179
7.7	Variation of σ_T/D and σ_V/D with respect to k for $x/D \simeq 5.7$	180
8.1	Estimated maximum excess temperature at full plant load when effluent is discharged only through large ports	187
8.2	Transverse distribution of normalized depth-averaged excess temperature 600 feet downstream from diffuser pipe in three-dimensional laboratory model	188
B.1	Observed excess temperatures in °F 500 ft downstream from diffuser pipe on November 2, 1972	208
B.2	Observed excess temperatures in °F 300 and 500 ft downstream from diffuser pipe on November 9, 1972	209

Figure		Page
B.3	Observed excess temperatures in °F 500 ft downstream from diffuser pipe on November 28, 1972	210
B.4	Observed excess temperatures in °F 300 and 500 ft downstream from diffuser pipe on January 16, 1973	211
B.5	Observed excess temperatures in °F 500 ft downstream from diffuser pipe on February 20 and July 23, 1973	212
B.6	Observed excess temperatures in °F 500 ft downstream from diffuser pipe on July 26 and July 31, 1973	213
B.7	Observed excess temperatures in °F 500 ft downstream from diffuser pipe on August 17 and August 30, 1973	214
B.8	Observed excess temperatures in °F 500 ft downstream from diffuser pipe on September 12 and October 8, 1973	215
B.9	Observed excess temperatures in °F 500 ft downstream from diffuser pipe on October 31 and November 14, 1973	216
B.10	Observed excess temperatures in °F 500 ft downstream from diffuser pipe on December 3, 1973, and January 16, 1974	217
B.11	Observed excess temperatures in °F 500 ft downstream from diffuser pipe on January 21, 1974, and 150 ft downstream from diffuser pipe on March 14, 1974	218
B.12	Observed excess temperatures in °F 150 ft downstream from diffuser pipe on April 15, 1974	219
B.13	Observed excess temperatures in °F 500 ft downstream from diffuser pipe on July 23 and July 25, 1974	220
B.14	Observed excess temperatures in °F 500 ft downstream from diffuser pipe on August 22 and September 10, 1974	221
B.15	Observed excess temperatures in °F 150 ft downstream from diffuser pipe on October 2 and November 11, 1974	222

Figure		Page
B.16	Observed excess temperatures in °F 500 ft downstream from diffuser pipe on January 8, 1975	223
C.1	Excess temperature in °F and velocity in ft/sec measured downstream from a main channel diffuser pipe port on November 16, 1973	225
C.2	Excess temperature in °F and velocity in ft/sec measured downstream from a main channel diffuser pipe port on March 12, 1974	227
C.3	Excess temperature in °F and velocity in ft/sec measured downstream from a shallow channel diffuser pipe port on March 13, 1974	229
C.4	Excess temperature in °F and velocity in ft/sec measured downstream from a main channel diffuser pipe port on July 24, 1974	232
C.5	Excess temperature in °F and velocity in ft/sec measured downstream from a main channel diffuser pipe port on October 1, 1974	235
C.6	Excess temperature in °F and velocity in ft/sec measured downstream from a main channel diffuser pipe port on October 25, 1974	238
C.7	Excess temperature in °F and velocity in ft/sec measured downstream from a main channel diffuser pipe port on October 30, 1974	241

LIST OF NOMENCLATURE

A_j - Individual discharge port area, $\pi D^2/4$

A_5 - Area within 5°F isotherm

B - Slot jet width = A_j/L

b - Jet radius (at distance s)

D - Discharge port diameter

d - Local flow depth

F - Dimensionless critical temperature rise, defined as

$$\frac{\Delta T_c}{\Delta T_{max}} = \frac{8}{k}\frac{\Delta T_c}{\Delta T_E}\frac{\bar{u}_{\Delta T}^A}{U_a}\left(\frac{\sigma_T}{D}\right)^2 \text{ in Eq. (7.13)}$$

F - Froude number (various forms are used)

g - Gravitational acceleration

H - Ambient flow depth

h - Height of port centerline above bed

I_u - Intercept on $\frac{U_j - U_a}{u_{max} - U_a}$ axis of Fig. 6.10

k - Velocity ratio U_j/U_a

L - Discharge port spacing distance

P - Percent of full plant operating load

P_A - Fractional area $\pi r_c^2/HL$ defined by Eq. (7.8)

$P_{A_{max}}$ - Maximum value, with respect to x, of P_A

P_Q - Fractional discharge defined by Eq. (7.9)

$P_{Q_{max}}$ - Maximum value, with respect to x, of P_Q

Q_a - Total ambient flow across diffuser

Q_E - Total effluent discharge into river

Q_C - Discharge through spray canal

Q_{jD} - Design prototype jet discharge

Q_5 - Discharge through 5°F isotherm

Q_j - Diffuser discharge from one port

Q_R - Total river discharge

Q_F - Total ambient discharge in flume

q - Ambient flow per unit length of diffuser

$\bar{q}$ - River width-averaged unit discharge

q_a - Average ambient discharge per unit width in cross-sectional region assigned to a single diffuser port

q_j - Diffuser discharge per unit length

$\bar{q}_j$ - River width-averaged unit effluent discharge

$\mathbb{R}$ - Reynolds number (various forms are used)

r - Radial distance from jet centerline

r_c - Value of r at which $\Delta T = \Delta T_c$

S - Minimum excess temperature dilution $(T_E - T_a)/(T - T_a)$

S_u - Slope of Eq. (6.10)

s - Distance measured along jet trajectory in Chapter 2. Dimensionless variance of radial temperature-rise distribution, $(\sigma_T/D)^2$, in Chapter 7.

T - Measured temperature

$\bar{T}$ - Computed mean temperature at a section

$\bar{T}_a$ - Average ambient river temperature

T_{aI} - Temperature of river water going into intake bay

T_a - Depth-averaged ambient flow temperature

T_E - Effluent temperature

$\bar{T}^d$ - Depth-averaged temperature

T_i - Temperature at the *ith* point (of a section)

T_I - Plant intake temperature

T_{max} - Maximum temperature T_i measured at a section

T_{mix} - Section temperature in a completely mixed flow

T_n - Dimensionless temperature rise $(T - T_a)/(T_E - T_a)$

ΔT - Temperature rise above the ambient, $T - T_a$; also called excess temperature due to jet

ΔT_c - Critical temperature rise, usually 5°F

ΔT_E - Temperature rise across condensers, $T_E - T_a$

ΔT_m - Mixed temperature rise, $\frac{Q_E(T_E - T_a)}{Q_R}$

ΔT_{max} - Temperature rise at centerline of jet

U_a - Ambient flow velocity

$\tilde{U}_5$ - Estimated average velocity with 5°F isotherm

U_j - Initial jet velocity

u - Local velocity

$\bar{u}^A_{\Delta T}$ - Excess temperature-weighted mean velocity in cross-sectional region assigned to a single diffuser port, defined by Eq. (7.2)

Δu - Excess velocity, $u - U_a$, due to jet

Δu_{max} - Excess velocity at centerline of jet

V - Volume flux ration $V = q_a/q_j$

W - River width

x - Distance measured downstream from discharge point

y - Vertical distance

y_M - Level of maximum transverse spreading

ZPA - Zone-of-passage with respect to area

ZPD - Zone-of-passage with respect to discharge

ZPRD - Zone-of-passage with respect to river discharge

Z_5 - Half width of measured 5°F isotherm

z - Transverse distance

α - Coefficient of entrainment in Chapter 2. Ratio of radial momentum-to-heat spreading in diffusing jet in Chapter 7, defined as σ_V/σ_T

θ - Local angle of jet centerline with horizontal

θ_o - Initial angle of inclination of jet (with respect to x-axis)

ν_a - Kinematic viscosity of ambient flow

ν_j - Kinematic viscosity of jet flow

ρ - Density of ambient flow

$\Delta\rho$ - Density difference (ambient - jet)

σ_T - Standard deviation of radial excess temperature distribution

σ_{yT} - Estimated standard deviation of the vertical excess temperature profile

σ_{zT} - Estimated standard deviation of the transverse excess temperature profile

σ_V - Standard deviation of radial excess velocity distribution

σ_{yV} - Estimated standard deviation of the vertical excess velocity profile

σ_{zV} - Estimated standard deviation of the transverse excess velocity profile

ABSTRACT

The performance of the multiple-port, submerged-jet diffuser pipe system for discharging heated condenser cooling water from the 1600 megawatt Quad Cities Nuclear Power Station into the Mississippi River was investigated in a comprehensive set of river surveys and thermal-hydraulic model studies. The objectives of the investigation were to: (1) verify that the system was operating in compliance with temperature standards established by Iowa and Illinois regulatory agencies that apply to the Mississippi River; (2) determine the river discharge below which plant load must be curtailed in order to remain in compliance with the temperature standards; (3) study the mixing characteristics of single and multiple submerged jets discharging into shallow, flowing receiving waters; and (4) compare model and prototype data for the initial mixing region close to the diffuser pipe.

The diffuser-pipe system was found to be in compliance with the applicable thermal standards by a comfortable margin during all of the river surveys. The results of the study indicate that with a minor modification in the distribution of the flow from the diffuser ports, satisfactory performance in the open-cycle mode can be achieved for river discharges as low as about 15,000 cfs.

The gross behavior of the jets in the initial mixing region was found to be in rough accordance with the behavior of a momentum jet discharging into a quiescent, infinite body of water. The momentum-jet type behavior began to break down when the confining

effects of the free surface and bottom boundaries came into play. Buoyancy effects only became evident farther downstream in cases where the momentum was largely diffused before complete mixing was achieved. For the most part, good agreement was obtained between prototype and model data. Based on the experimental results, dimensionless parameters can be used to classify the mixing zone downstream of the diffuser pipe into three regions; the individual-jet region, the transition region were the jets merged, and a two-dimensional region following merging of the jets.

Using generalized temperature- and velocity-distribution functions for the individual jet region, relationships were derived for predicting the zones-of-passage, with respect to both cross-sectional area and flow discharge, for the region of a channel assigned to a single diffuser port. Predicted, model, and prototype results, which were found to agree quite well, all indicate that the minimum zones-of-passage, within which the temperature rise does not exceed 5°F, occur about six port diameters downstream from the diffuser pipe.

CHAPTER I

INTRODUCTION

1.1 Waste Heat from Electrical Power Generation

Energy in the form of heat is a by-product of electrical power generation. Large-scale beneficial use of this energy is not foreseen in the near future; therefore, it is called waste heat. Conventional steam-electric generating stations operate at efficiencies of about 40 percent and nuclear stations at about 32 percent. This means that for each kW of electrical energy produced by a nuclear power station, roughly 2 kW of energy in the form of waste heat are produced. The ultimate heat sink for this waste heat is outer space. Various methods of transmitting the heat from the condenser cooling water in a plant to the atmosphere can be used. The methods can be divided into two groups: once-through cooling and closed-cycle cooling.

Once-through cooling systems draw the condenser cooling water from a water body, pass it through the condenser once, and return it to the water body. These water bodies include rivers, reservoirs, lakes, and coastal waters. The initial distribution of the heated water in the water body can be tailored to range from strong stratification to nearly complete mixing by using various discharge designs. Stratification is achieved by

discharging the heated water onto the surface of the ambient water at low velocity. The hot water tends to float on the surface in a thin layer; thus, the heat is more quickly dissipated to the atmosphere. Complete mixing can be approached by discharging the heated water as high-velocity submerged jets near the bottom of the water body. A large volume of ambient water is entrained into the heated jet. Therefore, a high degree of dilution is achieved within a short distance downstream from the jet discharge. Mixing somewhere between strong stratification and complete mixing can be achieved by discharging the hot water at a high velocity through a canal into the ambient water. Shearing force due to the high discharge velocity causes entrainment of ambient water. Such a discharge system would both dilute the hot water and dissipate the heat to the atmosphere at a reasonable rate.

Closed-cycle cooling systems are designed to transfer all of the waste heat load directly to the atmosphere. Examples of such systems are cooling towers, cooling ponds, and spray ponds. Cooling towers are of the following types: mechanical draft wet, natural draft wet, mechanical draft dry, natural draft dry, and combination wet and dry. The principal mode of heat transfer for wet cooling towers is evaporation, while sensible heat transfer is the principal mode for cooling towers. Although cooling towers discharge relatively small quantities of waste heat into water bodies, they consume more water than once-through systems. This

is due to water loss by evaporation and drift. Towers can also pose fogging and icing problems under certain climatological conditions. Evaporation and drift loss, as well as fog and ice problems, are avoided with dry towers; however, their use is limited in this country due to economic and technological considerations. Cooling ponds are bodies of water through which the condenser cooling water recirculates. Flow-through times of several days allow the heat to be dissipated to the atmosphere by radiation, convection, conduction, and evaporation. Spray ponds discharge the cooling water into the air in droplets, thereby increasing the evaporation rate.

Guidelines for the disposal of waste heat are determined by the Environmental Protection Agency (EPA), as directed by the 1972 amendments to the Federal Water Pollution Control Act. It appears that closed-cycle evaporative cooling processes will become mandatory for all plants by 1977 unless, as stated in the 1972 amendments, it can be demonstrated for specific cases that another type of cooling process is not ecologically damaging. Such exceptions are being dealt with by the EPA on a case-by-case basis. Many power companies are seeking this alternative because open-cycle cooling systems are more economical than closed-cycle systems. The present investigation is part of a large-scale biological and hydraulic study to determine if the Quad Cities diffuser-pipe cooling system has an adverse effect on the Mississippi River ecosystem.

1.2 Quad Cities Nuclear Power Station

The Quad Cities Nuclear Power Station produces electrical energy in two 800-MWe boiling water reactor units. The plant is located on the east bank of the Mississippi River about 3 miles north of Cordova, Illinois (Fig. 1.1). When the plant is operating at full capacity with a once-through heat rejection system, 2270 cubic feet per second (cfs) is withdrawn from the Mississippi River through the intake system, circulated through heat exchangers to remove waste heat from the condensers, and returned to the river through the discharge system at a temperature that is 23°F (12.8°C) higher than that of the ambient river water. When operating at partial capacity in the once-through mode, the effluent design discharge of 2270 cfs is usually maintained; therefore, the temperature rise decreases in proportion with the percent of full plant generating capacity.

The river at the plant site is approximately 2200 ft wide. The main river channel is on the west side and is approximately 800 ft wide and 25 ft deep. The remainder of the channel has an average depth of 8 ft. About 75 to 80 percent of the river flow passes through the main channel. The lowest daily flow and the 7-day low flow with a 10-year recurrence interval, for the period 1939 through 1968 (after construction of navigation dams), are about 10,900 cfs and 13,200 cfs, respectively.

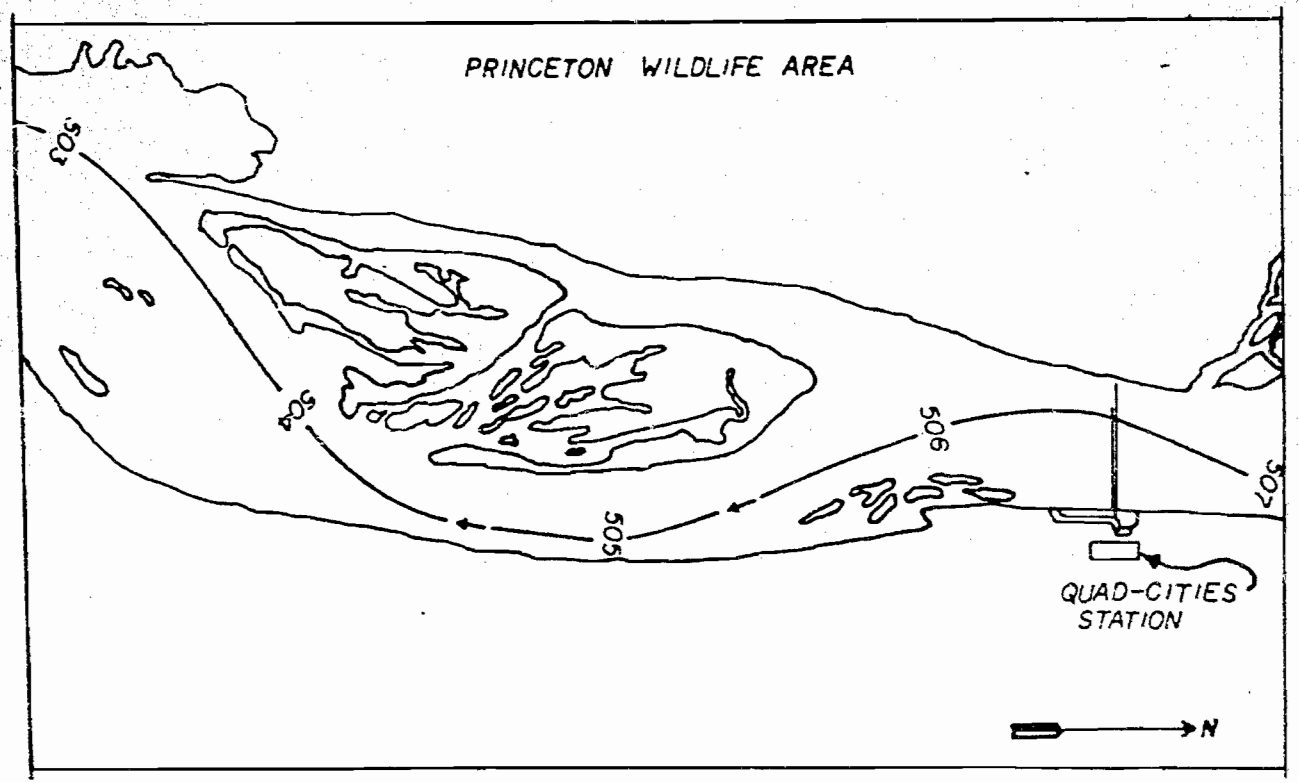

Fig. 1.1 Site of Quad Cities Nuclear Power Station.

The plant began producing electricity in April, 1972, and received full power licenses in December, 1972. A once-through system with a discharge canal terminating at the east bank of the river was originally proposed and was used as a temporary heat rejection system. Model studies conducted by the Iowa Institute of Hydraulic Research demonstrated that the system would not perform well enough to meet the thermal criteria of the regulatory agencies. As a result, a multiport diffuser-pipe discharge system that would thoroughly mix the heated cooling water with the ambient river water was adopted and put into operation in August, 1972.

The diffuser pipe system was designed to distribute the effluent discharge across the river more or less in proportion to the transverse distribution of the ambient river discharge. Essentially complete mixing was achieved within a short distance by discharging the effluent discharge as jets from a series of risers that were spaced along the length of two buried 16-ft diameter pipes located as shown in Fig. 1.2. Beginning at about 840 ft from the Illinois shore, ten 24-in. diameter risers, or ports, are spaced at intervals of 39.33 ft across the remainder of the shallow water region which extends 400 ft farther into the channel. Then across the deep-water region, which spans the next 780 ft, forty 36-in. diameter ports are spaced at intervals of 19.67 ft. Each port is inclined at an angle of 20° with the horizontal pointing in the downstream direction; and each port is

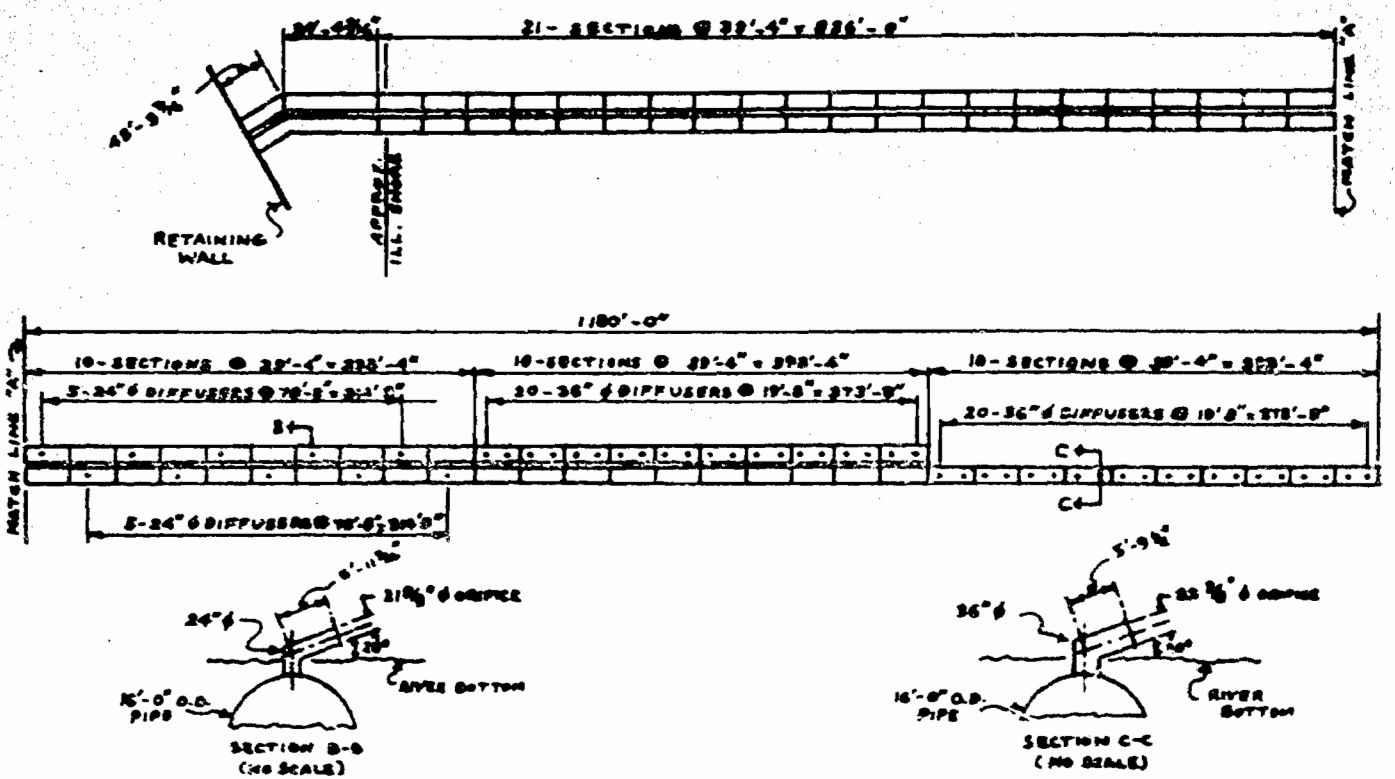

Fig. 1.2 Quad Cities multiport diffuser pipe.

equipped with a removable orifice plate at the discharge end. The orifice diameter is nine-tenths that of the port. The distribution of effluent discharge across the river can be modified as needed by replacing these orifice plates with ones of different sizes. This is called tuning the diffuser pipe. The jet velocities vary from 8.5 feet per second (fps) at the Illinois end to slightly more than 9 fps at the Iowa end. The purpose, layout, and design of the diffuser pipe system are described by Jain et al. (1971).

The station's operating permit specified that no more than 50 percent of the waste heat load could be discharged into the river as of May, 1974, and that by May, 1975, the plant had to go to a completely closed-cycle cooling system. Therefore, a closed-cycle spray canal system was constructed. During the initial operational period, beginning in May, 1974, the spray canal was used together with the short diffuser pipe to dissipate the waste heat. Three lift pumps drew approximately 1200 cfs from the discharge bay into the spray canal. The rest of the condenser cooling water flow was discharged through the short diffuser pipe. When operation of the plant in a completely closed-cycle mode was begun in 1975, spray canal performance was found to be unsatisfactory for summer conditions. Permission to operate the spray canal and diffuser pipe in the combined mode described above, for a limited period, was obtained. The final outcome is still uncertain.

1.3 Thermal Standards for Large Rivers in Iowa and Illinois

All discharge of waste heat from the Quad Cities Nuclear Power Station into the Mississippi River must comply with the thermal criteria for both Iowa and Illinois since the river borders both states. The regulatory agencies for the two states are the Iowa Water Quality Commission and the Illinois Pollution Control Board. The thermal criteria that apply to the Mississippi River, as compiled by Paily et al. (1975), are presented in Appendix A. The standards, as they apply to the Quad Cities Nuclear Power Station diffuser pipe, are discussed in this section.

The mixing zone as defined by the Iowa and Illinois regulatory agencies may not contain more than 25 percent of the cross-sectional area or volume of flow at any cross section, and temperature increases outside the mixing zone may not exceed 5°F. Therefore, for any cross section, no more than 25 percent of the cross-sectional area or volume of flow may contain water with temperature increases greater than 5°F. The portions of cross-sectional area and volume of flow not included in the mixing zone are called, respectively, the zone-of-passage with respect to area and the zone-of-passage with respect to discharge. Consequently, for the Mississippi River, both the zones-of-passage with respect to area and with respect to discharge must be equal to or greater than 75 percent. Temperature rises greater than 5°F are usually found only in regions close to the diffuser ports, so that each port has

its own mixing zone except when the river discharge is very low. Hence, the diffuser pipe system has 50 mixing zones, 1 for each port.

The Illinois regulations state, in addition, that no mixing zone shall exceed the area of a circle with a 600-ft radius (approximately 26 acres). At the Quad Cities plant site, if the mixing zone is assumed to span the entire river width which is about 2000 ft, this corresponds approximately to a zone extending from the diffuser pipes to a section 500 ft downstream.

1.4 Purpose and Scope of Study

The purpose of this study was to determine and analyze the performance of the Quad Cities Nuclear Power Station diffuser-pipe system and to predict effluent and river-flow conditions under which the system would fail to satisfy the thermal standards of the Iowa and Illinois regulatory agencies. In addition, laboratory and field studies were designed to provide a better understanding of the mixing characteristics of the individual-jet region of submerged multiport diffusers discharging into shallow, flowing receiving waters.

Two different types of surveys were performed to evaluate the performance of the diffuser pipe system with respect to the applicable thermal standards. Cross-sectional surveys, wherein the temperature distribution over the entire river cross section was measured, were performed at downstream distances of 500 ft or less to establish that the system was operating in compliance with the

26-acre mixing zone standard. Single-port surveys, wherein much more detailed measurements of temperature and velocity distributions in the higher temperature regions close to the diffuser pipe were obtained, were performed to evaluate the performance of the system with respect to the zone-of-passage standards.

Cross-sectional prototype surveys involved measuring the velocities and temperatures both upstream and downstream from the diffuser pipes in order to determine the effect of the effluent discharge on the velocity and temperature distributions in the river. Compliance with the 26-acre mixing zone limitation for this river site is guaranteed if maximum temperature increases at a cross section 500 ft downstream from the diffuser pipes are no more than 5°F. Consequently, most downstream cross-sectional measurements were taken at a section 500 ft downstream from the centerline of the two diffuser pipes.

Single-port prototype surveys involved measuring velocities and temperatures both upstream and downstream from a diffuser port in order to determine the 5°F temperature rise isotherms and, from these, the zones-of-passage. Seven surveys were made from November, 1973, to October, 1974. Each of the surveys consisted of detailed measurements at sections downstream from one diffuser port. A maximum of three downstream sections could be surveyed in one day. Usually, the lateral measurement span at each section was wide enough to also include the mixing zones of the adjacent ports.

Single-port, two-dimensional model studies were performed at the Iowa Institute of Hydraulic Research to enable zone-of-passage predictions to be made for flow conditions not observed in the single-port prototype studies. The ambient velocities in the flume were varied to correspond to river velocities in the diffuser-pipe section of the river for total river flows ranging from 13,200 to 50,000 cfs. Effluent jet velocities in the model correspond to a prototype jet velocity of 9 fps. Depths of flow in the flume correspond to river depths ranging from 9.25 ft to 26 ft. Different model set-ups were used for the large main-channel diffuser ports and the small shallow-water ports. Measurements were taken at increasing distances downstream from the effluent discharge section until the excess temperature distribution was essentially two-dimensional.

1.5 Characteristics of Multiport Diffusers

Submerged multiport diffusers are effective hydraulic structures for discharging wastewater into receiving waters when thorough mixing within limited mixing zones is required. A multiport diffuser consists of several discharge ports issuing from a large pipe located near the bottom of a water body. The high-velocity jets entrain surrounding ambient water, thus producing high dilution rates. Significantly higher rates of dilution are achieved when a multiport diffuser is used instead of a single, large submerged jet. Discussions of the internal hydraulics and

design of multiport diffusers is presented in Rawn, Bowerman, and Brooks (1960); Vigander, Elder, and Brooks (1970); Camp and Graber (1969, 1970); and Jain et al. (1971).

Power plants using diffuser-pipe heat rejection systems usually discharge the heated water in relatively shallow water. This results in very complex flow patterns due to the interaction of the buoyant jets with the surface and the bottom.

The basic component of multiport diffusers is the single submerged jet. Hence, familiarity with the behavior of single jets is essential to understanding the mixing characteristics of multiport diffusers. With this in mind, previous studies of single submerged jets and the effects of dynamic and geometric variables often encountered in multiport diffuser applications will be discussed in the next chapter. Previous studies on multiport diffusers will also be reviewed.

CHAPTER 2

PREVIOUS STUDIES OF SUBMERGED JETS

2.1 Single Jets

2.1.1. Momentum Jet

A momentum jet (simple jet) is formed when fluid is discharged, from a submerged outlet, into a fluid of the same density. Near the efflux section, steep velocity gradients exist between the jet and the surrounding fluid. The resulting high shearing stresses generate eddies at the border of the jet which, in turn, promote lateral mixing. The lateral mixing process extends outward, accelerating surrounding fluid, and inward, decelerating the fluid within the jet. Hence, the rate of flow and jet width continuously increase while velocities in the center of the jet continuously decrease. When the mixing process reaches the center of the jet, the flow is considered to be fully established. The region from the efflux section to the point where the jet flow becomes fully established is called the zone-of-flow establishment. The zones-of-flow establishment and fully established flow in a momentum jet are shown in Fig. 2.1.

The first comprehensive investigation of the momentum jet was presented by Albertson et al. (1950). For the case of a

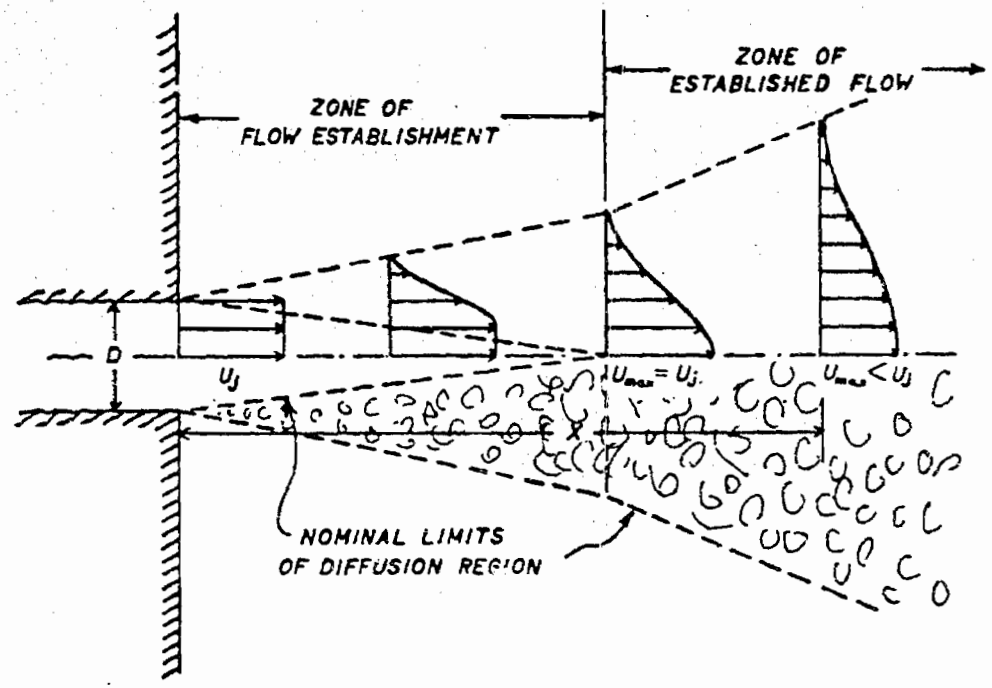

Fig. 2.1 Schematic representation of jet diffusion.
(From Albertson et al., 1950)

momentum jet discharging into a quiescent fluid, they showed that the nominal jet width varies linearly with distance of travel, x ($b \propto x$), and that the velocity profile follows a Gaussian distribution in the zone of established flow. The centerline velocity was found to be inversely proportional to x ($u \propto x^{-1}$). Since no external forces are applied to a momentum jet, momentum flux is constant at downstream sections and total jet discharge increases linearly with x. Albertson et al. determined that the length of the zone of flow establishment was approximately 6.2 nozzle diameters. They also determined the following relationship for the total jet discharge:

$$\frac{Q}{Q_0} = 0.32 \frac{x}{D} \qquad (2.1)$$

where

Q_0 = initial jet discharge

The relationship was confirmed by Ricou and Spalding (1961).

2.1.2. Buoyant Jet

A buoyant jet is generated by a continuous source of both momentum and buoyancy. If the jet discharges into denser surroundings, the buoyant force deflects the jet trajectory upward and causes the vertical momentum flux of the jet to increase with distance of travel. Buoyancy has little effect on the jet in the zone-of-flow establishment where momentum forces dominate the flow,

but becomes an increasingly important factor as jet velocities become small away from the efflux section.

Morton, Taylor, and Turner (1956) presented a theoretical analysis of the problem of a simple plume (no momentum flux) by applying an integral technique. Morton (1959) later used the approach to analyze the vertical buoyant jet. Fan (1967) extended Morton's integral technique to analyze an inclined round buoyant jet in a stagnant environment with linear density stratification. Morton's basic assumptions are:

1. The fluids are incompressible.
2. Flow is fully turbulent, implying no Reynolds-number dependence, and molecular diffusion is negligible compared to turbulent diffusion.
3. The effect of longitudinal diffusion is negligible compared to lateral diffusion.
4. The largest variation of fluid density through the flow field is small compared with the reference density. Hence, variation of density can be neglected when considering inertial terms but must be included in gravity terms.
5. Velocity profiles are similar in consecutive transverse sections of the jet in the zone of established flow. Morton et al. also assumed similar profiles for buoyancy.

In addition, Morton (1959) assumed that the rate of entrainment at the edge of the plume is proportional to some characteristic velocity u at that height.

$$\frac{dQ}{ds} = 2\pi\alpha ub \tag{2.2}$$

where

$\frac{dQ}{ds}$ = rate of change of volume flux

b = local characteristic length

α = entrainment coefficient assumed to be constant in the analysis

s = distance along jet trajectory

The problem was solved by applying the basic conservation equations of volume flux, momentum, and density deficiency. The three equations were solved for u, ρ, and b; characteristic jet velocity, density, and length.

Abraham (1963) investigated slot- and round-buoyant jets in stagnant, unstratified, ambient environment for different vertical and horizontal discharge angles. He applied a jet-spreading concept rather than the entrainment concept used by Morton for closure of the system of equations. Chan and Kennedy (1972) obtained a closed-form analytical solution of the jet properties, based on special assumptions of entrainment properties.

2.1.3. Effect of Crossflow

A round jet discharging into a crossflow produces a three-dimensional flow field. The jet is deflected in the downstream direction by a pressure force acting on the jet and by entrainment into the jet of fluid particles from the crossflow. At the upstream side of the jet, the crossflow is retarded and at the downstream side, a wake region forms resulting in a pressure force acting on the jet. Vortices develop in the wake region due to shearing force

between the crossflow and the edge of the jet. These vortices, in turn, generate smaller vortices in the jet. As a result, velocity and temperature profiles within the jet are horseshoe-shaped as shown in Fig. 2.2.

Fan (1967) made an extensive analytic and experimental study of a round-buoyant jet in a uniform cross stream of homogeneous density. He applied the integral technique of Morton et al. Additional assumptions adopted by Fan for the analysis are:

1. The entrainment relationship is represented by

$$\frac{dQ}{ds} = 2\pi\alpha b \left|\bar{U}_j - \bar{U}_a\right| \tag{2.3}$$

where

s = distance along the trajectory of the jet centerline

$\left|\bar{U}_j - \bar{U}_a\right|$ = magnitude of the vector difference of the two velocities $\bar{U}_j$ and $\bar{U}_a$

The variables $\bar{U}_j$ and $\bar{U}_a$ are defined by the following equations:

$$\bar{U}_j = \bar{i}\left(U_a \cos\theta + u\right) \tag{2.4}$$

$$\bar{U}_a = i\left(U_a \cos\theta\right) + \bar{j}\left(U_a \sin\theta\right) \tag{2.5}$$

where

$\bar{i}$ = a vector in the direction tangent to the jet axis

$\bar{j}$ = a vector perpendicular to the jet axis

α = a constant entrainment coefficient

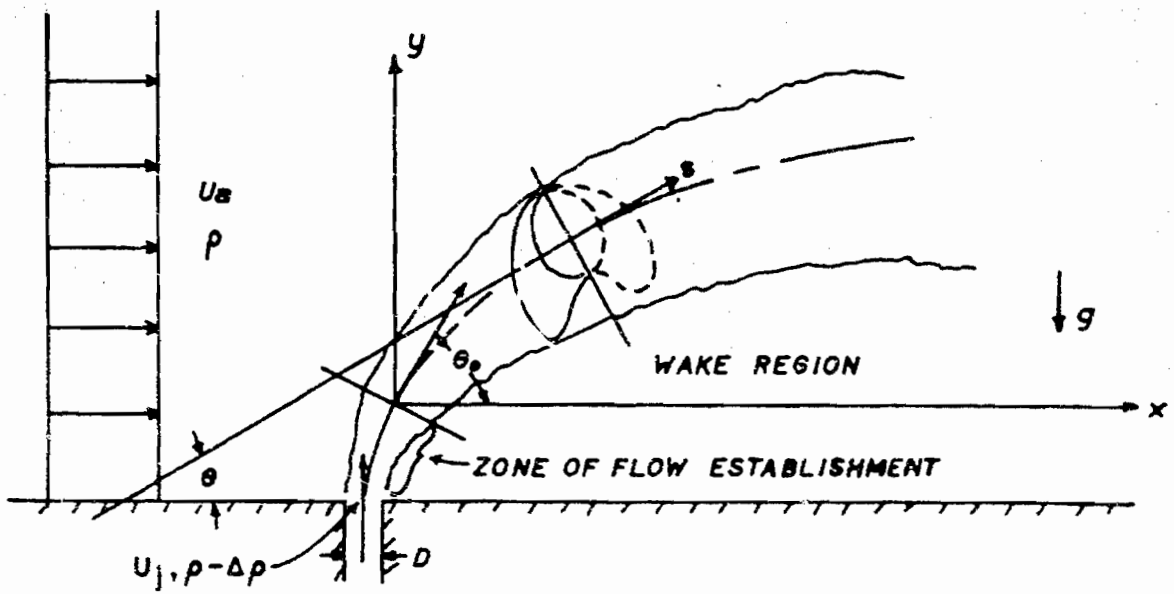

Fig. 2.2 Schematic diagram of a round jet in a uniform cross stream. (From Fan, 1967)

2. Profiles of the excess velocity above the component of the ambient velocity are assumed to be similar and Gaussian.

3. Buoyancy profiles are Gaussian.

4. Concentration profiles of a tracer are Gaussian.

5. The effect of the presence of the pressure field can be lumped into a gross drag term proportional to the square of the velocity component of the oncoming stream normal to the jet axis. The drag coefficient is assumed to be constant.

Chan and Kennedy (1972) analyzed the problem of a buoyant jet in a cross flow using an integral type solution with special entrainment coefficients. Experiments were also conducted for various jet velocity-to-crossflow velocity ratios to determine drag forces and jet trajectories, widths, and centerline velocities. Air was used as the fluid for all experiments.

2.1.4. Free-Surface and Bottom Effects

The free surface restricts the upward motion of the buoyant jet. The jet spreads laterally in a layer at the water surface and causes a slight surface rise that varies with the magnitude of vertical jet momentum at the surface. Abraham (1963) provided experimental results from which the thickness of the jet layer can be estimated. Entrainment into the jet decreases after it spreads at the surface. Analysis of entrainment into the surface layer was made by Jirka and Harleman (1973) for the two-dimensional (slot jet) case and by Lee, Jirka, and Harleman (1974) for the axisymmetric case. These studies were for stagnant receiving water.

The bottom usually reduces local entrainment into the jet. However, an experimental study by Sharp and Chung-su-Wang (1975) of a horizontal buoyant jet discharging at the bottom of a quiescent receiving environment showed surface dilutions ranging from 200 to 500 percent greater than for horizontal buoyant jets not experiencing bottom effects. They attributed this to increased turbulence and momentum exchange at the free interface and to the extension of the length of the trajectory caused by the jet's tendency to cling to the bottom.

The methods of jet analysis previously discussed apply only for deep receiving water in which free-surface and bottom effects can be neglected. In constricted shallow receiving environments, the pressure field cannot be considered hydrostatic. The velocity of fluid being entrained into the jet in regions of restricted flow increases; therefore, local pressures decrease. These low pressure regions can cause the jet to attach to boundaries as in the studies of Sharp and Chung-su-Wang mentioned previously. The jet flow field in shallow receiving environments is very complicated since assumptions of hydrostatic pressure distribution and similarity of velocity profiles are not valid. Therefore, the analytical models of Morton et al., Fan, Abraham, and Chan and Kennedy are not directly applicable to submerged buoyant jets in shallow receiving waters.

2.2 Multiport Diffusers

Multiport diffusers have been used for discharging sewage into the ocean for many years. More recently they have also been used for discharging condenser cooling water from electrical generating stations into fresh water bodies and coastal waters. Although multiport diffusers for these two cases are, in principle, the same, the receiving-water and density-difference characteristics are different. Power plants usually discharge into shallow water and the relative density difference between the receiving water and the buoyant jet is typically about 0.003. Sewage outfalls typically discharge in deep water with a relative density difference of about 0.025. Therefore, for power plant multiport diffusers, the receiving water is confined and the buoyancy forces are approximately an order of magnitude smaller than for sewage diffusers.

2.2.1. Round Jet Interference

The discharge from a multiport diffuser initially behaves like a row of single jets that spread with length of travel. At some distance downstream the single jets merge and eventually resemble a two-dimensional slot jet. The region where the flow is transformed from buoyant round-jet flow to slot-jet flow is called the transition zone. This process is shown in Fig. 2.3. Self-similarity profiles are not valid in the transition zone; consequently, the mathematical analysis of single jets, as discussed in

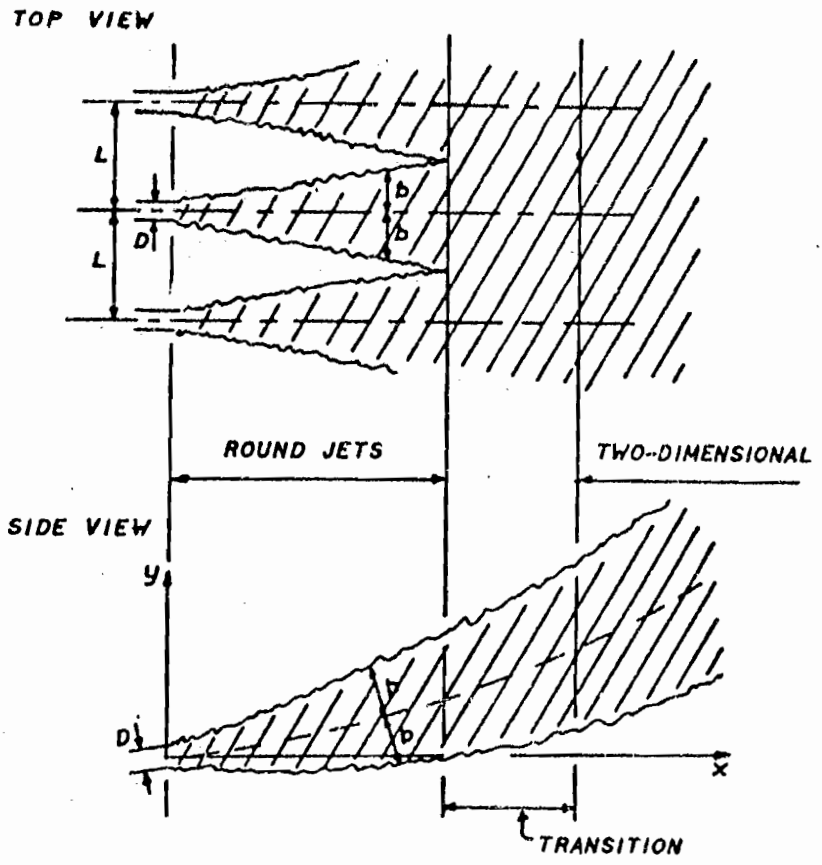

Fig. 2.3 Jet interference for a submerged multiport diffuser. (From Jirka and Harleman, 1973)

this chapter, cannot be extended to describe flow in the transition zone of multiport diffusers. A simplified analysis of the transition zone has been used by Abraham (1973), Cederwall (1971), and Jirka and Harleman (1973). The analysis is based on the "equivalent slot diffuser" concept which is discussed in the next section.

2.2.2. Equivalent Slot Diffuser Concept

The discharge from a multiport diffuser can be analyzed by assuming the flow to be from a slot diffuser having the same momentum flux and discharge per unit diffuser length. A multiport diffuser with discharge port diameter D and port spacing L is represented by an "equivalent slot diffuser" with a width B by the following relationship:

$$B = \frac{\pi D^2}{4L} \tag{2.6}$$

The question of when round jet interaction begins was studied by Koh and Fan (1970). They investigated two criteria for determining the point where merging begins. The criteria are:

1. The nominal half-width b of the jet equals half of the port-spacing length.

$$b = \frac{L}{2} \tag{2.7}$$

2. The entrainment of a round jet equals that of an equivalent slot jet.

Koh and Fan, as well as Jirka and Harleman (1973), found that adoption of either criterion results in essentially the same prediction for the initial point of jet interaction.

Jirka and Harleman discuss merging above the diffuser for nozzles in alternating directions.

2.2.3. Two-Dimensional Channel Model

A multiport diffuser discharging into a large stagnant water body induces a three-dimensional flow field as shown in Fig. 2.4. In the central portion of the flow field the flow is predominantly two-dimensional. Jirka and Harleman analyzed this portion of the flow field by introducing a two-dimensional channel model. They studied jet stability and dilution as well as the extension of two-dimensional results to the three-dimensional case. The "equivalent slot diffuser" concept was used for both the theoretical and the experimental analysis.

When a multiport diffuser is used in a river, the jet flow is affected by the ambient flow. If the diffuser pipe extends across the river width, the flow is laterally confined and the diffuser usually cannot induce additional flow. However, if the ambient discharge per unit width is too small to supply the round jets with sufficient entrainment water, the diffuser will induce a three-dimensional flow field that modifies the ambient discharge distribution in the vicinity of the diffuser ports. The discharge distribution across the river for a laterally confined installation

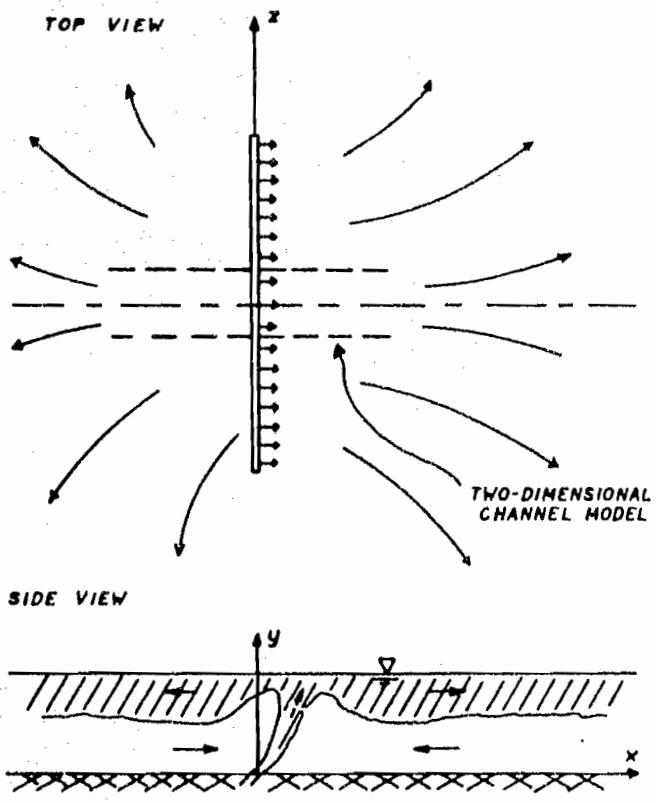

Fig. 2.4 Three-dimensional flow field for a submerged diffuser, two-dimensional behavior in center portion (stable flow away zone). (From Jirka et al., 1973)

will not be greatly changed by the diffuser discharge; therefore, the two-dimensional channel model can be applied reasonably well to the entire length of the diffuser. Studies of this type have been made by Cederwall (1971); Jirka and Harleman (1973); Argue and Sayre (1973); Cardenas (1974); and others.

2.2.4. Three-Dimensional Models

Many three-dimensional basin models have been used to predict multiport diffuser performance in rivers, lakes, ponds, and coastal waters. A few of these are Harleman, Hall, and Curtis (1968); Jain, Sayre, Akyeampong, McDougall, and Kennedy (1971); and Harleman, Jirka, and Stolzenbach (1971). Three-dimensional basin models have often been distorted in the vertical. Distorted models are less conservative in predicting near-field dilution and do not truly represent three-dimensional flow fluids.

CHAPTER 3

TWO-DIMENSIONAL CHANNEL MODEL OF THE QUAD CITIES MULTIPORT DIFFUSER

3.1 Objectives of the Study

The general objectives of the model study were discussed in Chapter 1 and the specific objectives are discussed here. The study includes river flow conditions encountered in the prototype for total Mississippi River discharges ranging from 13,500 to 50,000 cfs. Therefore, velocities and depths across that part of the channel occupied by the diffuser pipe for a range of discharges are modeled. The discharge distributions across the river for different discharges and bottom profiles were measured by staff of the Iowa Institute of Hydraulic Research. These field surveys will be discussed in Chapters 4 and 5. The objectives of the model study were to determine the following over the range of conditions indicated above:

1. Agreement between single-port prototype and single-port model results for the same flow conditions.
2. 5°F Isotherms with respect to area.
3. 5°F Isotherms with respect to discharge.
4. Jet trajectory.
5. Jet dilutions.

6. Jet spreading.

7. Transition from three-dimensional single buoyant jet flow to two-dimensional slot jet flow.

Dimensionless isotherms are based on dimensionless temperature rise, T_n, as defined by

$$T_n = \frac{T - T_a}{T_E - T_a} \tag{3.1}$$

where

T = measured temperature of water partially mixed with effluent discharge

T_a = ambient water temperature

T_E = discharge water temperature

The dimensionless isotherm of particular interest corresponds to a temperature rise of 5°F in the prototype. For example, if the ambient river temperature were 72°F, which is a typical ambient river temperature for July and August, and the effluent discharge temperature were 95°F, the dimensionless temperature for this isotherm would be

$$T_n = \frac{5}{95 - 72} = 0.217 \tag{3.2}$$

The denominator represents the 23°F temperature rise of the cooling water as it passes across the condensers of the Quad Cities reactor when the plant is at full generating capacity.

3.2 Characteristics of the Quad Cities Multiport Diffuser

The Quad Cities multiport diffuser was described in Chapter 1. Here additional characteristics of the diffuser that should be considered in the model study are discussed.

The Quad Cities diffuser has main-channel ports with a 2.7-ft orifice diameter in river water from about 16 to 25 ft deep, and shallow-water ports with 1.8-ft orifice diameter in water from about 7 to 22 ft deep. Therefore, the receiving water is nearly always less than 10 jet diameters deep, which is quite shallow for multiport diffuser installations. Argue and Sayre (1973) reasoned that for low river flows the individual buoyant jets for the Quad Cities diffuser do not merge before they reach the surface; hence, surface distortion predominates over jet interaction. Their analysis assumed that jet deflection due to buoyancy and ambient crossflow cancel one another so that the jet trajectory could be approximated by a straight line, at least until the jet approached the surface. In the present study, both high and low ambient velocities are modeled; therefore, cases of both surface distortion predominating over jet interaction and vice versa are investigated.

Adoption of the "equivalent slot diffuser" concept, as used by Jirka and Harleman (1973), for constructing a two-dimensional physical model of the Quad Cities multiport diffuser are not applicable for this study. Since the objectives stated in the previous section all pertain to the buoyant jet region, and the transition

zone and jet surface distortion may occur before jet interaction, a two-dimensional "sectional model" with individual discharge ports is required. The experimental setup is described in Chapter 4.

The Quad Cities multiport diffuser is laterally confined since it extends nearly across the width of the main channel of the river. Therefore, a two-dimensional "sectional model" can be applied except perhaps near the ends of the diffuser pipe.

3.3 Modeling Considerations

Single-port models of submerged round buoyant jet must be geometrically undistorted to correctly represent jet mixing. This means that geometric scaling factors between prototype and model must be equal for all coordinates. In this study, a three-port sectional model with a 1:29.5 length ratio was used for the main-channel ports and a single-port sectional model with a 1:19.7 length ratio was used for the shallow-water ports.

The parameters chosen to describe the flow in these studies were:

$$F_j = u_j / \left(g \frac{\Delta\rho}{\rho} D \right)^{\frac{1}{2}} = \text{jet densimetric Froude number} \qquad (3.3)$$

$$k = U_j / U_a = \text{velocity ratio} \qquad (3.4)$$

$$(H - h)/D = \text{relative submergence} \qquad (3.5)$$

where the symbols are shown in Fig. 3.1. Parameters such as vertical discharge angle, horizontal nozzle orientation, and diffuser pipe alignment with crossflow direction were constant for all experiments. Jet and ambient Reynolds numbers should be high enough to ensure turbulent flow. This requirement was satisfied by keeping

$$R_a \geq 600 \tag{3.6}$$

$$R_j \geq 2500 \tag{3.7}$$

When ambient discharge per unit width, $U_a H$, is small, the jets entrain most of the ambient flow and the following set of parameters may be more appropriate:

$$F_j = U_j / \left(g \frac{\Delta\rho}{\rho} D \right)^{\frac{1}{2}} = \text{jet densimetric Froude number} \tag{3.8}$$

$$V = U_a H / U_j B = \text{volume flux ratio} \tag{3.9}$$

$$H/D = \text{relative depth} \tag{3.10}$$

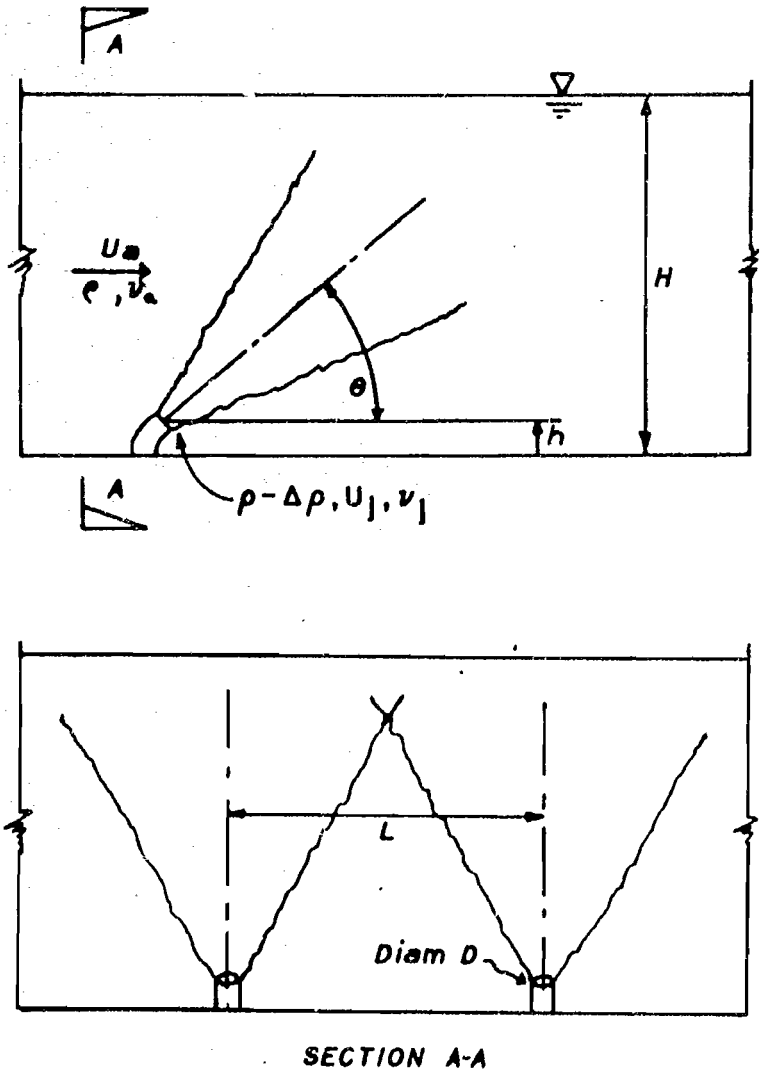

Fig. 3.1 Round jets in a flowing environment—terms defined.

CHAPTER 4

EXPERIMENTAL EQUIPMENT AND PROCEDURES

4.1 Prototype Studies

4.1.1. Temperature and Velocity Measuring Equipment

Temperatures were measured with a system designed by the Iowa Institute of Hydraulic Research electronic staff especially for reliable and accurate measurement of short-term average temperatures in the field. The system has a measurement range of -5°C to 45°C and digitally displays average temperature to the nearest 0.01°C. The system consists of a Model 710 Yellow Springs Instrument Company thermistor probe, an IIHR Portable Linear Thermistor Temperature Meter, and a Hewlett-Packard 5302-A Universal Counter. Unique features of the system are its linearity, stability, and meter-protection circuit. The linearity results from using a Yellow Springs Instrument Company thermistor probe and resistor composite, which together form two legs of a Wheatstone bridge; the other two legs are precision resistors. The thermistor probe has a linearity deviation of +0.065°C and a 3.7-sec time constant. Stability of the instrument is due to the low voltage-drift characteristic of the bridge amplifier. This low voltage-drift characteristic is achieved by using chopper operational amplifiers.

The meter-protection circuit protects the direct display meter from excessive current by supplying the meter current from a differential source. The reason for this is to preserve the 0.1°C resolution for the complete measurement range of -5°C to 45°C. The Portable Linear Thermistor Temperature Meter is powered by two Ni-Cd batteries and is equipped with battery-condition meters.

The system is ideal for measuring average temperature in mixing zones since temperature fluctuations can be observed on the direct meter display while they are being time-averaged by the counter. This enables the user to obtain several sequential 10-sec averages when significant fluctuations are indicated by the meter. Additional information on the IIHR Portable Linear-Thermistor Temperature Meter is given by Glover (1973).

Velocities were measured with an Ott Universal current meter, No. 19090 mounted about 6 in. above the thermistor probe. The meter responds to velocities as low as 3 cm/sec. The averaging period was usually 30 sec.

4.1.2. Boat and Positioning Equipment

Measurements were taken from an 18-ft Jon-boat equipped with a 25-horsepower outboard motor and a canvas top for winter surveys. The thermistor probe and velocity meter were mounted to a weighted-cable and sounding-reel assembly that could measure water depth to the nearest 0.1 ft. The cable transmitted velocity meter signals to a "beeper" on the boat. For single-port surveys,

the sounding reel was attached to a boat seat. From the sounding reel, the cable passed through a system of pulleys and a carriage on the bow of the boat. The carriage was attached to a 10-ft section of aluminum I-beam that ran perpendicular to the longitudinal axis of the boat. This system is shown in Fig. 4.1. Since the carriage could be positioned along the length of the I-beam from inside the boat, transverse measurement locations could be varied ± 5 ft from the center of the beam without repositioning the boat or climbing out onto the bow. For cross-sectional surveys, the sounding reel was attached to a boom that was mounted near the middle of the boat. The end of the boom extended over the water, about 3 ft from the right side of the boat. The weighted cable, which held the thermistor probe and current meter, passed from the sounding reel and over a pulley on the end of the boom.

Transverse boat location was measured with a Hewlett-Packard 3800-B Electronic Distance Meter. A pair of Motorola FM radios provided communication between boat and shore.

4.1.3. Experimental Procedure

4.1.3.1. Single-Port Surveys

Upstream ambient river temperatures and velocities were measured at two verticals 100 ft upstream from the centerline between the two diffuser pipes at the beginning and end of each day for the single-port surveys. The verticals were approximately 60 ft apart. Downstream cross sections were marked with survey stakes

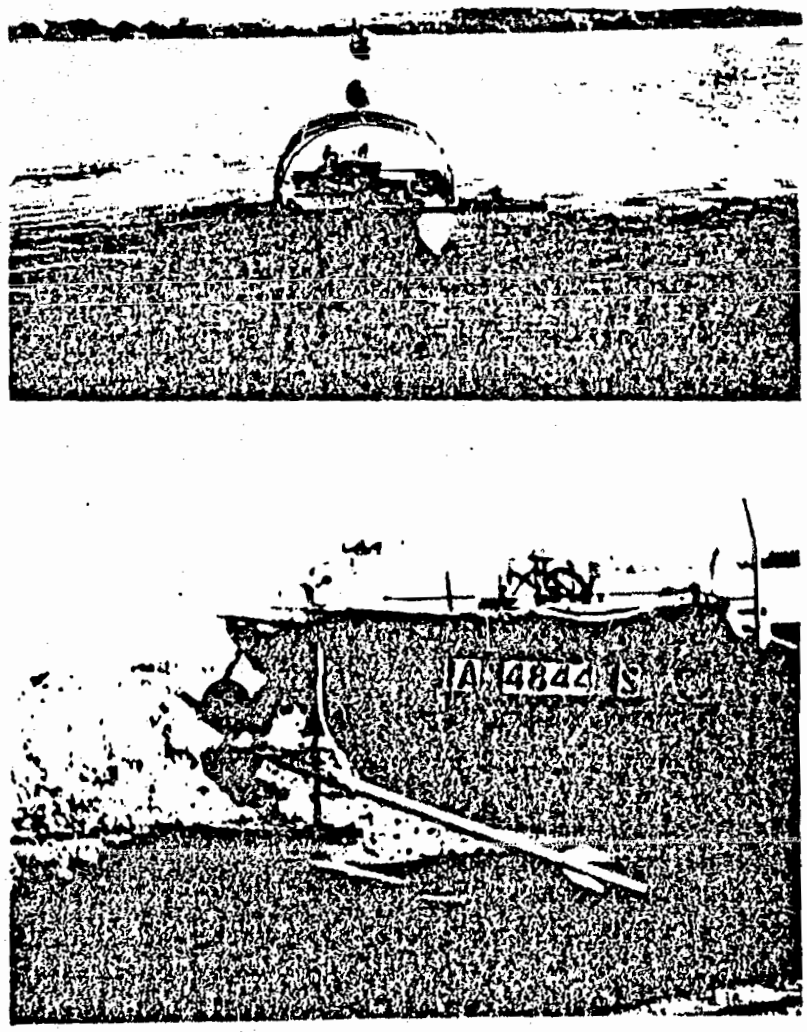

Fig. 4.1 Boat and measuring equipment.

and targets on both sides of the river. The boat operator was directed to the desired longitudinal location by a man on shore, who was positioned at one end of the corresponding cross section. The transverse location of the boat was then measured with the Hewlett-Packard distance meter from a survey stake at one end of the cross section. To ensure that the boat remained stationary during the velocity and temperature measurements, three anchors were used and distance-meter readings were taken every 10 minutes throughout the survey.

Temperatures and velocities were measured at several points in the vertical and at several verticals across each downstream cross section. More measurements were made in the higher-temperature zones. Usually, enough verticals were measured at the downstream cross sections so that the influence of three adjacent ports was observed.

4.1.3.2. Cross-Sectional Surveys

Temperature and velocity measurements were taken at several verticals in a cross section upstream from the diffuser pipes both at the beginning and at the end of each cross-sectional survey. The upstream cross section was located 1000 ft upstream from the centerline between the two diffuser pipes for the first six surveys and 200 ft upstream for all subsequent surveys. Most downstream measurements were made at a cross section 500 ft downstream from the centerline between the two diffuser pipes;

however, a few surveys were made at cross sections 150 and 300 ft downstream. Temperatures and velocities were measured at several verticals across each downstream cross section and at from three to six depths at each vertical.

The method of positioning the boat was the same as described for the single-port surveys. Only one anchor was used to hold the boat for the cross-sectional measurements.

4.2 Model Study

4.2.1. Experimental Equipment

4.2.1.1. Flume and Hot Water Supply

The single-port model experiments were performed in a glass-walled tilting flume 30-ft long, 2-ft wide and 1.5-ft deep, with a slope of 0.0002. The flume is on the first floor of the Iowa Institute of Hydraulic Research and its water supply comes from a constant-head tank on the third floor of the Institute (Fig. 4.2). The flow was regulated by valves and calibrated orifice meters located in parallel 4-in. and 6-in. pipes. A 1-in. orifice was used to measure flow in the smaller pipe and either a 2-in. or a 5-in. orifice was used in the larger pipe. The flow depth in the flume was controlled with an adjustable tailgate.

Heated water was discharged into the flume through round diffuser ports rising from the bottom of the flume. The hot water was supplied from five 75,000-BTU/hr natural-gas water heaters

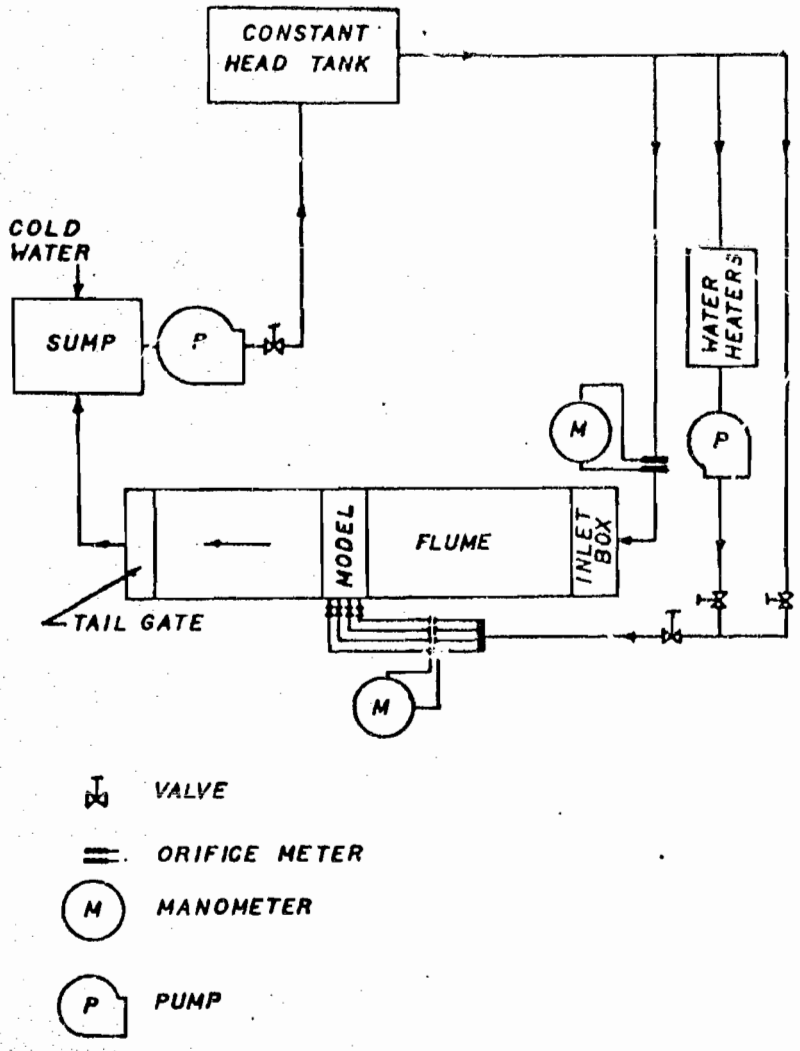

Fig. 4.2 Schematic layout of cold and hot water supply systems.

connected in parallel which drew water from the constant-head tank. The temperature of the heated water discharged into the flume was controlled by mixing cold water from the constant-head tank with hot water from the heaters at a T-joint. Each of the three branches of the T-joint had valves and the downstream branch was equipped with a thermometer so that the mixed water temperature could be monitored and adjusted accordingly with the valves in the hot and cold water lines. The mixed water flowed from the T-joint to a manifold from which it was discharged through insulated pipes that led through the bottom of the flume test section to the diffuser ports. Each of these pipes was equipped with a valve and an orifice for regulating the discharge through the ports. A schematic diagram of the flume and hot-water supply is shown in Fig. 4.3.

The discharge ports were made from brass pipe of 1.22 in. internal diameter with 1.10-in. diameter orifices attached to the discharge ends. These ports were scaled from the prototype ports which have removable orifices. A plan view of the one- and three-port experimental setups as well as an elevation view of a port are shown in Fig. 4.4. Notice that the initial jet centerline is 0.3 in. higher for the one-pipe layout.

4.2.1.2. Temperature Measuring Equipment

Temperatures were measured by 14 YSI thermistor probes. Each thermistor was incorporated as one leg of a Wheatstone bridge with a bridge output voltage of ± 10 mv. Each bridge was supplied

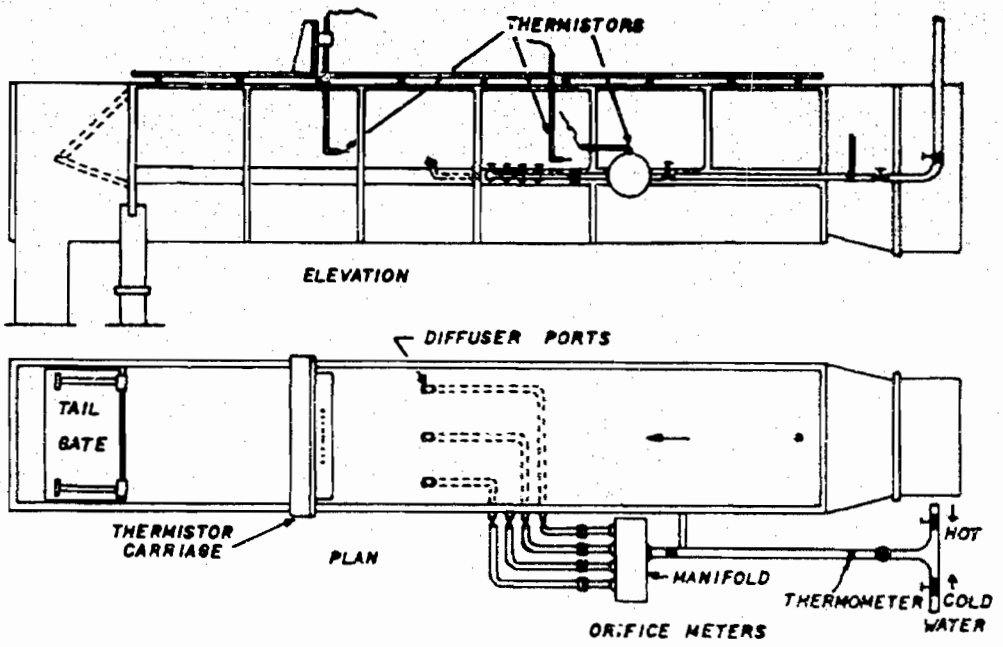

Fig. 4.3 Schematic diagram of flume (not to scale).

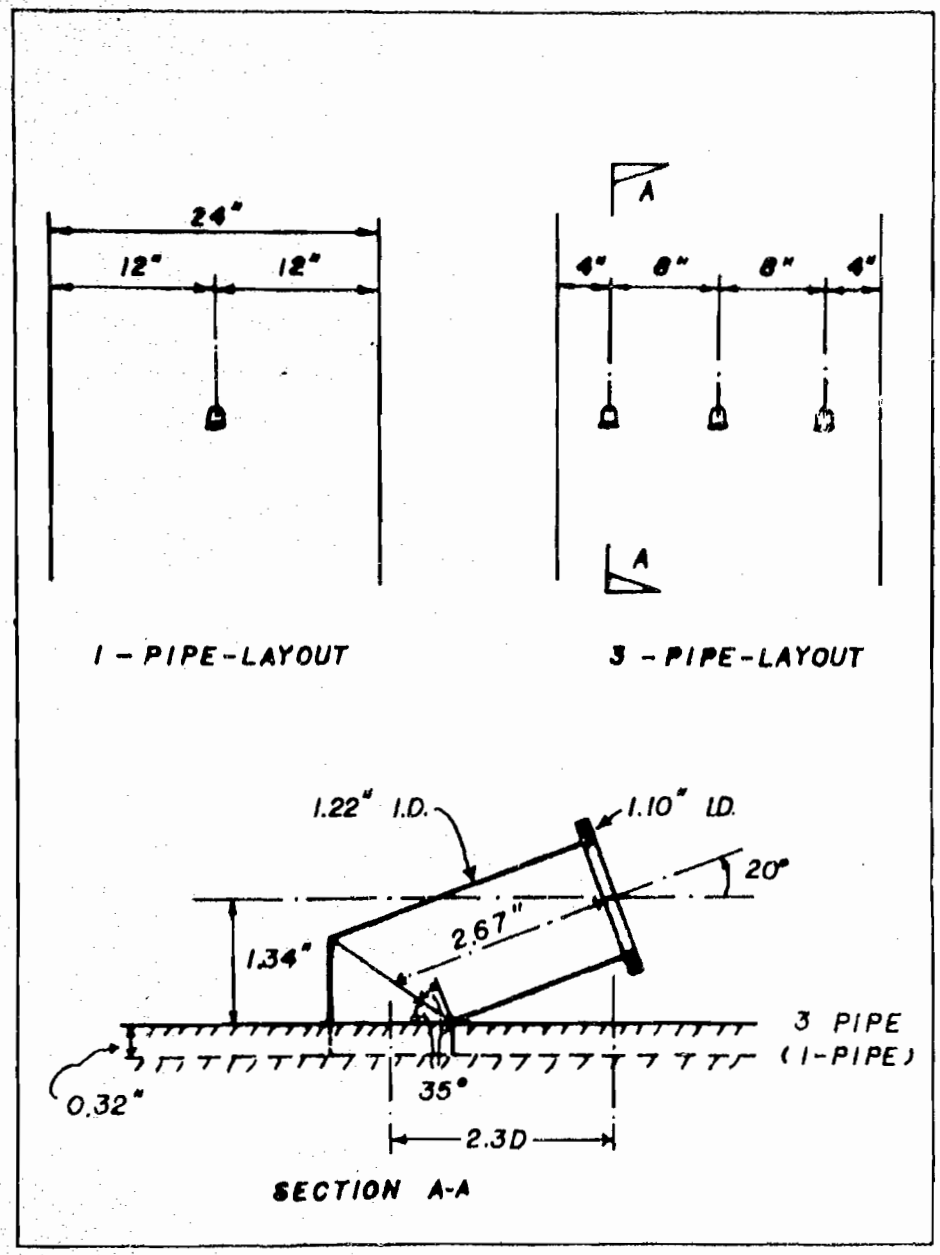

Fig. 4.4 Discharge ports.

through a 100,000 ohm resistor connected to a common 5-volt power supply, and the outputs were fed to the Institute's IBM 1801 Data Acquisition System. The resolution of the system was about 0.02°F.

The temperatures downstream from the ports were measured by 11 thermistor probes mounted on a rack that could be moved vertically which, in turn, was mounted to a carriage that could be moved along the length of the flume. The upstream ambient temperature was measured by one thermistor located in the middle of the channel a few feet upstream from the ports. The effluent temperature was measured by one thermistor installed in the heated-water manifold. An additional thermistor was used as a backup for any of the other thermistors that might malfunction and as a "rover" to take measurements at locations other than the primary upstream or downstream points. A fifteenth channel had a constant resistor that provided a check for the complete system.

All 14 thermistors were calibrated in a closed-cycle, circulating, calibration system. The system was well-insulated and equipped with a heater to heat the water, a variable-speed electric pump to circulate the water and a small diffuser pipe to discharge and mix the water in a calibration chamber. A precision thermometer with a resolution of 0.02°F was located along with the thermistor probes in the insulated calibration chamber. The thermistors were calibrated at approximately 1°F intervals over a range of 68 to 109°F. Thermistor voltage readings were taken over a 60-sec

averaging period during which time the temperature was measured and averaged with the precision thermometer. A second-degree polynomial calibration curve of temperature vs. voltage was then computed for each thermistor using a least-squares fitting program. Since the fit was good only for temperature increments of 15°F or smaller, maximum calibration ranges were limited to 15°F for each thermistor. For example, if the ambient water temperature in the flume was 72°F, the calibration curves for the upstream and downstream probes were computed from calibration data in the 72 to 87°F range. The calibration curve for the heated-water thermistor was computed from calibration data in a higher temperature range which depended on the ambient temperature in the flume as well as on the temperature rise called for in a specific experiment. The coefficients of the calibration curves for the thermistors were computed on the IBM computer and were stored on disk for subsequent use in experimental runs.

4.2.1.3. Velocity Measuring Equipment

Velocities in the flume were measured using a dual pressure-transducer system which is capable of making precision measurements for velocities down to about 0.1 fps. The system used a 1/16 in. outside diameter Prandtl-type Pitot tube with the dynamic and static pressures transmitted to two Model PM5-TC, Statham pressure transducers, both with maximum ranges of ± 0.15 psi. The outputs of the two transducers are both amplified by two noninverting chopper

amplifiers and fed into a difference amplifier. The output of the difference amplifier is converted to frequency by a voltage-to-frequency converter and displayed on an electronic counter. The sensitivities of the two transducers were equalized by the difference amplifier, thus ensuring a zero output when both transducers are subject to the same pressure. This sensitivity balancing reduces measurement errors due to temperature fluctuations and vibrations experienced by the transducers. A block diagram of the system is shown in Fig. 4.5.

The system was calibrated in a special calibration tank. The tank consisted of an enclosed head tank from which the water issued through a flow nozzle patterned after an ISA (Instrument Society of America) flow nozzle, like the one shown by Streeter 1975, Fig. 8.16, p. 469). Nozzles of 1-in. and 2-in. inside diameters were used in the calibration. Water flow from the Institute's constant head tank into the calibration system's enclosed constant head tank was varied with an intake valve in a 1-in. diameter pipe. Discharge through the system was measured by weighing, using a 5-gal. bucket, a scale, and a stopwatch. The Pitot tube was placed in the center of the jet from the flow nozzle. Calibration results are shown in Fig. 4.6.

4.2.2. Experimental Procedure

4.2.2.1. Planning of Experiments

Model verification of single-port prototype performance was based on ambient and jet densimetric Froude number similarity

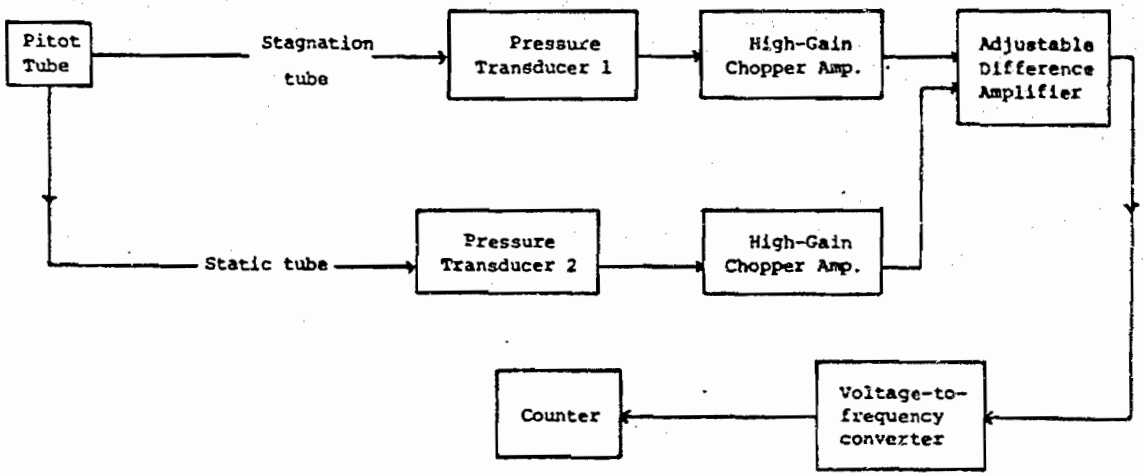

Fig. 4.5 Block diagram for dual pressure-transducer velocity measuring system.

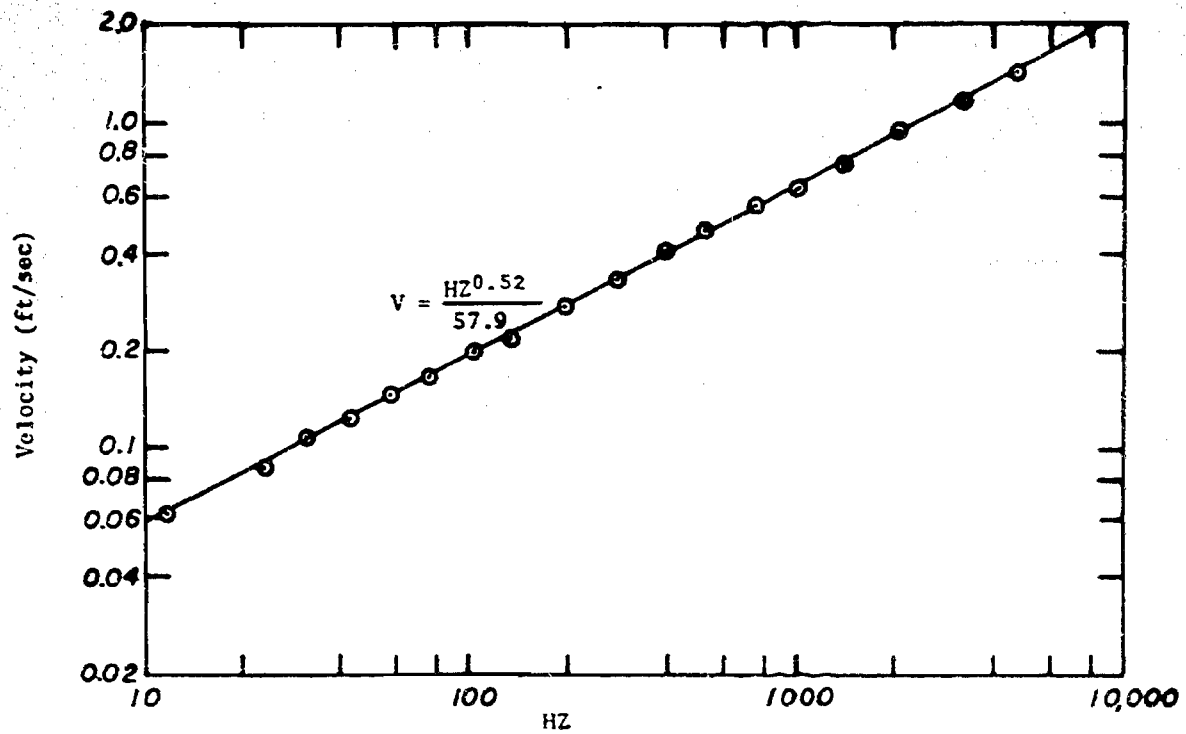

Fig. 4.6 Calibration curve for dual pressure—transducer velocity measuring system.

as discussed in Chapter 3. The principal dimensionless modeling parameters were the relative depth, H/D; the velocity ratio, U_j/U_a; and the relative density deficit $(\rho - \rho_a)/\rho_a$. In the model studies, temperatures and velocities were measured at distances downstream from the ports corresponding to the prototype measurement locations.

Model runs were designed to enable predictions of temperature and velocity fields downstream from the diffuser ports to be made for ranges of typical river flow and plant operation conditions not covered in the prototype experiments. These runs were also based on ambient and jet densimetric Froude number similarity. The initial jet velocity and the normalized density deficit at the efflux section were constant for most of the runs. The initial jet velocity in the model corresponded to the average design jet velocity of 9 fps. The normalized density difference was held at 0.003686, corresponding to the design temperature rise across the condensers of 23°F and an ambient river temperature of 72°F. The ambient temperature in the model could not be controlled, so the effluent temperature was varied as needed to maintain the desired normalized density difference of 0.003686 at the source. Ambient flow velocities and depths were varied so that Mississippi River flow conditions in the prototype for total river discharges ranging from 13,200 to 50,000 cfs were simulated. For a few additional runs, the jet velocity and the normalized density deficit were varied to test the effect of varying the densimetric Froude numbers while holding the submergence and the ambient flow conditions constant.

4.2.2.2. Temperature Measurements

Sampling of the voltage signals from each thermistor by the computer was initiated by pushing a button near the flume. The signals were sampled at an approximate rate of seven times per second and averaged over a 60-sec interval. The average voltages were then converted to the corresponding average temperature for each thermistor, based on the calibration curve coefficients stored on disk. These average voltages and average temperatures as well as calculated normalized temperature rises, T_n, $\left(T_n = (T - T_a)/(T_E - T_a)\right)$, were printed. The average temperatures and the normalized temperatures were stored on disk and later punched onto computer cards for analysis on the University of Iowa's IBM 360/65 system.

Temperature measurements downstream from the ports for the three-port runs were restricted primarily to a region of width equal to the spacing between ports centered on the port at the flume centerline. This was the middle 8 in. of the flume. The measurement locations for the one-port runs were also restricted to the middle 8 in. of the flume unless the transverse width of a modeled 5°F isotherm was found to extend beyond this region. For these cases, measurements were taken across the entire flume width. The central region of the jet was the main area of interest; therefore, spacing of thermistors and measurement procedures were designed to define as well as possible the characteristics of the central part of the jet. At each cross section, readings were taken from the top

downwards. Readings were taken at 0, 0.05H, 0.15H, 0.25H, 0.35H, 0.45H, 0.55H, 0.65H, 0.75H, 0.85H, 0.95H, and H, where H equals the water depth. At the surface, the thermistors were barely submerged and at the bottom they were as low as possible without touching the bed of the flume. Measurements were taken at cross sections every 0.508 ft downstream from the ports for both the one-port and three-port runs. The transverse spacing is shown in the measurement grid in Fig. 4.7. After measuring the temperatures in the first three cross sections downstream from the ports, the computer printout was examined. For each of the three sections, the depth of the hottest point was noted. Temperature measurements were then taken at ± 0.05H from the point of maximum temperature for each section. This procedure helped to improve definition of the central portion of the jet. Additional downstream cross sections were measured until the temperature field became two-dimensional, or until a total of 10 cross sections had been measured.

4.2.2.3. Velocity Measurements

The dual-transducer Pitot tube velocity measuring system was used to define the velocity field in the central portion of the jet. The location of the velocity readings was determined by the results of the temperature measurements. Velocity readings were taken in the region where the measured normalized excess temperature was greater than or equal to the value corresponding to a 5°F temperature rise in the prototype. Velocity measurements were also

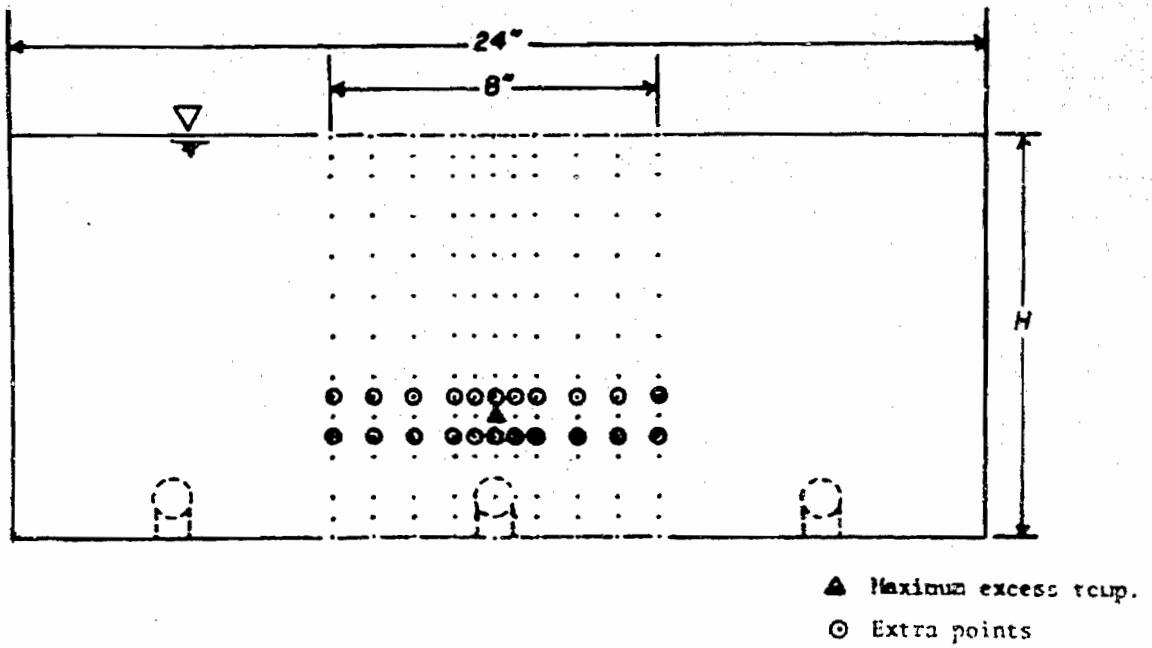

Fig. 4.7 Temperature measurement grid within a transverse section of the flume.

taken to determine the jet half-width at some sections. The sampling time for each velocity measurement was usually 10 sec. If excessive fluctuations were observed on the dial of the adjustable difference amplifier, longer sampling times were used.

CHAPTER 5

PROTOTYPE EXPERIMENTAL RESULTS

5.1 Cross-Sectional Surveys

Cross-sectional investigations were conducted from November, 1972, to January, 1975. During the period from November, 1972, to March, 1974, the power plant was operating as an open-cycle system using both diffuser pipes to discharge the condenser cooling water into the Mississippi River. From April, 1974, to January, 1975, the plant was operating either in the open-cycle mode or in a partial open-cycle mode with one of the diffuser pipes and the spray canal in parallel. With the exception of the March, 1974, survey, when only the long pipe was used, only the short diffuser pipe was being used during the surveys in the second period. Consequently, only part of the river was used for initial mixing at the time of these surveys. The cross-sectional prototype studies will, therefore, be divided into two sections: two-pipe studies and one-pipe studies.

5.1.1. Two-Pipe Surveys

Eighteen cross-sectional surveys were conducted when the plant was discharging all of its condenser cooling water into the river through both diffuser pipes. These investigations covered

total river discharges ranging from 31,400 to 73,600 cfs and total plant generating loads from 46 to 95 percent of full load.

5.1.1.1. Background Data

Background information for each of the survey days is presented in Tables 5.1 and 5.2. In Table 5.1, the distances from the centerline between the two diffuser pipes to the upstream and downstream measurement cross sections are given in columns 2 and 3. Column 4 gives the total river discharge data, as supplied by the U. S. Geological Survey. The values represent the Mississippi River flow (at Clinton, Iowa, 14 miles upstream from the plant), plus the inflow from the Wapsipinicon River. For surveys wherein velocity measurements were made, total river discharge was calculated from velocity and depth profiles. These measured discharges are presented in column 5. The measured discharges agreed well with the Geological Survey's values except during the winter months when the river was partially covered with ice and the U.S.G.S. discharges included corrections for the ice cover. For these days, the measured discharges were assumed to be correct. They were about 20 percent lower than the U.S.G.S. discharge estimates.

Column 2 of Table 5.2 shows the total river discharges used for all calculations. The ambient temperatures $\bar{T}_a$ in column 3 are weighted (with respect to river discharge per unit width) averages of sets of temperature readings taken at the upstream cross section both before and after the downstream data were obtained.

TABLE 5.1. Background Data for Two-Pipe Cross-Sectional Surveys

Date (1)	Distance to Downstream Section (ft) (2)	Distance to Upstream Section (ft) (3)	Total River Discharge from U.S.G.S. (cfs) (4)	Measured Total River Discharge (cfs) (5)
11-02-72	500	1000	70,700	--
11-09-72	300	1000	73,600	--
11-09-72	500	1000	73,600	--
11-28-72	500	1000	56,500	--
1-16-73	300	1000	38,000	--
1-16-73	500	1000	38,000	--
2-20-73	500	200	36,800	39,300
7-23-73	500	200	34,600	--
7-26-73	500	200	31,800	33,700
7-21-73	500	200	33,900	36,900
8-17-73	500	200	41,900	41,800
8-30-73	500	200	42,000	43,000
9-12-73	500	200	36,500	37,100
10-08-73	500	200	47,600	47,500
10-31-73	500	200	58,300	58,800
11-14-73	500	200	39,200	39,100
12-03-73	500	200	55,700	51,100
1-16-74	500	200	37,400	31,400
1-21-74	500	200	52,800	41,900
3-14-74	150	200	82,700	--

TABLE 5.2. Background River Flow and Plant Effluent Data

Date	River Discharge Q_R (cfs)	Average Ambient Temperature $\bar{T}_a$ (°C)	Plant Intake Temperature T_I (°C)	Plant Effluent Temperature T_E (°C)	Percent of Full Plant Load (P)	No. of Pumps Running	Estimated Plant Effluent Discharge Q_E (cfs)	Estimated Mixed Temperature Rise ΔT_m (°C)
(1)	(2)	(3)	(4)	(5)	(6)	(7)	(8)	(9)
11-02-72	70,700	8.0	8.1	23.4	90	6	1,710	0.37
11-09-72	73,600	6.7	6.4	20.4	95	6	1,970	0.37
11-28-72	56,500	1.4	1.1	16.1	90	6	1,740	0.45
1-16-73	38,000	0.5	0-4.4*	22.9	90	6	1,140	0.67
2-20-73	39,300	0.4	0.2	16.7	92	6	1,620	0.67
7-23-73	34,600	23.6	23.5	35.2	94	6	2,330	0.78
7-26-73	33,700	25.5	25.5	37.6	94	6	2,250	0.81
7-31-73	36,900	25.4	25.2	32.7	46	6	1,785	0.35
8-17-73	41,800	26.1	25.6	37.8	94	6	2,230	0.62
8-30-73	43,000	26.7	26.0	37.8	93	6	2,290	0.59
9-12-73	37,100	21.7	21.4	31.7	85.5	6	2,410	0.65
10-08-73	47,500	17.1	18.0	28.8	85.0	6	2,280	0.56
10-31-73	58,800	10.9	10.9	21.6	77.8	6	2,110	0.58
11-14-73	39,100	4.6	4.7	16.4	79.4	6	1,970	0.50
12-03-73	51,100	4.6	4.9	18.8	89.0	6	1,860	0.52
1-16-74	31,400	0.1	0.01	10.0	47.5	6	1,380	0.43
1-21-74	41,900	0.2	0.04	11.5	82.5	6	2,090	0.57
3-14-74	82,700	3.1	3.7	16.4	91.9	6	2,095	0.34

*Ice melting unit in operation.

The technical staff of the station provided hourly data on plant intake and effluent temperatures, percent of full plant load, and the number of circulating water pumps in operation for the days on which surveys were conducted. The estimated plant effluent discharge was computed from the formula

$$Q_E = \frac{12.8 \times 2270 \times P/100}{T_E - T_I} \qquad (5.1)$$

where

Q_E = plant effluent discharge in cfs

P = percent of full plant load

T_E = plant effluent temperature in °C

T_I = plant intake temperature in °C

Equation (5.1) is based on the design full-load plant temperature rise of 12.8°C, the design effluent discharge of 2270 cfs, and the assumption that the plant heat rejection rate is proportional to the plant load. The estimated values of Q_E are sometimes lower than the design value of 2270 cfs. The reduction in Q_E is attributed to partial blockage in the circulating water system due to the growth of slime deposits. The estimated fully-mixed temperature rise in the last column of Table 5.2 was computed according to the heat balance relationship

$$\Delta T_m = \left(Q_E/Q_R\right) \times \left(T_E - \bar{T}_a\right) \qquad (5.2)$$

5.1.1.2. Temperature Data

Raw Data. Temperature data for a typical survey at the upstream and downstream cross sections are shown in Fig. 5.1. The locations of the decimal points of the temperature readings correspond to the probe positions in the river cross sections when the readings were obtained except for the surface readings, where the probe was located 6 in. below the water surface, and the bottom readings, where the probe was located 10 in. above the bottom. The temperature in the upstream cross section for most surveys tended to vary more going across the channel than in the vertical. The only exception was near the Iowa shore where significant vertical stratification sometimes occurred. This was probably due to water of different temperature from the Wapsipinicon River either "sliding" under or floating on the Mississippi River water.

Transverse Distribution of Depth-Averaged Excess Temperature. Representation of the data as shown in Fig. 5.2 gives the best overall perspective because it maps the excess temperature across the channel in a context wherein it can be compared readily to the transverse variation of ambient temperature. The abscissa is the distance from the Illinois shore divided by the river width at the measurement cross section. The measured temperatures at the downstream sections are represented by $\bar{T}^d$, the depth-averaged temperature. The figure shows that the order of magnitude of the excess temperature is not much more than that of the variation of

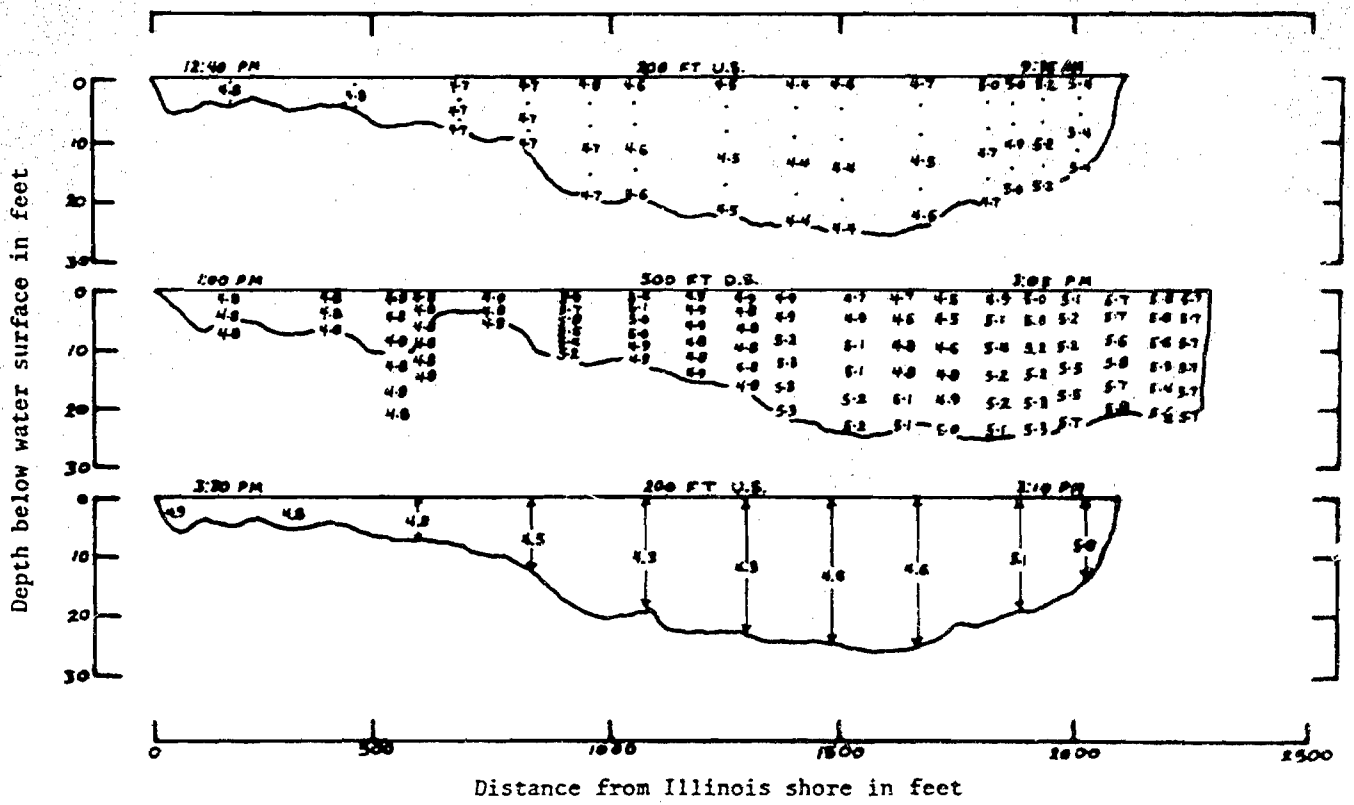

Fig. 5.1 Observed temperatures in °C 200 ft upstream and 500 ft downstream from diffuser pipe on December 3, 1973.

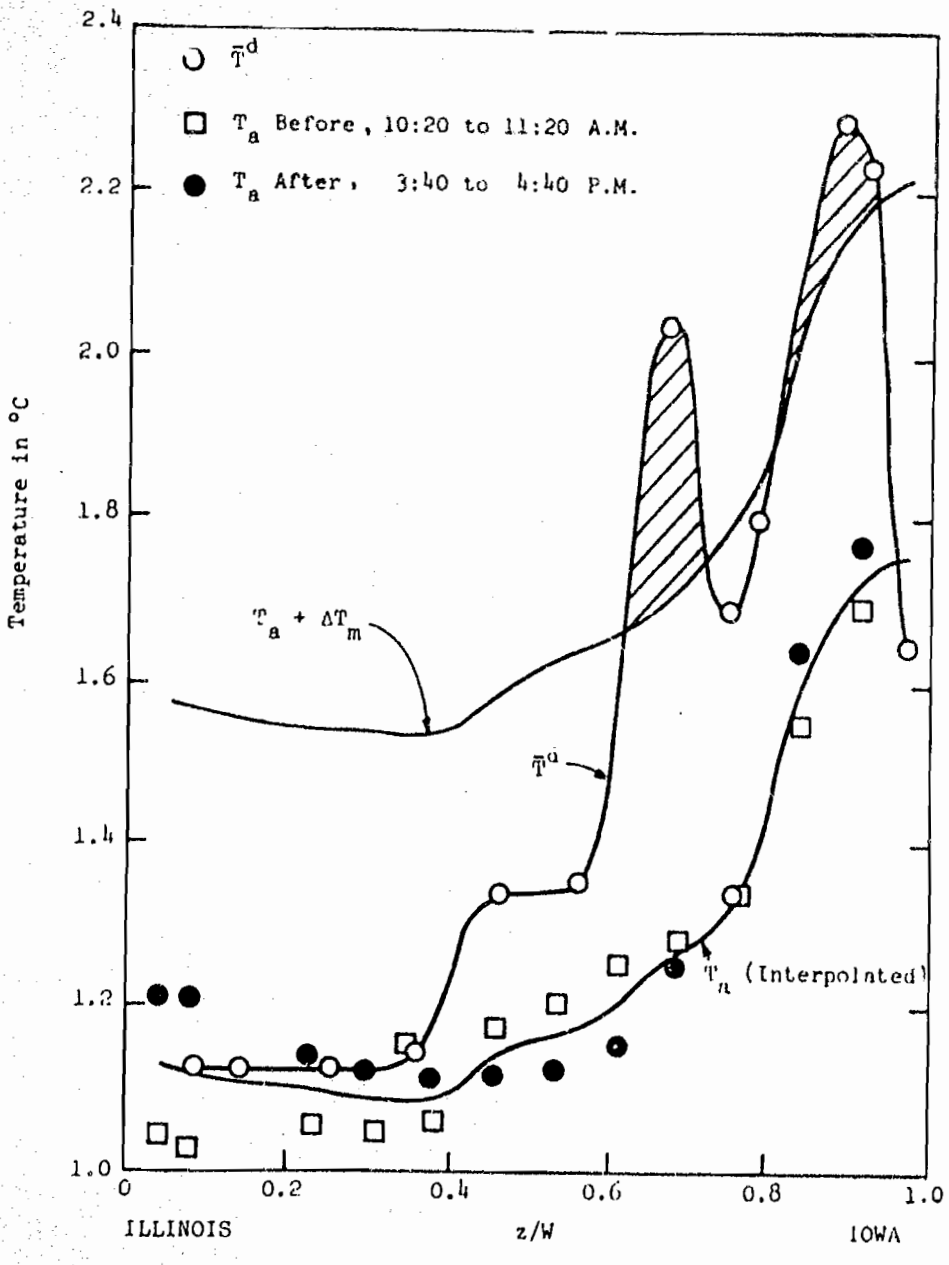

Fig. 5.2 Transverse distribution of depth-averaged temperature 500 ft downstream and ambient temperature 1000 ft upstream from diffuser pipe on November 28, 1972.

the natural ambient temperature. The change in magnitude and distribution of ambient temperature that can occur within a few hours can also be seen.

Representation of the data as shown in Fig. 5.3 is more helpful, however, in evaluating the performance of the diffuser-pipe system. The variable depth-averaged ambient temperature distribution pattern has been subtracted, leaving only the transverse distribution of the depth-averaged excess temperature. If there were no heat to transfer to the atmosphere and the heated effluent were completely mixed with the river water, the difference $\bar{T}^d - T_a$ would be equal to ΔT_m all the way across the channel, and $(\bar{T}^d - T_a)/\Delta T_m$ would have the uniformly distributed value of one. The amount by which the curves deviate from this value is a measure of the nonuniformity of excess heat distribution. In view of the short distance from the diffuser pipes to the two cross sections, it is safe to assume an adiabatic system and neglect the heat loss. If the excess heat is not uniformly distributed, the average value of $(\bar{T}^d - T_a)/\Delta T_m$ across the channel need not equal one unless the discharge per unit width of the ambient flow q_a is uniformly distributed. In the present case, the ambient flow is weighted heavily toward the Iowa shore, and the total heat balance has to be stated in terms of the excess heat flux distribution as

$$Q_E \Delta T_E = Q_R \Delta T_m = \int_0^W d\, \overline{u(T - T_a)}^d \, dz \qquad (5.3)$$

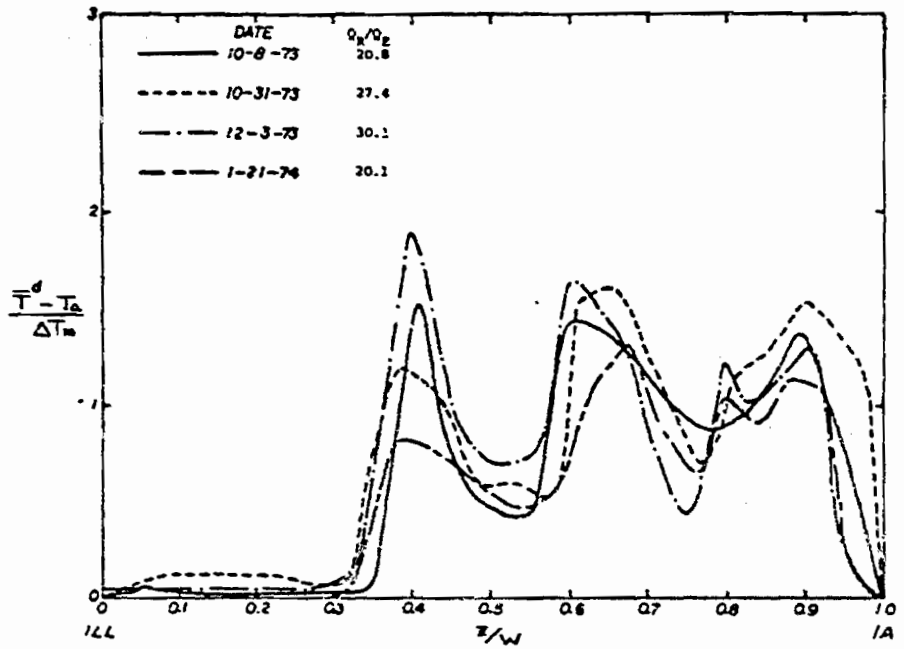

(a) Q_R > 40,000 cfs

Fig. 5.3 Transverse distribution of normalized depth-averaged excess temperature 500 ft downstream from diffuser pipe.

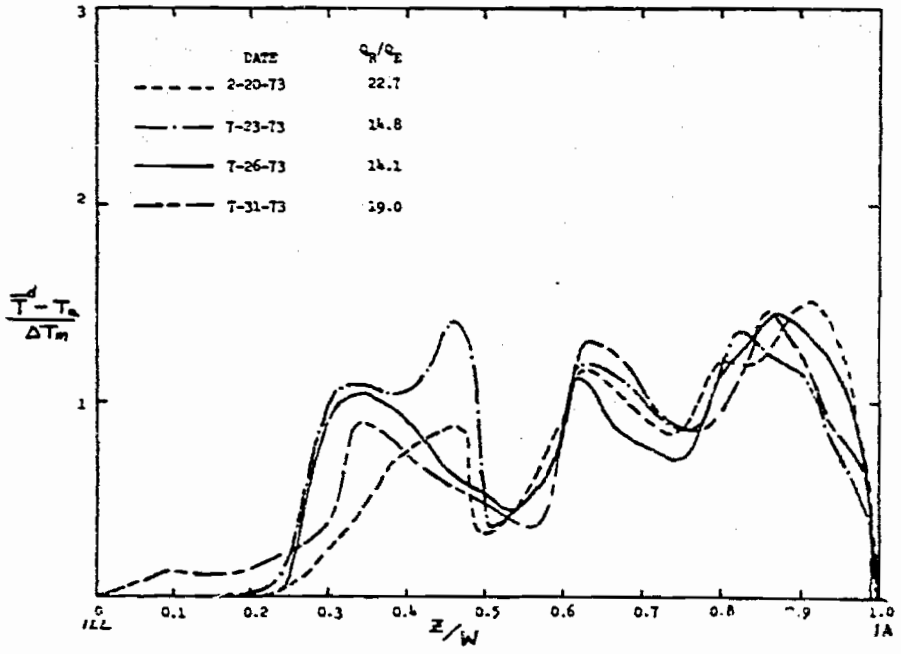

(b) 30,000 cfs < Q_R < 40,000 cfs

Fig. 5.3 (continued).

Still, the areas under the different curves in Fig. 5.3 should be roughly equal, provided there was no major shift in the distribution of either ambient flow or excess temperature.

An immediately obvious feature of Fig. 5.3 is the multi-peaked nature of the distributions. The reason for these peaks will be discussed in section 5.1.1.3.

Dilution at Point of Least Mixing. The excess temperature at each measurement point in the downstream cross sections was obtained by subtracting from the measured downstream temperature the depth-averaged upstream ambient temperature at the same value of z/W. These temperature rises for two typical surveys are shown in Fig. 5.4. Similar excess temperature plots are given in Appendix B for all surveys. The highest excess temperatures tend to occur near the water surface except in the winter months when the ambient river temperature falls below 39°F and the highest temperature rises are near the bottom of the river. This is caused by the sinking plume effect, which is due to the reversal in the density-temperature relationship below 4°C.

With regard to optimizing the performance of the diffuser-pipe system and ensuring that the stream temperature standards are satisfied, it is important to consider the points in the cross section where the excess temperature is highest. The data in Table 5.3 relate to points in the 500-ft downstream cross section where the maximum temperature rises, and hence minimum dilutions,

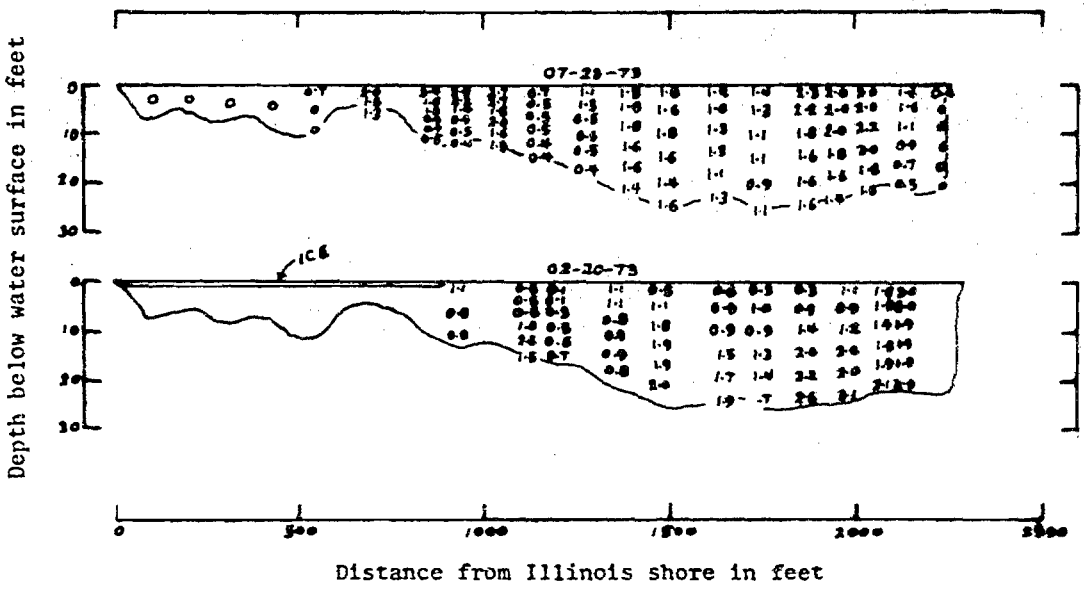

Fig. 5.4 Observed excess temperatures in °F 500 ft downstream from diffuser pipe on February 20 and July 23, 1973.

TABLE 5.3 Performance Characteristics of Diffuser Pipe 500 ft Downstream at Points where Minimum Dilution was Obtained

Date	Distance from Illinois Shore	Maximum Local Normalized Excess Temp. $\frac{(T-T_a)_{max}}{\Delta T_m}$	Maximum Local Excess Temp. $(T-T_a)_{max}$	Dilution at Point of Least Mixing $\frac{\Delta T_E}{(T-T_a)_{max}}$	Maximum Possible Dilution $\frac{Q_R}{Q_E} = \frac{\Delta T_E}{\Delta T_m}$
	(ft.)		(°F)		
(1)	(2)	(3)	(4)	(5)	(6)
11-02-72	1610	1.95	1.3	21.3	41.3
11-09-72	1675	1.50	1.0	24.7	37.4
11-28-72	1610	2.47	2.0	13.3	32.5
1-16-73	1640	2.07	2.5	16.2	33.3
2-20-73	1810	2.23	2.7	10.8	24.3
7-23-73	945	2.71	3.8	5.5	14.8
7-26-73	855	1.86	2.7	8.1	15.0
7-31-73	1420	2.20	1.4	9.4	20.7
8-17-73	2060	2.05	2.3	9.2	18.7
8-30-73	1015	2.73	2.9	6.9	18.8
9-12-73	700	2.22	2.6	6.9	15.4
10-08-73	930	2.58	2.6	8.1	20.8
10-31-73	955	2.03	1.4	13.8	27.9
11-14-73	1400	1.67	1.8	11.8	19.8
12-03-73	905	2.26	2.1	12.2	27.5
1-16-74	910	2.71	2.1	8.5	22.8
1-21-74	1045, 1820	1.66	1.7	12.0	20.0
3-14-74*	1310	3.62	2.2	10.9	39.5

*150 ft downstream from diffuser pipe.

were obtained. Distances from the Illinois shore to these points are listed in column 2. The maximum local temperature rises normalized by the mixed temperature rise, and in °F, are listed in columns 3 and 4, respectively. Column 5 lists the dilutions at the point of least mixing, i.e., the minimum observed dilutions. For comparison, column 6 lists the maximum possible dilutions which would be obtained for complete mixing.

As the data in column 4 of Table 5.3 shows, the highest temperature rise ever observed in the 500-ft downstream cross section was 3.8°F which is comfortably within the 5°F limit. However, because the maximum temperature rise tends to increase as river discharge decreases, and river discharges were higher than normal during this period, it is of interest to examine more closely the temperature data for those days on which the highest maximum normalized local temperatures occurred. The "hot spots" for the four days on which the highest $(T - T_a)/\Delta T_m$ values occurred are circled in Fig. 5.5. In each case, the hot spots are highly localized and are located in a part of the shallow region of the cross section downstream from the smaller 2-ft diameter ports. Evidently there is a relative deficiency of dilution water supplied by the ambient flow in this region.

The graph shown in Fig. 5.6 was plotted with a view toward estimating the river discharge Q_R at which the maximum temperature rise at full plant load in the 500-ft downstream cross

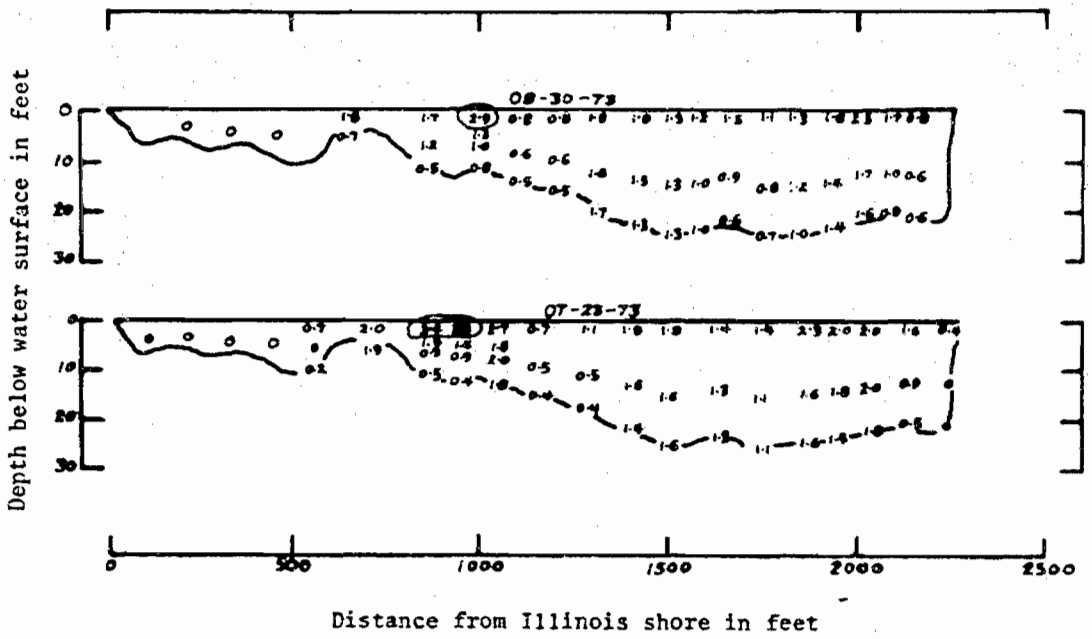

(a) July 23 and August 30, 1973

Fig. 5.5 Observed excess temperatures in °F 500 ft downstream from diffuser pipe.

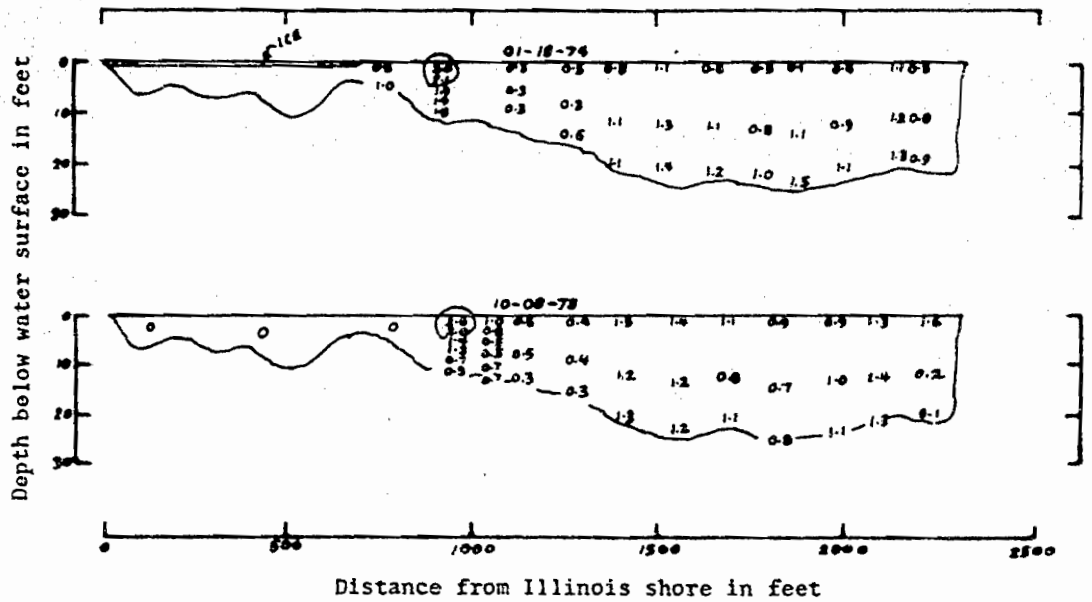

(b) October 8, 1973, and January 16, 1974

Fig. 5.5 (continued).

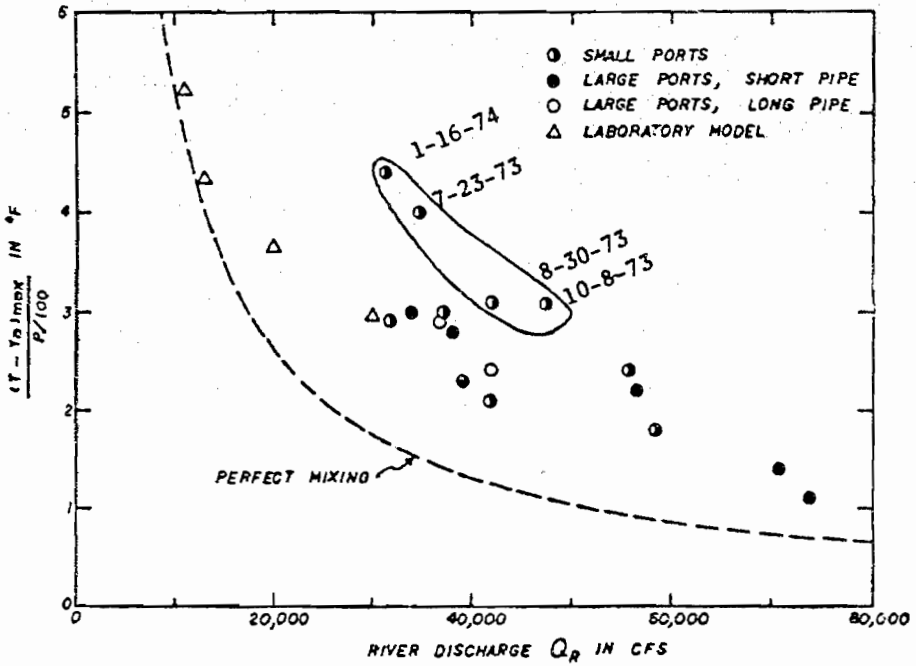

Fig. 5.6 Maximum excess temperature 500 ft downstream from diffuser pipe for full plant load versus river discharge.

section would reach 5°F. The denominator P/100 in the ordinate is the fractional plant load which ranges from zero at no load to one at full load. It is assumed here that the maximum temperature rise would increase in direct proportion to the plant load. Different symbols are used to identify sections of the diffuser pipes that are responsible for the hot spots. In addition, the four points corresponding to the hot spots mentioned in the previous paragraph are identified by date. For comparison, data from the laboratory model study (Jain et al., 1971) and the perfect mixing curve representing the equation

$$\frac{(T - T_a)_{max}}{P/100} = \frac{\Delta T_m}{P/100} = \frac{Q_E \Delta T_E}{P/100\ Q_R} \tag{5.4}$$

where

Q_E = 2270 cfs

ΔT_E = 23°F

are shown. This graph will be discussed further in Chapter 7.

5.1.1.3. Velocity and Heat Flux Data

Velocities as well as temperatures were measured on the days for which measured total river discharges are listed in Table 5.1. The velocity measurements for these days were used to determine the discharge distribution across the river at upstream and downstream cross sections. Some of these distributions, covering a range of total Mississippi River discharges from 31,400

to 58,300 cfs, are shown in Fig. 5.7. In the ordinate $q/\bar{q}$, q = local discharge per unit width obtained by multiplying the local depth d by the local depth-averaged velocity $\bar{u}^d$, and $\bar{q} = Q_R/W$ = width-averaged value of q. Also shown in Fig. 5.7, for comparison, is the normalized transverse distribution of discharge per unit width from the diffuser pipe, $q_j/\bar{q}_j$. No influence of the diffuser-pipe operation on the river-flow distribution is apparent in the data in Fig. 5.7 or in any of the other surveys wherein velocities were measured. However, the influence of the diffuser pipe system which takes the condenser cooling water from the region close to the Illinois shore and redistributes it across the deep portion of the channel could well become apparent at lower river discharges.

The measured discharge distributions tended to vary somewhat from survey to survey. At intermediate discharges, between 30,000 and 50,000 cfs, no systematic variation was observed. This was probably attributable to the the nearly constant river stage at the plant site maintained by the navigation dam near LeClaire, about 12 miles downstream, at intermediate and low river discharges.

Figure 5.8 shows the upstream and downstream $q/\bar{q}$ curves averaged for the surveys from February 20, 1973, to August 30, 1973. River discharge for these surveys ranged from 31,000 to 41,900 cfs. The diffuser pipe discharge distribution is also shown. Figure 5.9 shows the transverse distribution of the ratio of $q_j/\bar{q}_j$ to the corresponding average upstream $q/\bar{q}$ values from Fig. 5.8 which also

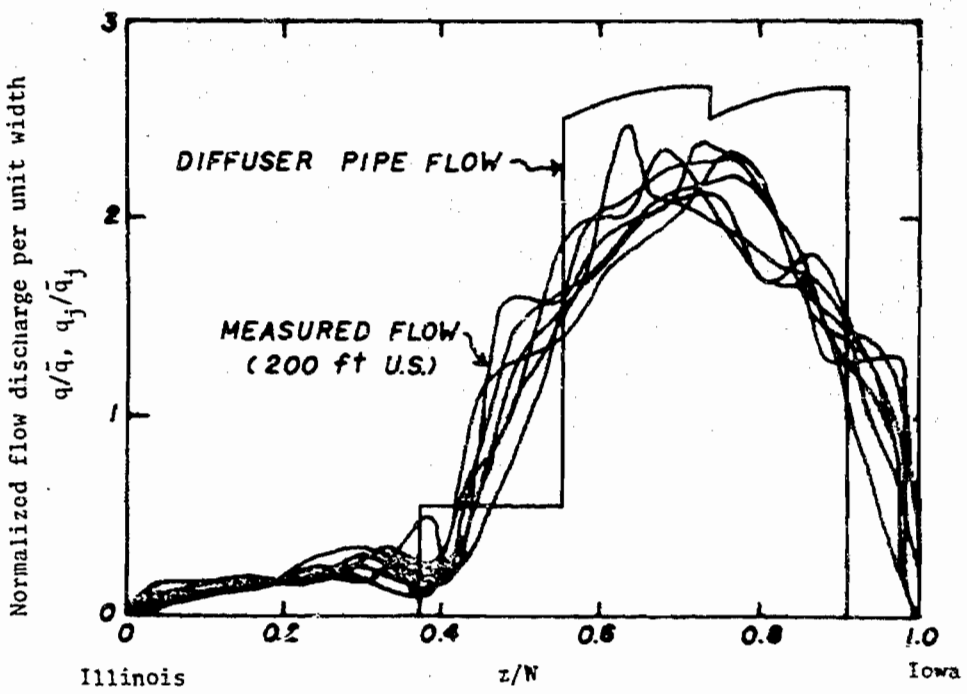

(a) 200 ft upstream from diffuser pipe

Fig. 5.7 Normalized transverse distributions of river flows.

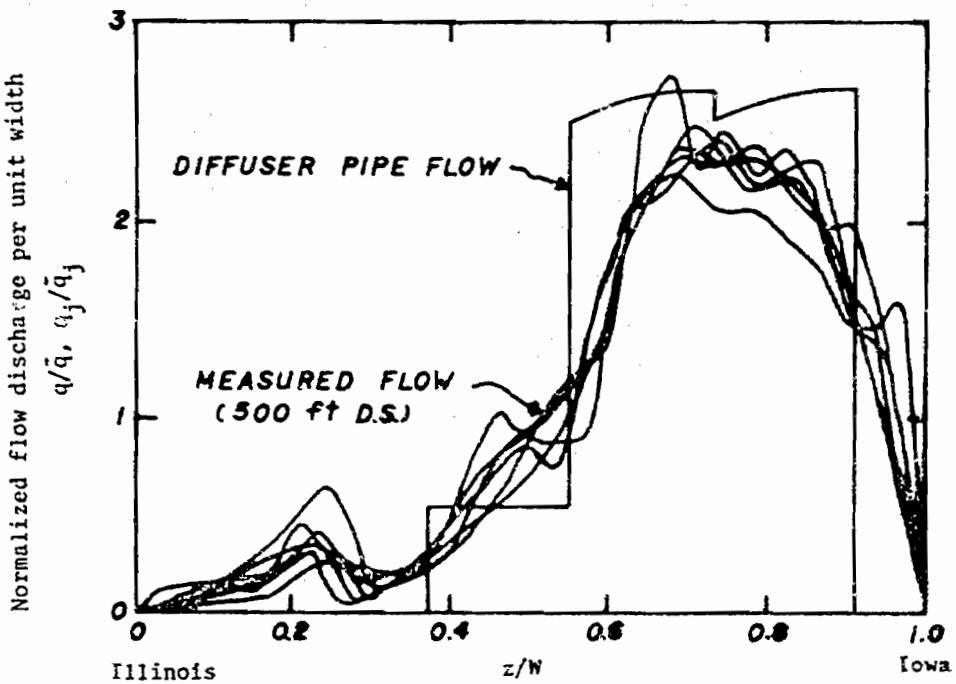

(b) 500 ft downstream from diffuser pipe

Fig. 5.7 (continued).

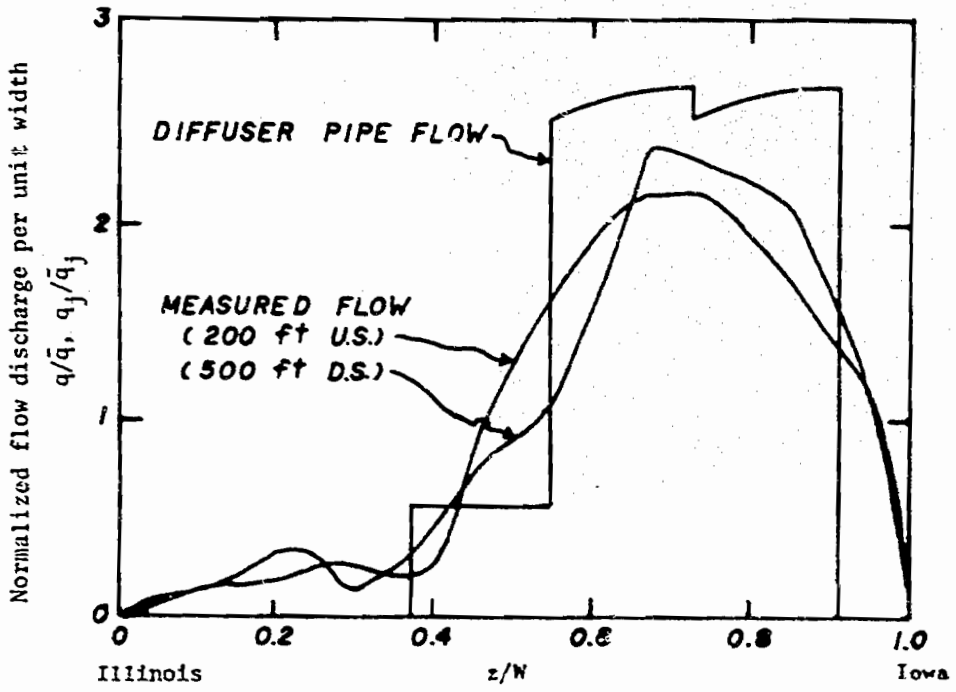

Fig. 5.8 Average normalized transverse distributions of river discharge 200 ft upstream and 500 ft downstream from diffuser pipe and diffuser pipe normalized discharge distribution at the pipe.

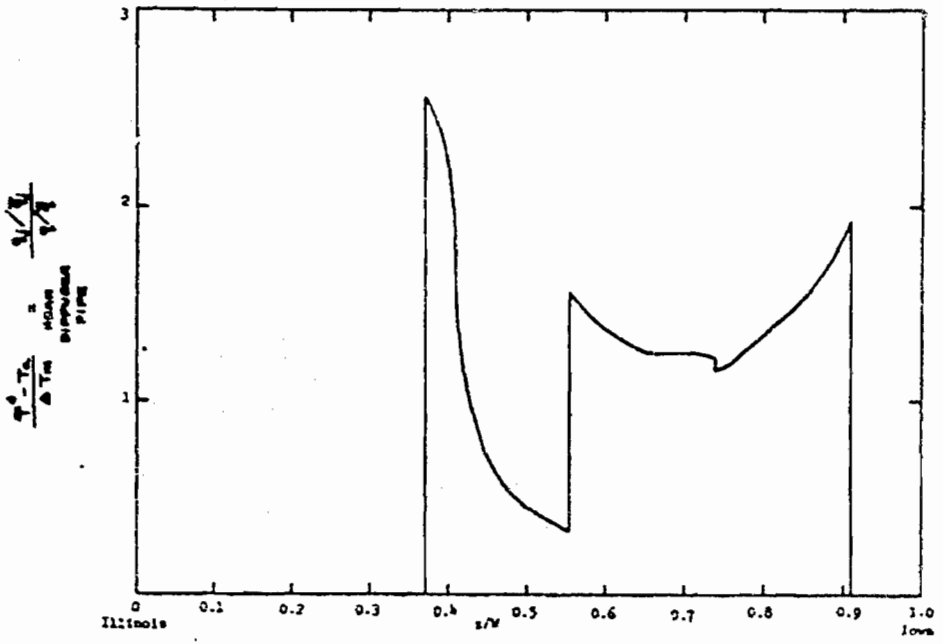

Fig. 5.9 Estimated transverse distribution of normalized excess temperature near the diffuser pipe.

represents an estimate of the transverse distribution of the normalized excess temperature $(\bar{T}^d - T_a)/\Delta T_m$ in the immediate vicinity of the diffuser pipes following initial mixing. The equivalence of the two ratios can be seen from the equality

$$\frac{q_j/\bar{q}_j}{q/\bar{q}} = \frac{q_j}{Q_E/W} \Big/ \frac{q}{Q_R/W} = \frac{q_j Q_R}{q Q_E} \tag{5.5}$$

combined with

$$\frac{Q_R}{Q_E} = \frac{\Delta T_E}{\Delta T_m} \tag{5.6}$$

which is a restatement of Eq. (5.2), and

$$q_j/q = \frac{\bar{T}^d - T_a}{\Delta T_E} \tag{5.7}$$

which is the dilution ratio for complete mixing of the local effluent discharge with the local ambient discharge. Comparison of the distribution in Fig. 5.9 with the distributions in Fig. 5.3 shows that they are indeed similar if allowance is made for some attenuation and smoothing due to transverse mixing occurring in the 500-ft reach between the diffuser pipes and the downstream survey section.

Distributions of the normalized excess heat load across the channel at the downstream cross section were determined from the temperature together with the velocity measurements. The distribution curves for two surveys are shown in Fig. 5.10. In the

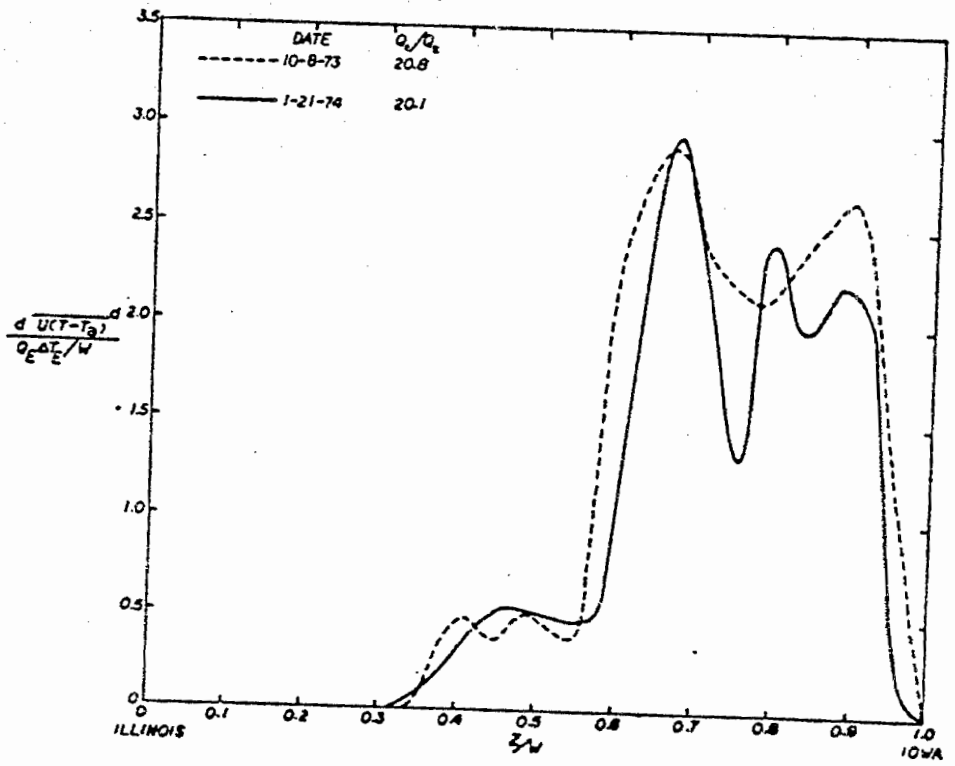

Fig. 5.10 Transverse distribution of normalized excess heat flux 500 ft downstream from diffuser pipe for Q_R = 30,000 to 40,000 cfs.

ordinate, the quantity $\overline{u(T - T_a)}^d$ is the local depth-averaged heat flux where u is the local velocity. The area under these curves represents the ratio of the total excess heat load measured at the downstream section to the total excess heat input from the diffuser pipes. Values of this ratio, which is called the heat recovery ratio, are listed in Table 5.4 for all the surveys for which velocity measurements were made. The value of the heat recovery ratio should equal one, if the heat loss in the 500-ft length of channel is assumed to be negligible. The level of agreement provides an overall check on the temperature, velocity, and background data. The results in Table 5.4 appear to be quite satisfactory.

TABLE 5.4. Heat Recovery Ratios 500 ft Downstream from Diffuser Pipe

Date	Heat Recovery Ratios
2-20-73	0.90
7-26-73	0.87
7-31-73	0.88
8-17-73	0.85
8-30-73	1.00
9-12-73	1.12
10-08-73	1.00
11-14-73	0.85
1-16-74	1.09
1-21-74	0.86

5.1.2. One-Pipe Surveys

Nine cross-sectional surveys were conducted when the plant was using only one diffuser pipe to discharge condenser cooling water. Six of these were made when the plant was using the spray canal in conjunction with the short diffuser pipe to dissipate the waste heat. This cooling system will be referred to as the combined system.

A schematic diagram of the combined system is shown in Fig. 5.11. The variables shown in the figure are defined as follows:

Q_C = flow discharge entering spray canal in cfs; depends on number of lift pumps operating

Q_E = effluent discharge from diffuser pipe in cfs; depends on number of circulating water pumps and lift pumps operating

T_E = effluent temperature from plant in °C; provided by technical staff

T_I = intake temperature to plant in °C

T_{aI} = ambient temperature in river entering intake in °C, measured by IIHR

ΔQ_L = loss of flow discharge in spray canal system due to evaporation in cfs; varies with plant operating conditions and meteorological conditions; $\Delta Q_L \approx 45$ cfs

ΔT_L = temperature reduction in spray canal system in °C; varies with plant operating conditions and meteorological conditions

$\Delta(QT)_L$ = loss of heat flux in spray canal system in cfs - °C; varies with plant operating conditions and meteorological conditions

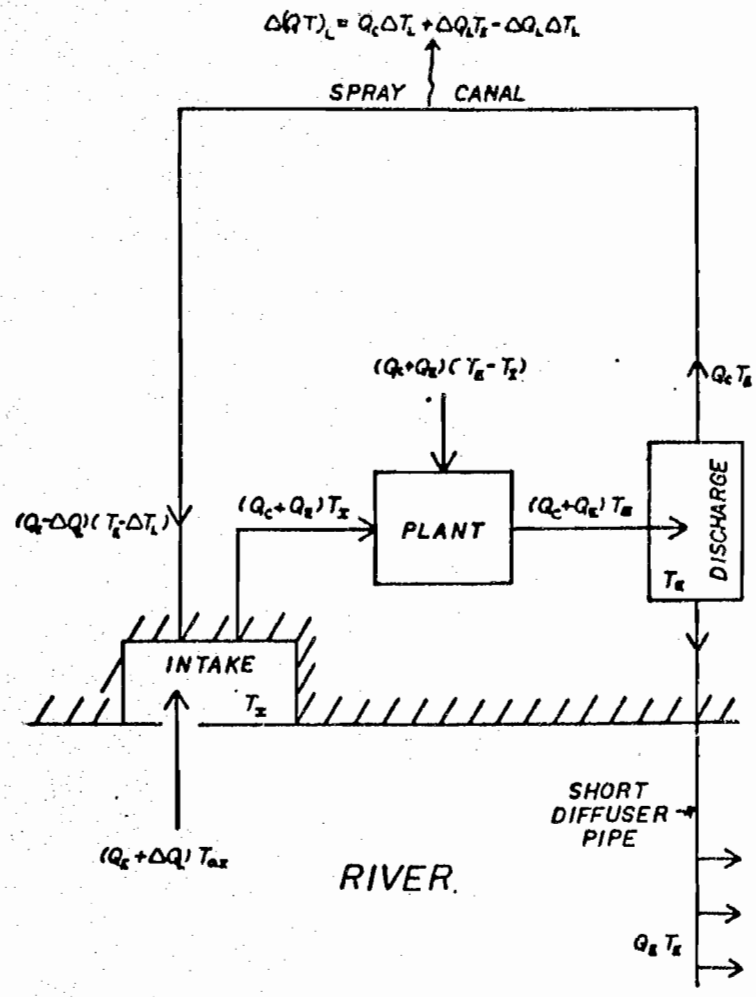

Fig. 5.11 Schematic diagram of combined spray canal-diffuser pipe cooling system.

Water flows into the intake bay from both the river and the downstream end of the spray canal and is drawn through the plant by the six circulating water pumps. The water is heated as it passes through the condensers and then flows into the effluent discharge bay. Three lift pumps each draw 401 cfs from the discharge bay into the upstream end of the spray canal. The remainder of the effluent is discharged in the river through the short diffuser pipe. When one or more of the lift pumps to the spray canal is not in operation, the discharge into the canal decreases proportionally and the discharge through the short diffuser pipe increases. The rate of heat dissipation from the canal is dependent on the effluent temperature, the meteorological conditions, and the heat transfer characteristics of the spray canal. The temperature of the spray canal adjusts until a thermodynamic balance is established between the rate of heat added by the condensers and the sum of the rates of heat transfer to the atmosphere and the net heat exchange with the river. When this occurs, the system reaches equilibrium. At this equilibrium condition, the effluent temperature has been observed to exceed the ambient river temperature by as much as 51°F.

The one-pipe studies covered total river discharges ranging from 22,200 to 103,000 cfs and percent of full plant load from 40.2 to 91.0 percent.

5.1.2.1. Background Data

Background data for each of the surveys is presented in Tables 5.5 and 5.6. These tables correspond to Tables 5.1 and 5.2 in section 5.1.1.1.

Column 2 of Table 5.6 indicates which of the two diffuser pipes, the long or the short one, was in operation during each survey. The number of lift pumps and circulating water pumps running for the days on which surveys were made are given in columns 8a and 8b. On the days when no lift pumps were running, the plant was operating open-cycle. The equation for computing Q_E for the surveys wherein the spray canal was not operating is Eq. (5.1). When the spray canal is in operation, this equation is no longer applicable. Since each of the three lift pumps is supposed to have a capacity of (401) cfs, and each of the six circulating water pumps a capacity of (378.3) cfs, the following equation should apply for the combined system:

$$Q_E = (378.3) \times NC - (401) \times NL \qquad (5.8)$$

where

NC = number of circulating water pumps in operation

NL - number of lift water pumps in operation

However, this method of computing Q_E is valid only if the pumps operate at their design capacities. This is questionable, in view of the results of the open-cycle studies. Since the heat-flux

TABLE 5.5. Background Data for One-Pipe Cross-Sectional Surveys

Date (1)	Distance to Downstream Section (ft) (2)	Distance to Upstream Section (ft) (3)	Total River Discharge from U.S.G.S. (cfs) (4)	Measured Total River Discharge (cfs) (5)
4-15-74	150	200	98,300	103,000
7-23-74	500	200	21,200	22,200
7-25-74	500	200	32,700	37,100
8-22-74	500	200	30,000	32,000
9-10-74	500	200	26,200	27,000
10-02-74	150	200	27,000	26,700
11-11-74	150	200	37,600	--
1-08-75	500	200	26,200	25,300

TABLE 5.6. Background River Flow and Plant Effluent Data when Operating with Spray Canal and/or One Diffuser Pipe Only

Date	Diffuser Pipe	River Discharge	Average Ambient Temp.	Plant Intake Temperature		Plant Effluent Temp.	Percent of Full Plant Load	Number of Pumps Running		Estimated Plant Effluent Discharge	Estimated Mixed Temperature Rise
			$\bar{T}_a$	T_{aI}	Est. T_I	T_E		Lift	CW	Q_E	ΔT_m
		(cfs)	(°C)	(°C)	(°C)	(°C)	(P)			(cfs)	(°C)
(1)	(2)	(3)	(4)	(5a)	(5b)	(6)	(7)	(8a)	(8b)	(9)	(10)
4-15-74	Long	103,000	8.6	8.9	8.9	20.8	46.9	0	3	1150	0.14
7-23-74	Short	22,200	26.8	26.4	27.4	33.3	40.2	2	6	1160	0.34
7-25-74	Short	37,100	26.4	26.1	31.2	40.4	65.2	3	6	850	0.32
8-22-74	Short	32,000	25.2	25.0	30.4	43.0	91.0	3	6	880	0.49
9-10-74	Short	27,000	21.7	21.6	30.0	42.4	79.0	3	5	650	0.50
10-02-74	Short	26,700	13.3	13.3	22.4	35.6	81.0	3	5	580	0.48
11-11-74	Short	37,600	9.0	8.9	22.2	34.3	79.0	3	5	690	0.46
1-08-75	Short	25,300	0.3	0.3	0.3	7.9	46.0	0	6	1750	0.53

measurement results shown in Table 5.4 for the open-cycle two-pipe studies were reasonably good, the heat flux measurements for surveys when the combined system was in operation were used to estimate the effluent discharge. The following equation was used to estimate Q_E:

$$Q_E = \frac{1}{(T_E - \bar{T}_a)} \int_0^W \overline{du(T - T_a)^d}\, dz \qquad (5.9)$$

where

W = river width

d = local depth

The integral was evaluated for each survey by measuring the area under the heat flux curves with a planimeter. The effluent discharges computed, using Eq. (5.9), are presented in column 9. Values of Q_E computed according to Eq. (5.8) ranged up to about 25 percent larger. Column 10 gives the estimated mixed temperature rises at the downstream cross sections.

5.1.2.2. Temperature Data

The methods of data collection and reduction for the one-pipe studies were the same as discussed previously for the two-pipe studies.

Transverse Distribution of Depth-Averaged Excess Temperature. The transverse distribution of excess temperature is presented in Fig. 5.12 which corresponds to Fig. 5.3 in section

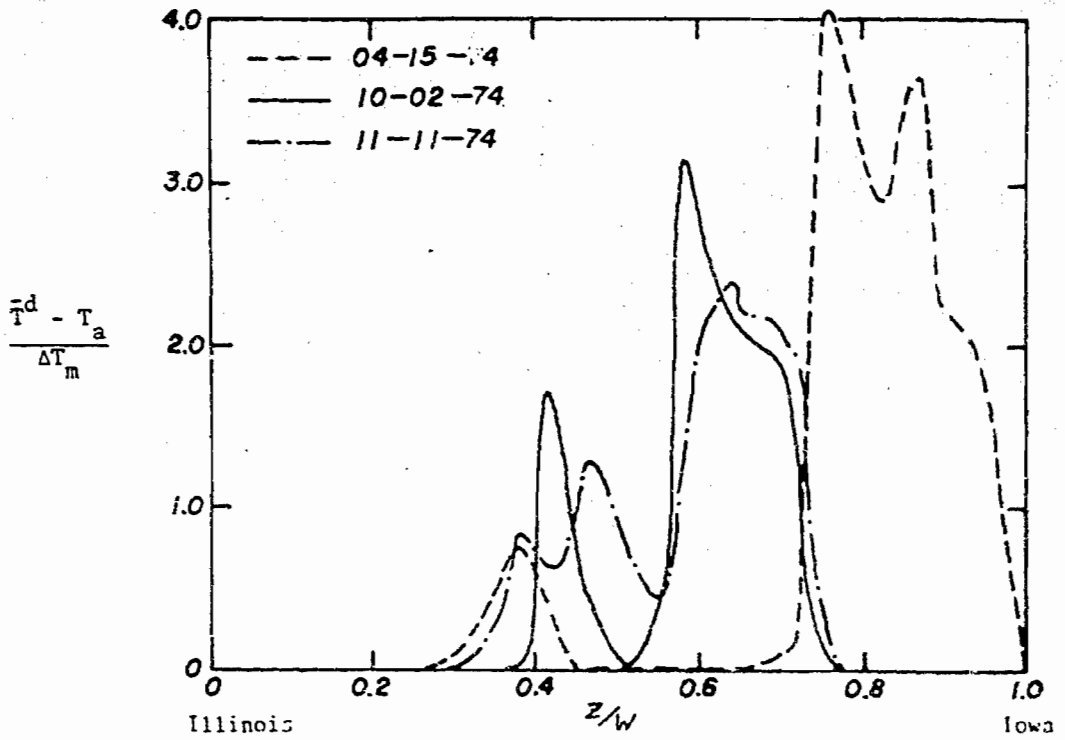

(a) April 15, 1974; October 2, 1974; and November 11, 1974

Fig. 5.12 Transverse distribution of normalized depth-averaged excess temperature 500 ft downstream from diffuser pipe.

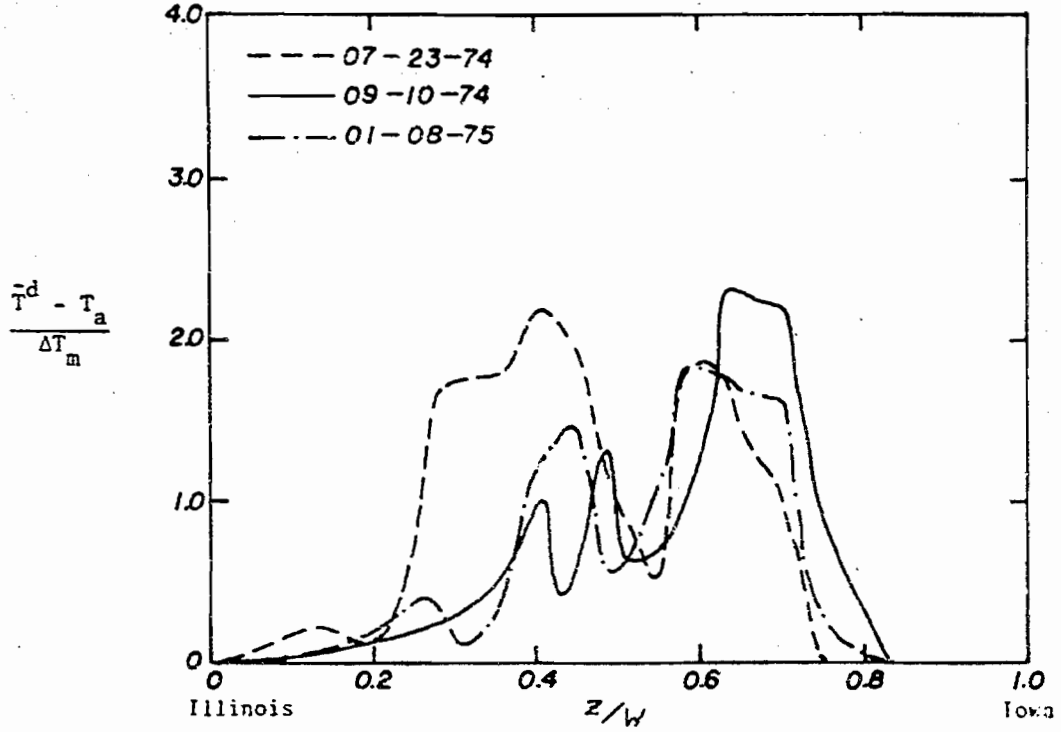

(b) July 23, 1974; September 10, 1974; and January 8, 1975

Fig. 5. 12 (continued).

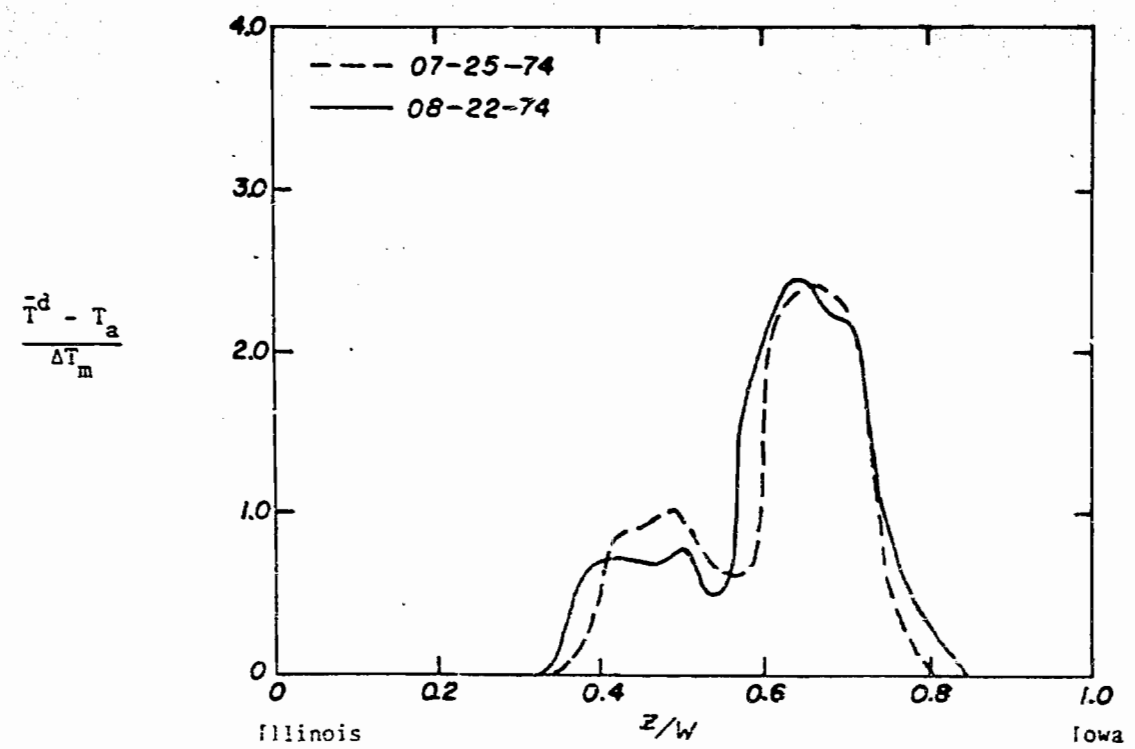

(c) July 25, 1974 and August 22, 1974

Fig. 5.12 (continued).

5.1.1.2. For all the surveys when only the short pipe was used, little excess heat was found in the Iowa side of the main channel. This, of course, was to be expected since the short diffuser pipe only extends across the east half of the main channel. The river discharge of 22,200 cfs on July 23, 1974, was the lowest of any for either the two-pipe or one-pipe surveys. The excess temperature on this day spread towards the Illinois shore across the water surface as shown in Fig. B.13.

Dilution at Point of Least Mixing. The temperature rises at the downstream measurement points are shown in Appendix B.

The data in Table 5.7 relate to points in the downstream cross section where maximum temperature rises were obtained. This table corresponds to Table 5.3 which was discussed in section 5.1.1.2. At the section 500 ft downstream, the maximum observed excess temperature was 3.2°F which is well under the 5°F limit. The estimated proportion of the total waste heat discharged through the diffuser pipe is presented in column 8 of Table 5.7 and will be discussed in Chapter 7.

5.1.2.3. Velocity and Heat Flux Data

Velocities were measured in eight of the surveys. Discharge distributions and total excess heat flux were determined as they were for the two-pipe studies. The 200-ft upstream discharge distributions for the lowest total discharge 22,200 cfs on July 23, 1974, and for the highest total discharge, 103,000 cfs

TABLE 5.7. Performance Characteristics of Diffuser Pipe at Points where Minimum Dilution was Obtained when Operating with Spray Canal and/or One Diffuser Pipe Only

Date	Downstream Distance (ft)	Distance from Illinois Shore (ft)	Maximum Local Excess Temperature $(T-T_a)_{max}$ (°F)	Maximum Local Normalized Excess Temperature $\frac{(T-T_a)_{max}}{\Delta T_m}$	Dilution at Point of Least Mixing $\frac{\Delta T_E}{(T-T_a)_{max}}$	Maximum Possible Dilution $\frac{Q_R}{Q_E} = \frac{\Delta T_E}{\Delta T_m}$	Estimated Proportion of Waste Heat to Diffuser Pipe*
(1)	(2)	(3)	(4)	(5)	(6)	(7)	(8)
4-15-74	150	1740	1.4	5.72	15.7	89.6	1.00
7-23-74	500	920	2.1	3.45	5.57	19.1	0.65
7-25-74	500	1495	1.8	3.12	14.0	43.6	0.63
8-22-74	500	1475	2.8	3.17	11.4	36.4	0.59
9-10-74	500	1475	3.2	3.57	11.6	41.5	0.59
10-02-74	150	950	4.2	4.82	9.56	46.0	0.55
11-11-74	150	1475	2.8	3.35	16.3	54.5	0.76
1-08-75	500	1345	1.9	2.01	7.20	14.5	1.00

*Estimated proportion of waste heat to diffuser pipe = $\frac{Q_E \Delta T_E}{(2270)(12.8)P/100}$.

on April 15, 1974, are shown in Fig. 5.13. Except in two of the surveys—those on July 23, 1974, and January 8, 1975—the upstream and downstream river-flow distributions did not differ appreciably and were close to the averaged distributions shown in Fig. 5.8. The result for those two surveys, shown in Fig. 5.14, indicate that the flow in the downstream section was much more heavily concentrated near the center of the channel. On both of these days, all of the effluent discharge was from the short pipe, the estimated effluent discharge was greater than the design discharge of 1135 cfs for one pipe, and the river discharge was comparatively low. The amount of additional flow concentrated near the center is greater than can be accounted for by the diffuser pipe discharge alone, particularly for the January 8, 1975, downstream distribution. Evidently conditions combined to cause the diffuser pipe discharge to behave like a jet pump and entrain additional ambient flow. When operating with one pipe, the diffuser-pipe system no longer discharges into a laterally-constrained receiving environment as it did when both pipes were in operation. Therefore, at sufficiently high effluent discharge-to-total river discharge ratios, some of the water on the Iowa side of the main channel is evidently drawn over to the part of the channel where the effluent is being discharged.

Distributions of the excess heat load across the channel at the downstream cross sections were determined from the velocity

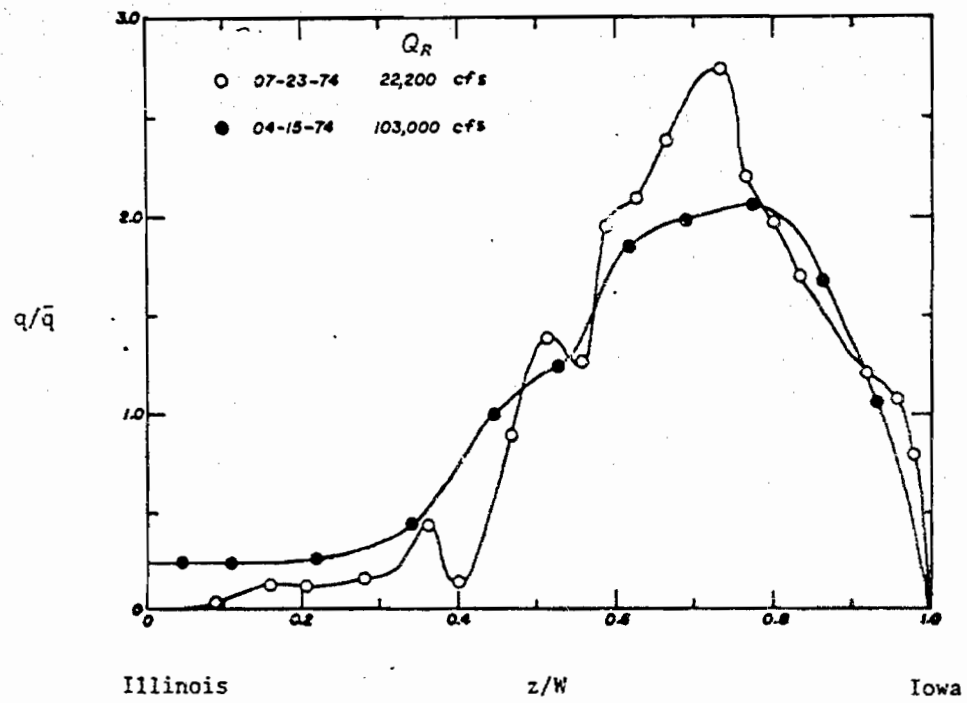

Fig. 5.13 Normalized transverse distribution of river discharge per unit width 200 ft upstream from the diffuser pipe on April 15 and July 23, 1974.

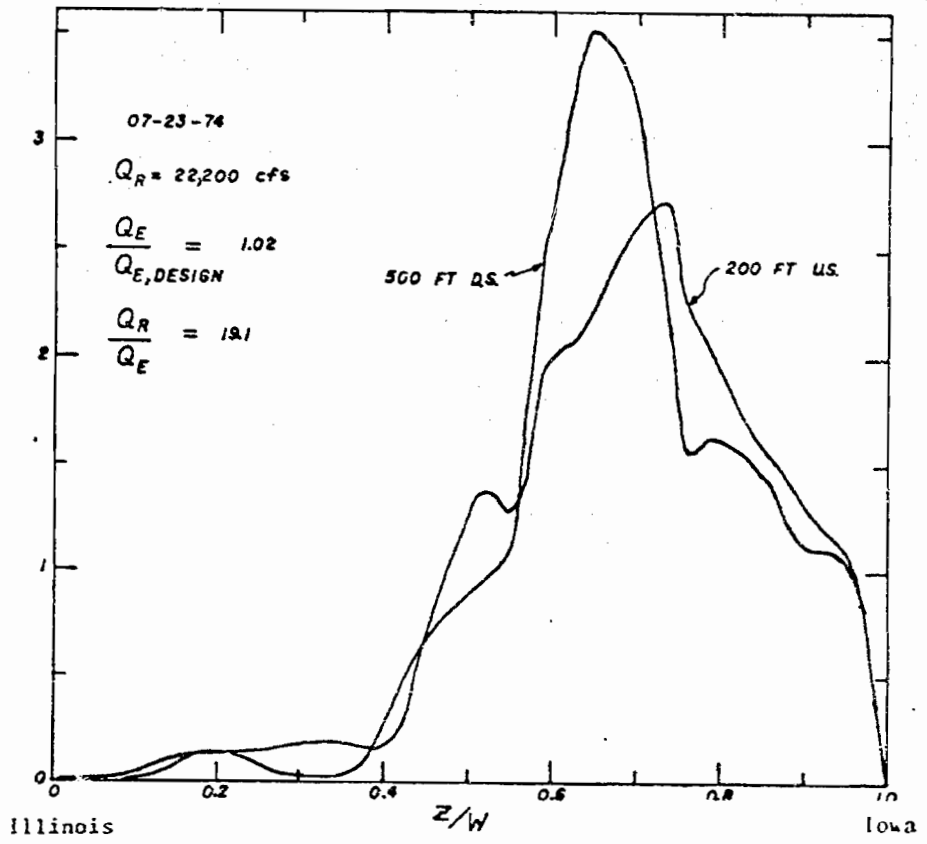

(a) July 25, 1974

Fig. 5.14 Normalized transverse distributions of river discharge 200 ft upstream and 500 ft downstream from diffuser pipe.

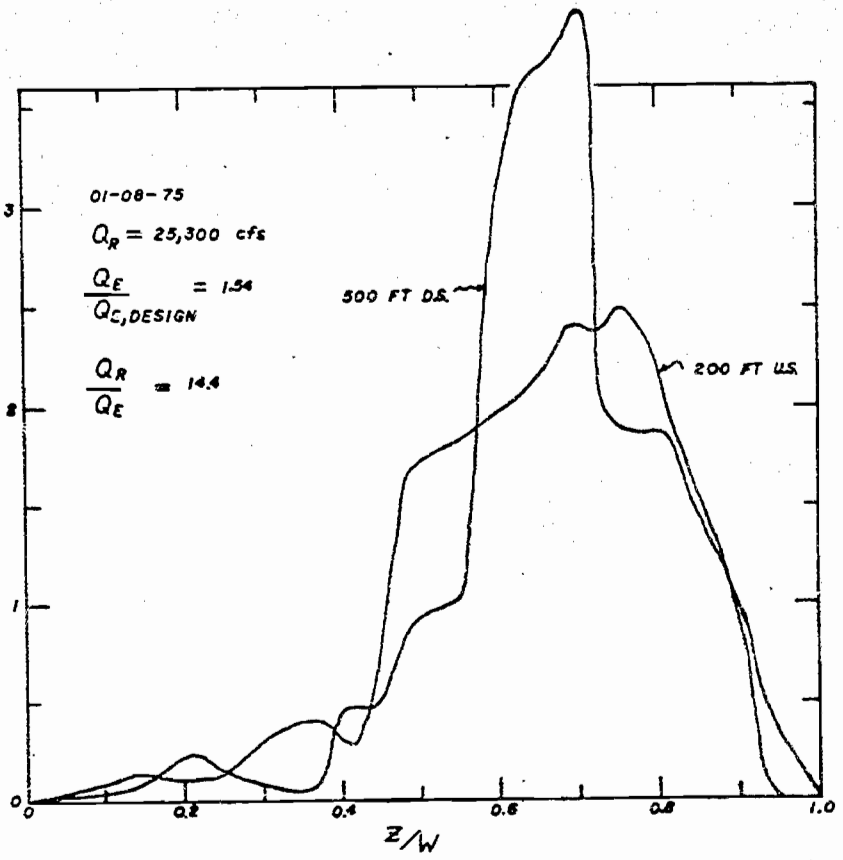

(b) January 8, 1975

Fig. 5.14 (continued).

and temperature measurements as for the two-pipe surveys. Most of the excess heat flux was found in the Illinois side of the main channel. These results are not shown here; however, the total heat flux can be determined by multiplying the mixed temperature rise ΔT_m in Table 5.6 (which was determined from the heat-flux distribution data) by the river discharge Q_R.

5.2 Single-Port Prototype Surveys

Seven single-port prototype surveys were conducted between November 11, 1973, and October 30, 1974. Five of the surveys were made downstream from 3-ft ports on the short diffuser pipe; one was made downstream from a 3-ft port on the long pipe and one was made downstream from a 2-ft port on the short pipe. Both velocities and temperatures were measured in all surveys.

5.2.1. Background Data

Background data for the days on which surveys were made is presented in Table 5.8. Column 2 gives the total river discharge as supplied by the U.S. Geological Survey. Column 3 gives the distance from the Illinois shore to the location of the heated jet centerline at the section 30 ft downstream from the centerline between two diffuser pipes and column 4 gives the port orifice diameters corresponding to the locations in column 3. The distances downstream from the port orifices where the measurements were made are shown in column 5. The Industrial Bio-Test unit and

TABLE 5.8. Background Data for Single-Port Prototype Studies in 1973 and 1974

Date	River Discharge Q_R (cfs)	Distance from Illinois Shore z (ft)	Outlet Diameter of Port D (ft)	Distance Downstream from Port x (ft)	Percent of Full Plant Load P (%)	Local Ambient Temp. T_a (°F)	Plant Effluent Temp. T_E (°F)	Estimated Discharge from Single Port Q_j (cfs)	Estimated Velocity from Single Port U_j (ft/sec)
(1)	(2)	(3)	(4)	(5)	(6)	(7)	(8)	(9)	(10)
11-16-73	39,600	1774	2.7	35 65	88.5	40.2	65.5	42.1	7.35
3-12-74	82,210	1345	2.7	15 45	91.2	37.2	61.4	46.7	8.16
3-13-74	82,900	968	1.8	35 65 95	89.5	38.1	61.4	19.9	7.82
7-24-74	26,900	1313	2.7	15 45 75	50.0	79.5	94.7	46.3	8.09
10-01-74	28,600	1273	2.7	15 45 75	78.0	57.2	96.0	27.3	4.77
10-25-74	25,900	1293	2.7	15 45 75	91.0	53.5	104.5	24.0	4.19
10-30-74	25,200	1391	2.7	15 45 75	87.8	56.1	106.8	25.3	4.42

the technical staff of the station provided the information on the percent of full plant load, the effluent discharge temperature, and the number of circulating pumps and lift pumps in operation. The local ambient temperature and velocity were measured by the Institute staff. The values were averaged for the period of the survey.

The estimated effluent discharge Q_j from the single port under investigation is given in column 9. When the plant was operating entirely in the open-cycle mode, the following equation was used:

$$Q_j = \frac{12.8 \times Q_{jD} \times P/100}{T_E - T_I} = \frac{Q_E Q_{jD}}{2270} \tag{5.10}$$

where

Q_{jD} = design discharge for the port in cfs

When the combined system was in operation, Q_j was calculated with the following equation:

$$Q_j = \frac{Q_T \Delta T_m}{T_E - T_a} \tag{5.11}$$

where

Q_T = measured discharge in a section of river whose width is equal to spacing between adjacent ports at the farthest downstream section

ΔT_m = measured mixed temperature at farthest downstream section

T_E = effluent temperature in discharge bay

T_a = local ambient river temperature

As in the one-pipe cross-sectional studies, a simple heat balance such as Eq. (5.10) could not be used for determining Q_j when the spray canal was in operation since the effluent discharge Q_E was not known with certainty. The jet velocities in column 10 were calculated from the values in columns 4 and 9.

5.2.2. Temperature Data

Ambient temperature and velocity were measured at two verticals upstream from the ports both before and after the downstream measurements were made for each survey. The ambient temperature was assumed to vary linearly with respect to time during the survey. Lateral variation of the ambient temperature across the relatively small test sections was negligible. Excess temperatures at the downstream sections were calculated by subtracting the upstream ambient temperature from the measured downstream temperature readings. Fig. 5.15 shows the data from a typical donwstream survey. Each solid circle represents the location of the midpoint between the thermistor probe and the current meter. The number above the point is the excess temperature in °F. The number below the point is the measured velocity (not the excess velocity) in feet per second. The vertical lines separate the regions assigned to adjacent ports. Similar figures for all single-port surveys are presented in Appendix C.

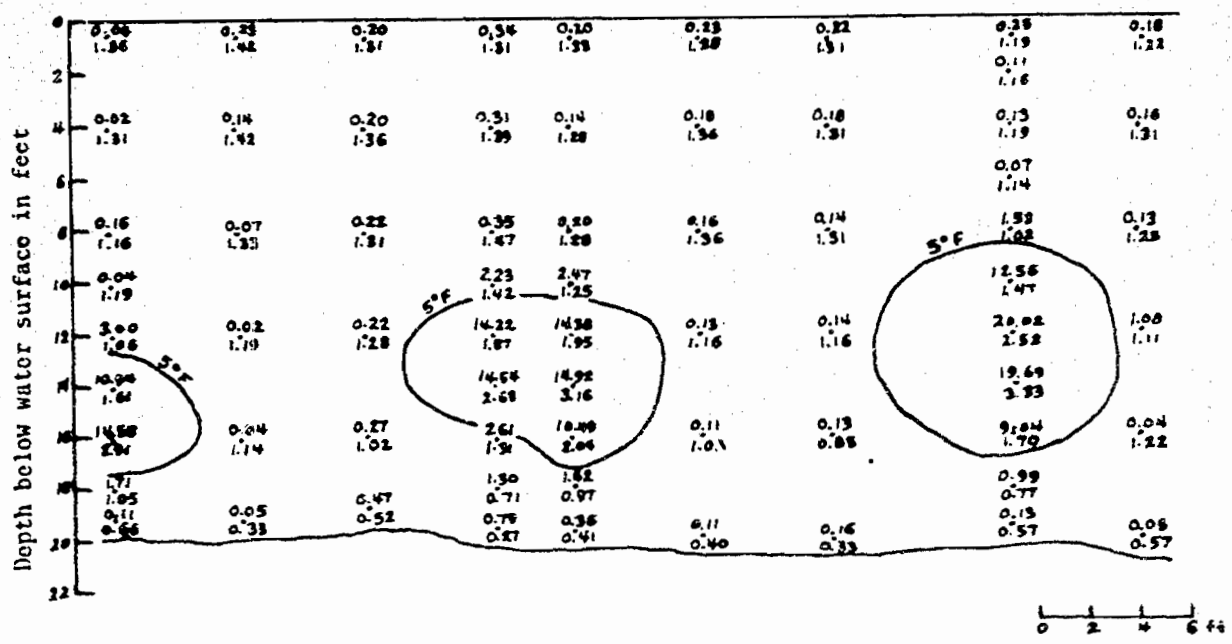

Fig. 5.15 Excess temperature in °F and velocity in ft/sec measured 15 ft downstream from a main channel dirfuser pipe port on October 30, 1974.

Table 5.9 gives the local average ambient velocity and depth, and the port spacing for each of the surveys in columns 3 to 5, respectively. Local average means an average taken over the region included in the survey. Column 6 lists the estimated effluent discharge from the ports under investigation. When the plant was operating in the open cycle mode, the estimated mixed temperature rise given in column 7 was based on the following equation:

$$\Delta T_m = Q_j \Delta T_E / \left(LHU_a\right) \tag{5.12}$$

When the plant was operating with the combined system, the mixed excess temperature was computed from the data at the section farthest downstream.

The 5°F temperature rise isotherms for the survey sections were determined by linear interpolation. They are shown for all the single-port surveys in Appendix C. Some of the plots also show isotherms for smaller temperature rise values. Excess temperatures greater than 5°F were not observed in some surveys. The percent of the area between the vertical lines wherein excess temperatures less than 5°F are presented in column 8 of Table 5.9. These percentages are zones-of-passage with respect to area, as defined in Chapter 1, for the region of the channel associated with a particular port. The maximum observed temperature in each survey section is given in column 9.

TABLE 5.9. Results for Single-Port Prototype Studies

Date	Distance Downstream from Port x (ft)	Local Average Ambient Velocity U_a (ft/sec)	Local Average Depth H (ft)	Port Spacing L (ft)	Estimated Effluent Discharge from Single Port Q_j (cfs)	Estimated Mixed Temperature Rise ΔT_m (°F)	Zone-of Passage wrt Area ZPA (%)	Maximum Observed Temperature Rise $(T-T_a)_{max}$ (°F)	Zone-of Passage wrt Discharge ZPD (%)
(1)	(2)	(3)	(4)	(5)	(6)	(7)	(8)	(9)	(10)
11-16-73	35	1.52	23.4	19.67	42.1	1.44	99.2	5.4	98.3
	65						100		100
3-12-74	15	2.88	21.7	19.67	46.7	0.89	97.3	7.7	96.5
	45						99.7	5.6	99.6
3-13-74	35	2.18	17.9	39.33	19.9	0.30	100	4.4	100
	65						100	1.7	100
	95						100	1.4	100
7-24-74	15	1.06	18.8	19.67	46.3	1.31*	100	4.9	100
	45						100	2.4	100
	75						100	1.9	100
10-01-74	15	1.18	22.0	19.67	27.3	2.11*	89.5	14.8	86.2
	45						94.4	6.7	91.9
	75						100	4.0	100
10-25-74	15	1.07	20.0	19.67	24.0	2.64*	86.1	19.0	81.2
	45						86.7	8.9	81.5
	75						97.5	6.0	97.0
10-30-74	15	1.09	20.4	19.67	25.3	2.71*	87.1	20.0	76.2
	45						87.2	8.7	85.3
	75						98.6	5.7	98.5

*Measured at farthest downstream section.

5.2.3. Velocity Data

The following equation was used to compute the percent of the discharge with excess temperature less than 5°F, i.e., the zone-of-passage with respect to discharge for a particular port,

$$ZPD = 100\left\{1 - A_5\bar{U}_5/(Q_a + Q_j)\right\} \qquad (5.13)$$

where

A_5 = area enclosed by the 5°F isotherm

$\bar{U}_5$ = estimated average velocity within 5°F isotherm

$Q_a = LHU_a$ = ambient discharge for local increment of river width equal to 1 port spacing

The values of the zones-of-passage with respect to discharge are given in column 10 of Table 5.9. It should be emphasized that the zones-of-passage given in columns 8 and 10 apply only to the segment or slice of the river downstream from the port being studied. The width of these slices equals the local port spacing, i.e., 19.7 ft for the main-channel ports and 39.3 ft for the shallow-water ports.

The excess heat fluxes are not presented in the tables but can be determined by multiplying the effluent temperature rise times the estimated discharge from a single port.

CHAPTER 6

MODEL EXPERIMENTAL RESULTS

6.1 Introduction

The objectives of the model study, as stated in Chapter 3, were satisfied by performing the following two main series of model investigations: (1) experiments for which model results were directly compared with field measurements to determine how well the two-dimensional channel model represented the prototype; and (2) experiments that systematically covered a wide range of field conditions in an effort to adequately predict zones-of-passage for the entire river channel for various ambient flow and plant operating conditions. In addition, characteristics of merging jets over the experimental range were investigated.

The first series of experiments consists of model runs corresponding to each of the single-port prototype surveys. Table 6.1 gives the conditions for the model runs. The modeling criteria were described in Chapter 3. Temperature and flow conditions for the October 25 and October 30 prototype surveys were nearly the same; therefore, only the October 25 survey was modeled. Column 3 of Table 6.1 gives the normalized density deficit of the jet at the point of discharge for each run.

TABLE 6.1. Conditions for Model Runs Simulating Single-Port Surveys

Date of Prototype Survey	Ambient Velocity (ft/sec) U_a	Normalized Density Deficit $\Delta\rho/\rho$	Relative Depth H/D	Velocity Ratio U_j/U_a	Jet Densimetric Froude Number $U_j/\sqrt{gD\ \Delta\rho/\rho}$	Jet Reynolds Number U_jD/ν_j	Ambient Temp. (°F) T_a	Effluent Temp. (°F) T_E
(1)	(2)	(3)	(4)	(5)	(6)	(7)	(8)	(9)
11-16-73	0.279	0.00149	8.67	4.80	20.22	15,700	86.0	94.4
3-12-74	0.530	0.00108	8.04	2.85	26.76	17,200	85.8	92.0
3-13-74	0.491	0.00108	9.94	3.58	31.20	20,000	85.5	91.7
7-24-74	0.195	0.00257	6.96	7.63	24.59	23,800	73.0	90.3
10-01-74	0.217	0.00538	8.15	4.04	7.89	12,800	73.1	104.1
10-25-74	0.197	0.00739	7.48	3.92	6.74	13,900	72.0	112.3
10-30-74	0.201	0.00762	7.48	4.06	6.63	13,900	72.0	112.3

Columns 4 and 5 give the relative depth and the velocity ratio. Columns 6 and 7 give the jet densimetric Froude number and the jet Reynolds number, respectively. The ambient and effluent model temperatures for each run are shown in columns 8 and 9.

Background data for the second series of model experiments is presented in Table 6.2. The port diameter was equal to 0.0915 ft for all runs. Table 6.3 gives the values of several parameters for each run. Figure 6.1 shows the values of the velocity ratio U_j/U_a and the relative depth H/D for each experimental run. The run numbers are indicated on the figure. Most of the results for this experimental series are presented in matrices like those shown in Fig. 6.1.

6.2 Comparison of Model and Prototype Results for Single-Port Surveys

The zone-of-passage with respect to the portion of cross-sectional area assigned to one port at each of the downstream sections for the prototype surveys and corresponding model runs are presented in columns 3a and 3b of Table 6.4. This zone-of-passage ZPA is related to the area A_5 enclosed by the 5°F isotherm by the equation

$$ZPA = 100\left(1 - \frac{A_5}{LH}\right) \tag{6.1}$$

The zones-of-passage with respect to the portion of the ambient discharge assigned to one port for corresponding prototype

TABLE 6.2. Background Data for Model Experiments

Run No.	Port Spacing L (ft)	Depth H (ft)	Ambient Velocity U_a (ft/sec)	Ambient Temp. T_a (°F)	Initial Jet Temp. T_E (°F)	Initial Jet Velocity U_j (ft/sec)	Normalized Density Deficit $\Delta\rho/\rho \times 10^3$
(1)	(2)	(3)	(4)	(5)	(6)	(7)	(8)
11	0.667	.475	.074	75.7	97.5	1.66	3.69
12	0.667	.475	.100	85.3	104.7	1.66	3.69
13	0.667	.475	.147	71.6	94.7	1.66	3.69
14	0.667	.475	.258	76.0	97.8	1.66	3.69
15	0.667	.475	.442	86.5	105.8	1.66	3.69
21	0.667	.610	.074	68.5	92.8	1.66	3.69
21a	0.667	.610	.074	73.1	79.6	1.66	0.92
22	0.667	.610	.100	85.0	104.6	1.66	3.69
23	0.667	.610	.147	75.2	97.2	1.66	3.69
23a	0.667	.610	.147	73.3	79.8	1.66	0.92
24	0.667	.610	.258	82.0	102.2	1.66	3.69
24	0.667	.610	.441	85.8	105.1	1.66	3.69
31	0.667	.746	.074	75.4	97.3	1.66	3.69
32	0.667	.746	.100	85.1	104.5	1.66	3.69
33	0.667	.746	.147	74.7	96.8	1.66	3.69
34	0.667	.746	.258	84.2	103.7	1.66	3.69
35	0.667	.746	.441	86.1	105.3	1.66	3.69
41	0.667	.881	.074	75.2	97.2	1.66	3.69
41a	0.667	.881	.074	72.6	79.2	1.66	0.92

TABLE 6.2.—Continued

Run No.	Port Spacing L (ft)	Depth H (ft)	Ambient Velocity U_a (ft/sec)	Ambient Temp. T_a (°F)	Initial Jet Temp. T_E (°F)	Initial Jet Velocity U_j (ft/sec)	Normalized Density Deficit $\Delta\rho/\rho \times 10^3$
(1)	(2)	(3)	(4)	(5)	(6)	(7)	(8)
42	0.667	.881	.100	84.9	104.4	1.66	3.69
43	0.667	.881	.147	75.1	97.1	1.66	3.69
43a	0.667	.881	.147	71.3	78.2	1.66	0.92
44	0.667	.881	.258	84.9	104.4	1.66	3.69
45	0.667	.881	.441	86.8	106.0	1.66	3.69
51	2.0	.501	.030	74.5	96.6	2.03	3.69
52	2.0	.501	.060	75.4	97.3	2.03	3.69
53	2.0	.501	.091	73.8	96.2	2.03	3.69
54	2.0	.501	.181	74.7	96.8	2.03	3.69
55	2.0	.501	.258	74.0	96.3	2.03	3.69
61	2.0	.636	.030	73.5	96.0	2.03	3.69
62	2.0	.636	.060	75.3	97.2	2.03	3.69
63	2.0	.636	.091	73.5	96.0	2.03	3.69
64	2.0	.636	.181	73.0	95.8	2.03	3.69
71	2.0	.772	.030	74.2	96.5	2.03	3.69
72	2.0	.772	.060	75.5	97.4	2.03	3.69
73	2.0	.772	.091	73.6	96.0	2.03	3.69
74	2.0	.772	.181	74.5	96.8	2.03	3.69
75	2.0	.772	.258	83.4	103.1	2.03	3.69
81	2.0	.907	.030	73.5	95.9	2.03	3.69
82	2.0	.907	.060	73.5	97.4	2.03	3.69
83	2.0	.907	.091	73.2	95.9	2.03	3.69
85	2.0	.907	.258	83.3	103.0	2.03	3.69

Note: D = 0.0915 ft.

TABLE 6.3. Dimensionless Parameters for Model Runs

Run No.	Velocity Ratio $k=U_j/U_a$	Relative Depth H/D	Volume Flux Ratio $V=q_a/q_j$	Jet Froude Number $F_j=\frac{U_j}{\sqrt{\frac{\Delta\rho}{\rho}gD}}$	Normalized Fully Mixed Temperature $\frac{\Delta T_m}{\Delta T_E}=\frac{q_j}{q_a+q_j}$
(1)	(2)	(3)	(4)	(5)	(6)
11	22.4	5.19	2.16	15.9	.316
12	16.6	5.19	2.91	15.9	.255
13	11.3	5.19	4.28	15.9	.189
14	6.43	5.19	7.52	15.9	.117
15	3.76	5.19	12.9	15.9	.072
21	22.4	6.66	2.77	15.9	.265
21a	22.4	6.66	2.77	31.8	.265
22	16.6	6.66	3.74	15.9	.211
23	11.3	6.66	5.32	15.9	.158
23a	11.3	6.66	5.32	31.8	.158
24	6.43	6.66	9.66	15.9	.094
25	3.76	6.66	16.5	15.9	.057
31	22.4	8.15	3.39	15.9	.228
32	16.6	8.15	4.58	15.9	.179
33	11.3	8.15	6.73	15.9	.129
34	6.43	8.15	11.8	15.9	.078
35	3.76	8.15	20.2	15.9	.047
41	22.4	9.63	3.99	15.9	.200
41a	22.4	9.63	3.99	31.8	.200

TABLE 6.3.—Continued

Run No.	Velocity Ratio $k=U_j/U_a$	Relative Depth H/D	Volume Flux Ratio $V=q_a/q_j$	Jet Froude Number $F_j = \frac{U_j}{\sqrt{\frac{\Delta\rho}{\rho} gD}}$	Normalized Fully Mixed Temperature $\frac{\Delta T_m}{\Delta T_E} = \frac{q_j}{q_a+q_j}$
(1)	(2)	(3)	(4)	(5)	(6)
42	16.6	9.63	5.40	15.9	.156
43	11.3	9.63	7.94	15.9	.112
43a	11.3	9.63	7.94	31.8	.112
44	6.43	9.63	13.9	15.9	.067
45	3.76	9.63	23.9	15.9	.040
51	67.6	5.47	2.25	19.5	.308
52	33.8	5.47	4.50	19.5	.182
53	22.3	5.47	6.83	19.5	.127
54	11.2	5.47	13.6	19.5	.069
55	7.93	5.47	19.4	19.5	.049
61	67.6	6.94	2.86	19.5	.259
62	33.8	6.94	5.72	19.5	.149
63	22.3	6.94	8.67	19.5	.103
64	11.2	6.94	17.2	19.5	.055
71	67.6	8.43	3.47	19.5	.224
72	33.8	8.43	6.94	19.5	.126
73	22.3	8.43	10.5	19.5	.087
74	11.2	8.43	20.9	19.5	.046
75	7.93	8.43	29.8	19.5	.033
81	67.6	9.91	4.08	19.5	.197
82	33.8	9.91	8.15	19.5	.109
83	22.3	9.91	12.4	19.5	.075
85	7.93	9.91	35.1	19.5	.028

H/D \ U_j/U_a	22.4	16.6	11.3	6.4	3.8
5.2	11	12	13	14	15
6.7	21	22	23	24	25
8.1	31	32	33	34	35
9.6	41	42	43	44	45

3-port series

H/D \ U_j/U_a	67.7	33.8	22.3	11.2	7.9
5.5	51	52	53	54	55
6.9	61	62	63	64	
8.4	71	72	73	74	75
9.9	81	82	83		85

1-port series

Fig. 6.1 Run numbers for different velocity ratios and relative depths.

TABLE 6.4. Comparison of Model and Prototype Results for Single-Port Surveys

Date of Prototype Survey	Distance Downstream from port (ft)	Zone of Passage (Area) (%)		Zone of Passage (Discharge) (%)		Minimum Dilution[a] (%)	
		P	M	P	M	P	M
(1)	(2)	(3a)	(3b)	(4a)	(4b)	(5a)	(5b)
11-16-73	35	99.2	96.5	98.3	93.1	4.7	4.1
	65	100	100	100	100	7.0	7.1
3-12-74	15	97.3	94.5	96.5	94.4	3.1	2.3
	45	99.7	96.3	99.6	96.2	4.3	3.9
		--	100	100	100	--	5.4
3-13-74	35	100	100	100	100	5.3	5.9
	65	100	100	100	100	13.7	10.5
	99	100	100	100	100	16.6	14.9
7-24-74	15	100	96.5	100	89.2	3.10	2.3
	47	100	100	100	100	6.33	5.1
	75	100	100	100	100	8.00	7.0
10-01-74	15	89.5	92.9	86.2	88.4	2.62	2.3
	45	94.4	93.6	91.9	92.7	5.79	5.9
	75	100	100	100	100	9.70	11.4
10-25-74	15	86.1	88.7	81.2	83.7	2.7	2.3
	45	86.7	89.5	81.5	86.9	5.7	7.2
	75	97.5	93.8	97.0	92.8	8.5	8.6
10-30-74	15	87.1	88.7[b]	76.2	83.7[b]	2.5	2.3[b]
	45	87.2	89.5[b]	85.3	86.9[b]	5.8	7.2[b]
	75	98.6	93.8[b]	98.5	92.8[b]	8.9	8.6[b]

[a] Minimum dilution = $\frac{T_E - T_a}{T_{max} - T_a}$.

[b] Used 10-25-74 results.

and model conditions are presented in columns 4a and 4b. The method of determining these values from the prototype data was discussed in section 5.2.3. For the model, the following equation was used:

$$ZPD = 100\left(1 - A_5\bar{U}_5/(Q_F/n + Q_j)\right) \tag{6.2}$$

where

Q_F = total ambient flume discharge

n = 1 for 3-13-74 modeled run and 3 for all other runs

The estimated average velocity through the 5°F isotherm $\bar{U}_5$ was determined from velocity measurements made during each model run.

Columns 5a and 5b give the minimum excess temperature dilution S as determined by the following equation:

$$S = \frac{T_E - T_a}{T_{max} - T_a} \tag{6.3}$$

The agreement between model and prototype results, as presented in Table 6.2, is fairly good; hence, one can conclude with reasonable confidence that model results can be used to predict the zones-of-passage for the entire channel.

The 5°F isotherms as measured in the model are sketched on the appropriate figures in Appendix C with dashed lines. These isotherms are included on Figs. C.1, C.2, C.5, and C.6. The location of the maximum excess temperature as measured in the

model is indicated by a large X in Figs. C.1, C.2, C.4, C.5, and C.6. Since the shapes of corresponding isotherms for adjacent ports are usually quite different, it is not expected that the shapes of the isotherms found in the model would closely match those for the prototype. However, the agreement between model and prototype for the location of the maximum excess temperature at corresponding sections is reasonably good.

6.3 Zones-of-Passage for Entire Channel

Because local depths and ambient velocities vary from port to port, determination of zones-of-passage for the entire river channel requires that mixing zone areas and discharges for each of the 50 ports be determined and then added together. Clearly, the single-port prototype surveys did not include either enough ports in different parts of the channel or a sufficiently detailed coverage over the range of ambient flow and plant operating conditions for such determinations to be made. Consequently, the results of the single-port model experiments, which were designed to provide the required coverage, were used for this purpose. More specifically, the model data were used to develop curves and equations relating the dimensionless ratios A_5/A_j and $\Delta\bar{U}_5/\Delta U_j$ to the dimensionless ratios H/D and U_j/U_a, which were used to estimate values of A_5 and $\bar{U}_5$ for each port as a function of river discharge for the condition of full plant load.

Figure 6.2 shows the variation of mixing zone area, within which ΔT exceeds 5°F, with distance downstream from the port for various combinations of U_j/U_a and H/D. The plots were made dimensionless by using the area and diameter of the ports as scaling factors. Although the simulated 5°F temperature rise isotherms are actually isotherms for a dimensionless temperature rise of 5/23 = 0.217, rather than the actual temperature rise of 5°F, they are called 5°F isotherms herein. At low values of relative submergence and at high velocity ratios, the mixing zones tended to be larger in area and to extend farther downstream than for higher relative submergences and lower velocity ratios. When the normalized fully-mixed temperature rise exceeded 0.217, the 5°F isotherm engulfed the entire measurement section within a short distance downstream from the ports. The normalized fully mixed temperature rise is given by the equation

$$\frac{\Delta T_m}{\Delta T_E} = nQ_j / \left(Q_F + nQ_j \right) \tag{6.4}$$

where

n = number of discharge ports

As can be seen in Table 6.3, $\Delta T_m/\Delta T_E$ exceeded 0.217 only in runs 11, 12, 21, 21a, 31, 51, 61, and 71. The persistence and magnitude of the mixing zones did not vary a great deal for flows with moderate to high relative submergences and moderate to low velocity

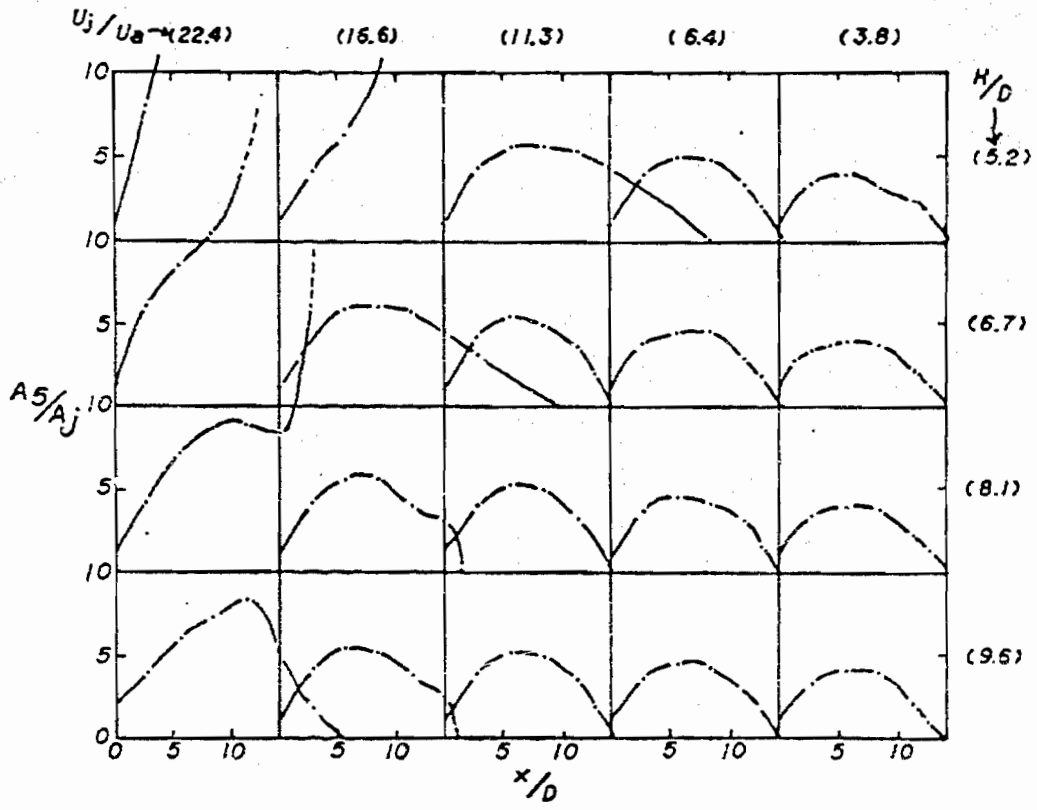

(a) 3-port series

Fig. 6.2 Normalized mixing zone areas versus distance downstream.

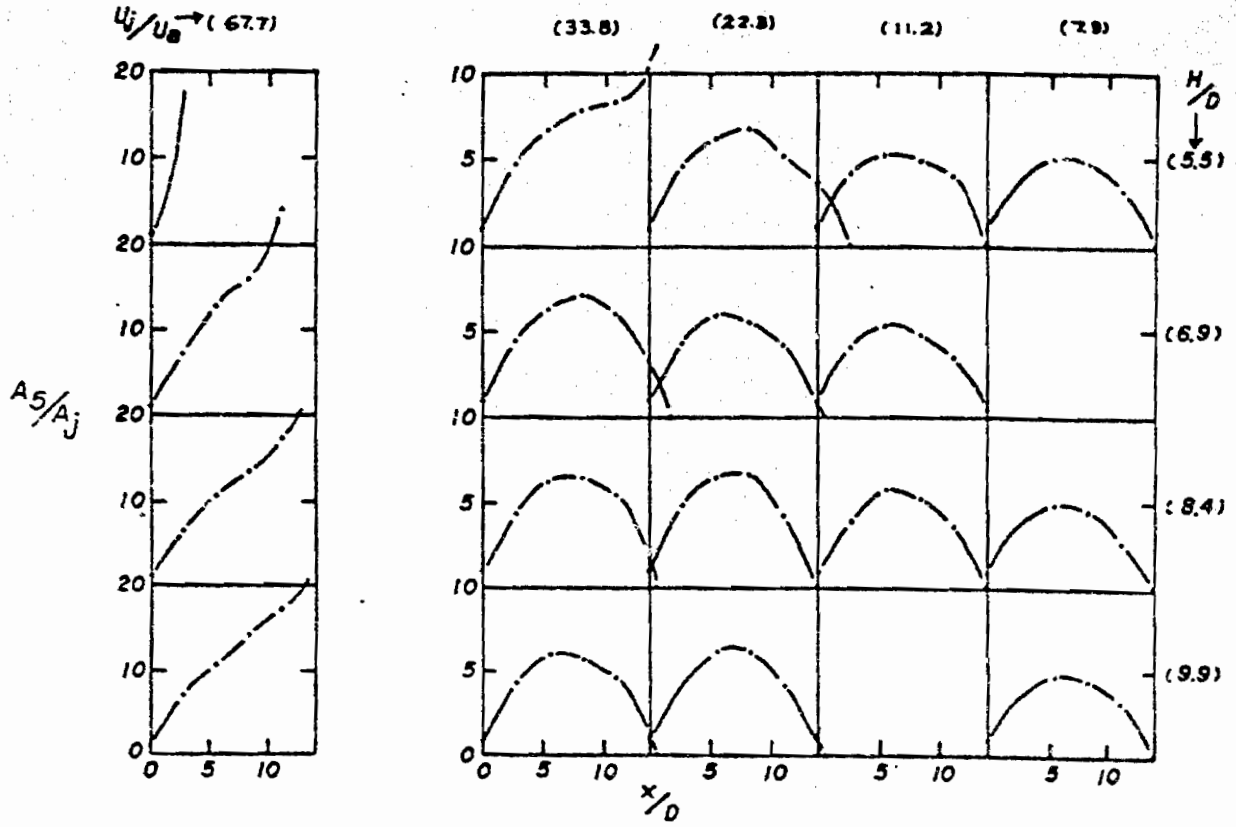

(b) 1-port series

Fig. 6.2 (continued).

ratios (i.e., for moderate to high volume flux ratios). For these conditions, the 5°F isotherms disappeared about 14 jet diameters downstream.

The shape of the 5°F isotherms was nearly elliptical. For the higher velocity ratios, the major axes tended to be oriented vertically; and for the lower velocity ratios they tended to be oriented horizontally, approaching the horseshoe-shape discussed in Chapter 2. Most of the isotherms for the intermediate velocity ratios were approximately circular. Figure 6.3 shows isotherms determined for runs with high, intermediate, and low velocity ratios at a section 8.3 jet diameters downstream from the ports. The areas enclosed by the 5°F isotherms and the areas of corresponding ellipses with principal axes equal to the vertical and transverse widths of the measured isotherms differed by less than 5 percent for most of the experiments.

At each measurement cross section in the model, velocity profiles were measured along the vertical and transverse lines which intersect at the point of maximum temperature rise. Some typical profiles for run number 22 are shown in Fig. 6.4. The excess velocity profiles were approximately Gaussian. Consequently, the excess velocity, due to the jet, was assumed to be distributed according to the bivariate normal distribution with zero correlation, so that the velocity distribution in the section could be represented by the equation

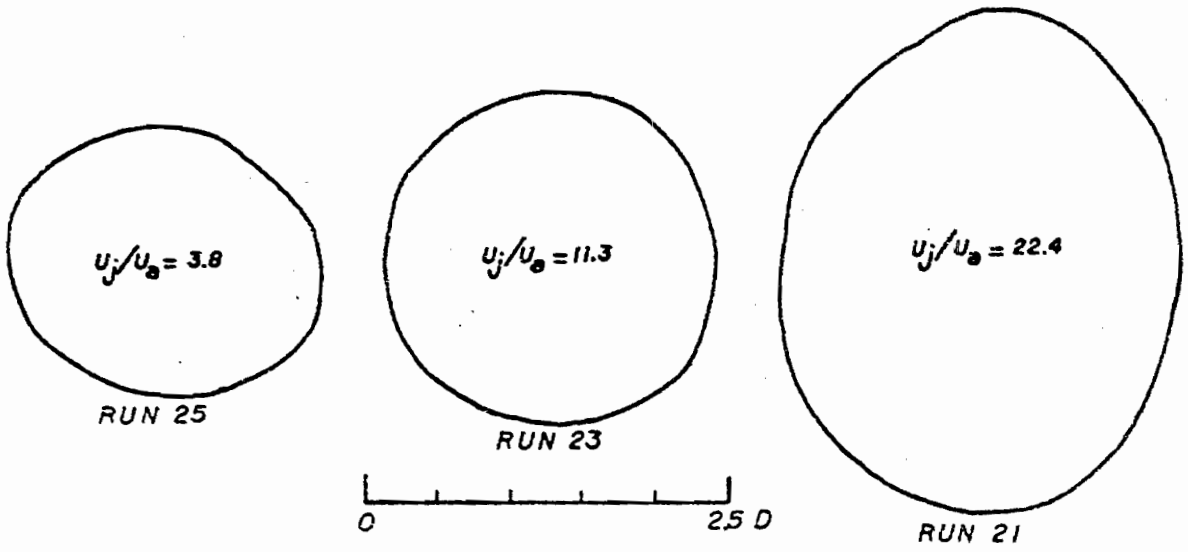

Fig. 6.3 5°F isotherms at a section 8.3 jet diameters downstream from a port.

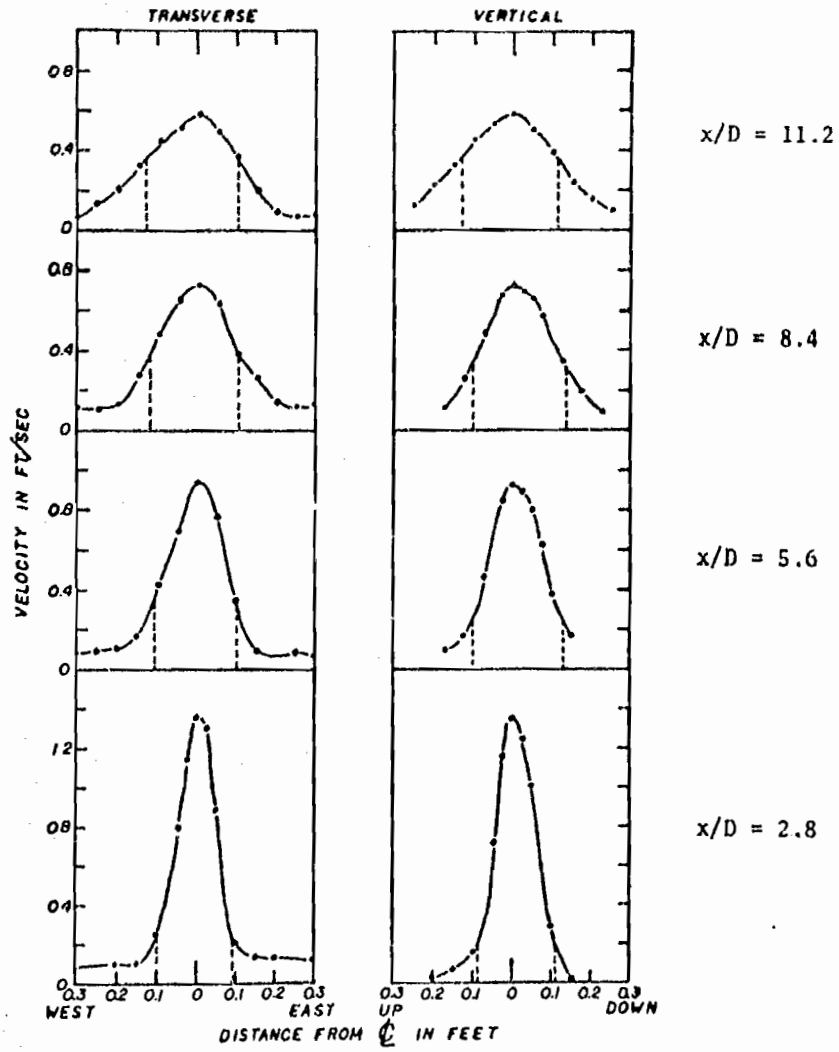

Fig. 6.4 Measured transverse and vertical velocity profiles for run 22.

$$u(y,z) = U_a + \Delta u_{max} \exp\left[-\frac{1}{2}\left(\left(\frac{y}{\sigma_{yV}}\right)^2 + \left(\frac{z}{\sigma_{zV}}\right)^2\right)\right] \qquad (6.5)$$

where

$u(y,z)$ = local velocity

Δu_{max} = maximum excess velocity in section (always at or very close to location of maximum temperature rise)

σ_{yV}, σ_{zV} = standard deviations of vertical and transverse excess velocity distributions, respectively

Since data on the jet trajectories (presented in section 6.4.4) showed that the upward inclination of the trajectories was usually less than 20° from the horizontal and cos 20° = 0.94, the magnitudes of the horizontal velocity components were assumed to be equal to the measured magnitudes of the total velocity vectors. According to Eq. (6.5), the transverse distributions of Δu at any y and the vertical distribution of Δu at any z are also Gaussian.

The solid curves passing through the data points in Fig. 6.4 were drawn by eye. The vertical dashed lines represent the corresponding transverse and vertical widths of the 5°F isotherms. The estimated standard deviations for the excess velocity distributions were determined so that the distributions predicted by Eq. (6.5) matched the measured velocity profiles at the peaks and at the edges of the 5°F isotherms (i.e., in Fig. 6.4, at the peaks and at the points where the dashed lines meet

the velocity profiles). The standard deviation σ_{zV} of the transverse distribution was estimated from the relationship

$$\sigma_{zV} = \frac{z_5}{\sqrt{-2 \ln R}} \tag{6.6}$$

where

Z_5 = half width of the measured 5°F isotherm

R = ratio of the average of the excess velocity at the transverse edges of the 5°F isotherm to the maximum excess velocity within the isotherm

An equation of the same form was used to estimate the vertical standard deviation σ_{yV}.

The average velocity within a modeled 5°F isotherm was determined by numerically integrating the velocity distribution given by Eq. (6.5) over the area of an ellipse with axes equal to the vertical and transverse isotherm widths. The total discharge within the isotherm was then determined from the equation

$$Q_5 = \int_{A_5} u \, dA = A_5 \bar{U}_5 \tag{6.7}$$

where

$\bar{U}_5$ = average velocity within the 5°F isotherm

It includes both the ambient and the excess velocity components. Figure 6.5 shows dimensionless discharge within the 5°F isotherms for the three-port and one-port series, respectively. As would be expected, these Q_5 curves vary with velocity ratio and relative

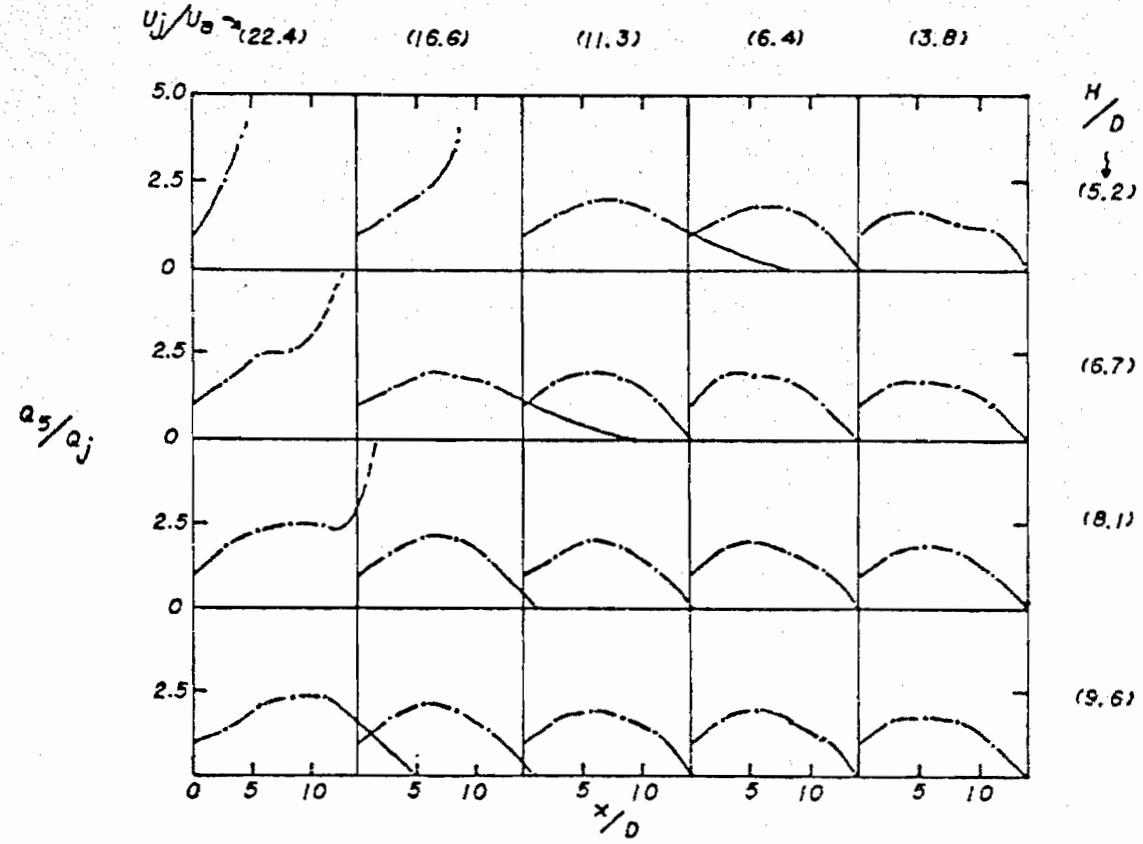

(a) 3-port series

Fig. 6.5 Normalized discharge within 5°F isotherms.

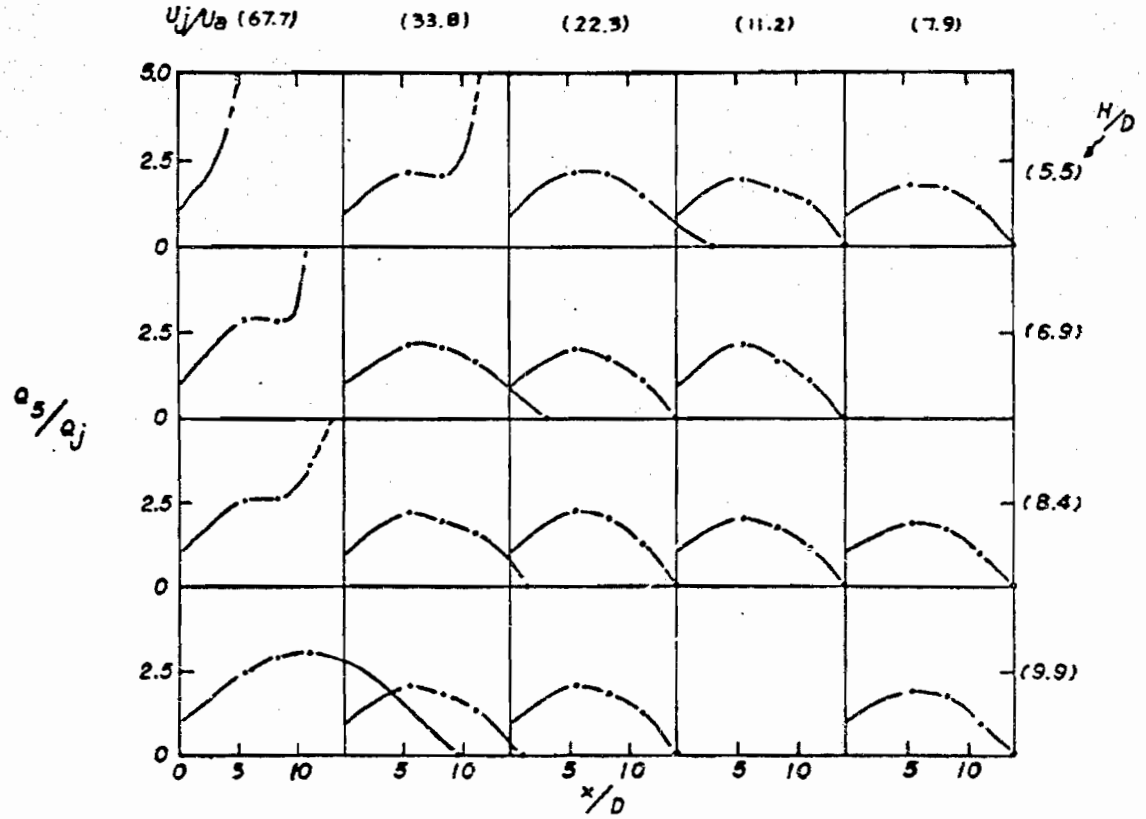

(b) 1-port series

Fig. 6.5 (continued).

depth in a manner that is very similar to the variation of the A_S curves in Fig. 6.2.

Zone-of-passage with respect to area for the entire river cross section was not determined since the zone-of-passage with respect to discharge is always smaller, and, hence, is the limiting restriction when velocities within the 5°F isotherms are greater than the ambient velocity. The method for determining zone-of-passage with respect to discharge for various Mississippi River flows using Fig. 6.5 will now be discussed. A similar method could be used together with Fig. 6.2 to determine the zone-of-passage with respect to the total cross-sectional area of the river.

Zones-of-passage with respect to river discharge at different distances downstream from the centerline between the two diffuser pipes were determined by the following equation:

$$ZPRD(x) = 100 \left[1 - \frac{1}{Q_R} \left(\sum_{i=1}^{25} Q\,(i, x - 15.6) + \sum_{j=1}^{25} Q\,(j, x + 4.4) \right) \right] \tag{6.8}$$

where

x = distance downstream from the centerline between the diffuser pipes

i = ith port from the Illinois shore on the short diffuser pipe which is located 10 ft downstream from the centerline between the two pipes

j = jth port from the Illinois shore on the long diffuser pipe which is located 10 ft upstream from the centerline between the two pipes

$Q_S(i,x)$ and $Q_S(j,x)$ = discharges obtained from Fig. 6.5 given local ambient and effluent flow conditions for ports on the short and long pipes, respectively

The depth corresponding to each port was obtained from the bottom profile shown in the diffuser pipe construction blueprints. The local ambient river velocity for a given river discharge at each port was determined from the depth profile and the appropriate ambient river discharge distribution as measured by IIHR staff at the section 200 ft upstream from the centerline between the two pipes. No ambient river discharge distributions were measured for flows below 20,000 cfs. Therefore, the normalized ambient discharge distribution shown in Fig. 5.13 for the July 23, 1974, when the Mississippi River discharge was 22,200 cfs, was used for discharges of 20,000 cfs or less. Since the curves in Fig. 6.5 vary with x, Eq. (6.8) was evaluated at several distances downstream from the centerline of the two pipes for each river discharge calculation. The zone-of-passage for a specific river discharge was then taken to be the value at the downstream section where Eq. (6.8) was minimum.

Fig. 6.6 shows the minimum zones-of-passage with respect to river discharge as defined by Eq. (6.8). Based on the model results, the standard for 75 percent zone-of-passage with respect to discharge would be violated at river discharges below 15,300 cfs, as indicated by the dashed lines in Fig. 6.6.

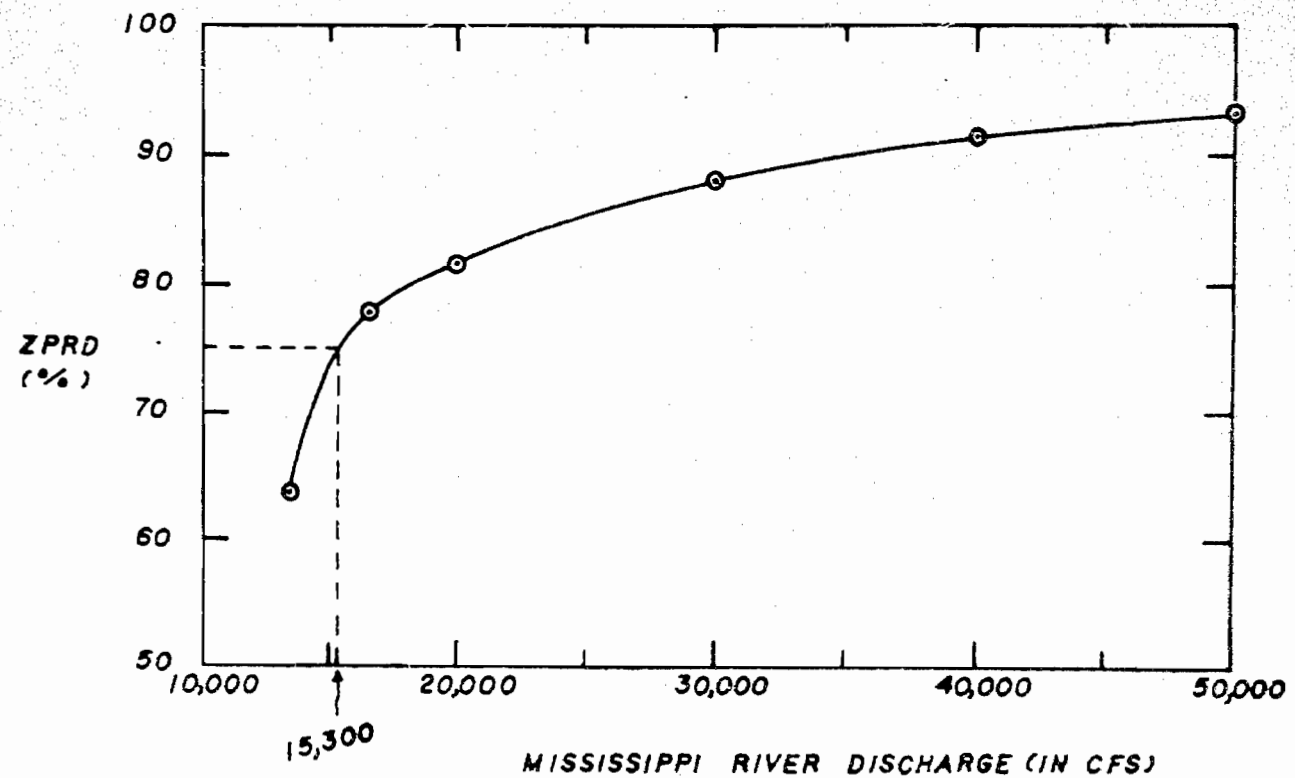

Fig. 6.6 Minimum zone-of-passage with respect to total river discharge.

6.4 Jet Characteristics

6.4.1. Zone of Flow Establishment

Temperatures and velocities were measured in planes normal to the jet trajectory from the efflux section to a section 2.7 jet diameters downstream to determine excess temperature and the jet velocity distributions in the region just downstream from the port for run numbers 31 and 33.

Figure 6.7 shows normalized excess temperature profiles for vertical profiles 0.55, 1.10, 1.60, 2.20, and 2.7 jet diameters downstream for run number 33. The orientation of the profiles shown in the figure is arbitrary. The results show that excess temperature distribution becomes established and approximates a Gaussian distribution within 1 jet diameter downstream. Similar results were obtained for run number 31, although the normal fit was not quite as good at the tails of the profile. Transverse profiles very close to the port were not measured.

Velocity profiles were obtained at the same sections in the same runs. Some typical vertical normalized excess velocity profiles are also shown for run number 33 in Fig. 6.7. These data represent resultant velocities, not horizontal components. The velocity distribution was not uniform at the efflux section. The efflux velocity at the top of the jet was about twice as great as the velocity at the bottom and was about 25 percent greater than the mean jet velocity $U_j = Q_j/A_j$. The maximum measured

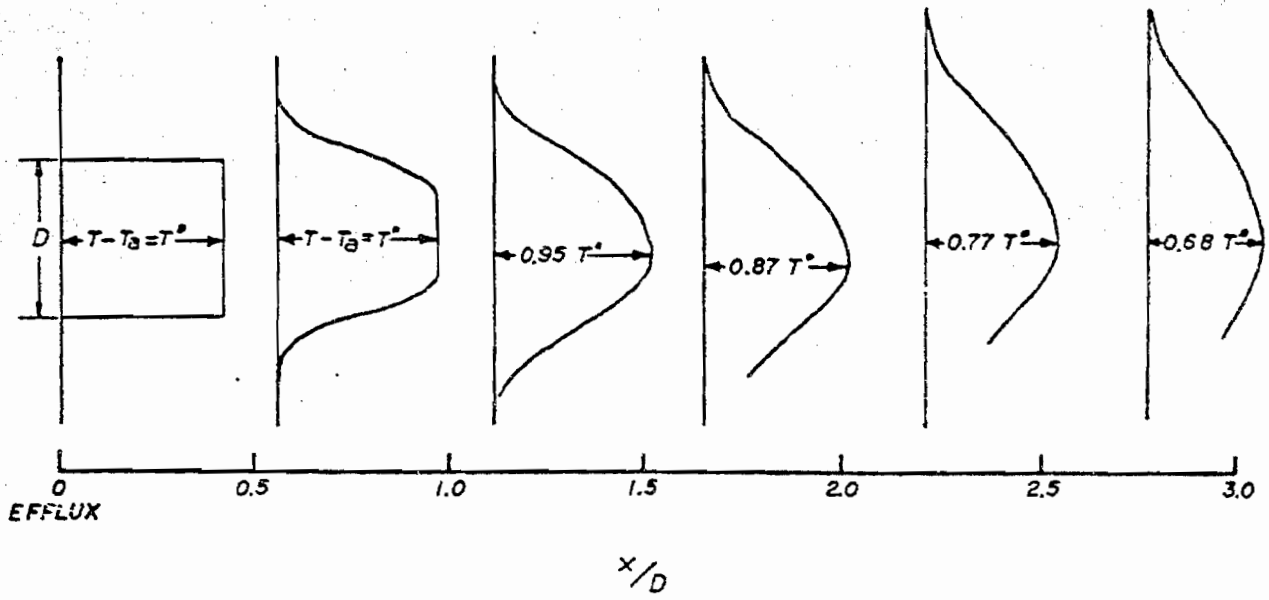

(a) Temperature

Fig. 6.7 Normalized excess temperature and velocity profiles just downstream from a port.

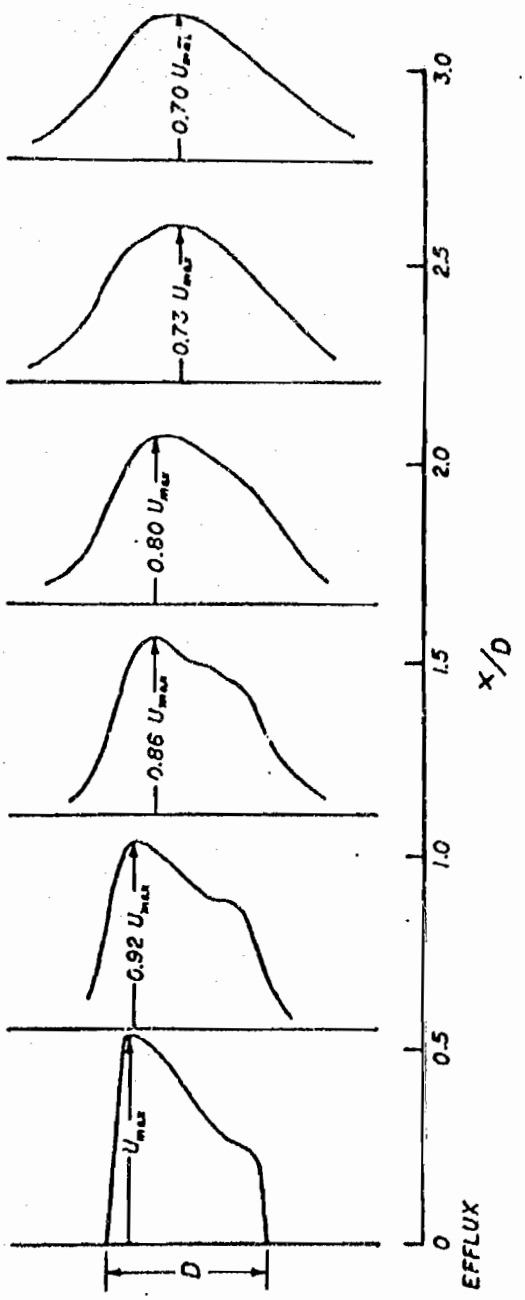

(b) Velocity

Fig. 6.7 (continued).

velocity equaled the mean jet velocity about 1.5 jet diameters downstream. The transverse distribution of velocity matched a normal distribution fairly well about 2 jet diameters downstream; however, the vertical distribution at the same section was still skewed toward the bottom. For run number 31 with the velocity ratio equal to 22.4, the vertical profile at the furthest downstream section was even more skewed. The positions of the maximum temperature and velocity coincided at sections beyond about 3 jet diameters downstream from the efflux section.

6.4.2. Centerline Dilution

The point of minimum excess temperature dilution at any section is the point in the section with the maximum normalized excess temperature. These points occur along the centerline or trajectory of the jet. Figure 6.8 shows the centerline temperature dilutions at most of the downstream sections obtained in both the one-port and three-port series of experiments. The curves in Fig. 6.8 characteristically show a linear increase of $(T_E - T_a)/(T_{max} - T_a)$ at low values of x/D, followed by a gradual leveling off as the limiting fully-mixed dilution, $\Delta T_E/\Delta T_m$, is approached. This asymptotic limit is shown as a dashed line for some of the shallow-water runs in the three-port series. Since a dilution of 4.6 corresponds to a model temperature rise of 5°F, the 5°F isotherm disappears when the centerline dilution exceeds 4.6. Part (c) of Fig. 6.8 compares the minimum excess temperature

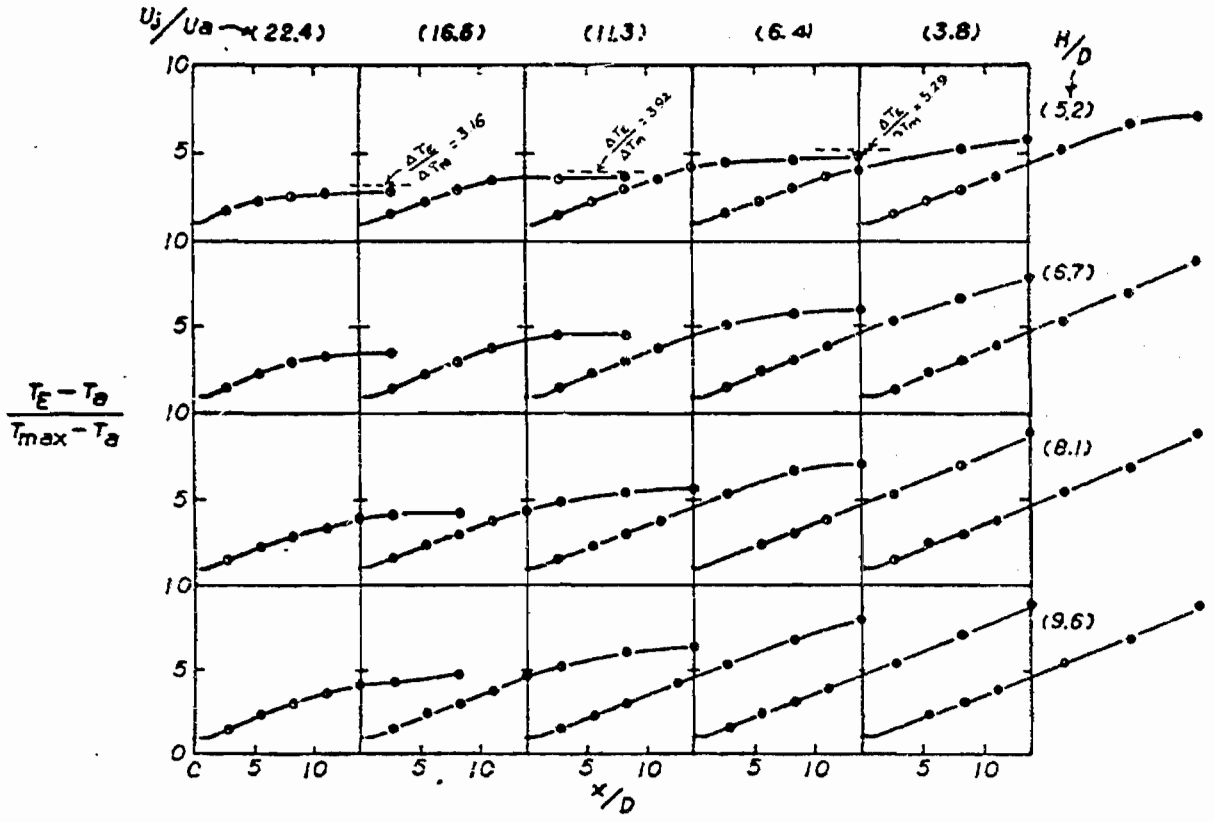

(a) 3-port series

Fig. 6.8 Centerline excess temperature dilution versus distance downstream.

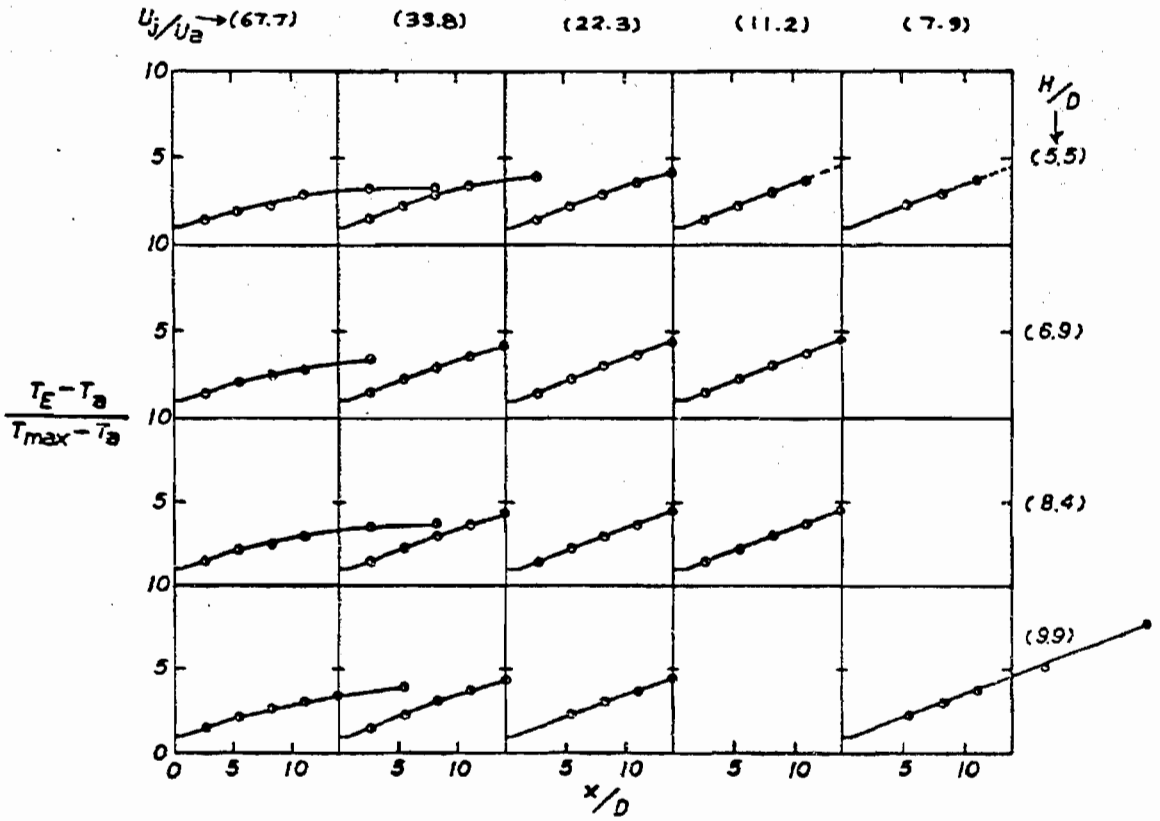

(b) 1-port series

Fig. 6.8 (continued).

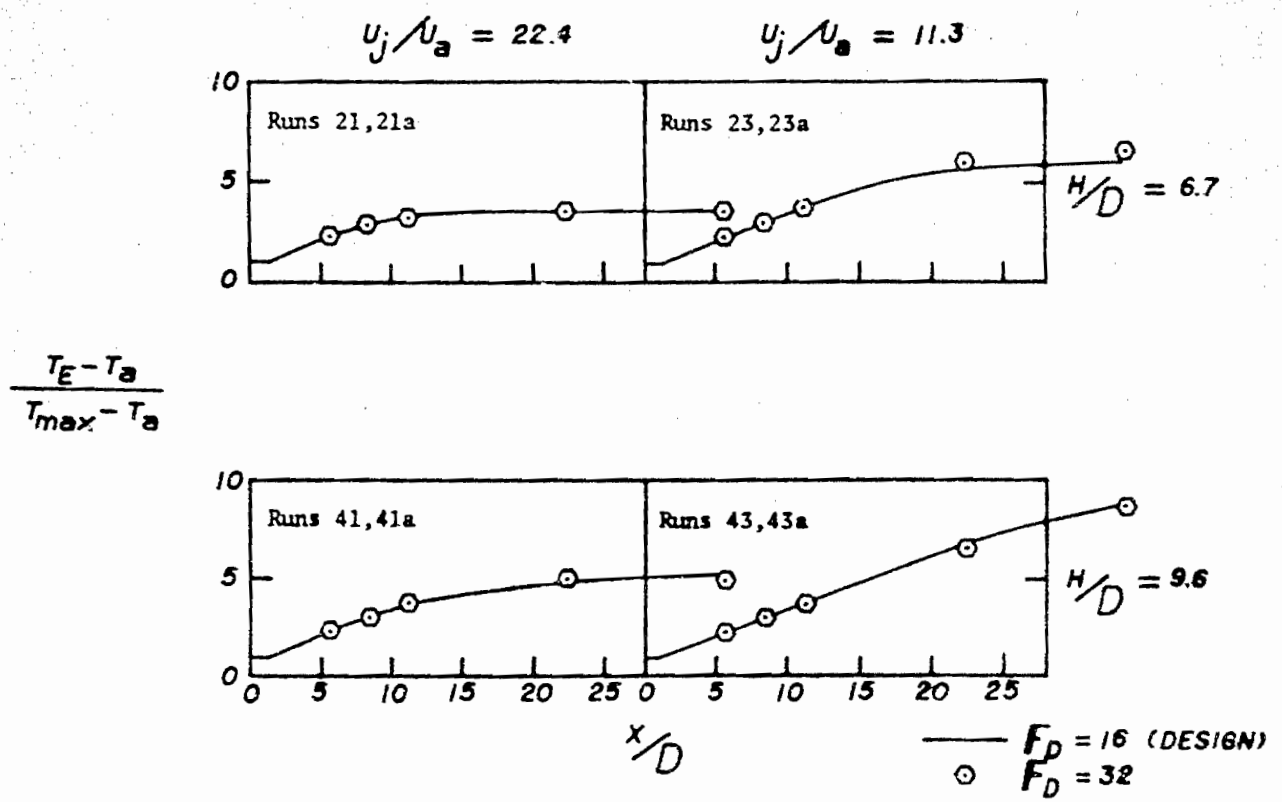

(c) 3-port runs for different Froude numbers

Fig. 6.8 (continued).

dilution for runs 21, 21a, 23, 23a, 41, 41a, 43, and 43a. These results indicate that in the region close to the ports doubling the Froude number by reducing the initial density difference has little effect on dilution rates.

Figure 6.9 presents the minimum excess temperature dilutions at all downstream sections for all the runs in generalized form. The abscissa is the distance downstream, x, divided by the product of the jet diameter D and the ratio V + 1, of the ambient plus jet discharge to the jet discharge. The ordinate is the measured minimum excess temperature dilution $(T_E - T_a)/(T_{max} - T_a)$ divided by the normalized fully mixed excess temperature dilution $\Delta T_E/\Delta T_m$. Part (a) of Fig. 6.9 shows the three-port results. For all runs except 11, 12, 13, 14, 15, 24, and 25, the plotted points follow the solid curve shown on the figure. The curve was estimated by eye. The runs for which the plotted points "peeled off" from the solid curve had shallow receiving water depths, suggesting that surface and bottom interaction probably retarded the dilution process. High values of the ratio of fully mixed excess temperature dilution $\Delta T_E/\Delta T_m$ to relative submergence (H - h)/D are characteristic of those runs. Part (b) of Fig. 6.9 shows the one-port results. The solid curve estimated from the data points in part (a) is also shown on part (b). The plotted points in part (b) follow the solid curve until reaching an ordinate value of about 0.6 where the points veer from the curve. All of the runs

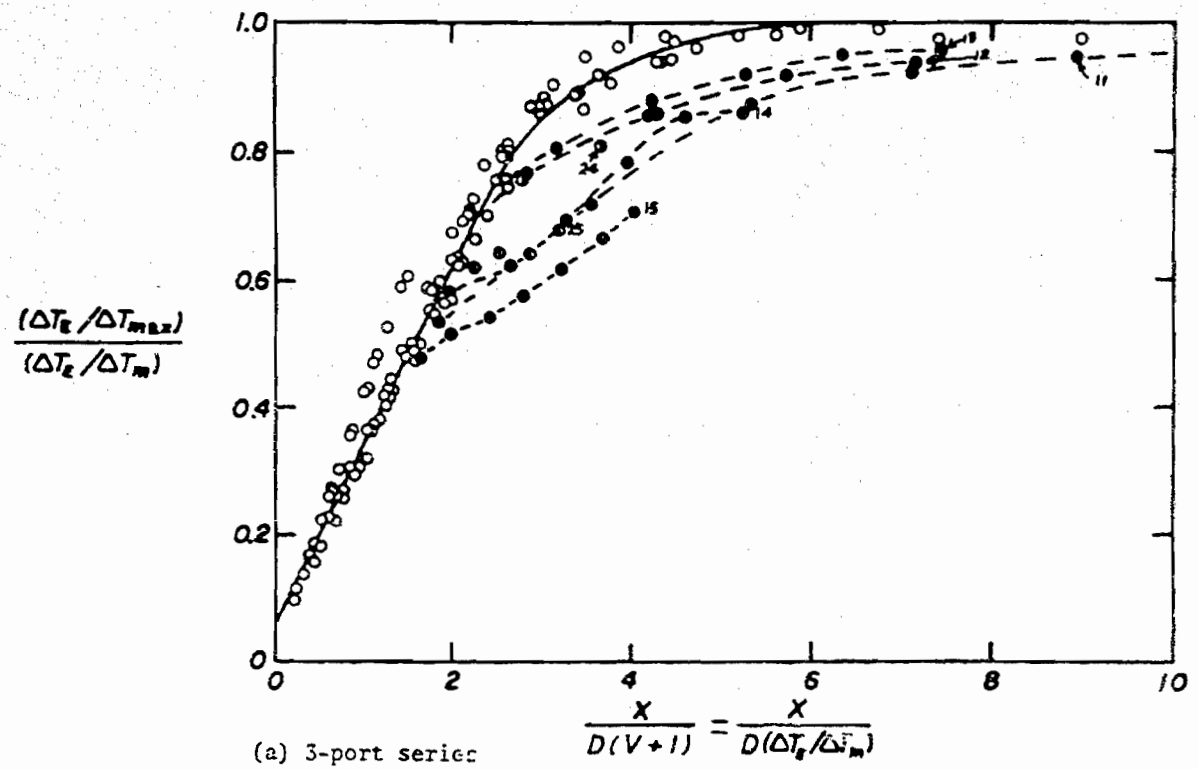

(a) 3-port series

Fig. 6.9 Generalized minimum excess temperature dilutions.

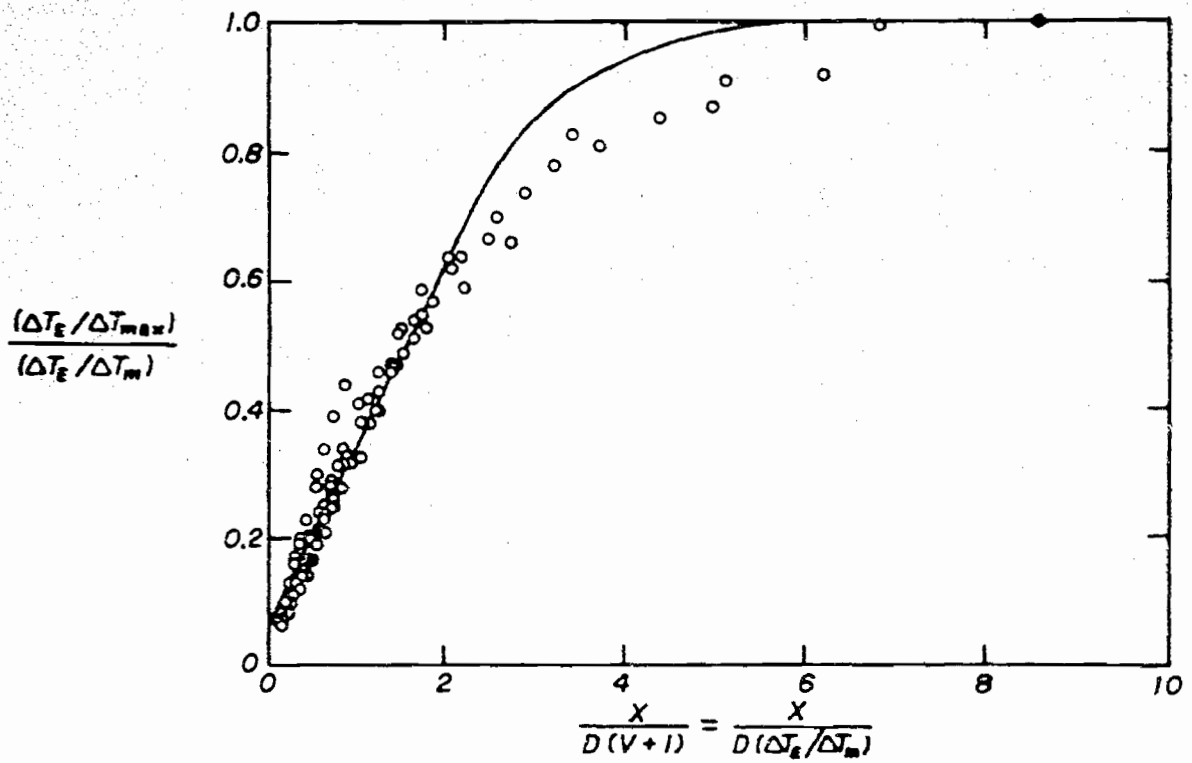

(b) 1-port series

Fig. 6.9 (continued).

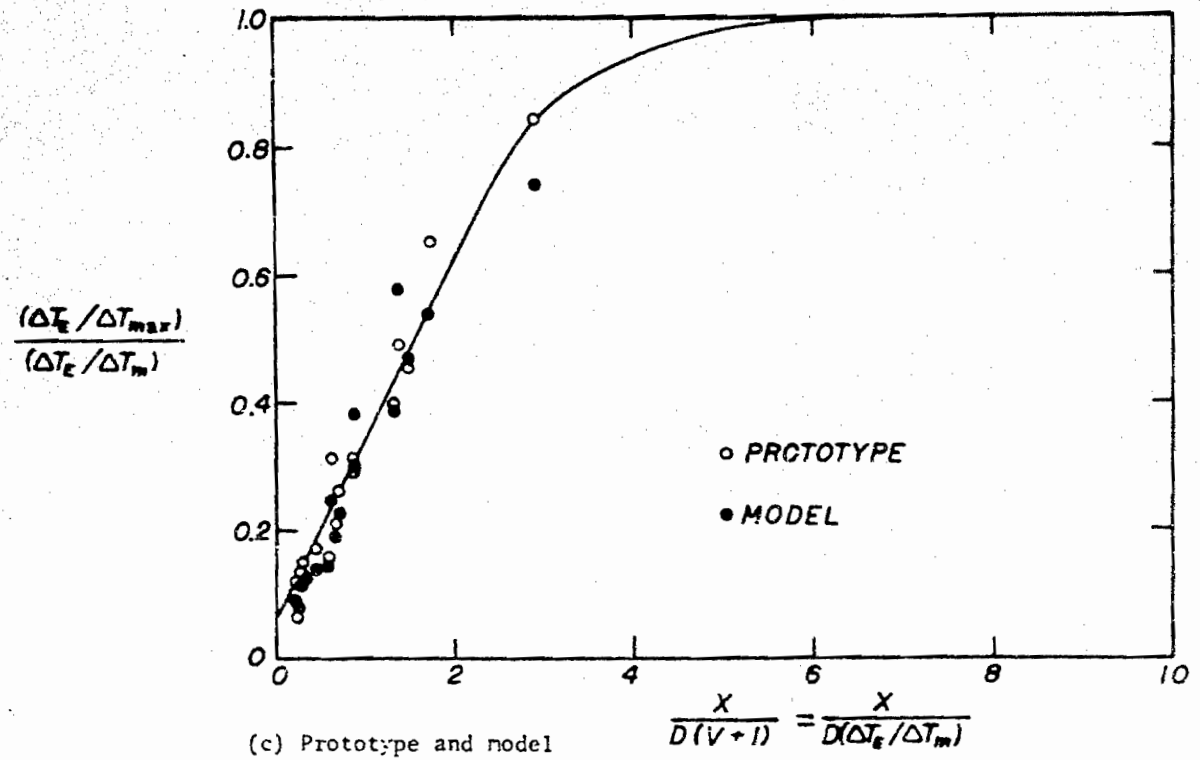

(c) Prototype and model

Fig. 6.9 (continued).

(51, 52, 61, 62, 71, 81) in the one-port series for which ordinate values above 0.6 were obtained are characterized by relatively low values of $\Delta T_E/\Delta T_m$ and/or H/D. This, together with the larger spacing between ports in the one-port series, evidently gave rise to surface and/or bottom interactions which increased the work of entrainment, resulting in a retardation of the later stages of dilution. Part (c) of Fig. 6.9 shows results of the single-port prototype surveys and the corresponding model runs together with the same solid curve shown in parts (a) and (b). The agreement is quite good.

In the range $x/D(V + 1) < 2$, the curves in Figs. 6.8 and 6.9 can be represented by the linear relationship

$$\frac{T_E - T_a}{T_{max} - T_a} = 0.28 \frac{x}{D} + 0.7 = 0.28 \left(\frac{x}{D} + 2.5\right) \qquad (6.9)$$

The coefficient 0.28 in Eq. (6.9) agrees fairly closely with the coefficient 0.32 in Eq. (2.1) for the average dilution in terms of discharge for a momentum jet in a quiescent fluid of infinite extent. The agreement would be better if the distance in Eq. (6.9) were measured along the jet trajectory instead of horizontally; assuming a trajectory angle of 20° the coefficient in Eq. (6.9) would then be 0.30. The value of the x intercept, -2.5D, corresponds closely to the location of the 70° bend in the discharge port, suggesting that the bend essentially eliminates the zone of flow establishment and contributes to increased initial mixing.

6.4.3. Maximum Excess Velocity

For easy comparison, ratios of initial to maximum excess velocity, $(U_j - U_a)/(U_{max} - U_a)$, along the jet centerline are plotted as a function of x/D in Fig. 6.10 in the same manner as the excess temperature dilution in Fig. 6.8 Over the range of x/D covered by the data, data for all runs can be represented by the linear relationship

$$\frac{U_j - U_a}{U_{max} - U_a} = S_u\left(\frac{x}{D}\right) + I_u \qquad (6.10)$$

The slopes S_u of the lines in Fig. 6.10 are related to the rates of excess center-line velocity reduction. For the three-port experimental runs shown in part (a) of Fig. 6.10 S_u varies from about 0.18 to 0.29 depending on the velocity ratio U_j/U_a and the relative depth H/D. Figure 6.11 shows S_u plotted as a function of velocity ratio U_j/U_a. The data define a family of curves with H/D as the third variable. Apparently surface interaction increases the excess velocity reduction for relative depths H/D below a value somewhere between 6.7 and 8.1. Figure 6.11 shows that this surface effect is reduced as U_j/U_a decreases. The smallest slope of 0.18 was observed at the highest relative velocity of 22.4. This value of S_u can be compared to the experimentally determined coefficient in the equation (corresponding to Eq. (6.10))

$$\frac{U_j}{U_{max}} = 0.16\,\frac{x}{D} \qquad (6.11)$$

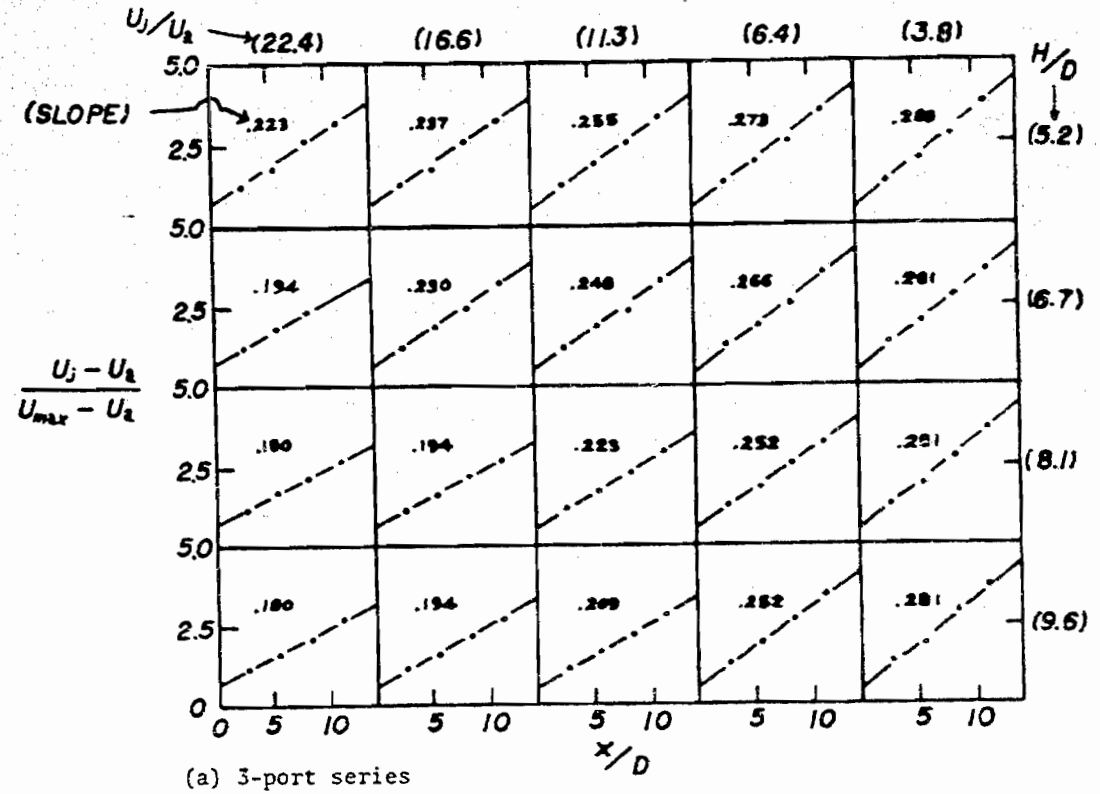

(a) 3-port series

Fig. 6.10 Ratios of initial to maximum excess velocity along centerline of jet.

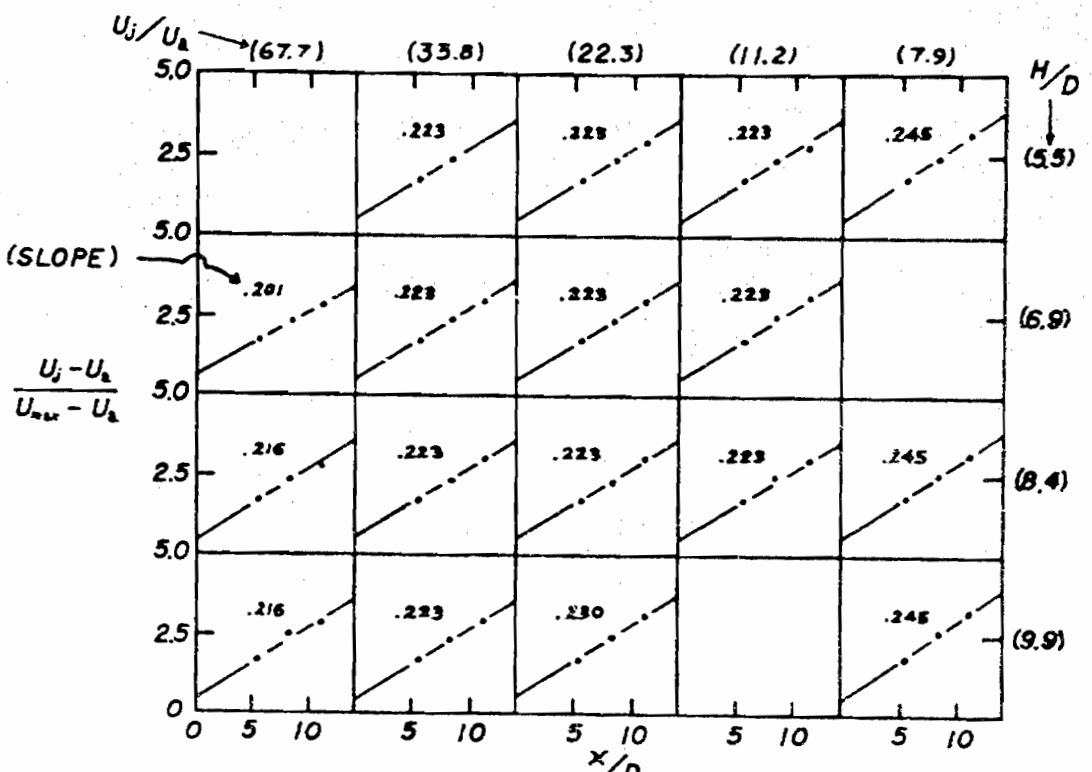

(b) 1-port series

Fig. 6.10 (continued).

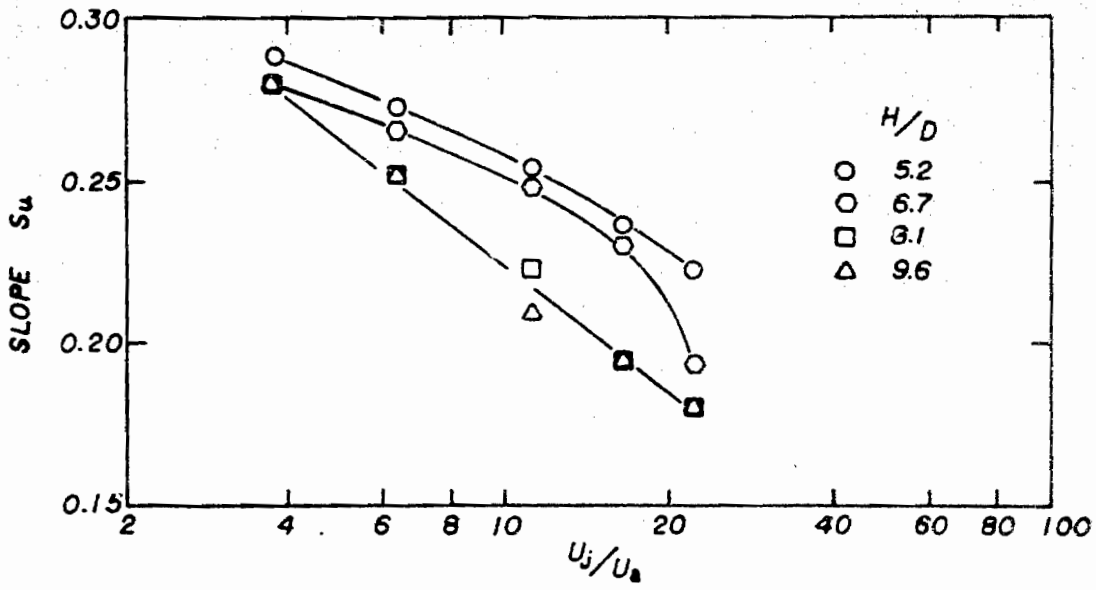

Fig. 6.11 Slopes of curves for 3-port series in Fig. 6.10.

given by Albertson et al. (1950) for a round momentum jet discharging into a quiescent fluid $(U_j/U_a = \infty)$ in the zone of established flow. Variation of S_u with velocity ratio U_j/U_a and relative depth H/D is not as pronounced for the one-port data shown in part (b) of Fig. 6.10 as for the three-port results. With the exception of the data set for $U_j/U_a = 7.9$, a slope of 0.22 fit all data from the one-port experiments reasonably well. For the runs with $U_j/U_a = 7.9$, $S_u = 0.25$ provided a better fit. These results are generally consistent with those shown in Fig. 6.11 for the three-port studies.

Three of the single-port prototype surveys for the main channel diffuser ports were performed when effluent flow conditions were approximately equal to design conditions. Values of S_u determined from these surveys are shown in Table 6.5. They compare reasonably well with the results given in Fig. 6.11 for the three-port model studies as regards both the magnitude of the S_u values and the trend.

A similarity relationship, analogous to the one in Fig. 6.9 for centerline temperature dilution, may exist for centerline velocity reduction. However, velocity measurements were not obtained sufficiently far downstream to determine if it does. The value of the ordinate intercept I_u in Eq. (6.10) varies only between 0.5 and 0.7. Because of the variation in S_u, the x intercept, $-I_u D/S_u$, would vary from about -2D to -4D.

TABLE 6.5. Rate of Centerline Excess Velocity Reduction for Single-Port Prototype Surveys

Date	Velocity Ratio U_j/U_a	Relative Depth H/D	Slope S_u
11-16-73	4.80	8.67	0.29
3-12-74	2.85	8.04	0.28
7-24-74	7.63	6.96	0.25

Comparison of Figs. 6.8 and 6.10, and Eqs. (6.9) and (6.10), shows that excess temperature and excess velocity along the jet centerline attenuate in a similar manner during the early stages of mixing. For low values of the velocity ratio U_j/U_a, the initial growth of the normalized reciprocal maximum excess temperature $(T_E - T_a)/(T_{max} - T_a)$ and velocity $(U_j - U_a)/(U_{max} - U_a)$, are nearly identical. As the velocity ratio increases above about $U_j/U_a = 6$, however, $(U_j - U_a)/(U_{max} - U_a)$ grows more slowly with respect to x/D, indicating a slower reduction in excess velocity along the centerline.

6.4.4. Jet Spreading

To characterize the spreading of the jets, data on the transverse and vertical standard deviations of both excess temperature and excess velocity distributions in cross-sectional

planes downstream from the diffuser ports are presented in this section. These cross-sectional planes were oriented normally to the flume, not the jet axis. The profiles, for which the standard deviations were estimated by the method of Eq. (6.6), were taken along the transverse and vertical axes of a cross-sectional plane whose origin was located at the point of maximum excess temperature in the plane.

Estimated standard deviations σ_{zT} and σ_{yT} of the excess temperature profiles, are shown in Fig. 6.12 as functions of x/D for both the one-port and three-port series. For all three-port and one-port runs in the three right hand columns of both parts (a) and (b) of Fig. 6.12 and for runs 32 and 42, the equation

$$\frac{\sigma_T}{D} = 0.5 + 0.086 \frac{x}{D} \tag{6.12}$$

provides a good fit to the data for transverse standard deviation of excess temperature. Although the data for the vertical standard deviation tends to scatter more, Eq. (6.12) fits it reasonably well also. The only systematic exception was for the three-port runs with velocity ratio k equal to 3.8. For these runs, the rate of vertical spreading of excess temperature was appreciably smaller than the rate of transverse spreading. This was previously discussed in section 6.3.

Curves for the one-port runs with velocity ratio U_j/U_a of 33.8 had a slope of about 0.11. The curves for runs with low volume

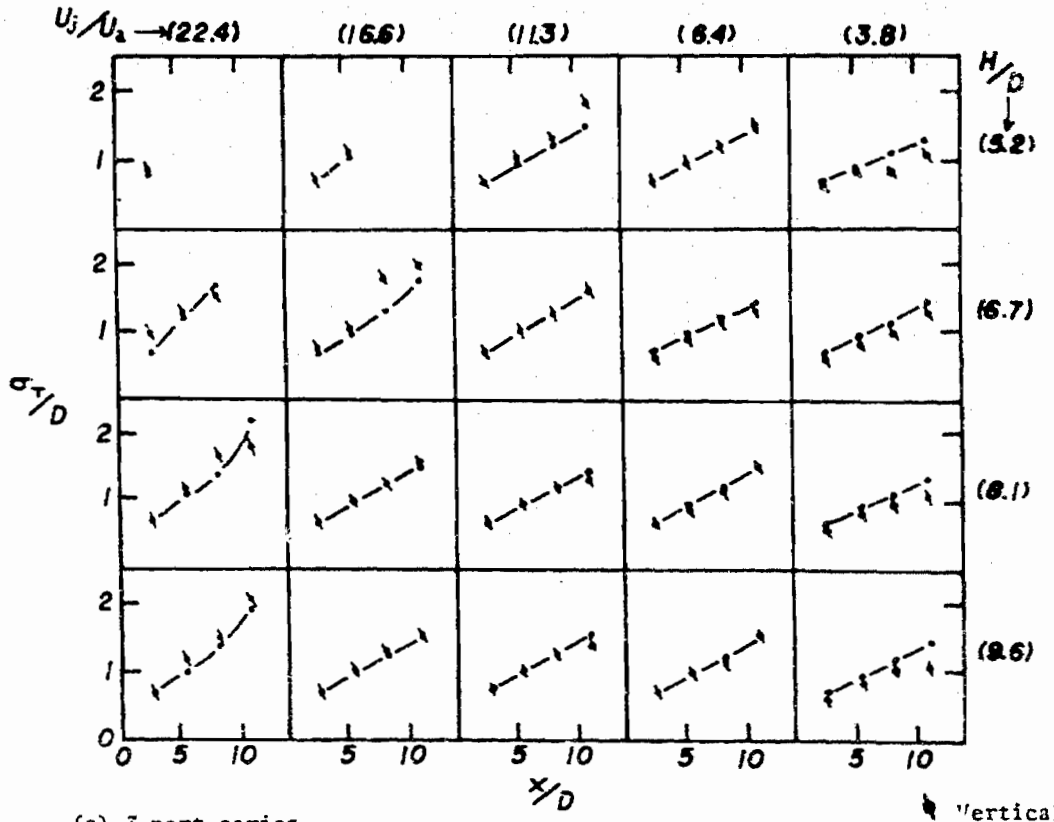

(a) 3-port series

Fig. 6.12 Estimated standard deviations of vertical and transverse temperature distribution.

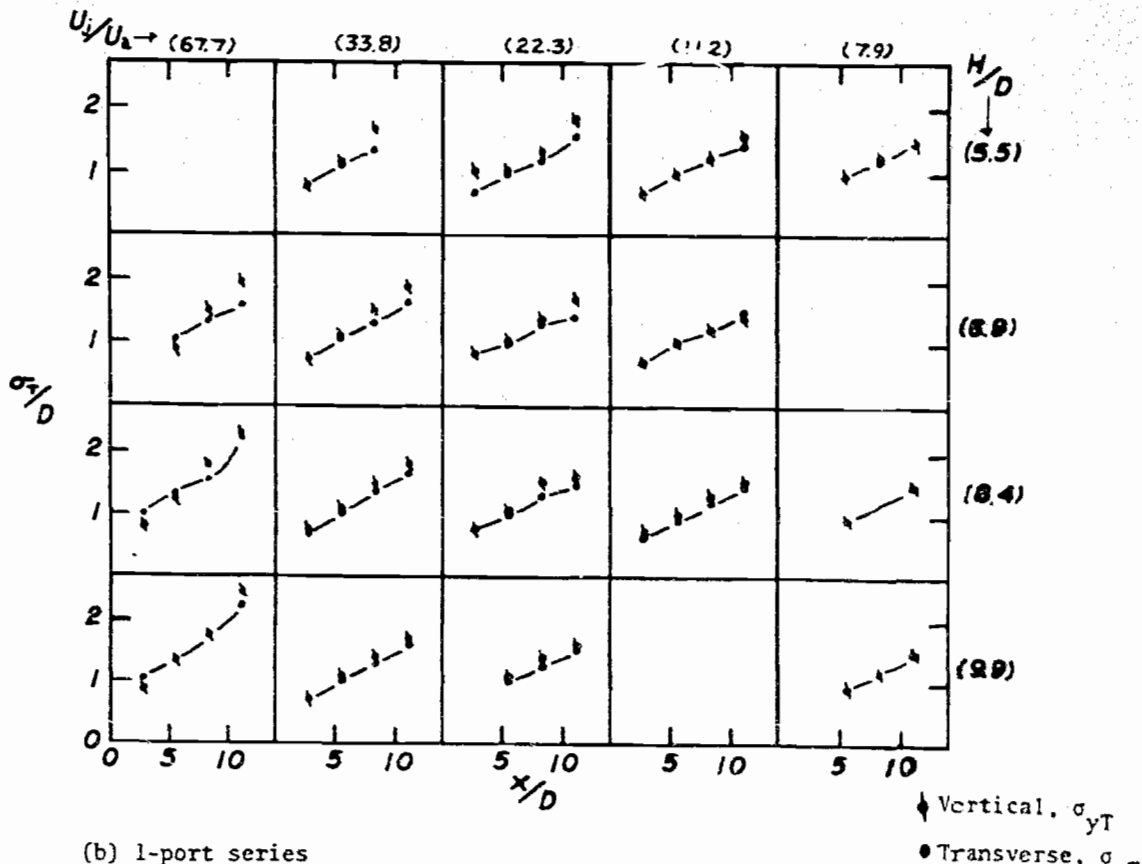

(b) 1-port series

Fig. 6.12 (continued).

flux ratios sloped upward rapidly due to the rapid increase in the standard deviation as complete mixing was approached.

Figure 6.13 shows the estimated transverse and vertical standard deviations σ_{zV} and σ_{yV} of the excess velocity profiles such as described in section 6.2. The data in Fig. 6.13 can be fitted roughly by the equation

$$\frac{\sigma_V}{D} = 0.25 + 0.076 \frac{x}{D} \tag{6.13}$$

The only obvious trend is the retarded rate of excess velocity spreading for three-port runs with low velocity ratios. There is too much scatter in the data to establish whether there is quantitative dependence on any of the flow parameters.

As shown in Eqs. (6.12) and (6.13), the ratios of the rate of excess temperature spreading to excess velocity spreading was approximately 1.13. This value was obtained by dividing the slope in Eq. (6.12) by the slope in Eq. (6.13). The equation for a round momentum jet discharging into a quiescent fluid, Albertson et al. (1950), that corresponds to Eq. (6.13) is

$$\sigma_V = 0.081\ x \tag{6.14}$$

6.4.5. Jet Trajectories

Figure 6.14 shows the centerline trajectories of the jet where the centerline at each section was located at the point of

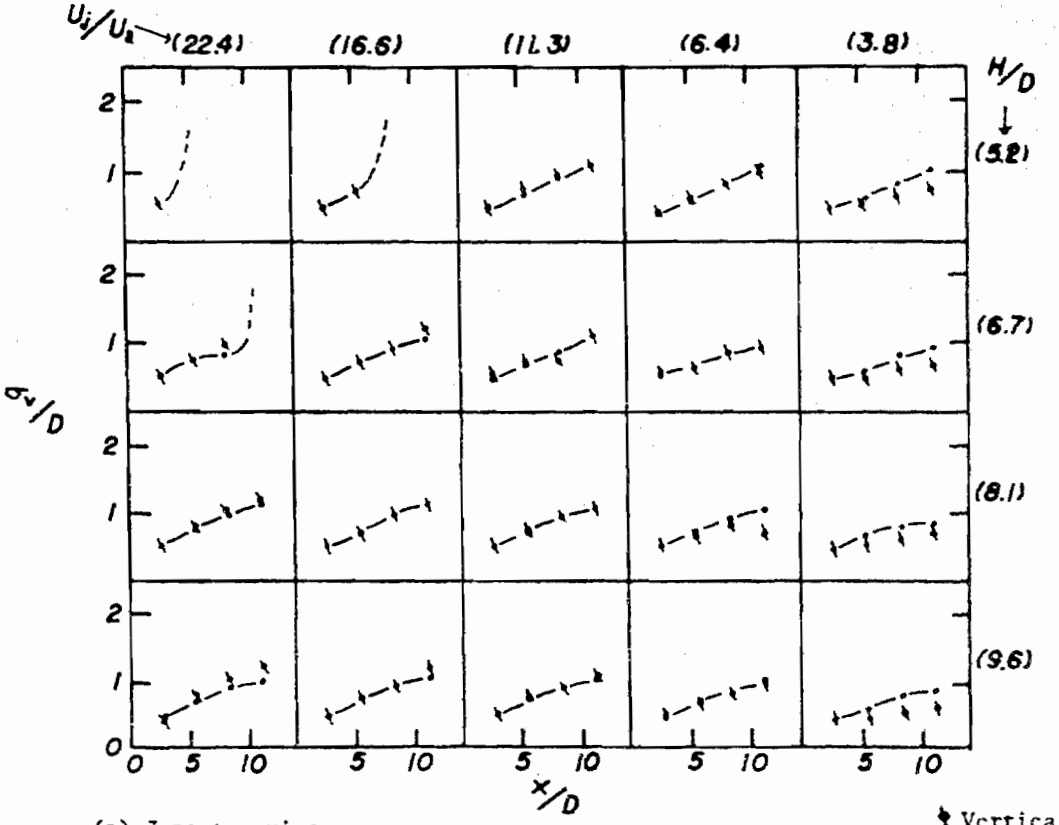

(a) 3-port series

Fig. 6.13 Estimated transverse and vertical standard deviations of excess velocity distribution.

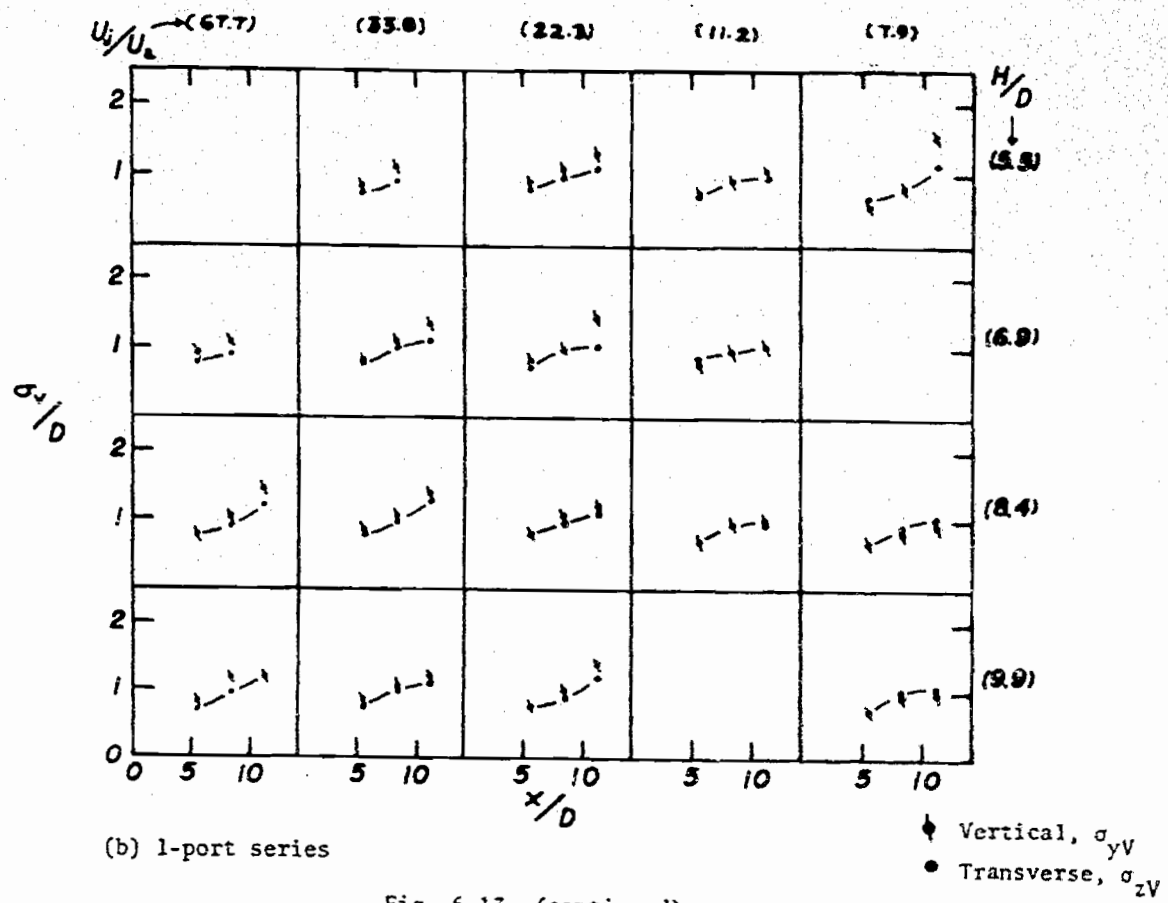

(b) 1-port series

Fig. 6.13 (continued).

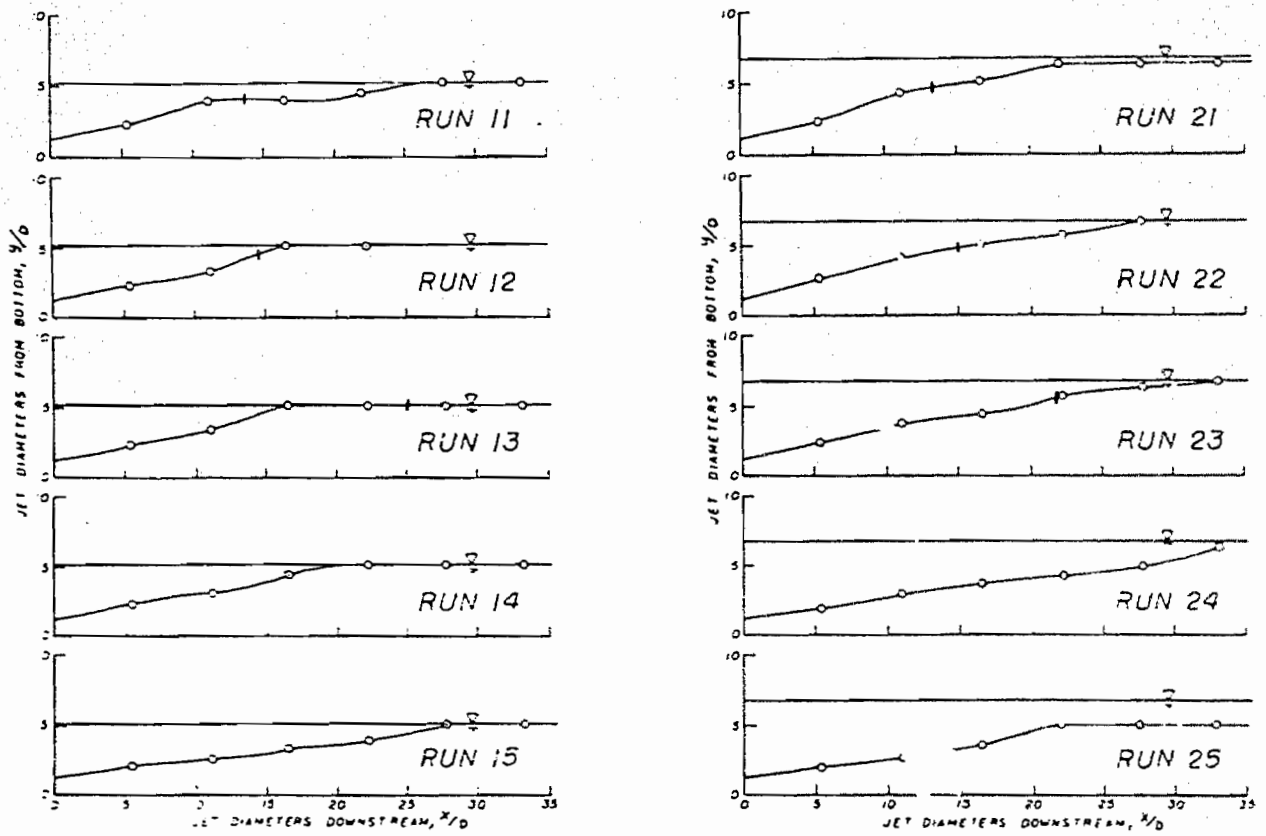

(a) 3-port series

Fig. 6.14 Jet trajectories.

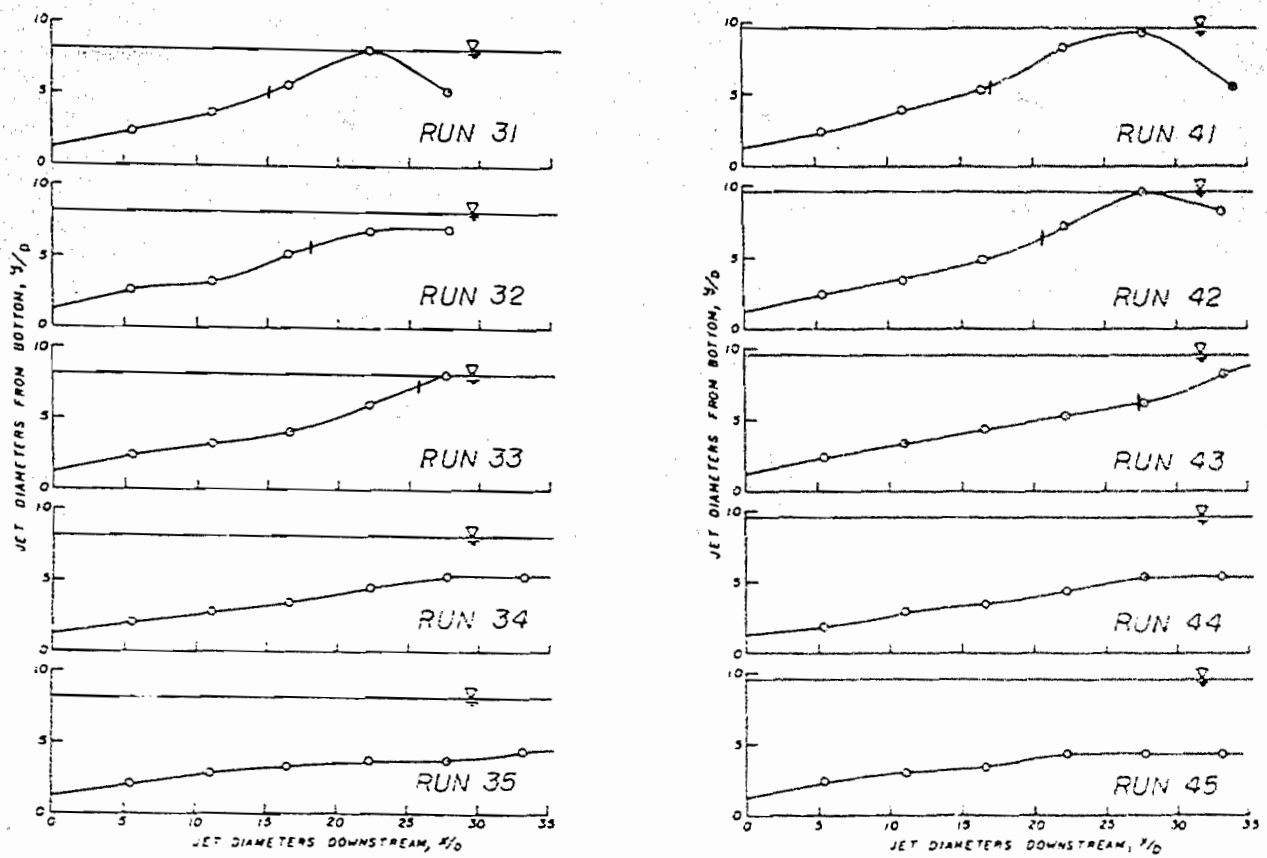

(a) (continued)

Fig. 6.14 (continued).

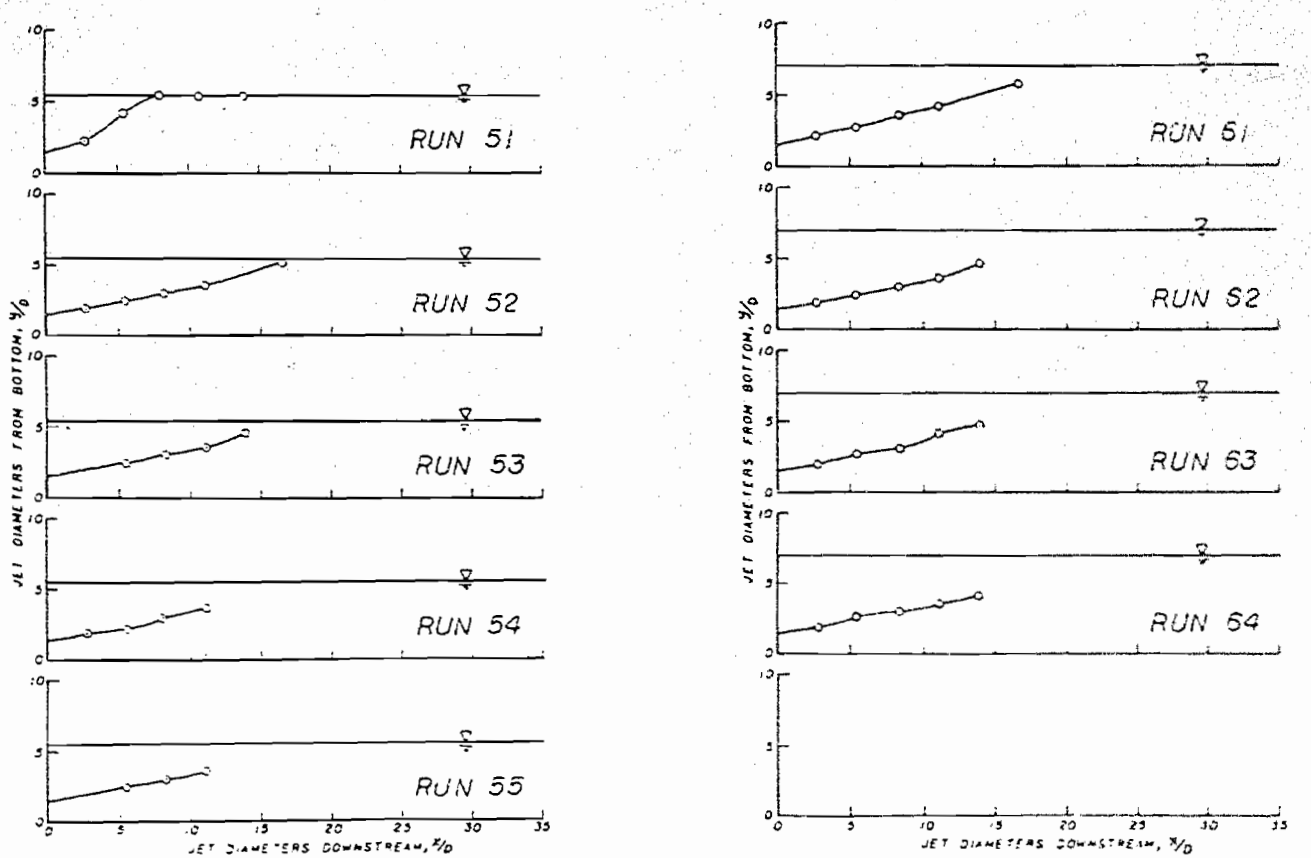

(b) 1-port series

Fig. 6.14 (continued).

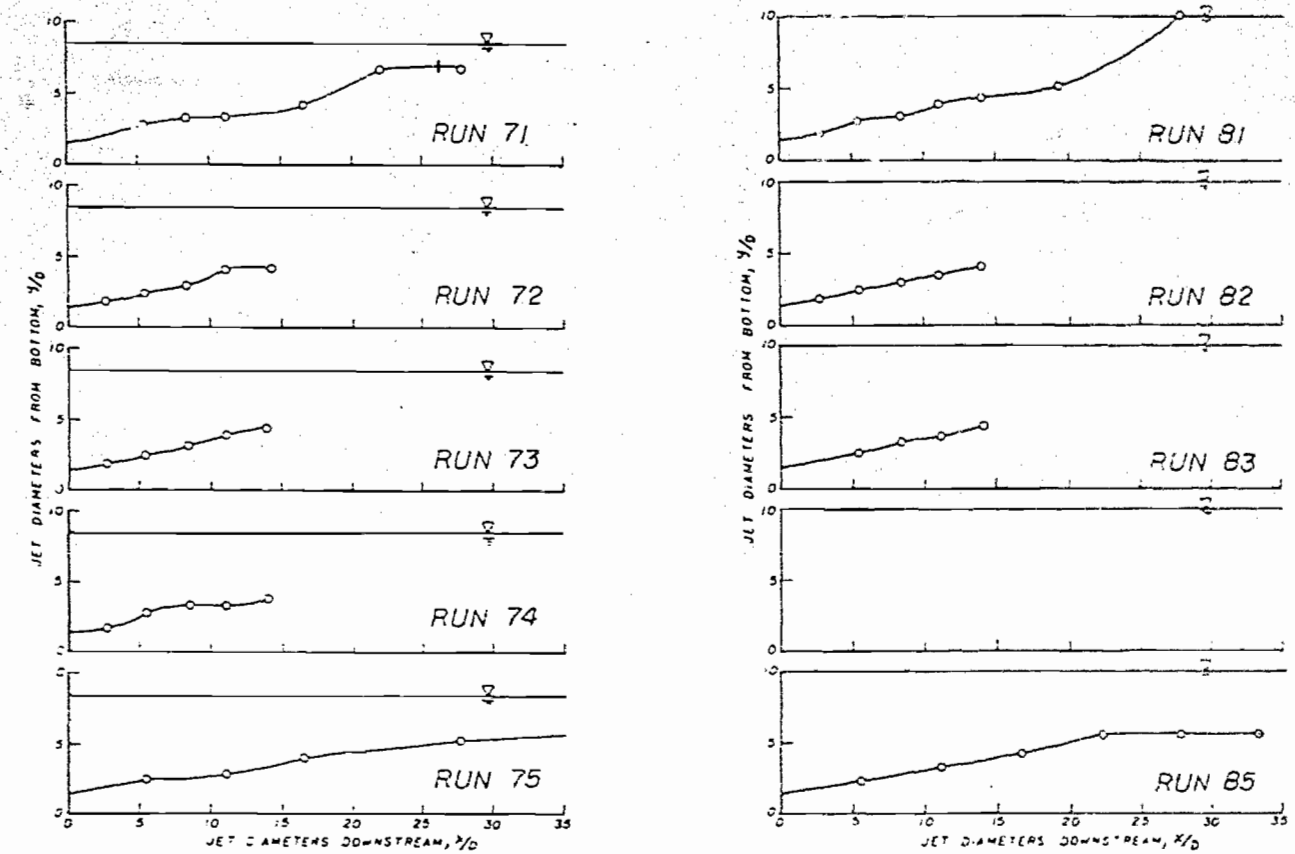

(b) (continued)

Fig. 6.14 (continued).

maximum excess temperature for both the three- and one-port series of experiments. The velocity ratio decreases from top to bottom in Fig. 6.14, which explains the consistent bending over of the jet trajectory for the runs toward the bottom of the figure. In nearly all cases, the average angle above the horizontal is significantly less than the initial angle of 20°, indicating that the effect of buoyancy, in comparison to that of the ambient velocity, is small.

Since these trajectories are based on temperature measurements, the location of the trajectories is not well defined as complete mixing is approached and the temperature distribution becomes nearly uniform. This condition occurs when the centerline excess temperature dilution plots shown in Fig. 6.8 approach the reciprocal of the normalized fully mixed excess temperature values given in Table 6.3. Note, for example, the trajectories for runs 31 and 41 which appear to bounce off the surface. Tic marks are shown on the trajectories for all runs in which the condition of complete mixing was approached, at the values of x/D where $(T_E - T_a)/(T_{max} - T_a)$ reaches 90 percent of the limiting value corresponding to complete mixing.

6.5 Individual-Jet, Transition, and Two-Dimensional Regions

The mixing and flow field downstream from a multiport diffuser can be divided into three regions or zones: the

individual-jet region; the transition region; and the two-dimensional region. These concepts, introduced briefly in Chapter 2, are amplified and quantified in this section.

In the individual-jet region—as its name implies—each jet and its properties are independent of all the other jets. The jets may be either buoyant or momentum jets, and in shallow water there may be free-surface and/or bottom boundary effects.

The individual-jet region ends and the transition region begins at the cross section where a significant amount of interaction between neighboring jets begins to occur. In special cases, e.g., when there is an upstream thermal wedge, the transition region could begin upstream from the ports and there may be no individual-jet region. In this study, the cross section marking the beginning of the transition region is taken to be the one at which the jet has spread transversely to the point where its nominal half width, $b = 2\sigma_{z,T}$, at the vertical level y_m of maximum transverse spreading, becomes just equal to half the distance between neighboring ports, L/2. Assuming that the excess temperature $\Delta T(x,y_m,z)$ at this level is distributed transversely according to the normal probability law, the transition region would then begin at the value of x, where

$$T(x,y_m,L/2) = 0.270\ \Delta T(x,y_m,0) \tag{6.15}$$

wherein 0.270 is twice the ratio of the normal probability density

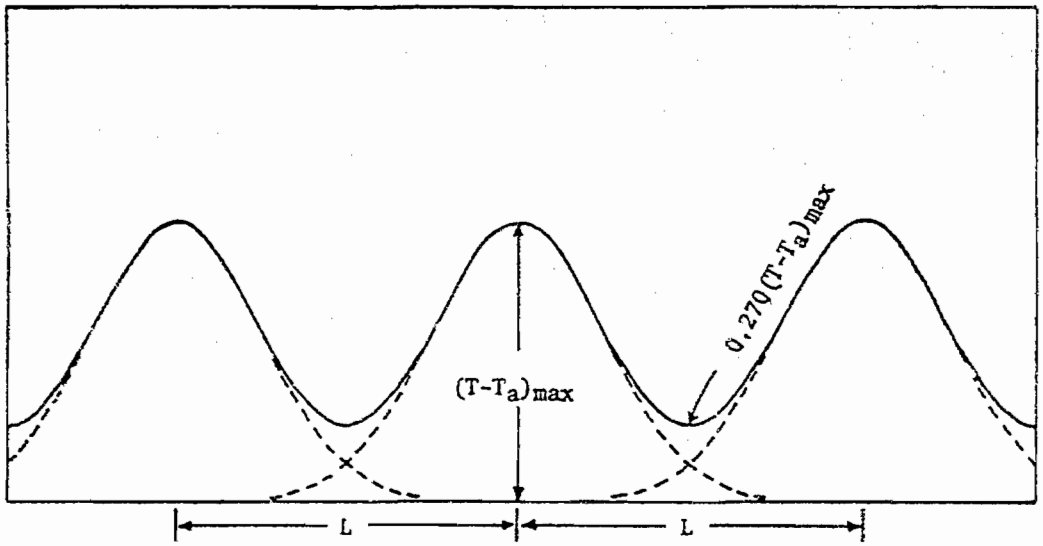

Fig. 6.15 Transverse excess temperature distributions through centerlines of three adjacent jets when interaction begins.

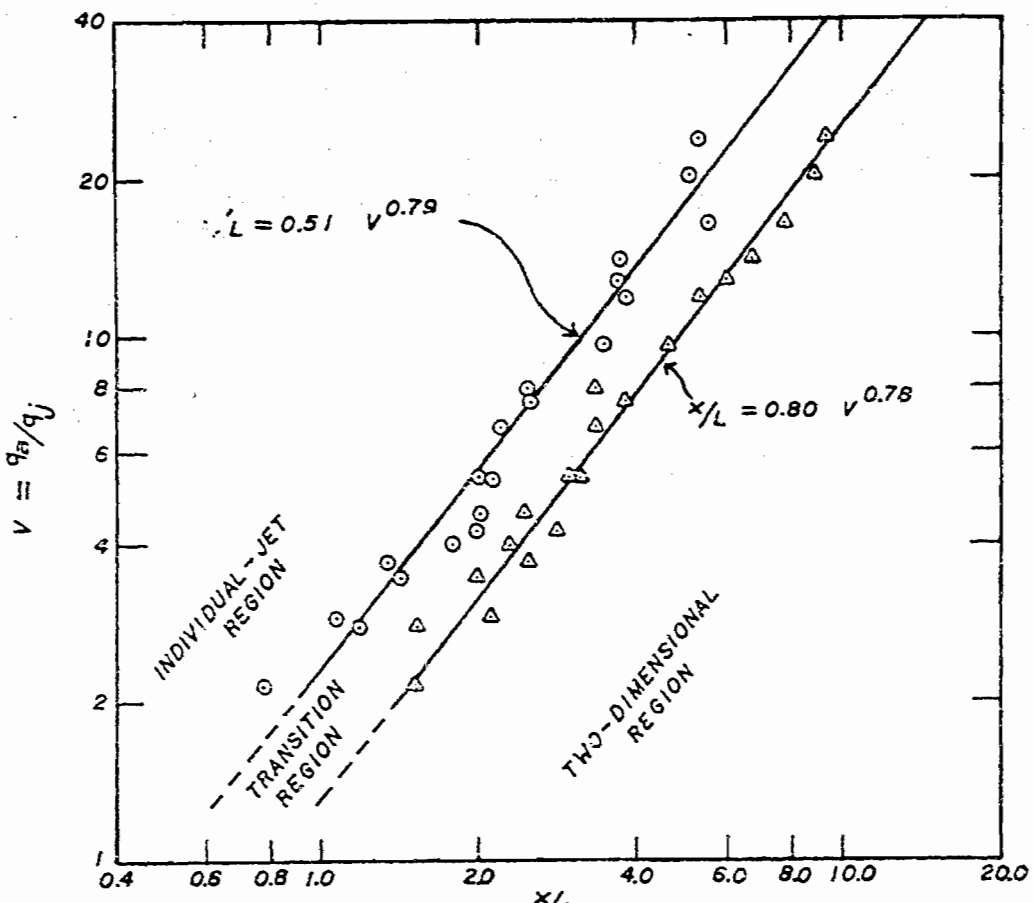

Fig. 6.16 Individual jet, transition, and two-dimensional regions for 3-port series.

Since the two lines are nearly parallel, the three regions may be defined by the following:

$$\left.\begin{array}{lll} \text{Individual jet region} & - & 0 < \dfrac{x}{LV^{0.79}} \leq 0.51 \\ \text{Transition region} & - & 0.51 < \dfrac{x}{LV^{0.79}} \leq 0.80 \\ \text{Two-dimensional flow region} & - & \dfrac{x}{LV^{0.79}} > 0.80 \end{array}\right\} \qquad (6.17)$$

where V is the volume flux ratio $\dfrac{U_a H}{U_j B}$.

CHAPTER 7

PREDICTING ZONES OF PASSAGE

7.1 Preliminary Considerations

In this chapter relationships are derived for predicting minimum zones-of-passage, with respect to both cross-sectional area and flow discharge, in the region of a channel assigned to a single diffuser port. A definition sketch for such a region, of depth H and width L, is shown in Fig. 7.1. The cross-hatched circular zone of radius r_c represents the mixing zone wherein the temperature rise $\Delta T = T - T_a$ is greater than some critical value ΔT_c, usually 5°F. Outside this zone is the zone-of-passage wherein $\Delta T < \Delta T_c$. Hypothetical temperature-rise distributions along the axes a-a and b-b are shown above and to the right. Note the contributions from the neighboring ports along a-a, and the influence of the reflections from the water surface and bed on the distribution along b-b. Except for the contributions from neighboring ports and the reflections, the distribution of ΔT along any radius is assumed to be the same, that is, independent of ϕ. The distribution of the excess velocity $\Delta u = u - U_a$ due to the jet is assumed to be qualitatively similar except near the bed and the water surface. For zones-of-passage larger than the minimum allowable of 75 percent, the area of the circular cross-hatched region in Fig. 7.1 is 0.25 HL or less. Consequently, as depicted in Fig. 7.1, the influence of contributions from neighboring ports and of bottom and free-surface effects should be minimal in this region and the

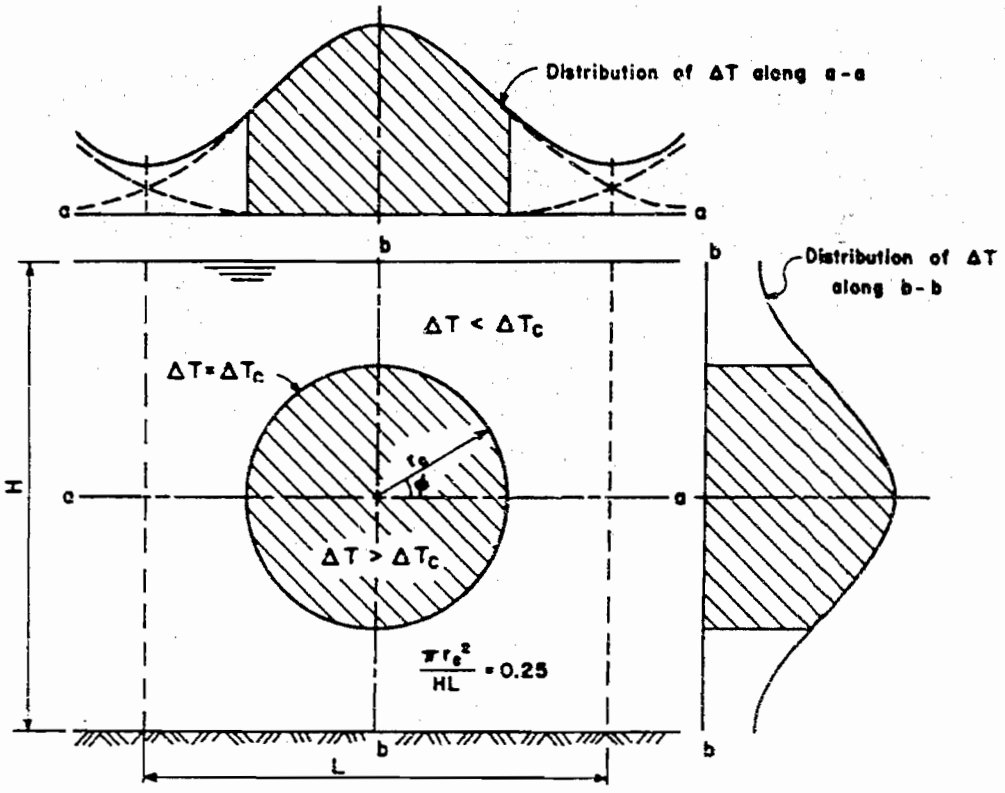

Fig. 7.1 Definition sketch for single-port region.

distributions therein are assumed to be axisymmetric.

Assuming that the amount of flow and heat escaping to the neighboring regions is exactly compensated for by the contributions from the neighboring regions, and that there is no heat loss to the atmosphere, the total volume and temperature-rise fluxes in the area HL remain constant and are given respectively by

$$Q = \int_{HL} u \, dA = \int_{HL} (U_a + \Delta u) dA$$

$$= q_a L + Q_j = Q_j (V + 1) \tag{7.1}$$

and

$$Q_j \Delta T_E = \int_{HL} u \, \Delta T \, dA = \bar{u}^{A}_{\Delta T} \int_{HL} \Delta T \, dA \tag{7.2}$$

In Eq. (7.1) the ambient velocity is assumed to be constant throughout the area HL. In Eq. (7.2) $\bar{u}^{A}_{\Delta T}$ is the excess temperature-weighted mean velocity in the area HL, which varies from a maximum of U_j at the port to a minimum of $(V + 1)U_a/V$ following complete mixing.

From the results in Chapter 6, the distributions of ΔT and Δu in the cross-hatched circular region of Fig. 7.1 can be approximated quite well by the radial normal distributions

$$\Delta T(r;\sigma_T) = \underbrace{\frac{Q_j \Delta T_E}{\bar{u}^{A}_{\Delta T}} \frac{1}{2\pi\sigma_T^2}}_{\Delta T_{max}} \underbrace{\exp[-\frac{1}{2}(\frac{r}{\sigma_T})^2]}_{\frac{\Delta T}{\Delta T_{max}}} \tag{7.3}$$

and

$$\Delta u(r;\sigma_V) = \Delta u_{max} \underbrace{\exp\left[-\frac{1}{2}\left(\frac{r}{\alpha\sigma_T}\right)^2\right]}_{\frac{\Delta u}{\Delta u_{max}}} \tag{7.4}$$

The bracketed expression for ΔT_{max} results from consideration of the total temperature-rise flux. In Eqs. (7.3) and (7.4) the parameters σ_T and $\sigma_V = \alpha\sigma_T$ are the respective standard deviations of the ΔT and Δu distributions. According to Eqs. (6.12) and (6.13), the value of α is approximately 0.7 over the range of x/D that is of interest, indicating that the rate of lateral spreading is somewhat less for Δu than for ΔT.

The excess temperature-weighted mean velocity in the area HL is defined by

$$\bar{u}^A_{\Delta T} = \frac{\int_{HL} u\Delta T \, dA}{\int_{HL}\Delta T \, dA} = U_a + \frac{\int_{HL}\Delta u\Delta T \, dA}{\int_{HL}\Delta T \, dA} \tag{7.5}$$

From Eqs. (7.3) and (7.4),

$$\Delta u\Delta T = \Delta u_{max} \, \Delta T_{max} \exp\left[-\frac{1}{2}\left(\frac{1+\alpha^2}{\alpha^2}\right)\left(\frac{r}{\sigma_T}\right)^2\right] \tag{7.6}$$

Now assume that the integrations of $\Delta u\Delta T$ and ΔT over the area HL are respectively equal to

$$2\pi \int_0^\infty \Delta u\Delta T \; r \, dr \quad \text{and} \quad 2\pi \int_0^\infty \Delta T \; r \, dr,$$

which in effect assumes that $\Delta u\Delta T$ and ΔT go to zero toward the outer boundaries of the region HL. The indicated integrations then lead to

$$\frac{\bar{u}^A_{\Delta T}}{U_a} = 1 + \left(\frac{\alpha^2}{1+\alpha^2}\right)\frac{\Delta u_{max}}{U_a} = 1 + \left(\frac{\alpha^2}{1+\alpha^2}\right)(k-1)\frac{\Delta u_{max}}{U_j - U_a} \tag{7.7}$$

Using Eqs. (6.12) and (6.13) to evaluate α and Eq. (6.10) to evaluate $\frac{u_{max}}{U_j - U_a}$, $\bar{u}^A_{\Delta T}/U_a$ can be estimated as a function of x/D and k, for the range of conditions covered in the flume experiments, as shown in Fig. 7.2.

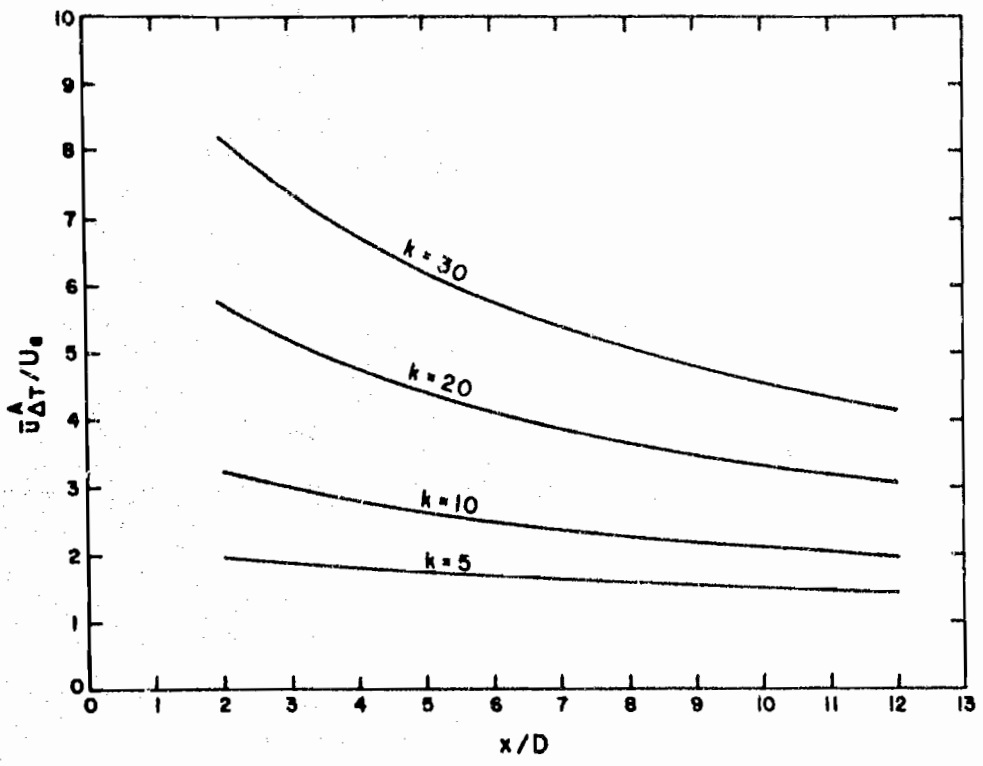

Fig. 7.2 Variation of $\bar{u}^{A}_{\Delta T}/U_a$ with x/D for different values of k, according to Eq. (7.7).

In plotting the curves, average values of 0.23 for S_u and 0.6 for l_u were used in Eq. (6.10).

7.2 Expressions for P_A and P_Q

In deriving relationships for the zones-of-passage with respect to area, ZPA, and with respect to discharge, ZPD, it is convenient to work with the fractional area

$$P_A = \frac{\pi r_c^2}{HL} \tag{7.8}$$

and the fractional discharge

$$P_Q = \frac{2\pi \int_0^{r_c} ur\, dr}{Q_j(V + 1)} \tag{7.9}$$

within which $\Delta T > \Delta T_c$. They are related to ZPA and ZPD by

$$ZPA = 100(1 - P_A) \tag{7.10}$$

and

$$ZPD = 100(1 - P_Q) \tag{7.11}$$

Eliminating r_c between Eqs. (7.8) and (7.3), and using the definitions $k = U_j/U_a$ and $V = q_a/q_j$, results in

$$P_A = -\frac{8}{kV}\left(\frac{\sigma_T}{D}\right)^2 \ln F \tag{7.12}$$

where

$$F = \exp\left[-\frac{1}{2}\left(\frac{r_c}{\sigma_T}\right)^2\right] = \frac{\Delta T_c}{\Delta T_{max}} = \frac{8}{k}\frac{\Delta T_c}{\Delta T_E}\frac{\bar{u}_{\Delta T}^{\Lambda}}{U_a}\left(\frac{\sigma_T}{D}\right)^2 \tag{7.13}$$

In a similar manner, replacing the local velocity u in Eq. (7.9) by

$$u = U_a + \Delta u(r;\ \sigma_V) \tag{7.14}$$

where Δu is given by Eq. (7.4), followed by the integration in Eq. (7.9), leads to

$$P_Q = \frac{8}{k(V+1)} \left(\frac{\sigma_T}{D}\right)^2 \left[-\ln F + \alpha^2 \frac{\Delta u_{max}}{U_a}(1 - F^{1/\alpha^2})\right] . \qquad (7.15)$$

7.3 Determination of $P_{A_{max}}$ and $P_{Q_{max}}$

Two different methods for predicting $P_{A_{max}}$ and $P_{Q_{max}}$ are presented in this section. The first method is based on the simplifying assumptions that P_A and P_Q vary with respect to $(\sigma_T/D)^2$, but that $\bar{u}^A_{\Delta T}/U_a$ and α^2 do not. Also, no direct use is made of the experimental results. In the second method P_A and P_Q are evaluated as functions of x/D using generalized relationships based on the experimental results, wherein σ_T/D, F, α, and $\frac{\Delta u_{max}}{U_j - U_a}$ are all represented as functions of x/D.

7.3.1 Using Simplifying Assumptions

With the simplifying assumptions indicated above, $P_{A_{max}}$ and $P_{Q_{max}}$ can be determined by the classical maximization procedure of elementary calculus. Letting $s = (\sigma_T/D)^2$ and $F = \frac{8}{k} \frac{\Delta T_c}{\Delta T_E} \frac{\bar{u}^A_{\Delta T}}{U_a} s$, and setting $\frac{dP_A}{ds} = 0$, leads to

$$P_{A_{max}} = \frac{1}{eV} \frac{\Delta T_E}{\Delta T_c} \frac{U_a}{\bar{u}^A_{\Delta T}} \qquad (7.16)$$

where e is the base of the natural logarithm. Using the lower limit $(V+1)/V$ as an estimate for $\bar{u}^A_{\Delta T}/U_a$ gives

$$P_{A_{max}} = \frac{1}{e(V + 1)} \frac{\Delta T_E}{\Delta T_c} \tag{7.16a}$$

which should provide a conservatively high estimate.

A similar procedure is followed to determine $P_{Q_{max}}$. Here, setting $\frac{dP_Q}{ds} = 0$ leads to the equation

$$-\ln F - 1 + (1 + \alpha^2)\left(\frac{\bar{u}_{\Delta T}^{A}}{U_a} - 1\right)\left[1 - \left(\frac{\alpha^2}{1 + \alpha^2}\right)F^{1/\alpha^2}\right] = 0$$

for which no explicit solution for F is apparent. Letting $\frac{\bar{u}_{\Delta T}^{A}}{U_a} = \frac{V + 1}{V}$ again, this equation reduces to

$$\ln F + 1 - \frac{(1 + \alpha^2)}{V}\left[\left(\frac{\alpha^2}{1 + \alpha^2}\right)F^{1/\alpha^2} - 1\right] = 0 \tag{7.17}$$

which is shown graphically for $\alpha = 0.7$ and $\alpha = 1$ in Fig. 7.3. This leads to

$$P_{Q_{max}} = \frac{\Delta T_E}{\Delta T_c} \frac{V}{(1 + V)^2} F\left[-\ln F + \frac{(1 + \alpha^2)}{V}(1 - F^{1/\alpha^2})\right] \tag{7.18}$$

wherein F and V values for a given value of α are paired according to Eq. (7.17). Because of the interdependencies contained in Eq. (7.17) it is not clear in this case whether or not Eq. (7.18) should give a conservative estimate of $P_{Q_{max}}$.

7.3.2 P_A and P_Q as Functions of x/D

To obtain P_A and P_Q as functions of x/D, the appropriate equations based on experimental results presented in Chapter 6 are substituted into Eqs. (7.12) and (7.15). For P_A, the result is

$$kV\ P_A = \frac{A_{\Delta T_c}}{A_j} = -8\left(\frac{\sigma_T}{D}\right)^2 \left[\ln \frac{\Delta T_c}{\Delta T_E} \frac{\Delta T_E}{\Delta T_{max}}\right] \tag{7.19}$$

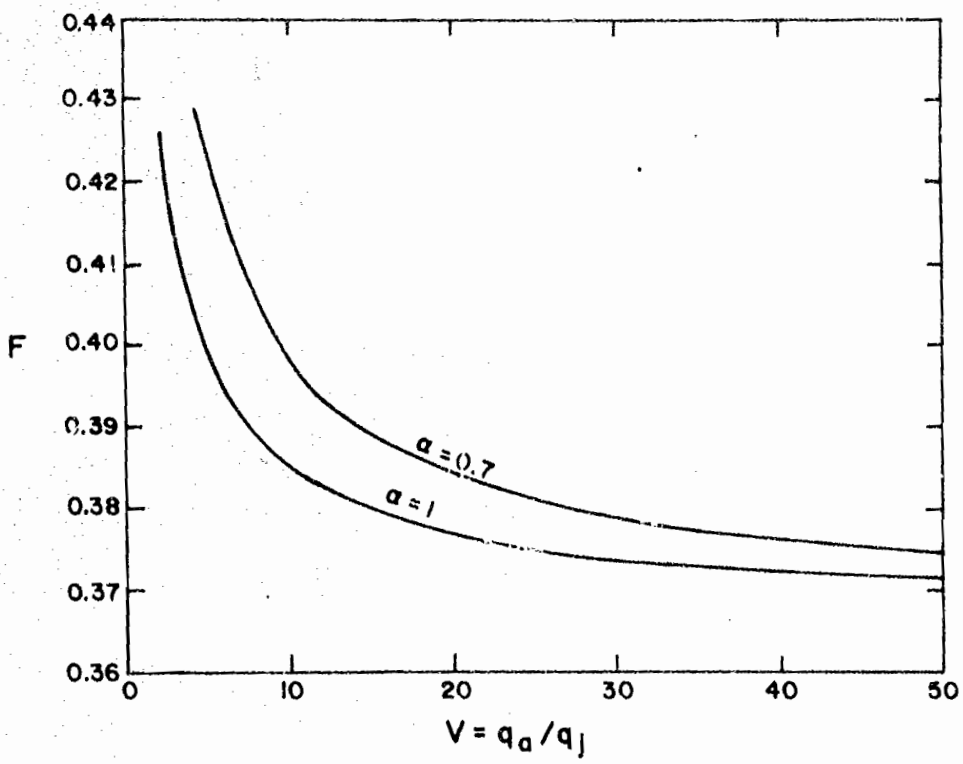

Fig. 7.3 Relationships between F and V for $\alpha = 0.7$ and $\alpha = 1$ according to Eq. (7.17), for determining $P_{O_{max}}$ according to Eq. (7.18).

where

$$\frac{\sigma_T}{D} = 0.086\left(\frac{x}{D}\right) + 0.5 \tag{6.12}$$

and

$$\frac{\Delta T_E}{\Delta T_{max}} = 0.28\left(\frac{x}{D}\right) + 0.7 \tag{6.9}$$

For P_Q, the result is

$$(V + 1)P_Q = \frac{Q_{\Delta T_c}}{Q_j} = \frac{8}{k}\left(\frac{\sigma_T}{D}\right)^2 \left[-\ln F + \alpha^2(k - 1)\,\frac{\Delta u_{max}}{U_j - U_a}\,(1 - F^{1/\alpha^2})\right] \tag{7.20}$$

where, in addition to Eqs. (6.12) and (6.9),

$$F = \frac{\Delta T_c}{\Delta T_E}\,\frac{\Delta T_E}{\Delta T_{max}} \qquad \text{from Eq. (7.13)}$$

$$\alpha = \frac{\sigma_V}{\sigma_T} = \frac{\sigma_V/D}{\sigma_T/D}$$

$$\frac{\sigma_V}{D} = 0.076\,\frac{x}{D} + 0.25 \tag{6.13}$$

$$\frac{U_j - U_a}{\Delta u_{max}} = 0.23\left(\frac{x}{D}\right) + 0.6 \tag{6.10}$$

The numerical coefficients 0.23 and 0.6 in Eq. (6.10) are respectively the average values of S_u and I_u, as they were in plotting the curves in Fig. 7.2.

Eqs. (7.19) and (7.20) for $\Delta T_E/\Delta T_c = 4.6$, corresponding to the experiments, are plotted in Fig. 7.4. In this format, the curves in Fig. 7.4 can be compared directly with the experimental curves in Figs. 6.2 and 6.5.

Because Eqs. (7.19) and (7.20), after making all of the

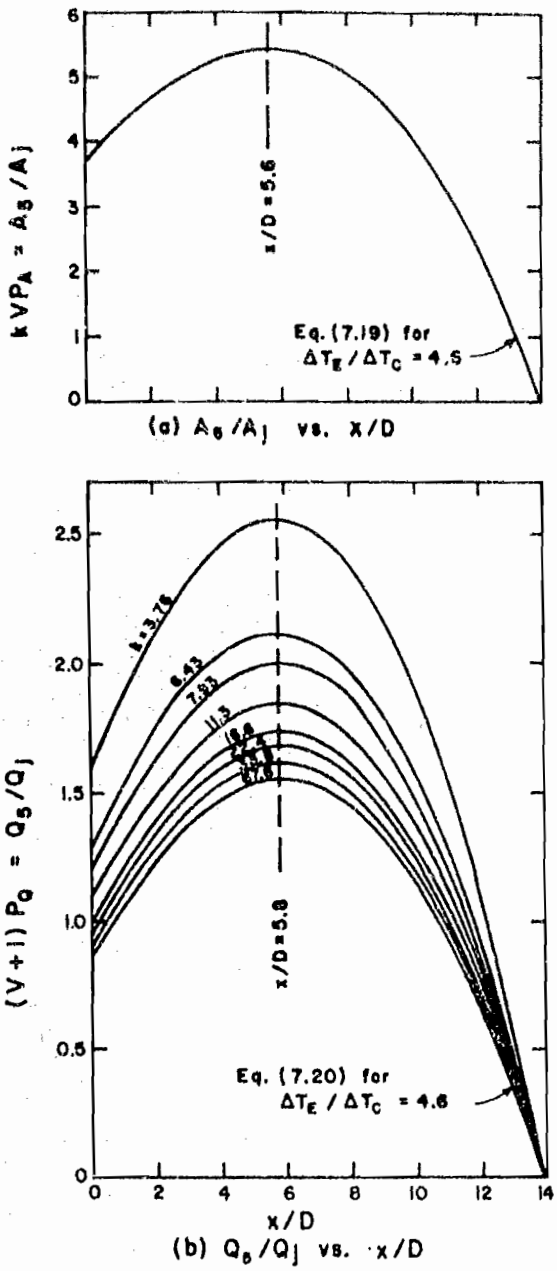

Fig. 7.4 Predicted A_5/A_j and Q_5/Q_j vs x/D using generalized experimental excess temperature and velocity distributions.

substitutions, are quite complicated functions of x/D, no attempt was made to obtain analytical expressions for $P_{A_{max}}$ and $P_{Q_{max}}$ by the methods of calculus as was done in section 7.3.1. Though it lacks generality, it is simpler to plot curves like those in Fig. 7.4 for the conditions of interest and read the maxi from the curves.

7.4 Comparisons with Experimental Data

Comparisons between the relationships developed in section 7.3 for predicting $P_{A_{max}}$ and $P_{Q_{max}}$ and the flume data are shown in Figs. 7.5 and 7.6.

Fig. 7.5 compares the data with the relationships presented in section 7.3.1 wherein the simplifying assumptions that $\bar{u}^A_{\Delta T}/U_a$ and α^2 do not vary with respect to $(\sigma_T/D)^2$ were used. Experimental values of $P_{A_{max}}$ are compared with Eq. (7.16a) for $\Delta T_E/\Delta T_c = 4.6$ in Fig. 7.5(a), and experimental values of $P_{Q_{max}}$ are compared with Eq. (7.18) for $\Delta T_E/\Delta T_c = 4.6$ and $\alpha = 1$ in Fig. 7.5(b). As anticipated, representation of $\bar{u}^A_{\Delta T}/U_a$ by its lower limit $(V + 1)/V$ in Eq. (7.16a), leads to predicted values of $P_{A_{max}}$ which are decidedly on the conservative side. Also, the data suggests a strong correlation between $P_{A_{max}}$ and k, which Eq. (7.16a) does not reflect. The dashed-line curve in Fig. 7.6(a) representing Eq. 7.16 reflects this correlation much better. In obtaining this curve, Eq. (7.7), for x/D = 5.6 , was used to represent $\bar{u}^A_{\Delta T}/U_a$.

In Fig. 7.5(b), Eq. (7.18), for $\Delta T_E/\Delta T_c = 4.6$ and $\alpha = 1$, agrees surprisingly well with the $P_{Q_{max}}$ data, although it tends to underpredict somewhat for V + 1 less than about 20. Correlation with k is much weaker for the $P_{Q_{max}}$ data than for the $P_{A_{max}}$ data. Another significant

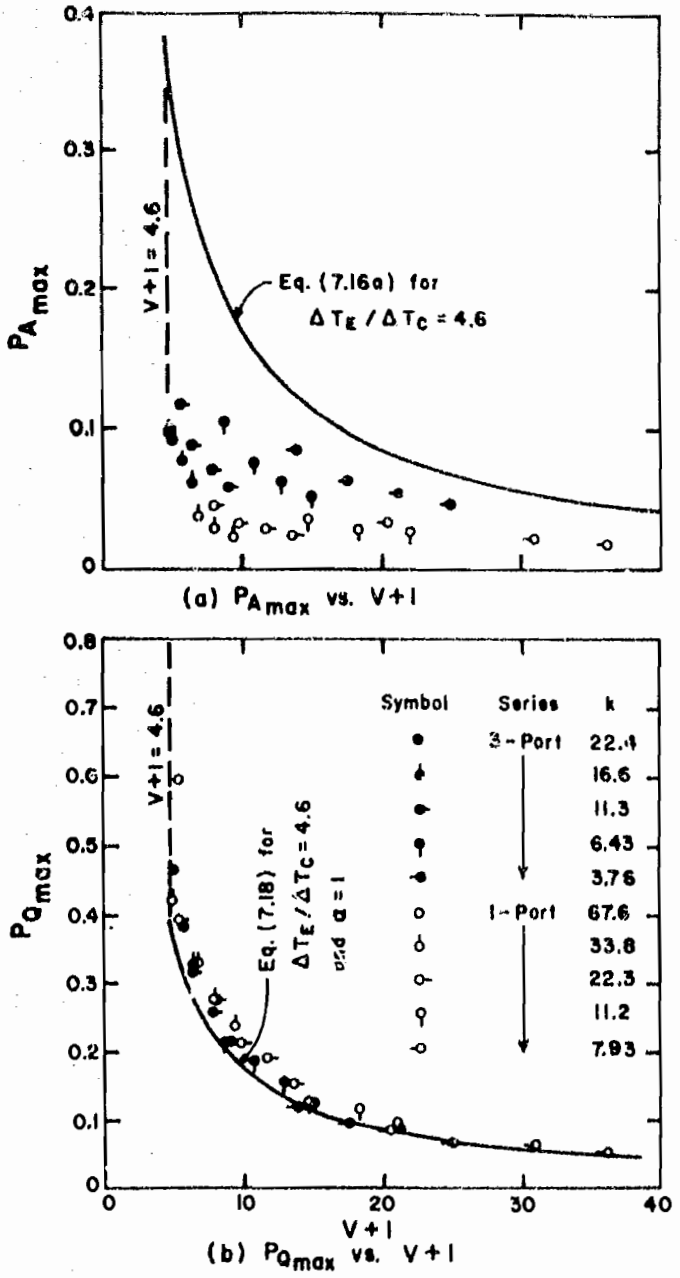

Fig. 7.5 Comparison between observed $P_{A_{max}}$ and $P_{Q_{max}}$ and predicted relationships which assume constant $\bar{u}_{\Delta T}^{A}/U_a$ and α^2.

feature of the $P_{Q_{max}}$ data is that it tends to follow the curve reasonably closely almost all the way to $V + 1 = \Delta T_E/\Delta T_m = 4.6$, at which value $P_{Q_{max}}$, because of complete mixing, must become equal to one. Eq.(7.18)is evidently very insensitive to α. Values of $P_{Q_{max}}$ computed for $\alpha = 0.7$ are almost identical to those for $\alpha = 1$ except for $V \leq 5$. where they are about one to four percent higher.

Before going on to discuss Fig. 7.6, some comparisons between Fig. 7.4 and the experimental A_5/A_j and Q_5/Q_j curves in Figs. 6.2 and 6.5 will be made. The general characteristics of the curves in Fig. 7.4 resemble those of most of the curves in Figs. 6.2 and 6.5. The predicted A_5/A_j and Q_5/Q_j curves peak at $x/D = 5.6$ and 5.8 respectively, compared with an average value of $x/D = 6.4$ for those A_5/A_j and Q_5/Q_j curves in Figs. 6.2 and 6.5 which have well-defined maxima. The predicted A_5/A_j and Q_5/Q_j curves all return to zero at about $x/D = 13.9$, compared to X/D values ranging fromabout 14 for most of the experimental curves up to about 20 for a few of them. For $x/D \to 0$, predicted Q_5/Q_j values agree reasonably well with the experimental ones, but the predicted A_5/A_j values are significantly larger than the experimental ones. Comparison of the predicted and experimental peak values of A_5/A_j and Q_5/Q_j is deferred until the discussion of Fig. 7.6, since that figure compares them directly.

The predicted A_5/A_j and Q_5/Q_j vs. x/D curves do not agree well with the experimental curves for runs 11, 12, 21, 31, 41, 51, 52, 61, 71, 81, almost all of which blow up, going to large values of the

ordinate from which they do not return to zero. The predicted curves show no such tendency. This difference is to be expected, however, since the value of $V + 1 = \frac{\Delta T_E}{\Delta T_m}$, the dilution ratio for complete mixing, for all of the experimental curves that blow up is either less than or only slightly larger than the critical value of $\Delta T_E/\Delta T_c = 4.6$. This means that $P_A = \frac{1}{kV}\frac{A_S}{A_j}$ and $P_Q = \frac{1}{V+1}\frac{Q_S}{Q_j}$ for all of these runs must either go to or closely approach a value of one. The predicted curves cannot be expected to blow up in this way since they are based on the properties of the generalized ΔT and Δu distributions which do not reflect the distortion in the distributions which must occur as complete mixing is approached.

Turning now to Fig. 7.6, the data for both $(A_S/A_j)_{max}$ and $(Q_S/Q_j)_{max}$ vary with k in ways that differ from those indicated by the solid curves representing Eqs. (7.19) and (7.20). The data indicate that both $(A_S/A_j)_{max}$ and $(Q_S/Q_j)_{max}$ increase with k, whereas the curve for Eq. (7.19) indicates no variation, and the curve for Eq. (7.20) indicates a decrease. The discrepancies are due mainly to a weak dependence of σ_T/D and σ_V/D on k that is not included in Eq.s (6.12) and (6.13) which were used as estimators for σ_T/D and σ_V/D. Close examination of the data in Figs. 6.12 and 6.13 shows that σ_T/D and σ_V/D in the neighborhood of x/D = 5.6 to 5.8 vary with k as shown in Fig. 7.7. Using the σ_T/D and σ_V/D values from the curves in Fig. 7.7 instead of Eqs. (6.12) and (6.13) in Eqs. (7.19) and (7.20) brings the curves into good agreement

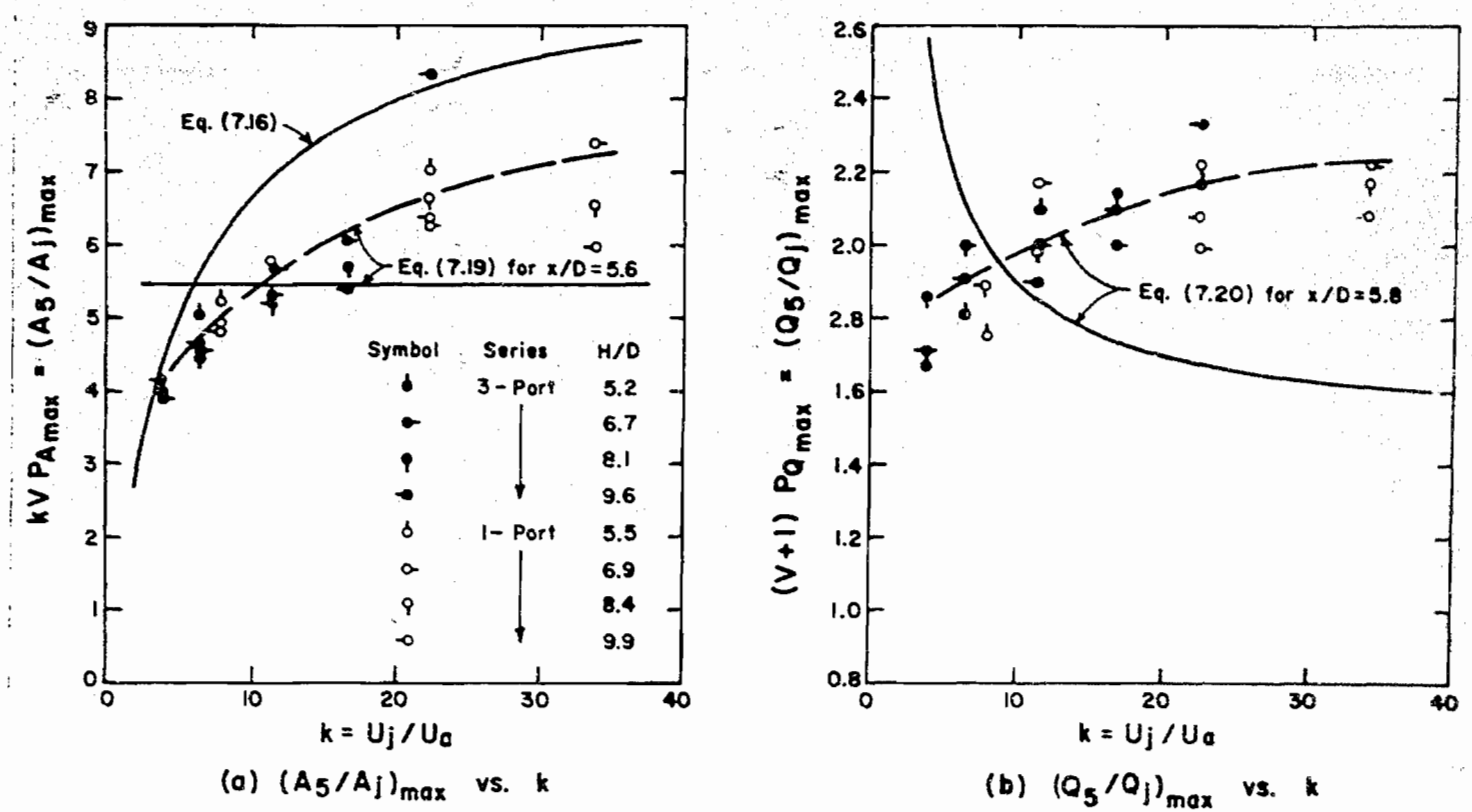

Fig. 7.6 Comparison between observed $(A_5/A_j)_{max}$ and $(Q_5/Q_j)_{max}$ and predicted relationships for $\Delta T_E/\Delta T_C = 4.6$ based on generalized experimental excess temperature and velocity distributions.

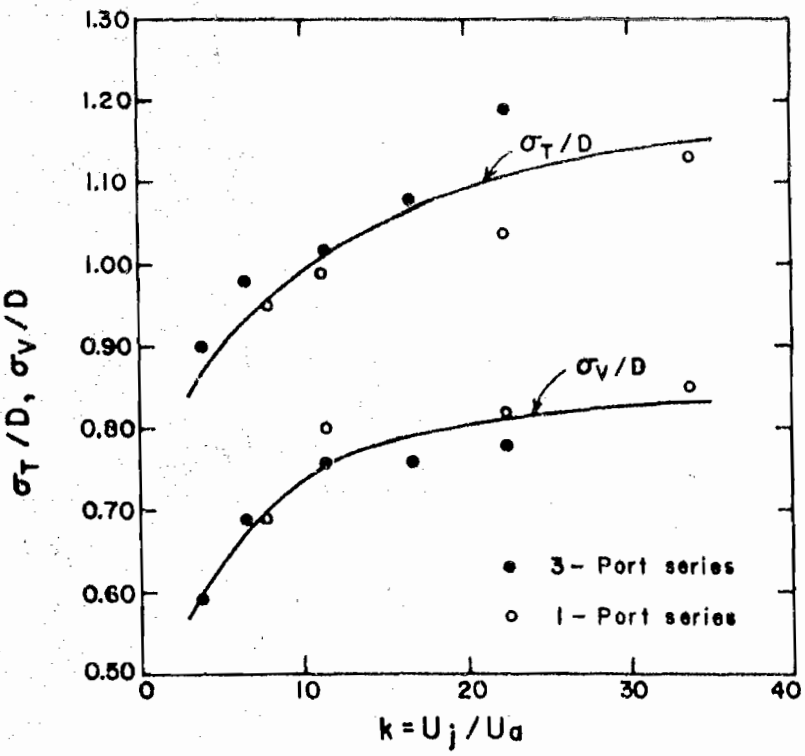

Fig. 7.7 Variation of σ_T/D and σ_V/D with respect to k for $x/D \simeq 5.7$.

with the data as shown by the dashed curves. A similar examination of the data in Figs. 6.8 and 6.10 for the other parameters (F and $\frac{\Delta u_{max}}{U_j - U_a}$) in Eqs. (7.19) and (7.20) reveals no consistent variation with respect to k. Considerably less improvement in the fit of the curve representing Eq. (7.16) to the data in Fig. 7.6(a) is obtained by using experimentally-determined α^2 and $\frac{\Delta u_{max}}{U_j - U_a}$ values to evaluate $\bar{u}^A_{\Delta T}/U_a$ in Eq. (7.16). Evidently the discrepancy between this curve and the data is at least partially due to ignoring the variation of $\bar{u}^A_{\Delta T}/U_a$ with respect to $(\sigma_T/D)^2$ when taking the derivative of Eq. (7.12) to obtain Eq. (7.16).

As regards the data in Fig. 7.6, neither $(A_S/A_j)_{max}$ nor $(Q_S/Q_j)_{max}$ appear to vary with relative depth H/D or lateral port spacing in any consistent way. The vertical spread is thought to be due to experimental scatter. In Fig. 7.7, σ_T/D appears to be somewhat larger for the 3-port series than for the 1-port series; the average α values are 0.69 for the 3-port series and 0.75 for the 1-port series.

Table 7.1 shows a comparison between measured and computed P_A and P_Q values for the prototype and model single-port surveys for which zone-of-passage data was presented in Tables 5.9 and 6.4. The values listed for the prototype and model data, and those computed by Eqs. (7.19) and (7.20), are all for x/D = 5.6, which corresponds to a prototype downstream distance of 15 ft. Those computed by Eqs. (7.16) and (7.18) are $P_{A_{max}}$ and $P_{Q_{max}}$ values, which should occur in the neighborhood of x/D = 5.6. The σ_T/D and σ_V/D relationships in Fig. 7.7 were used instead of Eqs. (6.12) and (6.13) in computing P_A and P_Q according to Eqs. (7.19) and (7.20). The agreement in Table 7.1 is

TABLE 7.1. Comparison Between Measured and Predicted P_A and P_Q for Single-Port Surveys

Date	P_A at x/D = 5.6				P_Q at x/D = 5.6			
	Prototype	Model	Eq. (7.16)	Eq. (7.19)	Prototype	Model	Eq. (7.18)	Eq. (7.20)
3/2/74	0.027	0.055	0.052	0.056	0.035	0.056	0.066	0.080
7/24/74	0	0.035	0.062	0.033	0	0.108	0.122	0.109
10/01/74	0.105	0.071	0.100	0.099	0.138	0.116	0.147	0.149
10/25/74	0.139	0.113	0.141	0.131	0.188	0.163	0.204	0.183
10/30/74	0.129	0.113	0.143	0.130	0.238	0.163	0.209	0.185

reasonably good, considering that initial jet velocities and excess temperatures at the times of these surveys differed significantly from the design values for the diffuser pipe which were simulated in all of the flume experiments on which the generalized ΔT and Δu distributions used in deriving the predictive relationships are based.

For the most part, the agreement between the relationships developed in this chapter for predicting $P_{A_{max}}$ and $P_{Q_{max}}$ and the data is considered encouraging. Eqs. (7.19) and (7.20) evaluated for $x/D = 5.7$, and with σ_T/D and σ_V/D evaluated as functions of both x/D and k as in Fig. 7.7, provide the best estimates of $P_{A_{max}}$ and $P_{Q_{max}}$. The weak variation of σ_T/D and σ_V/D with respect to k should be investigated further over a range of x/D values for the purpose of replacing Eqs. (6.12) and (6.13) with equations that represent σ_T/D and σ_V/D as joint functions of both x/D and k. The curves in Fig. 7.4 should then be revised accordingly. Eqs. (7.16) and (7.18) although less reliable than Eqs. (7.19) and (7.20), require less input information and may be useful for preliminary estimating purposes. To some extent all of the predictive relationships tend to break down as $V + 1 \rightarrow \Delta T_E/\Delta T_C$. However, this is a condition that in any case should be avoided if possible in designing diffuser-pipe systems. All in all, the methods, equations and curves developed herein should be useful tools for designing submerged-jet systems to meet zone-of-passage requirements, and for predicting zones-of-passage for different ambient flow conditions.

CHAPTER 8

SUMMARY AND CONCLUSIONS

8.1 Cross-Sectional Prototype Surveys

Cross-sectional prototype surveys were performed over a wide range of ambient flow and plant operating conditions. Initially the diffuser system was used as designed, with condenser cooling water discharging into the river through both pipes. In May, 1974, restrictions imposed by regulatory agencies went into effect that limited the discharge through the diffuser-pipe system to only one of the two pipes which was to be operated in combination with a spray canal. Several surveys were made for both operating conditions. The principal findings of these surveys are summarized in two parts: two-pipe surveys and one-pipe surveys.

8.1.1. Two-Pipe Surveys

Eighteen cross-sectional surveys covering river flows ranging from 31,400 to 73,600 cfs were performed while the plant was discharging all of its condenser cooling water into the river through both diffuser pipes. The highest excess temperature observed at the 500-ft downstream cross section was 3.8°F on July 23, 1973, when the total river flow was 34,600 cfs. If there are no excess temperatures greater than 5°F at this section, then

the area of the mixing zone cannot exceed 26 acres. Hence, the diffuser-pipe system was found to be operating in compliance with the 26-acre mixing zone limitation in all two-pipe surveys.

Because the plant was not operating at full capacity during any of the surveys, Fig. 5.6 was plotted with a view towards estimating the river discharge Q_R below which the maximum local temperature rise at full plant load in the 500-ft cross section would exceed $5^{o}F$. For several surveys, the maximum local excess temperatures were attributed to the small ports discharging into the shallow section of the river. If the small ports were to be closed and all of the effluent discharged through the large ports, the flow--and the waste heat load--discharged through each of the large ports would be increased approximately by the factor $(1 - Q_{E,S}/Q_E)^{-1} \approx 1.11$, where $Q_{E,S}/Q_E \approx 0.10$ is the proportion of the total effluent flow discharged through the small ports. Assuming that the maximum temperature rise 500 ft downstream from the large ports would be increased by the same factor, the maximum temperature rise in the 500-ft downstream cross section for conditions corresponding to those observed in the temperature surveys, and the plant operating at full load with the small ports closed, could be estimated by the equation

$$(T-T_a)_{max\ est} = 1.11\ (T-T_a)_{max,L}/(P/100) \qquad (8.1)$$

where

$(T-T_a)_{max,L}$ = maximum observed temperature rise 500 ft downstream attributable to a large port

P = percent of full plant load

The assumption on which Eq. (8.1) is based should be valid for conditions approaching complete mixing. For less than complete mixing, Eq. (8.1) would tend to somewhat overestimate maximum downstream temperature rises.

Values of $(T-T_a)_{max\ est}$ according to Eq. (8.1) are plotted in Fig. 8.1 for each 500-ft downstream cross-sectional survey along with data from the laboratory model study by Jain et al. (1971) and the perfect mixing curve. In comparison to Fig. 5.6, Fig. 8.1 indicates that better performance with respect to maximum excess temperature rise and closer agreement with the three-dimensional model study would be realized by blocking off the small ports.

The transverse distribution of the excess temperature was observed to be multipeaked, typically having three peaks. This was attributed to differences in the transverse distributions of the normalized effluent and river discharges. The distribution of excess temperature should become more uniform across the channel as total river discharge decreases. This is suggested in Fig. 8.2 which shows the normalized depth-averaged excess temperature for the three-dimensional model results of Jain et al. (1971) at a downstream section corresponding to 600 ft in the prototype. Since distorted models tend to significantly increase the relative effect of transverse turbulent mixing, the degree of improvement in the river would be less dramatic. Still, it is anticipated that temperature rises 500 ft downstream would not begin exceeding $5^{\circ}F$ until the river discharge goes below about 15,000 cfs.

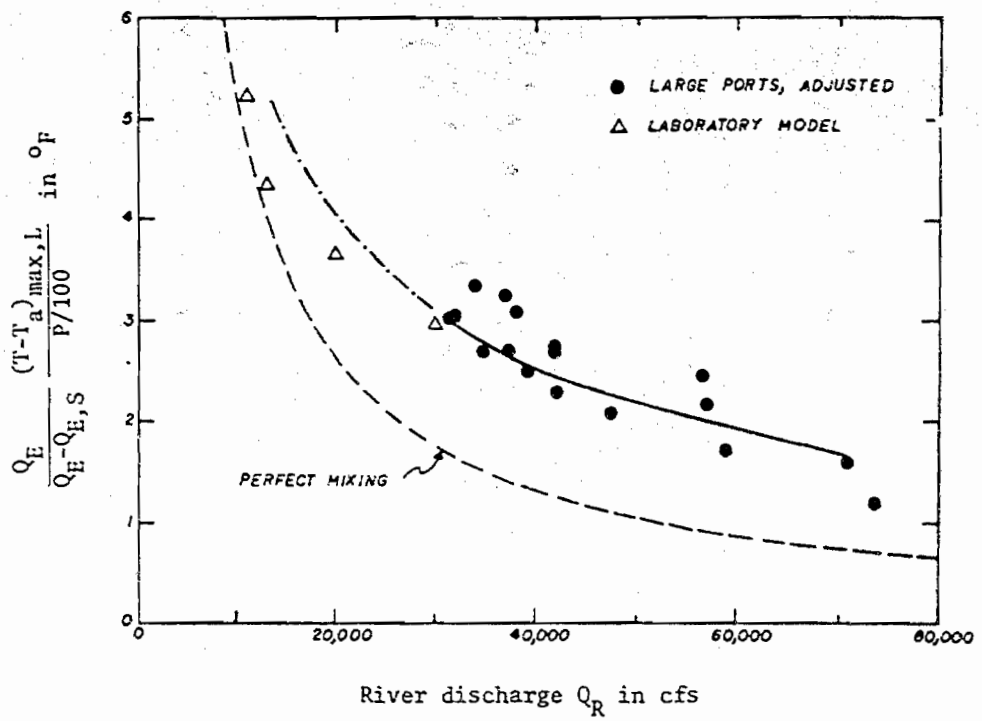

Fig. 8.1 Estimated maximum excess temperature at full plant load when effluent is discharged only through large ports.

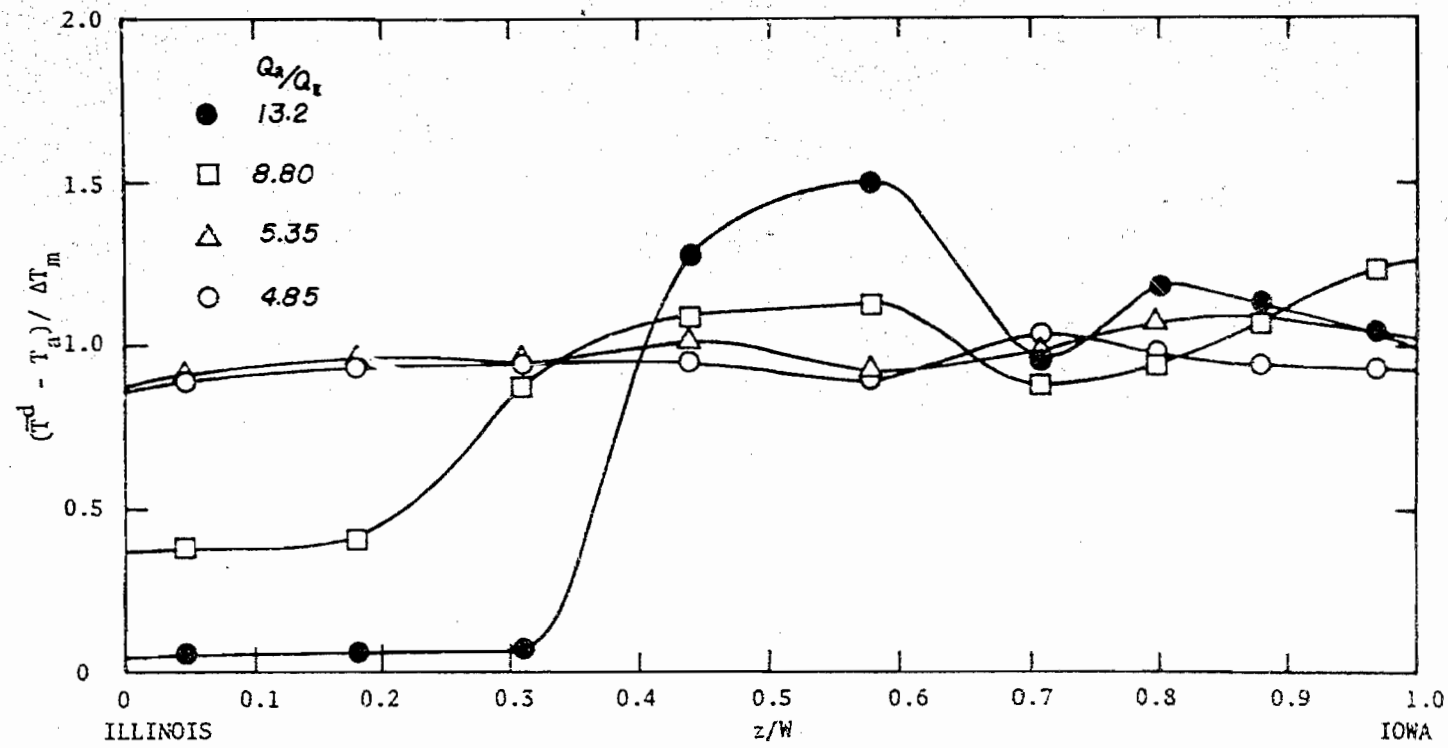

Fig. 8.2 Transverse distribution of normalized depth-averaged excess temperature 600 feet downstream from diffuser pipe in three-dimensional laboratory model.

Flow velocities were measured both upstream and downstream from the diffuser pipes for most of the surveys. No influence of the diffuser-pipe operation on the river flow distribution was apparent when two-pipes were used. The total measured excess heat load in the cross section 500 ft downstream from the diffuser pipes agreed closely with the total calculated excess heat input from the diffuser-pipe system.

8.1.2. One-Pipe Surveys

Nine cross-sectional surveys were performed when the plant was using only one diffuser pipe. Of these, six were conducted while the diffuser pipe was operating in parallel with the spray canal. The highest excess temperature at the 500-ft downstream cross section was 3.2°F; therefore, the cooling system was operating within the 26-acre mixing zone limitations during all of these surveys.

The transverse distribution of excess temperature had either one or two peaks in the sections of the river downstream from the pipe in use at the time of the survey. The distribution across the river was significantly less uniform for the one-pipe than for the two-pipe operating condition since, for the former, effluent was discharged into only half of the main channel of the river.

Results of the surveys in which the diffuser pipe was operated in parallel with the spray canal, indicated that the spray

canal was dissipating less than its share of the heat load at the existing meteorological conditions. Consequently, the temperature of the circulating water in the cooling system increased until an equilibrium condition was reached. At this equilibrium condition, the effluent temperature has been observed to exceed the ambient river temperature by as much as 51°F. This resulted in very high temperatures for the water discharging into the river from the diffuser pipe. Table 8.1 gives the estimated proportions of waste heat and condenser cooling water discharged through the diffuser pipe for the surveys conducted while the combined system was in operation. Column 4 shows the estimated effluent temperature rise that would occur at full plant generating capacity. This was computed from heat balance considerations according to the scheme shown in Fig. 5.11. Note that in the open-cycle mode this temperature rise was 12.8°C for the design Q_E at 2270 cfs. It can be concluded that the diffuser pipe carried more than its share of the waste heat in every case. In addition, this excessive heat load was discharged into only part of the river channel.

The transverse river flow distribution was considerably altered in the diffuser pipe discharge region during two of the one-pipe cross-sectional surveys. The ratio of river discharge Q_R to effluent discharge Q_E was relatively small at the time of these surveys. The diffuser pipe discharge apparently acted like a jet pump in drawing the ambient flow from other parts of the

TABLE 8.1. Estimated Proportions of Waste Heat and Condenser Cooling Water Discharged Through Diffuser Pipe When Combined System was in Operation

Date	Estimated Proportion of Waste Heat to Diffuser Pipe $\frac{Q_E \Delta T_E}{(2270)(12.8)P/100}$	Estimated Proportion of Cooling Water to Diffuser Pipe $\frac{Q_E}{Q_E + Q_S}$	Est. ΔT_E for P=100 (^oC)
(1)	(2)	(3)	(4)
7-23-74	0.65	0.59	21.2
7-25-74	0.63	0.41	25.5
8-22-74	0.59	0.42	20.8
9-10-74	0.59	0.35	29.5
10-07-74	0.55	0.33	31.2
11-11-74	0.76	0.36	33.7

Note: $\Delta T_E = T_E - \bar{T}_a$

Q_E from Eq. (5.9)

$Q_S = 401(NL)$ = spray canal discharge in cfs

NL = number of lift pumps in operation

river into the diffuser pipe region. One would expect this effect to be insignificant for the same effluent and river discharge magnitudes when both pipes are in operation.

8.2 Single-Port Studies

Both prototype and laboratory single-port experiments were conducted. Comparison of prototype and laboratory results for the same flow parameter values indicated that the two-dimensional channel model provided a good representation of the prototype. Hence, model runs were made for flow conditions corresponding to prototype full plant load operating conditions and river flows ranging from 13,200 to 50,000 cfs to fill in the gaps not covered by the prototype conditions. The results of these model studies were used to predict the river discharge Q_R for which zone-of-passage limitations would be violated.

The zone-of-passage with respect to discharge restriction is violated before the zone-of-passage with respect to area whenever, as in the present case, the velocity of flow in the zone occupied by the heated water exceeds the average ambient velocity. The results of the two-dimensional model studies together with Eq. (6.8) were combined to prepare Fig. 6.6 from which the river discharge Q_R at which the zone-of-passage criterion with respect to river discharge will be violated was estimated to be 15,300 cfs.

8.3 General Laboratory Results

Individual jets were modeled over a wide range of flow conditions to predict the performance of the Quad Cities diffuser pipe. In addition to flow characteristics directly related to zones-of-passage, characteristics such as excess temperature dilution, excess velocity reduction, jet trajectory, jet spreading and merging of adjacent jets were investigated.

Excess temperature dilution was presented in a generalized form in Fig. 6.9. Both model and field data were plotted on the figure. The results indicate that excess temperature dilution along the jet centerline proceeds in accordance with a similarity relationship until retardation due to surface and/or bottom interaction sets in.

In the region immediately downstream from the diffuser ports, the gross behavior of the jets was found to be in rough accordance with the behavior of momentum jets discharging into a quiescent, infinite body of fluid as described by Albertson et al. (1950). One important difference is that the zone of established flow in the present experiments was found to extend back into the diffuser ports, approximately to the location of the 70° bend. The momentum jet-type behavior began to break down when the confining effects of the free-surface and bottom boundaries came into play. In general, the velocity field was affected sooner and more strongly by these effects than was the temperature field.

Buoyancy effects appeared to be negligible in the region immediately downstream from the ports. Evidently over the range of jet densimetric Froude numbers covered in this investigation, buoyancy effects came into play only further downstream in cases where the volume flux ratio $V = q_a/q_j$ is too high for complete mixing to have been achieved before the mixing and entrainment capacity of the jet is dissipated due to diffusion and loss of momentum.

The mixing and flow field downstream from a multiport diffuser can be described as consisting of three regions. They are: the individual-jet region; the transition region; and the two-dimensional region. The definitions for these regions, as discussed in section 6.5, were used in formulating quantitative criteria for identifying the three regions. The results reduced to simple quations for locating the beginning and end of the transition region in terms of distance downstream x, port spacing L, and volume flux ratio V.

8.4 Predicting Zones of Passage

Two approaches were taken to predict the maximum fractional area $P_{A_{max}}$ and fractional discharge $P_{Q_{max}}$ for the mixing zone assigned to a single discharge port wherein the temperature rise exceeds some critical value ΔT_c, usually 5°F. The first approach, which utilizes some simplifying assumptions and makes no direct use of the experimental temperature- and velocity-distribution data, resulted in Eqs. (7.16) and (7.18). The second approach, which uses generalized functions for

the distribution of excess temperature and velocity due to the jet that are based on the model data, resulted in Eqs. (7.19) and (7.20). Comparison with the model data shows that Eqs. (7.16) and (7.18) provide rough estimates of $P_{A_{max}}$ and $P_{Q_{max}}$, the former tending to substantially overpredict, and the latter to slightly underpredict. Eqs. (7.19) and (7.20), and the model and prototype data all indicate that the minimum zones-of-passage, wherein the temperature rise does not exceed 5°F, usually occurs about six port diameters downstream from the diffuser ports. Eqs. (7.19) and (7.20) predict $P_{A_{max}}$ and $P_{Q_{max}}$ much more accurately than Eqs. (7.16) and (7.18), provided that the weak variation of the jet spreading parameters, σ_T/D and σ_V/D, with respect to $k = U_j/U_a$ is taken into account. In this regard, it is recommended that the excess temperature and velocity distributions due to the jet be investigated further so that Eqs. (6.12) and (6.13) can be replaced by equations which represent σ_T/D and σ_V/D as joint functions of both x/D and k.

All in all, the results of the zone-of-passage prediction analysis are considered to be encouraging. They should be useful for designing submerged jet systems to meet zone-of-passage environmental standards, and for predicting zones-of-passage for different ambient flow conditions.

REFERENCES

Abraham, G. 1963. "Jet Diffusion in Stagnant Ambient Fluid," Delft Hyd. Lab., Publ. No. 29.

Adams, E. E. June 1972. "Submerged Multiport Diffusers in Shallow Water with Current," M.I.T., S.M. Thesis (Civil Engineering).

Albertson, M. L., Dai, Y. B., Jensen, R. A., and Rouse, H. 1950. "Diffusion of Submerged Jets," *Trans. ASCE*, 115.

Argue, J. R. July 1973. "The Mixing Characteristics of Submerged Multiple-Port Diffusers for Heated Effluents in Open Channel Flow," M.S. Thesis, The University of Iowa, May 1973, and IIHR Report No. 147, Iowa City.

Camp, T. R. and Graber, S. D. February 1968. "Dispersion Conduits," Proc. ASCE, *J. Sanitary Engineering Division*, 94, 31-39.

Cederwall, K. April 1971. "Buoyant Slot Jets into Stagnant or Flowing Environments," W. M. Keck Laboratory for Water Resources and Hydraulics, Report No. KH-R-25, California Institute of Technology.

Chan, T. L. and Kennedy, J. F. August 1972. "Turbulent Nonbuoyant or Buoyant Jets Discharged into Flowing or Quiescent Fluids, IIHR Report No. 140, Iowa City.

Fan, L.-N. October 1967. "Turbulent Buoyant Jets into Stratified or Flowing Ambient Fluids," W. M. Keck Laboratory of Hydraulics and Water Resources, Report No. KH-R-15, California Institute of Technology.

Fan, L.-N. and Brooks, N. H. March 1966. Discussion of "Horizontal Jets in Stagnant Fluid of Other Density," by Abraham, G., Proc. ASCE, *J. of Hyd. Div.*, HY2.

Fan, L.-N. and Brooks, N. H. January 1969. "Numerical Solution of Turbulent Buoyant Jet Problems," W. M. Keck Laboratory, Report No. KH-R-18, California Institute of Technology.

Glover, J. R. March 1973. "The IIHR Portable Linear-Thermistor Temperature Meter," IIHR Report No. 144, Iowa City.

Harleman, D. R. F., Hall, L. C., and Curtis, T. G. September 1968. "Thermal Diffusion of Condenser Water in a River During Steady and Unsteady Flows," Ralph M. Parsons Laboratory for Water Resources and Hydrodynamics, M.I.T. Report No. 111, Cambridge, Massachusetts.

Harleman, D. R. F., Jirka, G. and Stolzenbach, K. D. June 1971. "A Study of Submerged Multiport Diffusers for Condenser Water Discharge with Application to the Shoreham Nuclear Power Station," M.I.T. Parsons Laboratory for Water Resources and Hydrodynamics, Technical Report No. 139.

Harleman, D. R. F., Jirka, G., Adams, E. E. and Watanabe, M. October 1971. "Investigation of a Submerged, Slotted Pipe Diffuser for Condenser Water Discharge from the Canal Plant, Cape Cod Canal," M.I.T. Parsons Laboratory for Water Resources and Hydrodynamics, Technical Report No. 141.

Jain, S. C., Sayre, W. W., Akyeampong, Y. A., McDougall, D., and Kennedy, J. F. September 1971. "Model Studies and Design of Thermal Outfall Structures Quad-Cities Nuclear Plant," IIHR Report No. 135, Iowa City.

Jirka, G. and Harleman, D. R. F. March 1973. "The Mechanics of Submerged Multiport Diffusers from Buoyant Discharges in Shallow Water," Ralph M. Parsons Laboratory for Water Resources and Hydrodynamics, M.I.T. Report No. 169, Cambridge, Massachusetts.

Koh, R. C. Y. and Fan, L.-N. October 1970. "Mathematical Models for the Prediction of Temperature Distributions Resulting from the Discharge of Heated Water in Large Bodies of Water," EPA Water Pollution Control Research Series 16130 DWO.

Larsen, J. and Hecker, A. M. January 1972. "Design of Submerged Diffusers and Jet Interaction," ASCE Nat. Water Resources Engineering Meeting, Atlanta, Georgia, Preprint 1614.

Lee, J. H. W., Jirka, G. H. and Harleman, D. R. F. 1974. "Stability and Mixing of a Vertical Round Buoyant Jet in Shallow Water," R. M. Parsons Laboratory for Water Resources and Hydrodynamics, Department of Civil Engineering, M.I.T. Technical Report No. 195.

Liseth, P. November 1970. "Mixing of Merging Buoyant Jets from a Manifold in Stagnant Receiving Water of Uniform Density," Hydraulic Engineering Laboratory, Report No. HEL 23-1, University of California, Berkeley.

Paily, P. P. November 1975. "Thermal Regime of the Upper Mississippi and Missouri Rivers," IIHR Report No. 185, Iowa City.

Parker, F. L. and Krenkel, P. A. December 1969. "Thermal Pollution: Status of the Art," Vanderbilt University, Department of Environmental and Water Resources Engineering, Report No. 3, Nashville, Tennessee.

Parr, A. D. and Sayre, W. W. October 1973. "Performance of the Diffuser-Pipe System for Discharging Condenser Cooling Water at the Quad Cities Nuclear Power Station, February–August, 1973," IIHR Limited Distribution Report No. 19, Iowa Institute of Hydraulic Research, The University of Iowa.

Parr, A. D. and Sayre, W. W. July 1974. "Performance of the Diffuser-Pipe System for Discharging Condenser Cooling Water at the Quad Cities Nuclear Power Station, September, 1973–January, 1974," IIHR Limited Distribution Report No. 25, Iowa Institute of Hydraulic Research, The University of Iowa.

Rawn, A. M., Bowerman, F. R., and Brooks, N. H. 1961. "Diffusers for Disposal of Sewage in Sea Water," *Trans ASCE*, 126, Part III.

Rouse, H., Yih, C. S., and Humphreys, H. W. 1952. "Gravitational Convection from a Boundary Source," *Tellus*, 4.

Sayre, W. W. and Parr, A. D. September 1972. "Water Temperatures in Mississippi River Downstream from Quad Cities Nuclear Power Station During Operation of Side-Jet Condenser Cooling Water Discharge System, June–July, 1972," IIHR Limited Distribution Report No. 13, Iowa Institute of Hydraulic Research, The University of Iowa.

Sayre, W. W. and Parr, A. D. March 1973. "Performance of the Diffuser-Pipe System for Discharging Condenser Cooling Water of the Quad Cities Nuclear Power Station, September, 1972–January, 1973," IIHR Limited Distribution Report No. 15, Iowa Institute of Hydraulic Research, The University of Iowa.

Sayre, W. W. and Parr, A. D. July 1974. "Summary of Thermal Monitoring Results for Quad Cities Generating Station, September, 1972–January, 1974," IIHR Limited Distribution Report No. 26, Iowa Institute of Hydraulic Research, The University of Iowa.

Sharp, J. J. and Wang, C.-su. 1973. "Boundary Effects on Dilution of Buoyant Jets," in *Water Pollution Research in Canada* (edited by G. J. Farquhar). Toronto, Canada: University of Toronto Press.

Streeter, V. L. and Wylie, E. B. 1975. *Fluid Mechanics.* (6th ed.). New York: McGraw-Hill.

Vigander, S., Elder, R. A., and Brooks, N. H. February 1970. "Internal Hydraulics of Thermal Discharge Diffusers," *Proc. ASCE, J. Hydraulics Division,* 96, 509-527.

APPENDIX A

REGULATIONS OF THE IOWA WATER QUALITY COMMISSION AND THE ILLINOIS POLLUTION CONTROL BOARD CONCERNING THE DISCHARGE OF WASTE HEAT INTO THE MISSISSIPPI RIVER NEAR CLINTON, IOWA

IOWA

The Water Quality Standards (Chapter 16, Code of Iowa, 1973) of the Iowa Water Quality Commission, Department of Environmental Quality classify the Missouri and Mississippi Rivers among the Class A waters. The temperature criteria for this classification are as follows:

1. No heat shall be added to interior streams that would cause an increase of more than 5°F. The rate of temperature change shall not exceed 2°F per hour. In no case shall heat be added in excess of that amount that would raise the stream temperature above 90°F.

2. No heat shall be added to streams designated as cold water fisheries that would cause an increase of more than 3°F. The rate of temperature change shall not exceed 2°F per hour. In no case shall heat be added in excess of that amount that would raise the stream temperature above 68°F.

3. No heat shall be added to lakes and reservoirs that would cause an increase of more than 3°F per hour. In no case shall heat be added in excess of that amount that would raise the temperature of the lake or reservoir above 90°F.

4. No heat shall be added to the Missouri River that would cause an increase of more than 5°F. The rate of temperature change shall not exceed 2°F per hour. In no case shall heat be added that would raise the stream temperature above 90°F.

5. No heat shall be added to the Mississippi River that would cause an increase of more than 5°F. The rate of temperature change shall not exceed 2°F per hour. In addition, the water temperature at representative locations in the Mississippi River shall not exceed the maximum limits in the below table during more than one percent of the hours in the 12-month period ending with any month. Moreover, at no time shall the water temperature at such locations exceed the maximum limits in the below table by more than 3°F.

Zone II - Iowa-Minnesota State Line to the Northern Illinois Border

Zone III - Northern Illinois Border to Iowa-Missouri State Line

Month	Zone II (°F)	Zone III (°F)
January	40	45
February	40	45
March	54	57
April	65	68
May	75	78
June	84	85
July	84	86
August	84	86
September	82	85
October	73	75
November	58	65
December	48	62

Mixing Zone in the Receiving Water

The area of diffusion of an effluent in the receiving water is a mixing zone and the Water Quality Standards shall be applied beyond the mixing zone.

The mixing zone shall be a specified linear distance, volume, or area which is determined on a case-by-case basis using the following criteria:

a. The zone shall be as small as practicable and shall not be of such size or shape as to cause or contribute to the impairment of water uses.

b. The mixing zone shall contain not more than twenty-five (25) percent of the cross-sectional area of volume of flow in the receiving body of water.

c. The mixing zone shall be designed to allow an adequate passageway at all times for the movement or drift of aquatic life.

d. Where there are two or more mixing zones in close proximity, they shall be so defined that a continuous passageway for aquatic life is available.

e. The mixing zone shall not intersect any area of any waters in such a manner that the maintenance of aquatic life in the body of water as a whole would be adversely affected.

In determining the size and location of the mixing zone for any discharge on a case-by-case basis, the following shall be considered:

f. The size of the receiving water, the volume of discharge, the stream bank configuration, the mixing velocities, and other hydrologic or physiographic characteristics.

g. The present and anticipated future use of the body of water.

h. The present and anticipated future water quality of the body of water.

i. The ratio of the volume of waste being discharged to the 7-day, 10-year low flow of the receiving stream.

ILLINOIS

The Illinois Pollution Control Board Rules and Regulations (Chapter 3: Water Pollution) specify the temperature criteria for the Mississippi River as follows:

1. There shall be no abnormal temperature changes that may adversely affect aquatic life unless caused by natural conditions.

2. The normal daily and seasonal temperature fluctuations that existed before the addition of heat due to other than natural causes shall be maintained.

3. The maximum temperature rise above natural temperatures shall not exceed 5°F.

4. In addition, the water temperature at representative locations in the main river shall not exceed the maximum limits in the following table during more than one percent of the hours in the 12-month period ending with any month. Moreover, at no time shall the water temperature at such locations exceed the maximum limits in the following table by more than 3°F.

Zone 1: Mississippi River (Wisconsin Border to Iowa Border)

Zone 2: Mississippi River (Iowa Border to Alton Lock and Dam)

Zone 3: Mississippi River (South of Alton Lock and Dam)

Month	Zone 1 (°F)	Zone 2 (°F)	Zone 3 (°F)
January	45	45	50
February	45	45	50
March	57	57	60
April	68	68	70
May	78	78	80
June	85	86	87

Month	Zone 1 (°F)	Zone 2 (°F)	Zone 3 (°F)
July	86	88	89
August	86	88	89
September	85	86	87
October	75	75	78
November	65	65	70
December	52	52	57

5. The owner or operator of a source of heated effluent which discharges 0.5 billion British thermal units per hour or more shall demonstrate in a hearing before this Board not less than 5 nor more than 6 years after the effective date of these regulations, or, in the case of new sources, after the commencement of operation, that discharges from that source have not caused and cannot be reasonably expected to cause significant ecological damage to the receiving waters. If such proof is not made to the satisfaction of the Board, appropriate corrective measures shall be ordered to be taken within a reasonable time as determined by the Board.

6. Permits for heated effluent discharges, whether issued by the Board or the Environmental Protection Agency, shall be subject to revision in the event that reasonable future development creates a need for reallocation of the assimilative capacity of the receiving stream as defined in the regulation above.

7. The owner or operator of a source of heated effluent shall maintain such records and conduct such studies of the effluents from such source and of their effects as may be required by the Environmental Protection Agency or in any permit granted under the Environmental Protection Act.

8. Appropriate corrective measures will be required if, upon complaint filed in accordance with Board rules, it is found at any time that any heated effluent causes significant ecological damage to the receiving stream.

Mixing Zones

a. In the application of any of the rules and regulations, whenever a water quality standard is more restrictive than its corresponding effluent standard, then an opportunity shall be allowed for the mixture of an effluent with its

receiving waters. Water quality standards must be met at every point outside of the mixing zone. The size of the mixing zone cannot be uniformly prescribed. The governing principle is that the proportion of any body of water or segment thereof within mixing zones must be quite small if the water quality standards are to have any meaning. This principle shall be applied on a case-by-case basis to ensure that neither any individual source nor the aggregate of sources shall cause excessive zones to exceed the standards. The water quality standards must be met in the bulk of the body of water, and no body of water may be used totally as a mixing zone for a single outfall or combination of outfalls. Moreover, except as otherwise provided, no single mixing zone shall exceed the area of a circle with a radius of 600 feet. Single sources of effluents which have more than one outfall shall be limited to a total mixing area no larger than that allowable if a single outfall were used.

In determining the size of the mixing zone for any discharge, the following must be considered:

1. The character of the body of water.
2. The present and anticipated future use of body of water.
3. The present and anticipated water quality of the body of water.
4. The effect of the discharge on the present and anticipated future water quality.
5. The dilution ratio.
6. The nature of the contaminant.

b. In addition to the above, the mixing zone shall be so designed as to assure a reasonable zone of passage for aquatic life in which the water quality standards are met. The mixing zone shall not intersect any area of any such waters in such a manner that the maintenance of aquatic life in the body of water as a whole would be adversely affected, nor shall any mixing zone contain more than 25% of the cross-sectional area or volume of flow of a stream except for those streams where the dilution ratio is less than 3:1.

APPENDIX B

EXCESS TEMPERATURE PLOTS FOR CROSS-SECTIONAL SURVEYS

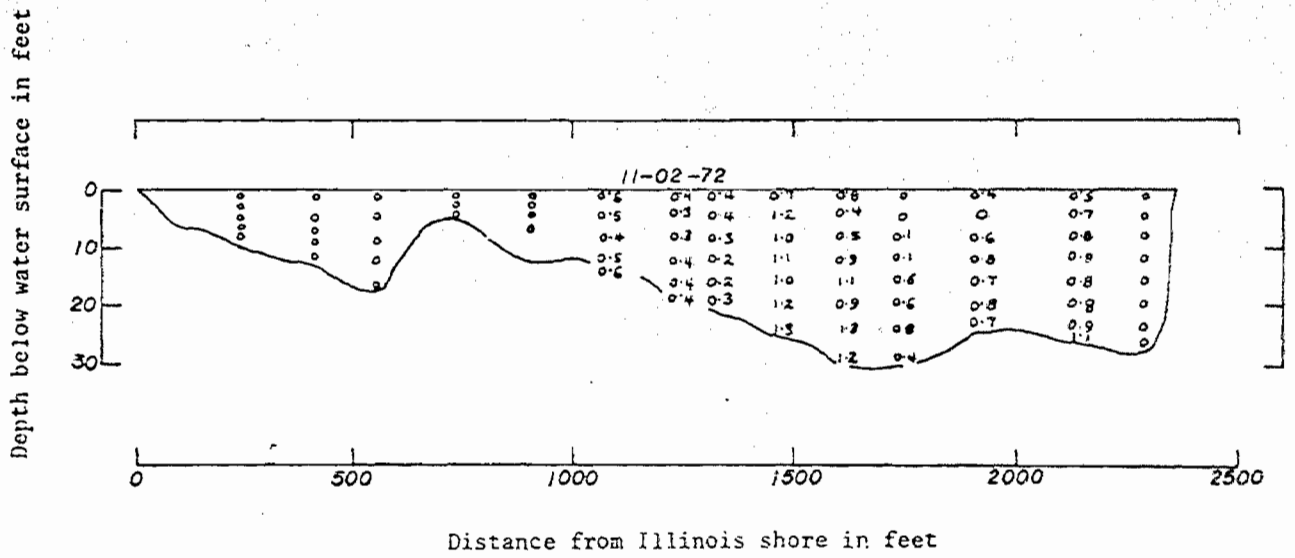

Fig. B.1 Observed excess temperatures in °F 500 ft downstream from diffuser pipe on November 2, 1972.

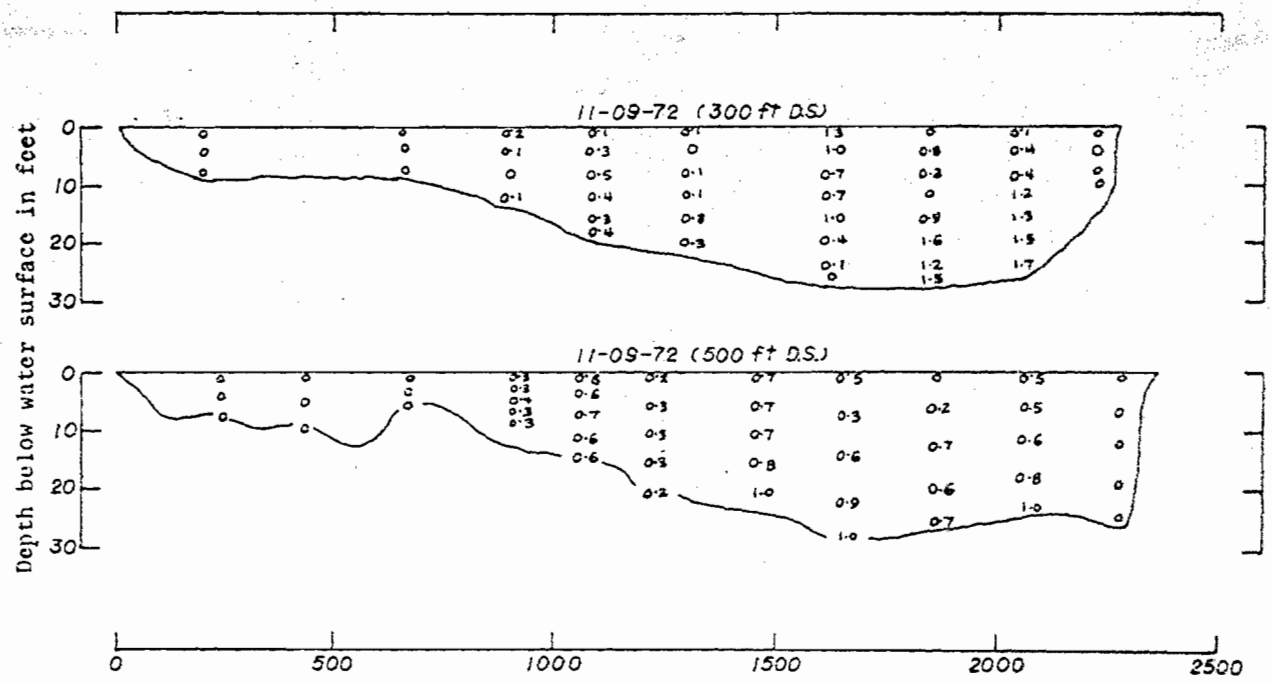

Fig. B.2 Observed excess temperatures in °F 300 and 500 ft downstream from diffuser pipe on November 9, 1972.

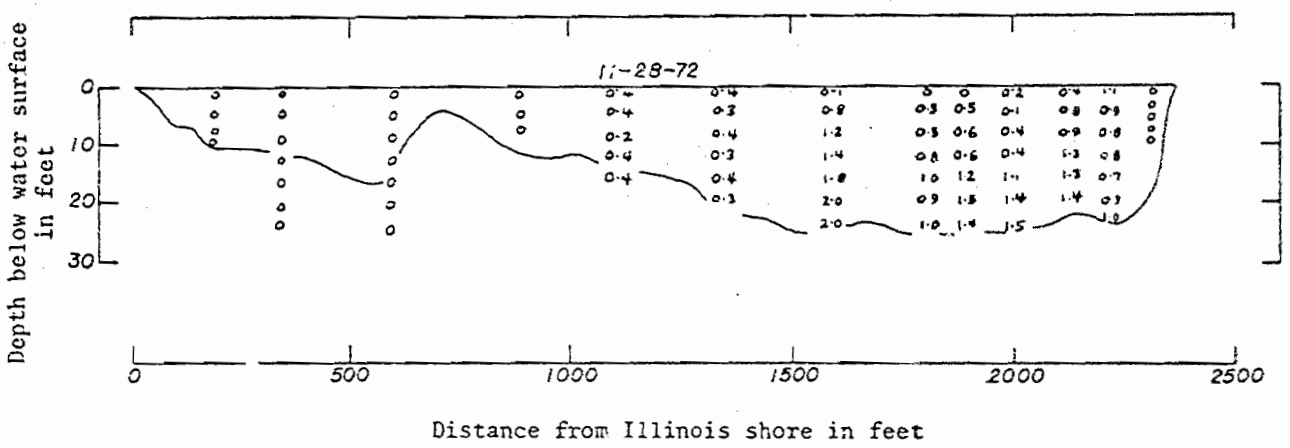

Fig. B.3 Observed excess temperatures in °F 500 ft downstream from diffuser pipe on November 28, 1972.

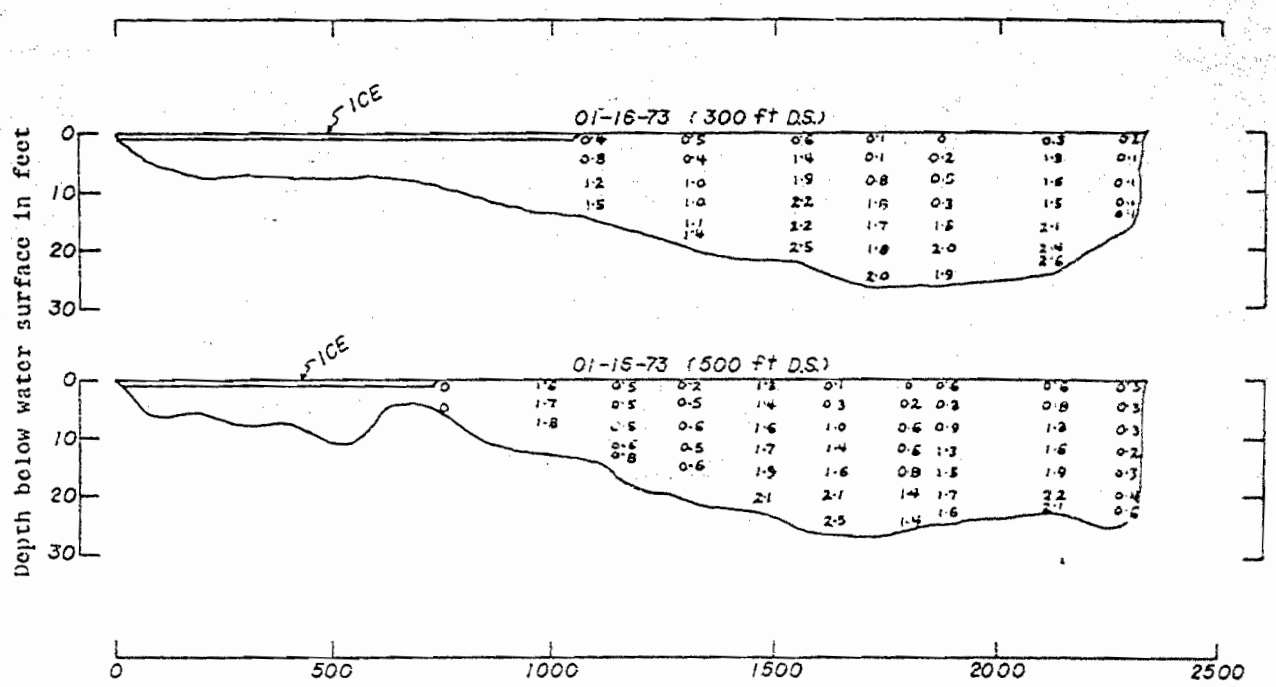

Fig. B.4 Observed excess temperatures in °F 300 and 500 ft downstream from diffuser pipe on January 16, 1973.

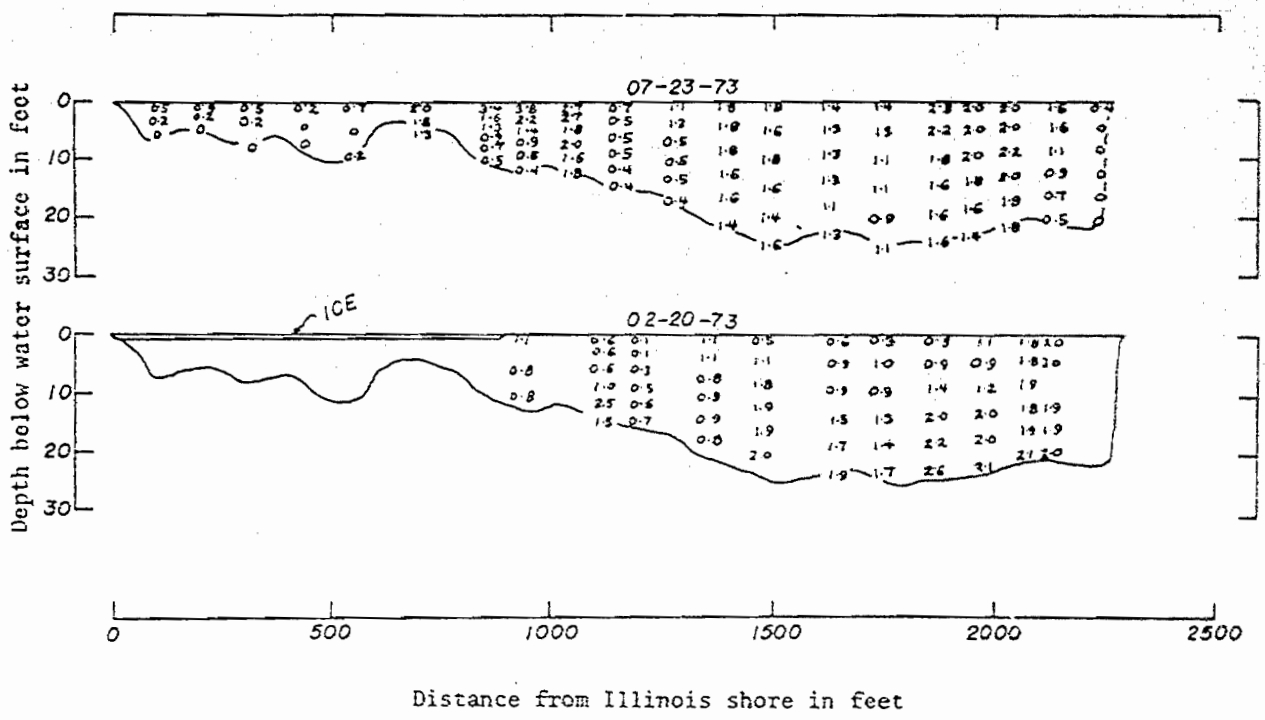

Fig. B.5 Observed excess temperatures in °F 500 ft downstream from diffuser pipe on February 20 and July 23, 1973.

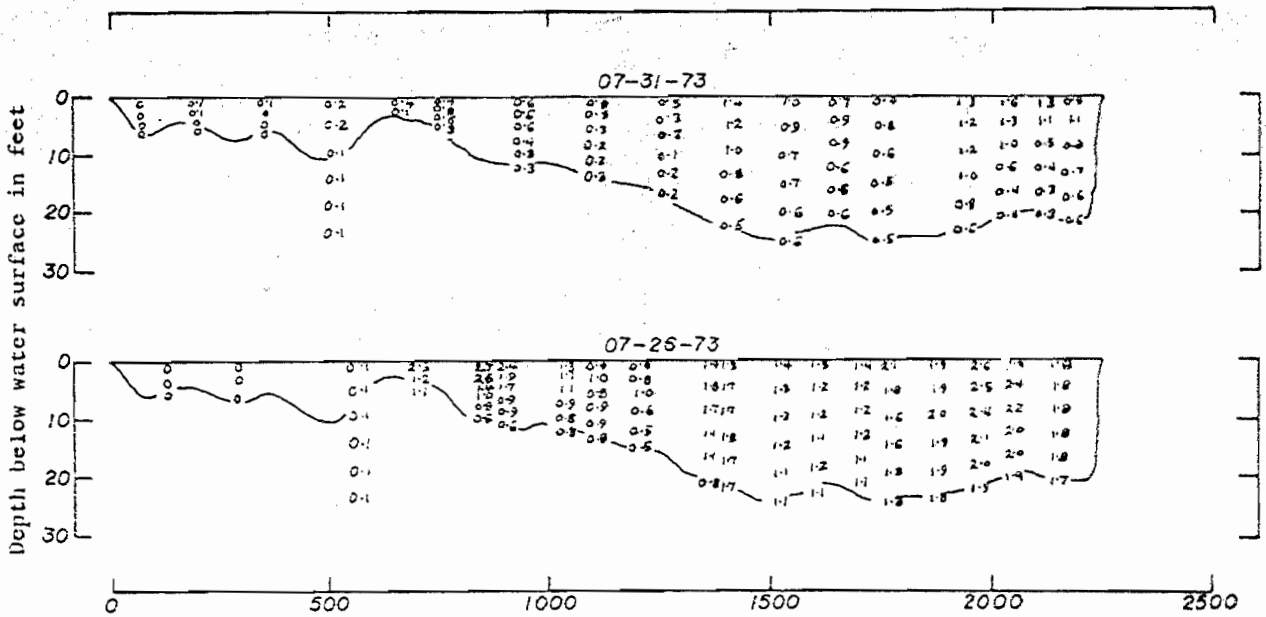

Fig. B.6 Observed excess temperatures in °F 500 ft downstream from diffuser pipe on July 26 and July 31, 1973.

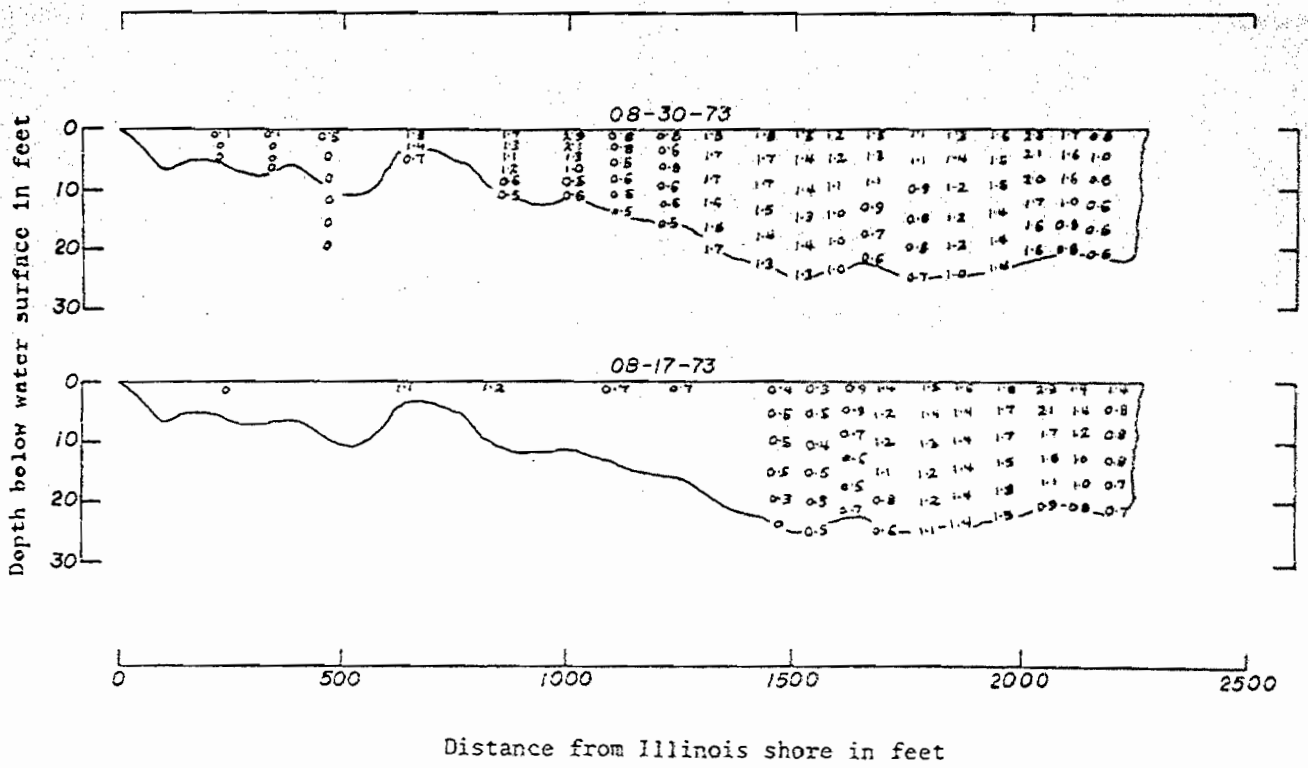

Fig. B.7 Observed excess temperatures in °F 500 ft downstream from diffuser pipe on August 17 and August 30, 1973.

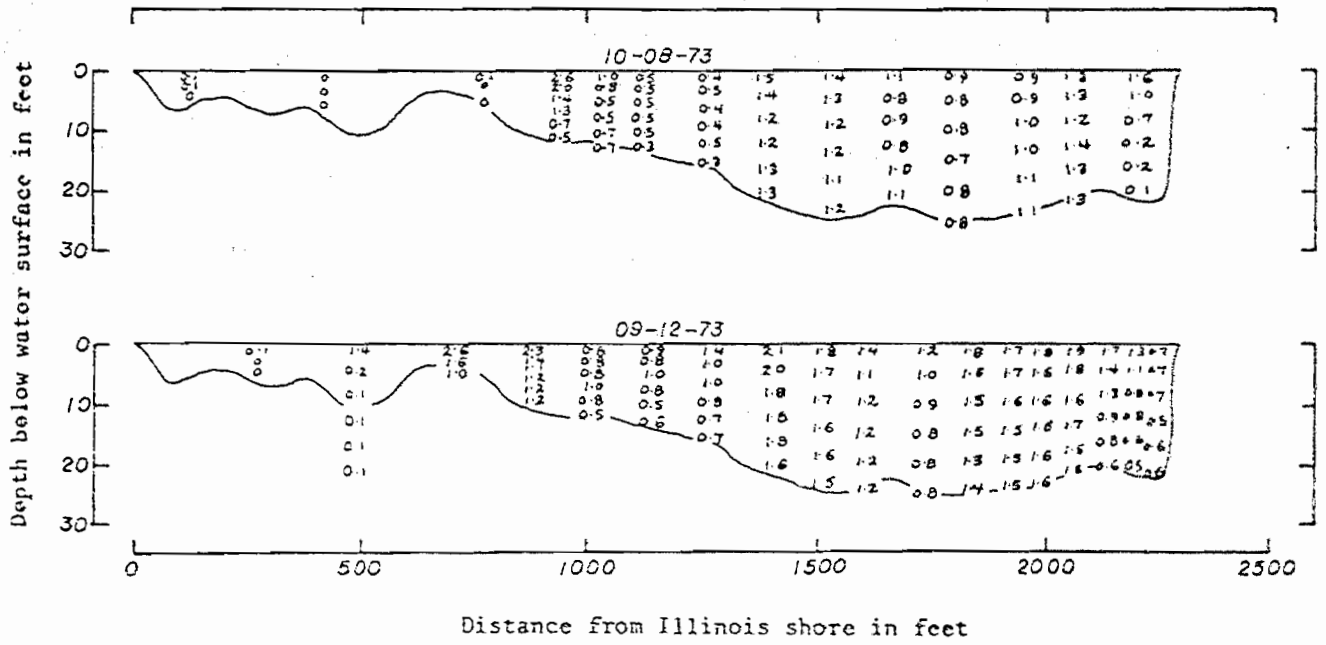

Fig. B.8 Observed excess temperatures in °F 500 ft downstream from diffuser pipe on September 12 and October 8, 1973.

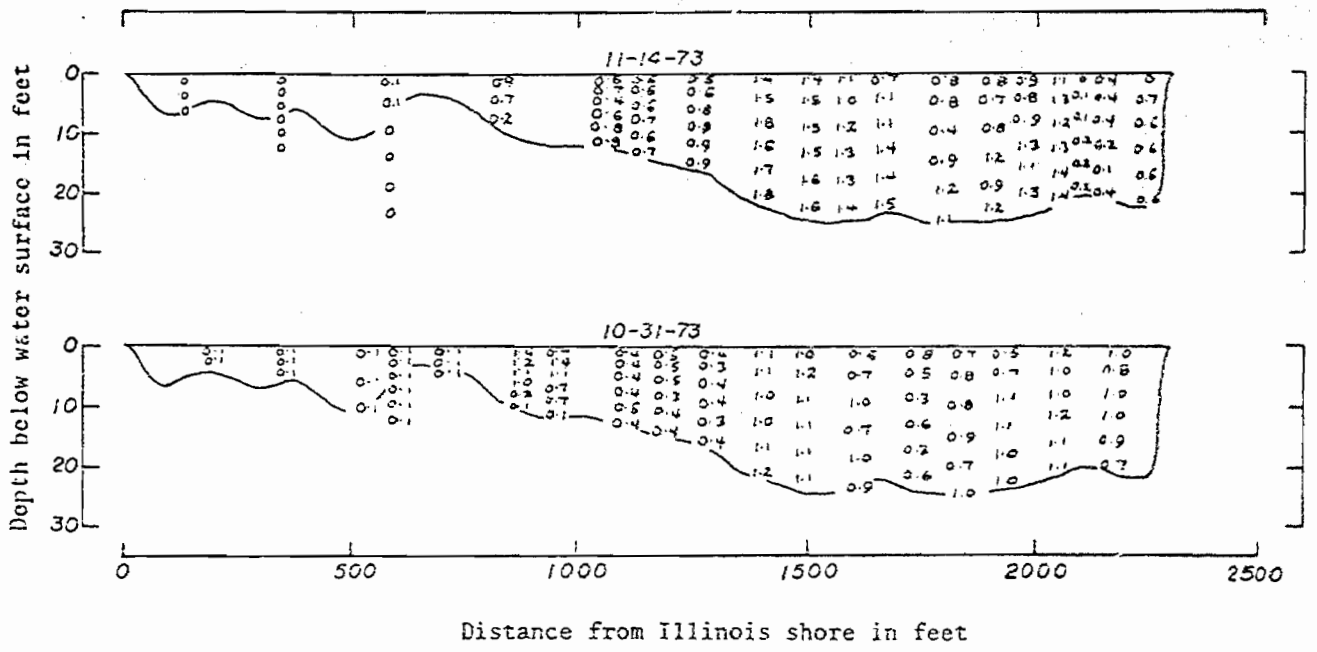

Fig. B.9 Observed excess temperatures in °F 500 ft downstream from diffuser pipe on October 31 and November 14, 1973.

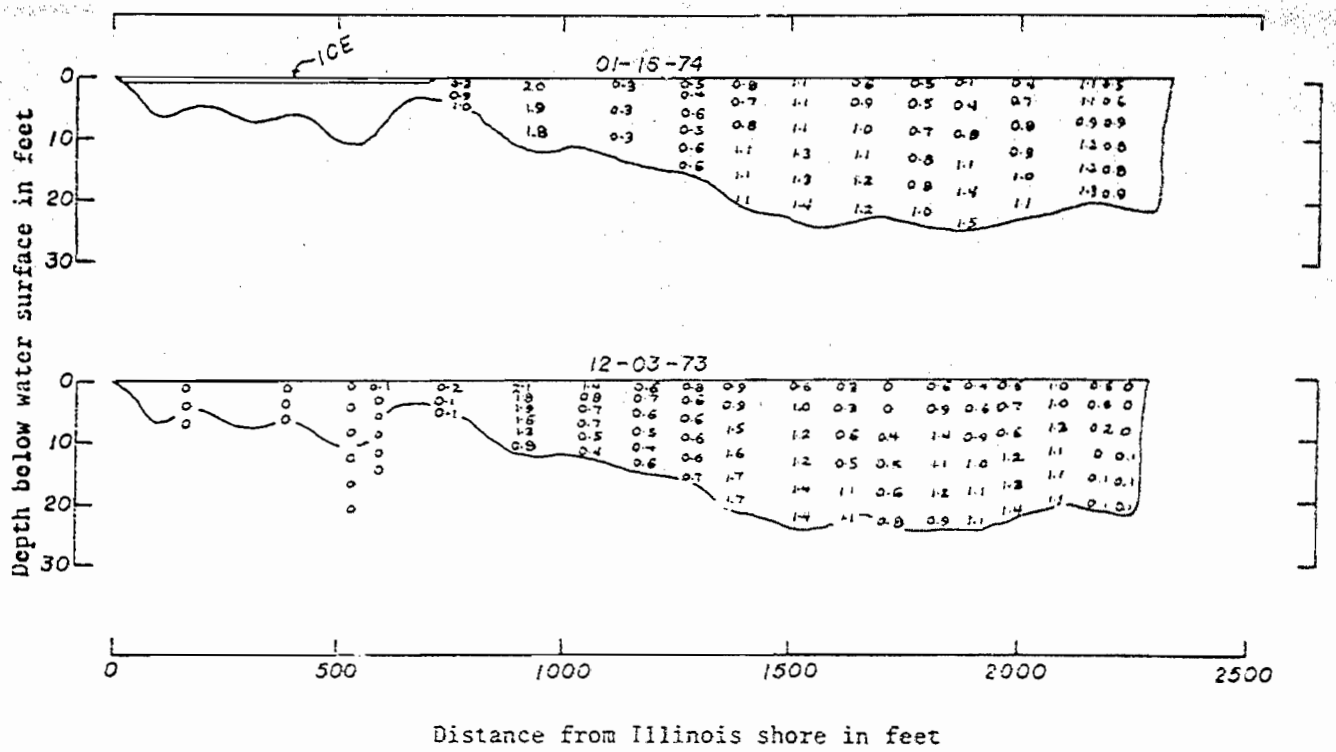

Fig. B. 10 Observed excess temperatures in °F 500 ft downstream from diffuser pipe on December 3, 1973, and January 16, 1974.

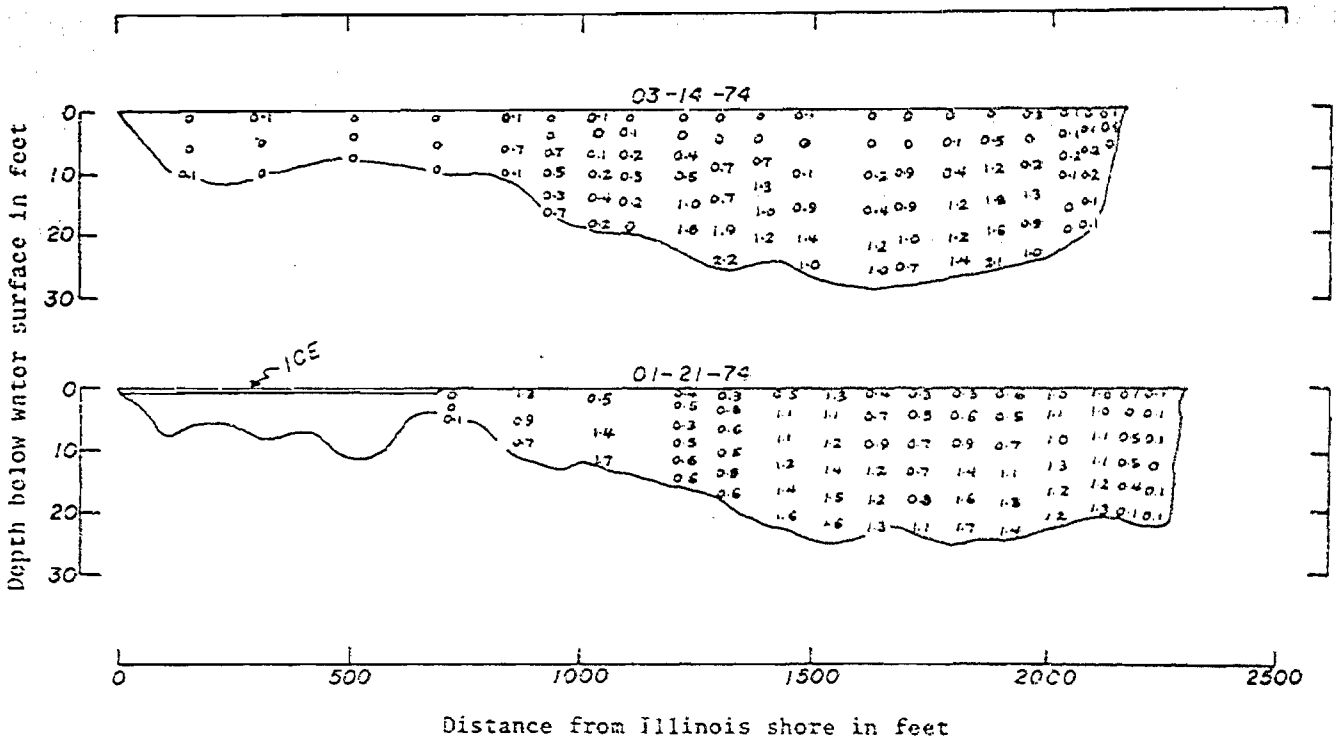

Fig. B.11 Observed excess temperatures in °F 500 ft downstream from diffuser pipe on January 21, 1974, and 150 ft downstream from diffuser pipe on March 14, 1974.

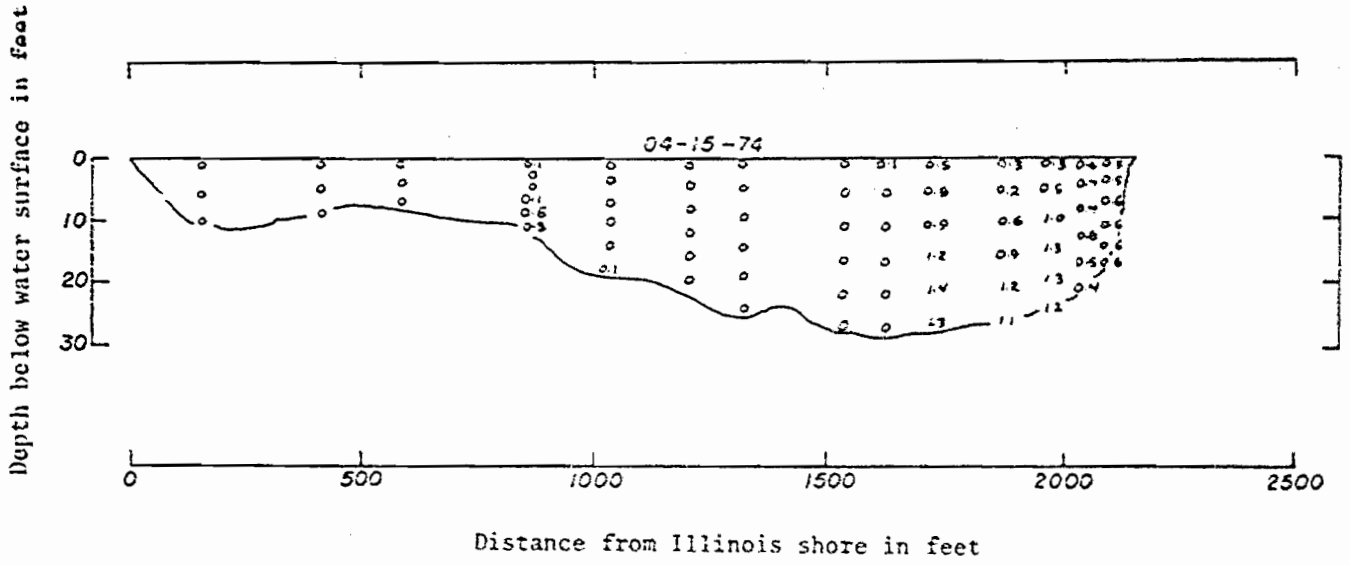

Fig. B. 12 Observed excess temperatures in °F 150 ft downstream from diffuser pipe on April 15, 1974.

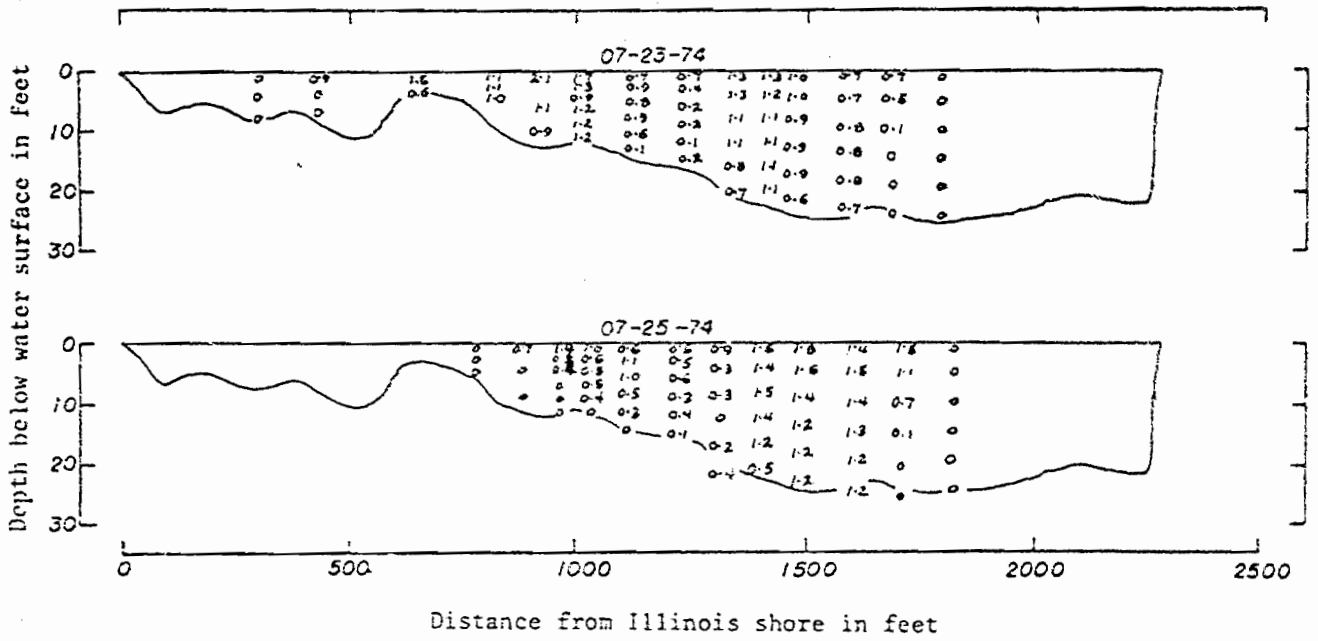

Fig. B.13 Observed excess temperatures in °F 500 ft downstream from diffuser pipe on July 23 and July 25, 1974.

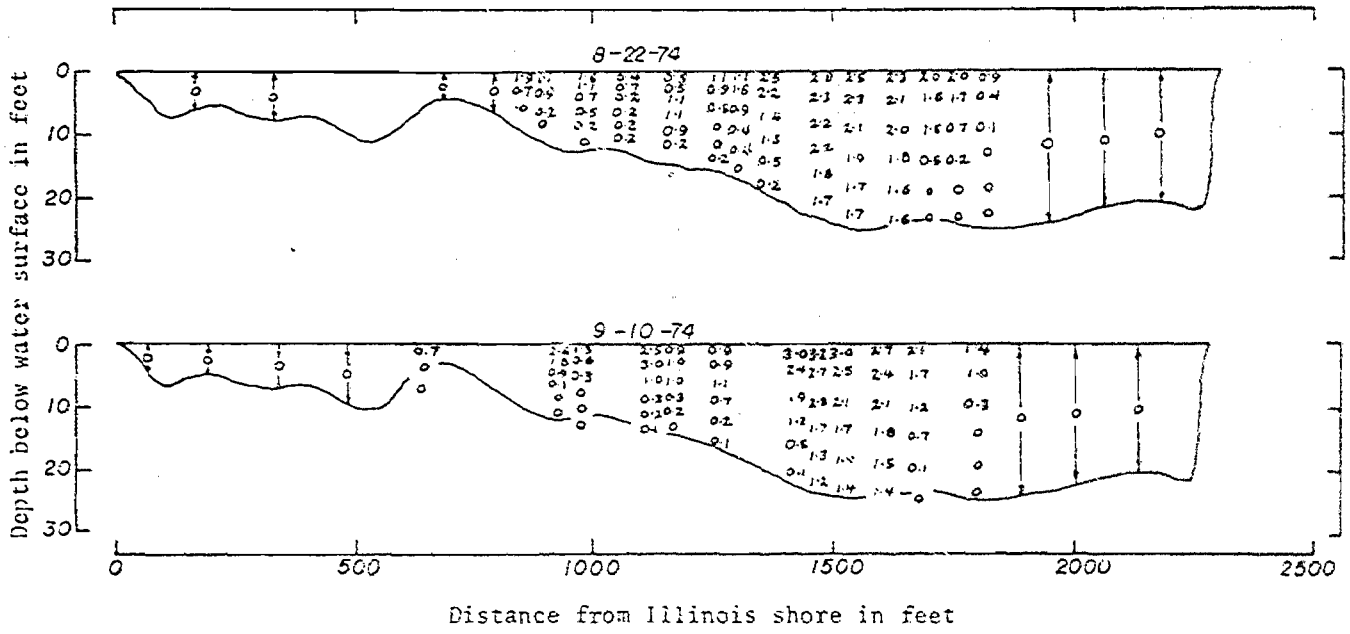

Fig. B.14 Observed excess temperatures in °F 500 ft downstream from diffuser pipe on August 22 and September 10, 1974.

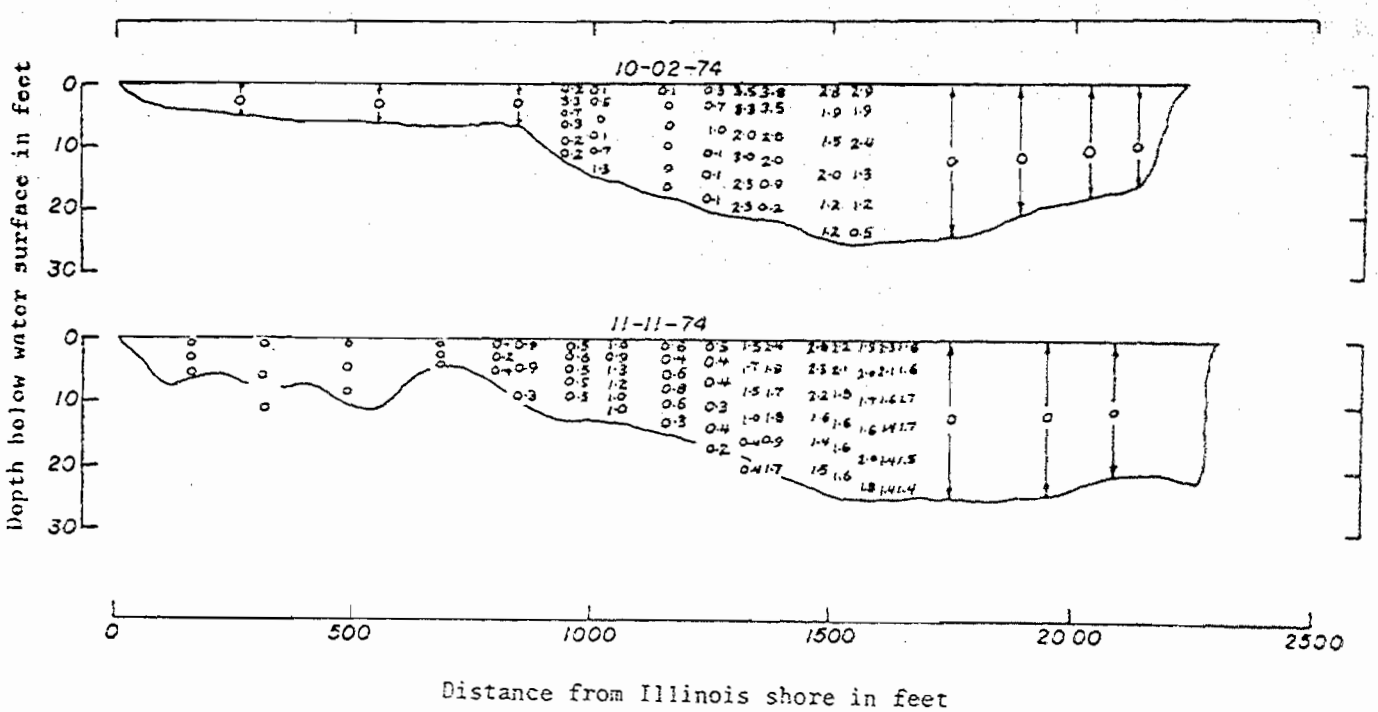

Fig. B.15 Observed excess temperatures in °F 150 ft downstream from diffuser pipe on October 2 and November 11, 1974.

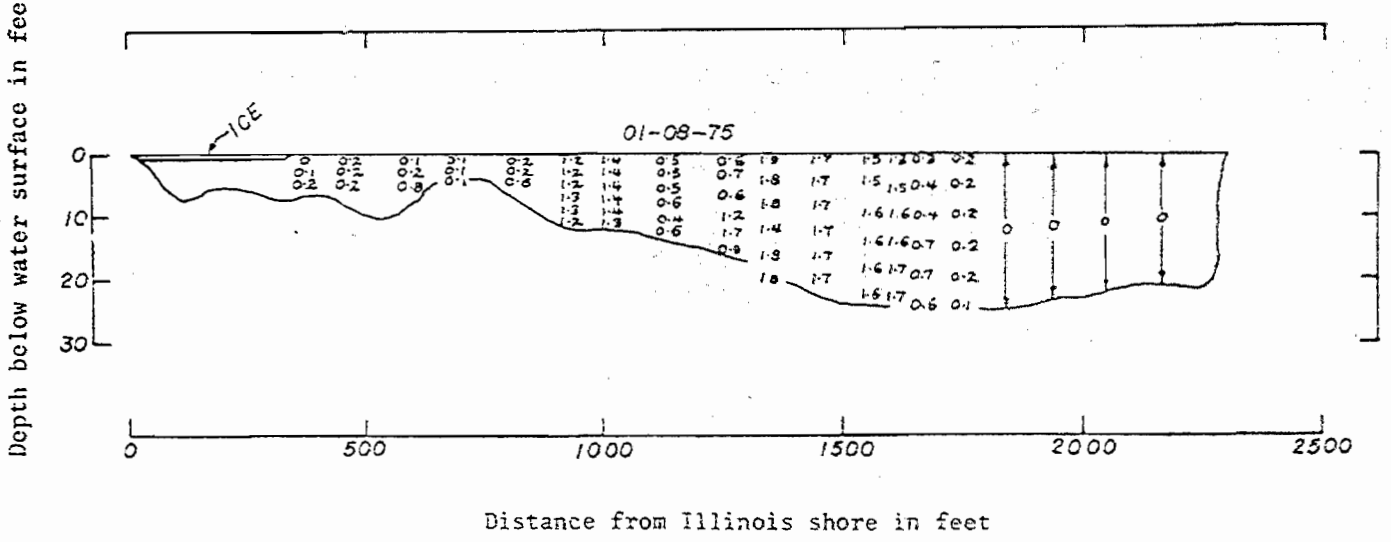

Fig. B.16 Observed excess temperatures in °F 500 ft downstream from diffuser pipe on January 8, 1975.

APPENDIX C

EXCESS TEMPERATURE AND VELOCITY PLOTS FOR SINGLE-PORT SURVEYS

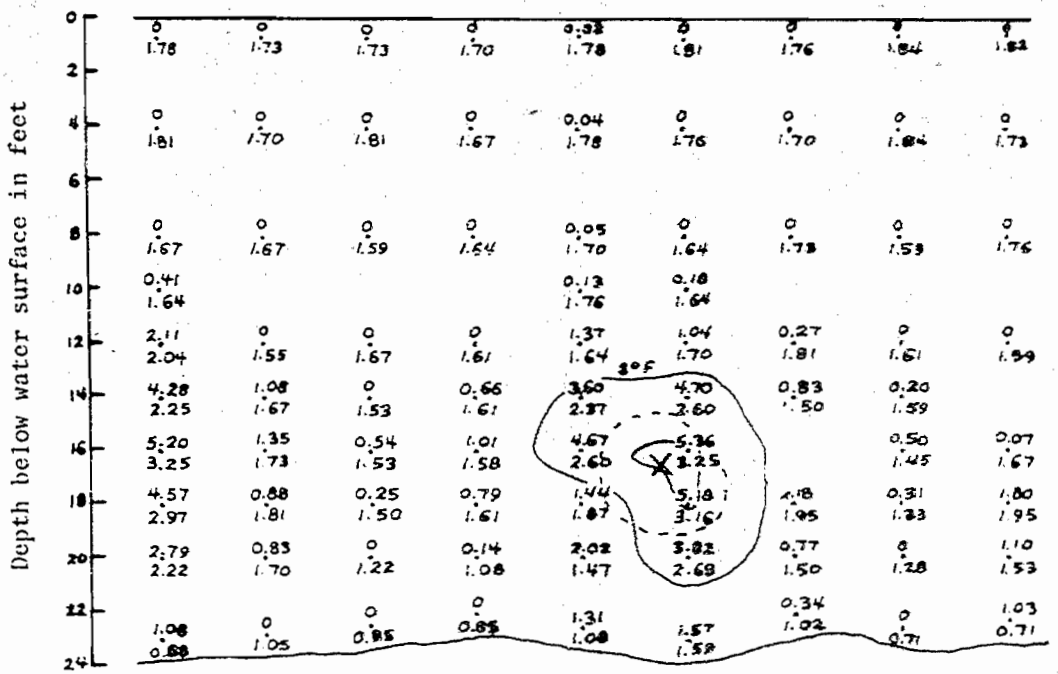

(a) 35 feet downstream

Fig. C.1 Excess temperature in °F and velocity in ft/sec measured downstream from a main channel diffuser pipe port on November 16, 1973.

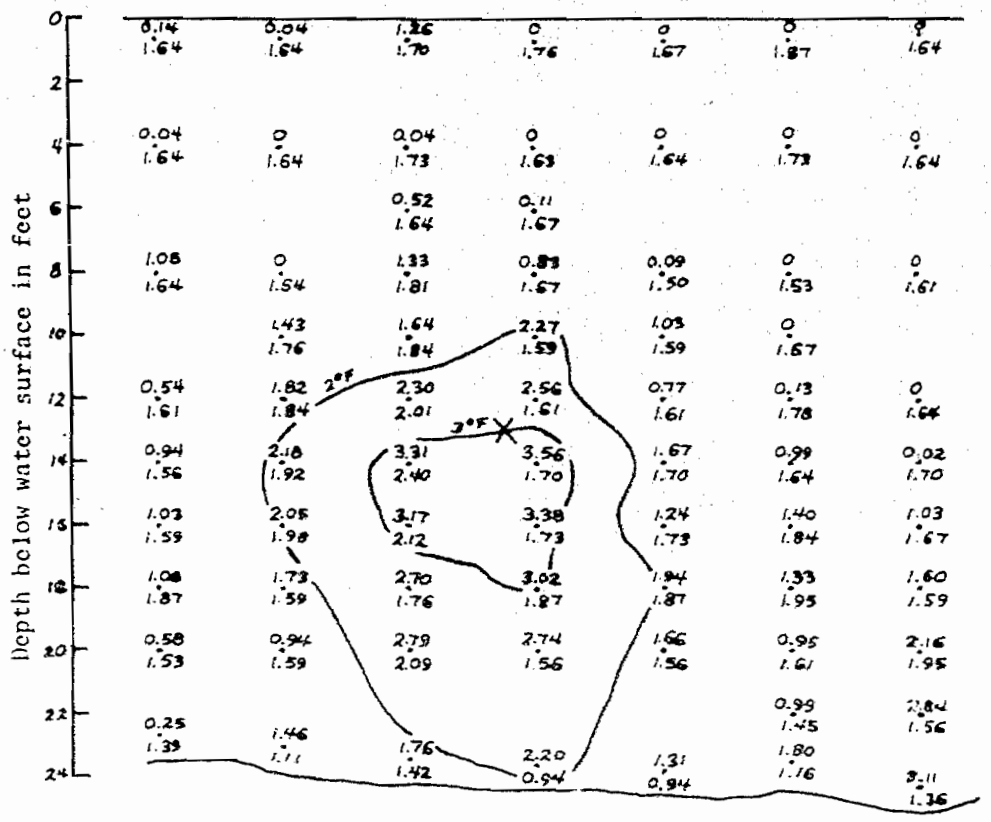

(b) 05 feet downstream

Fig. C.1 (continued).

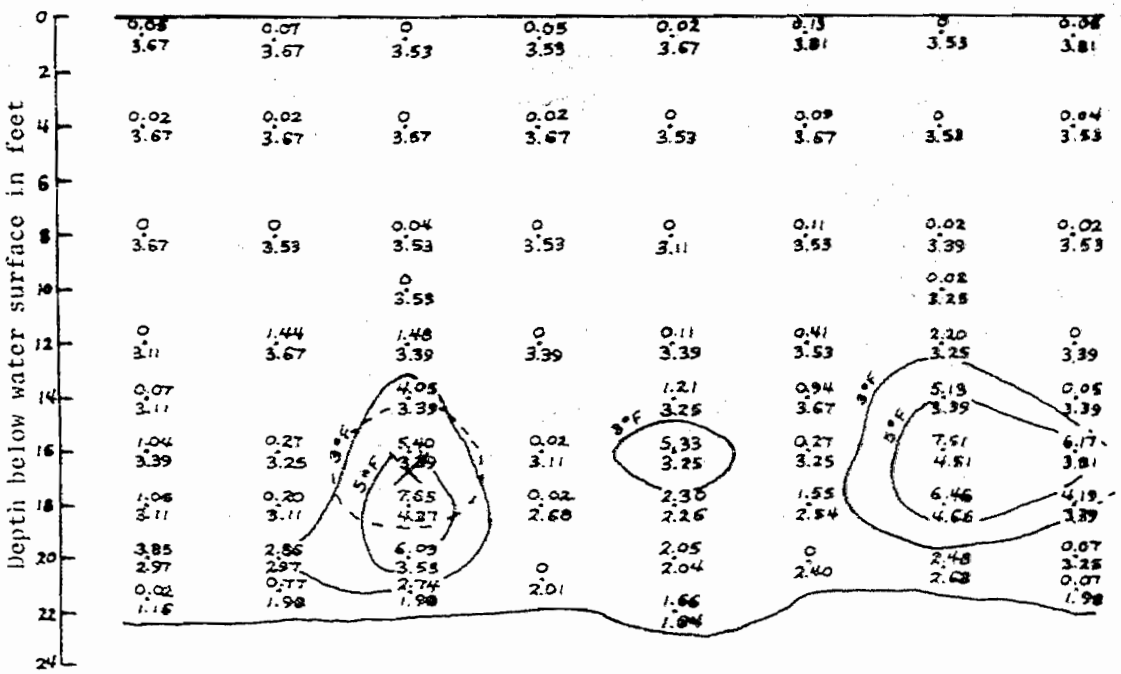

(a) 15 feet downstream

Fig. C.2 Excess temperature in °F and velocity in ft/sec measured downstream from a main channel diffuser pipe port on March 12, 1974.

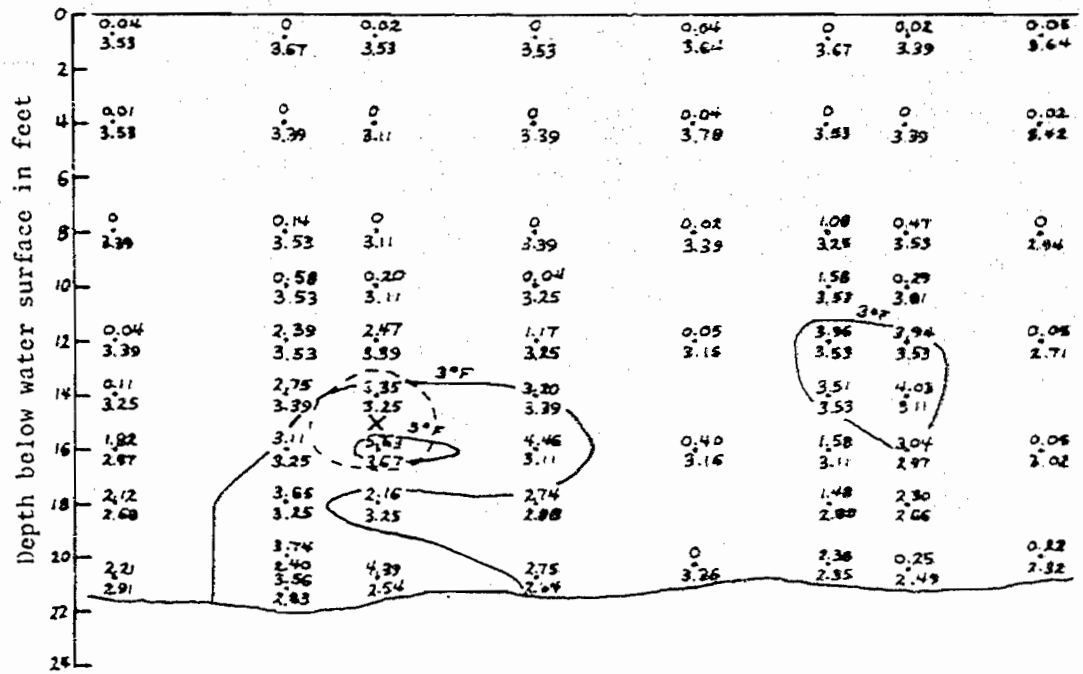

(b) 45 feet downstream

Fig. C.2 (continued).

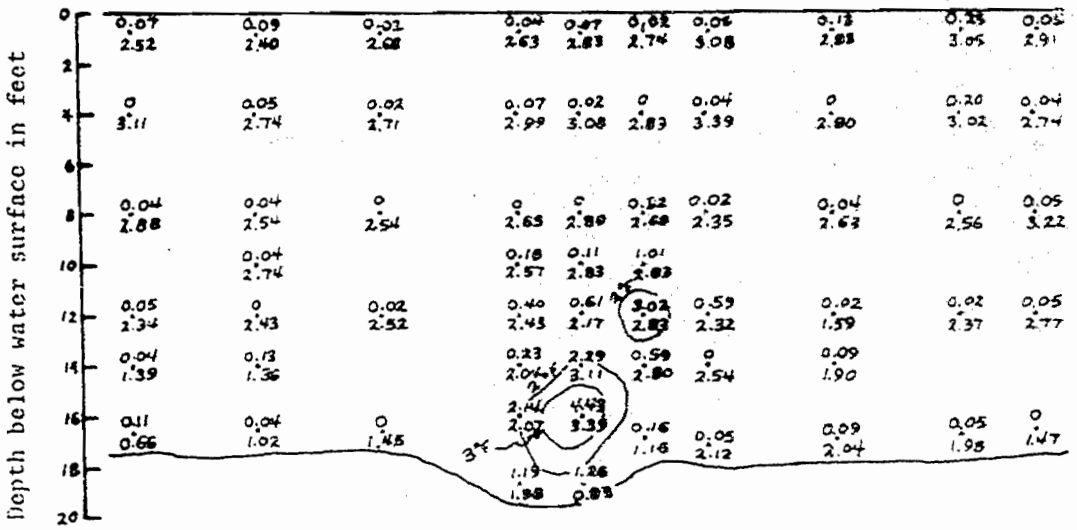

(a) 35 feet downstream

Fig. C. 3 Excess temperature in °F and velocity in ft/sec measured downstream from a shallow channel diffuser pipe port on March 13, 1974.

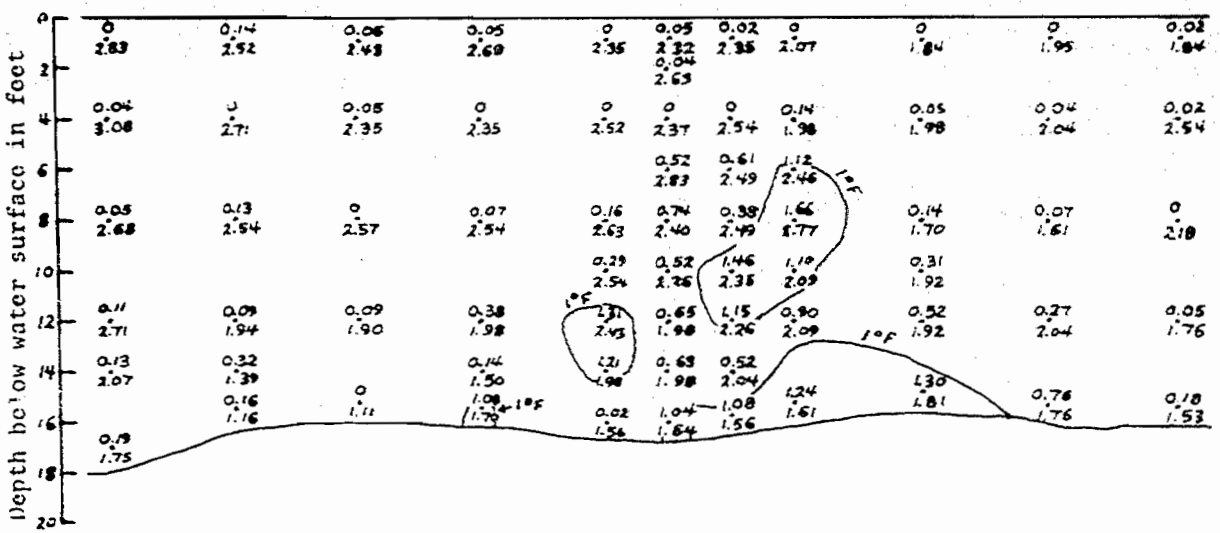

(b) 65 feet downstream

Fig. C.3 (continued).

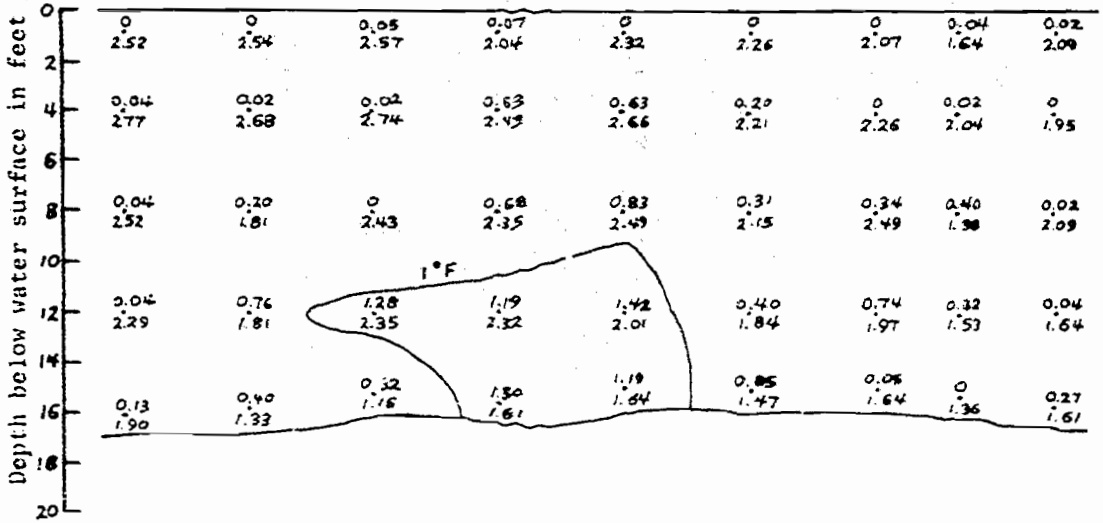

(c) 95 feet downstream

Fig. C.3 (continued).

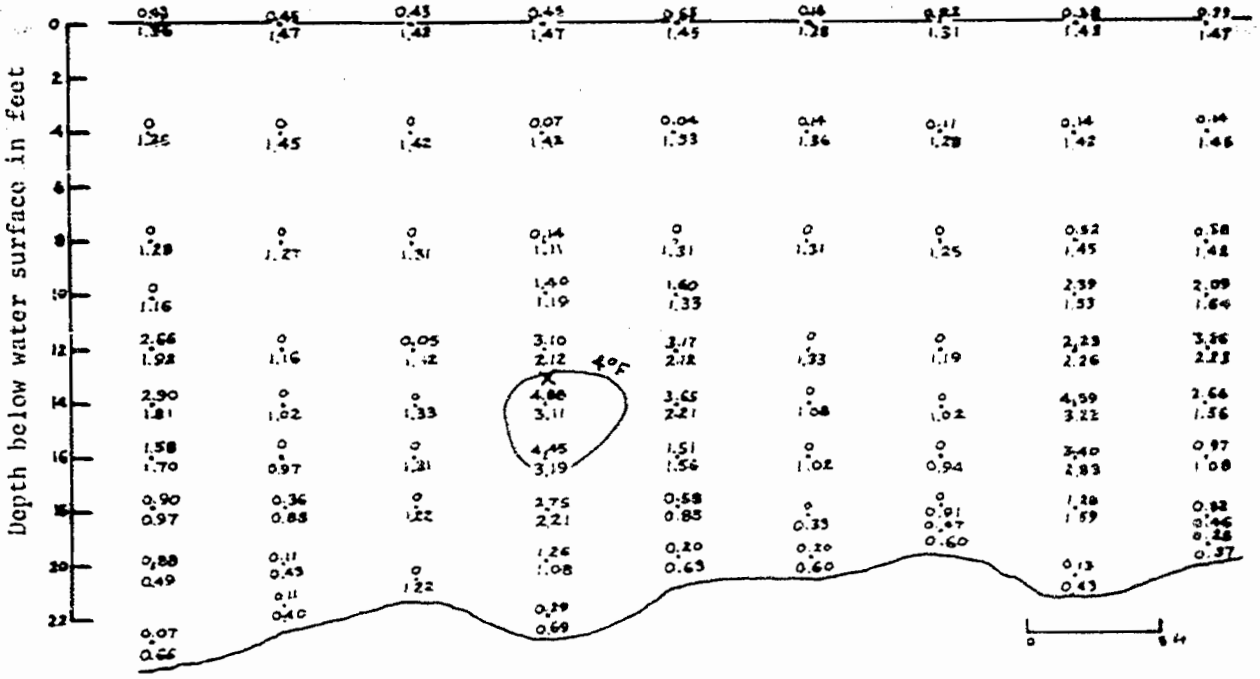

(a) 15 feet downstream

Fig. C.4 Excess temperature in °F and velocity in ft/sec measured downstream from a main channel diffuser pipe port on July 24, 1974.

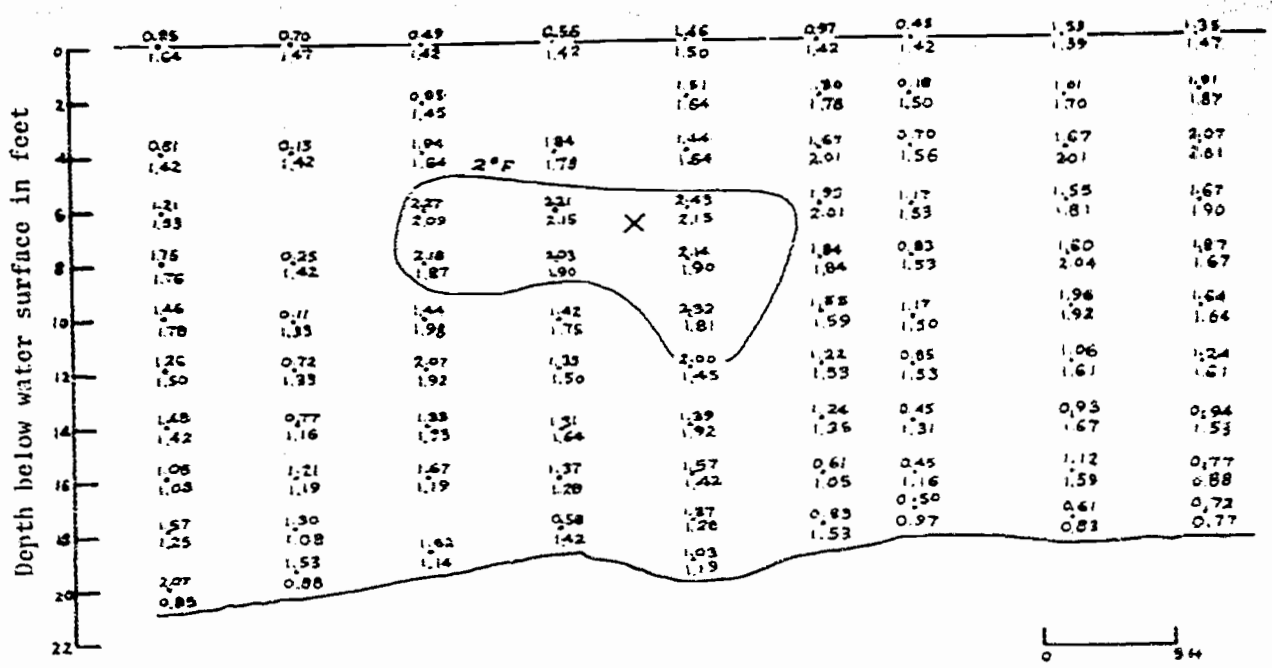

(b) 45 feet downstream

Fig. C.4 (continued).

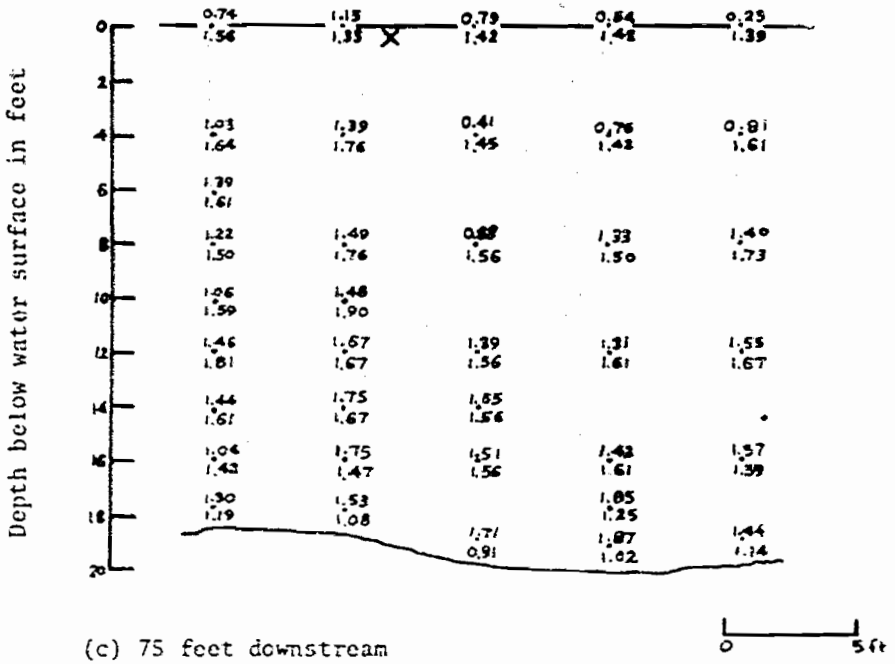

(c) 75 feet downstream

Fig. C.4 (continued).

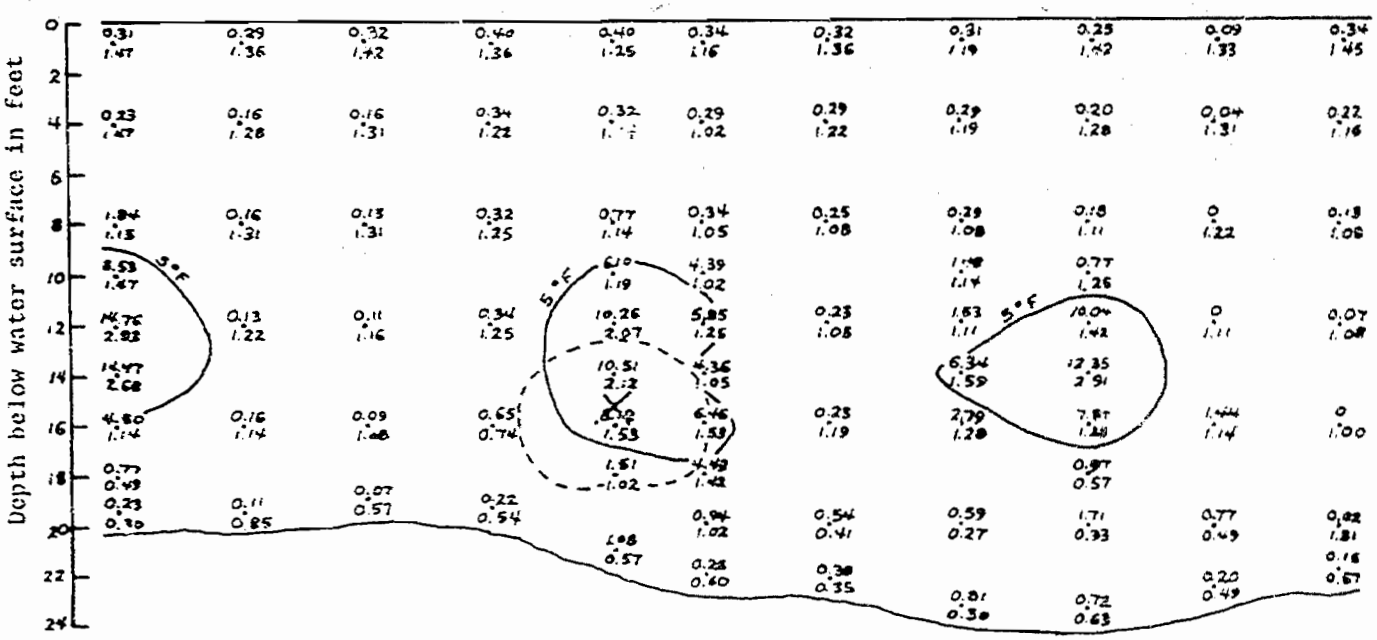

(a) 15 feet downstream

Fig. C.5 Excess temperature in °F and velocity in ft/sec measured downstream from a main channel diffuser pipe port on October 1, 1974.

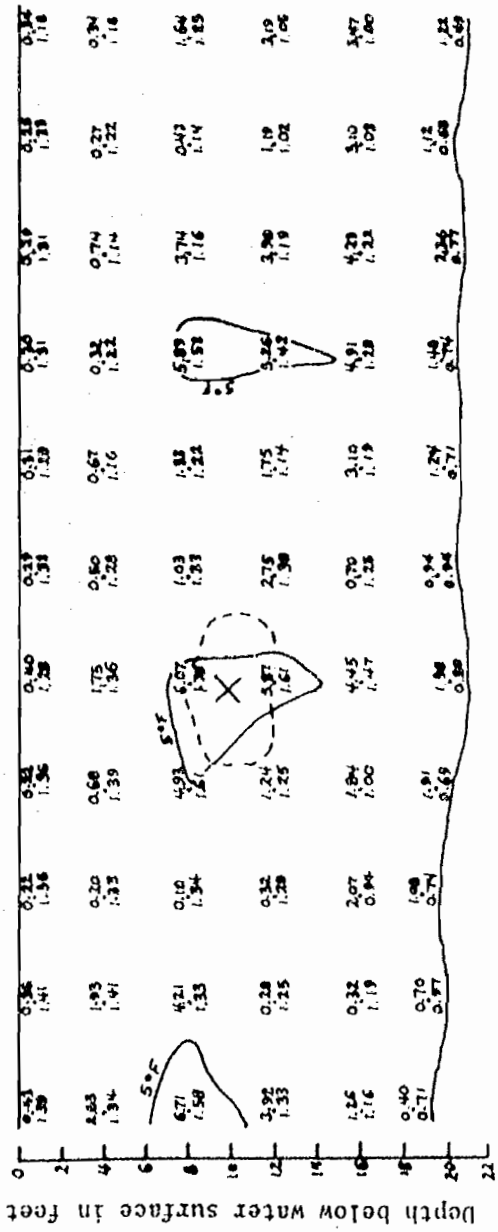

(b) 45 feet downstream

Fig. C.5 (continued).

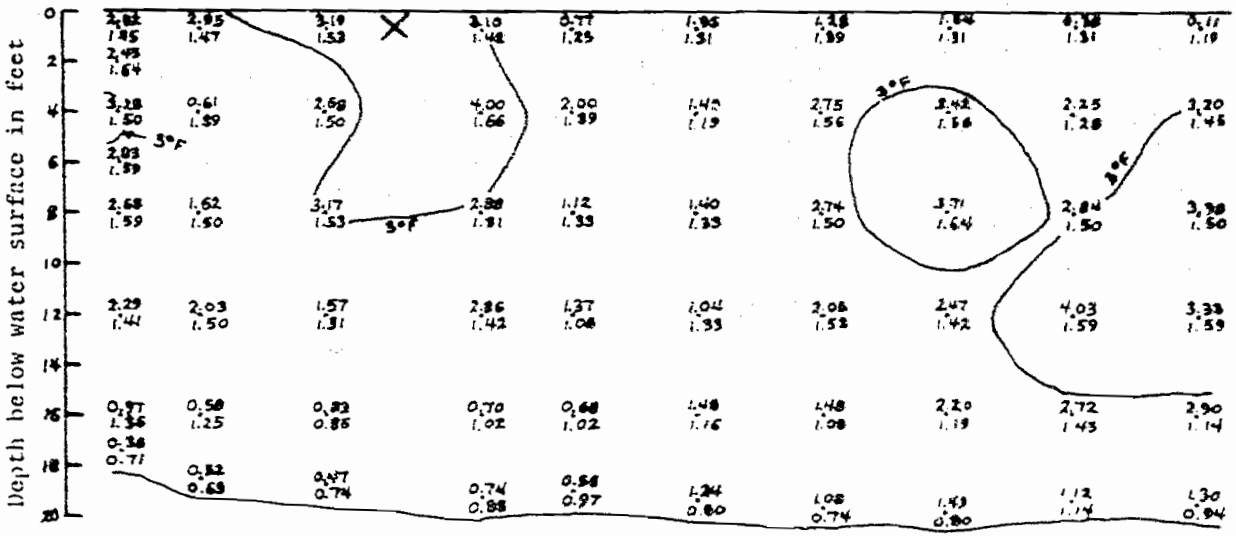

(c) 75 feet downstream

Fig. C.5 (continued).

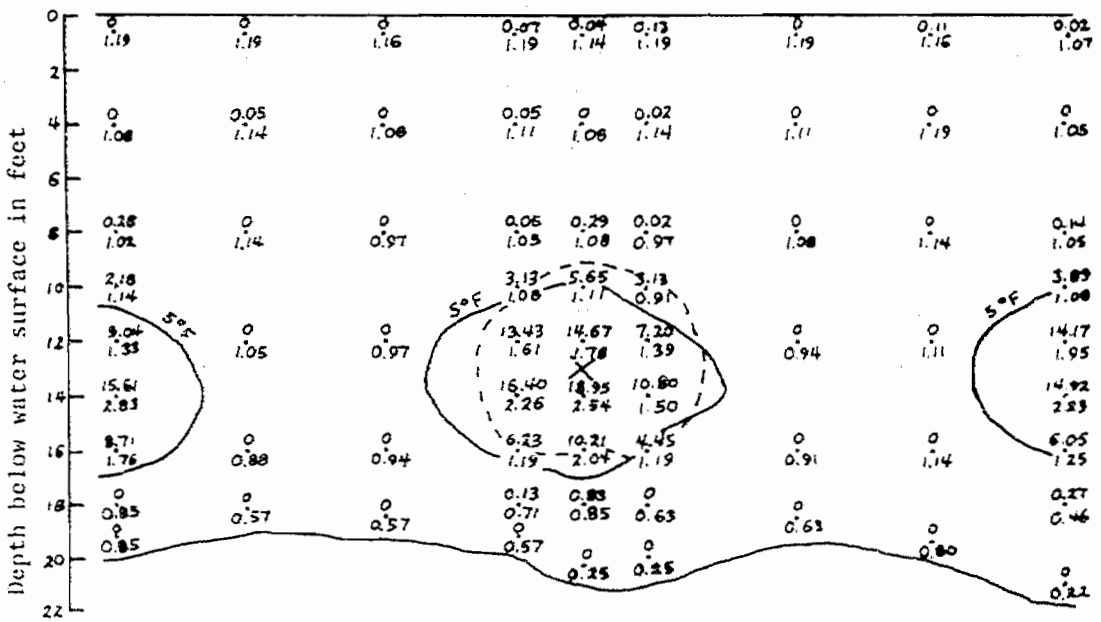

(a) 15 feet downstream

Fig. C.6 Excess temperature in °F and velocity in ft/sec measured downstream from a main channel diffuser pipe port on October 25, 1974.

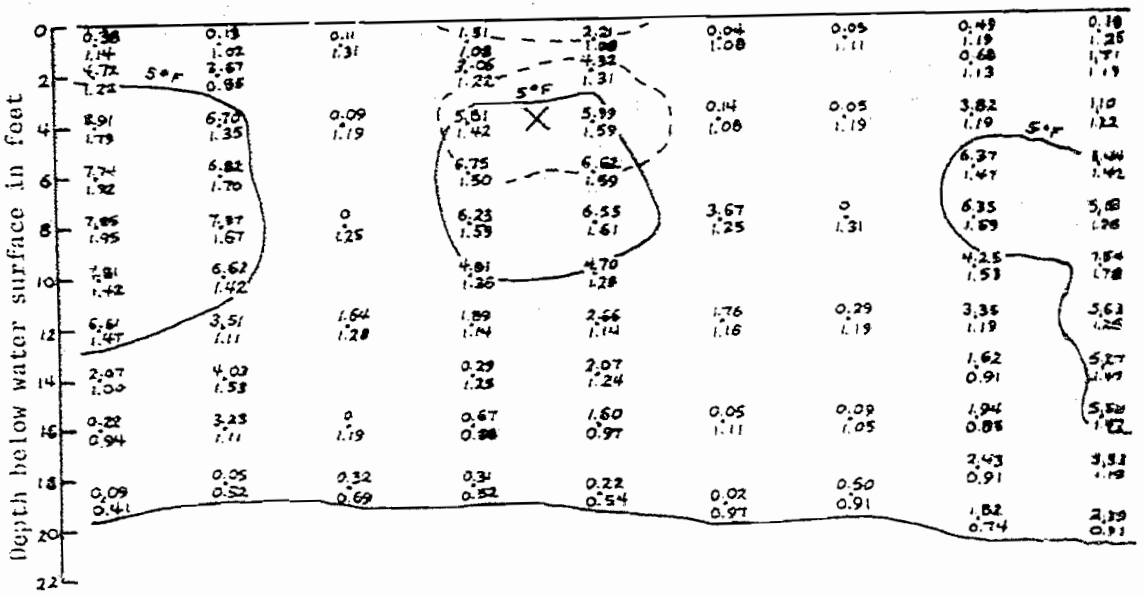

(b) 45 feet downstream

Fig. C.6 (continued).

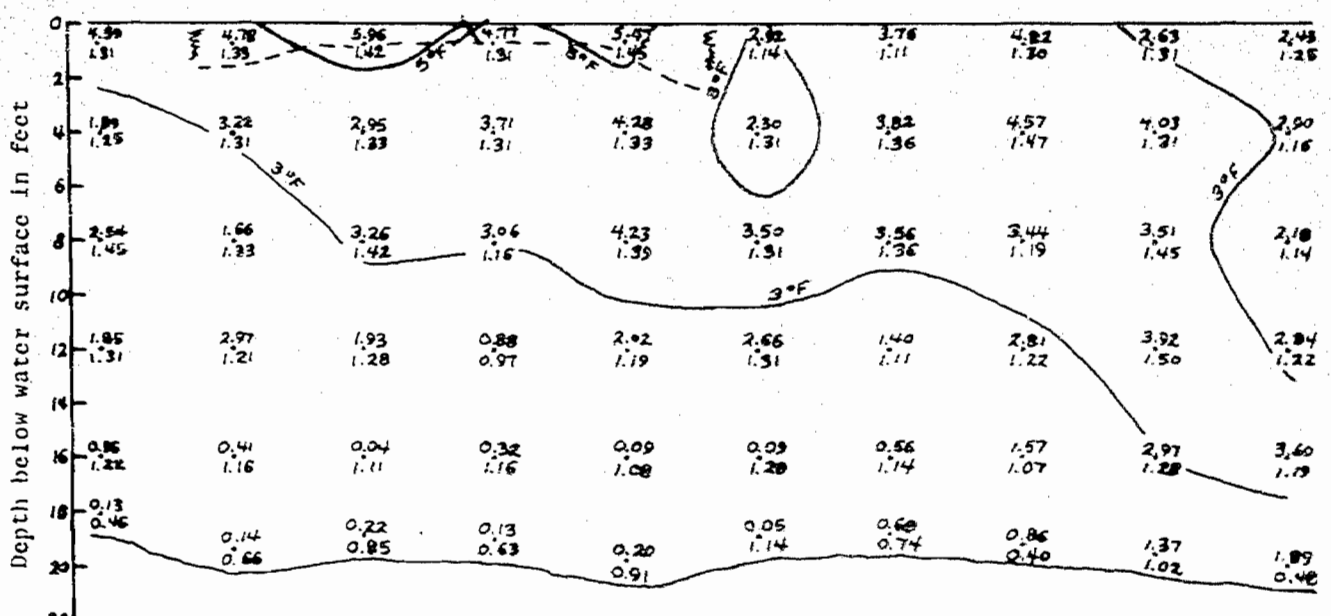

(c) 75 feet downstream

Fig. C.6 (continued).

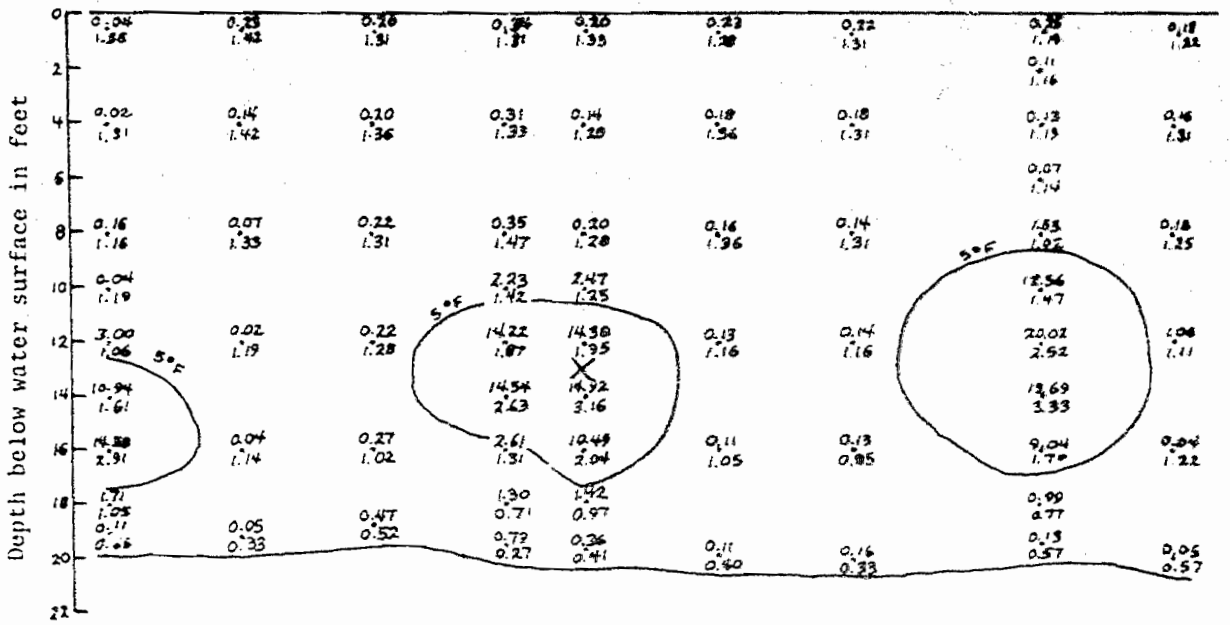

(a) 15 feet downstream

Fig. C.7 Excess temperature in °F and velocity in ft/sec measured downstream from a main channel diffuser pipe port on October 30, 1974.

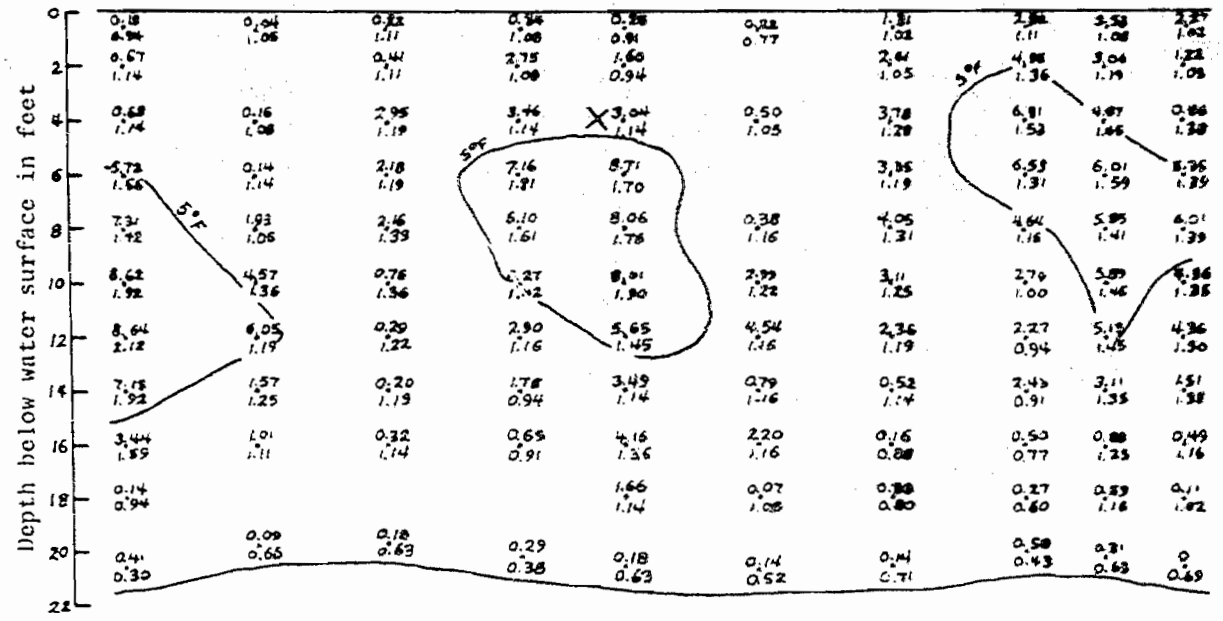

(c) 45 feet downstream

Fig. C.7 (continued).

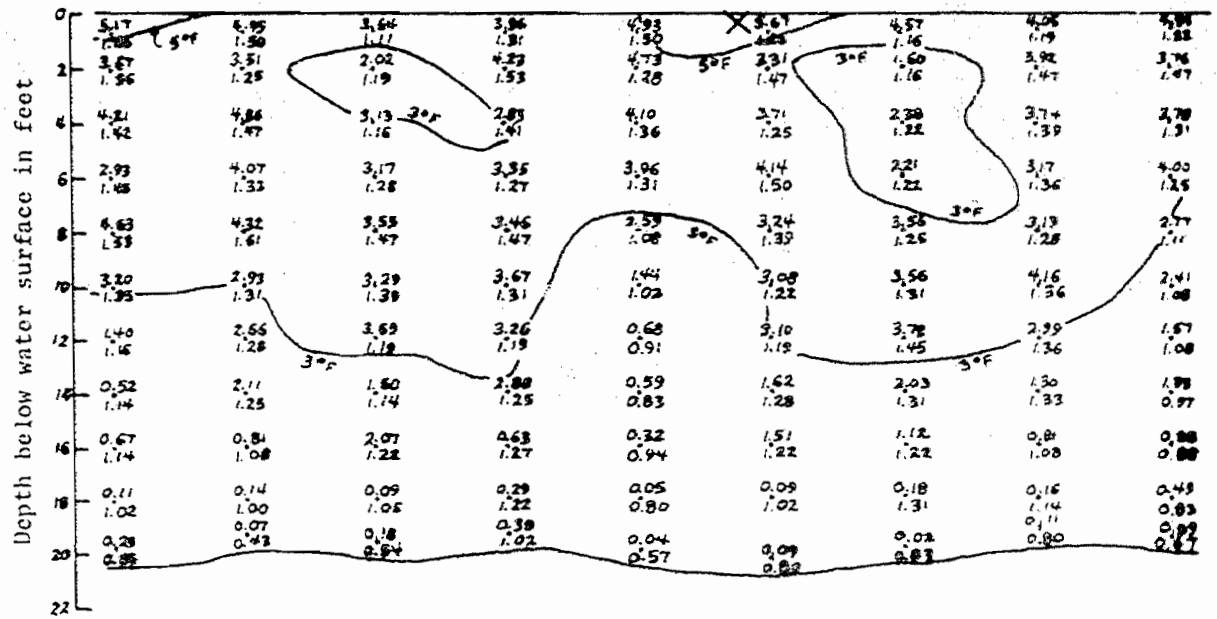

(c) 75 feet downstream

Fig. C.7 (continued).